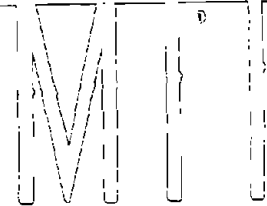


Publication No. R76-38

Order No. 555

NSF/RA-761753



PB80-102858



# NONLINEAR DYNAMIC RESPONSE OF REINFORCED CONCRETE FRAMES

by  
**KENNETH MUN SUNG MARK**

Supervised by  
**José M. Roesset**

DEPARTMENT  
OF  
CIVIL  
ENGINEERING

SCHOOL OF ENGINEERING  
MASSACHUSETTS INSTITUTE OF TECHNOLOGY  
Cambridge, Massachusetts 02139

**August 1976**

REPRODUCED BY  
U.S. DEPARTMENT OF COMMERCE  
NATIONAL TECHNICAL  
INFORMATION SERVICE  
SPRINGFIELD, VA 22161

**Sponsored by the National Science Foundation  
Division of Advanced Environmental Research  
and Technology  
Grant GI-4310**

ASRA INFORMATION RESOURCES  
NATIONAL SCIENCE FOUNDATION

Additional Copies May be Obtained from  
National Technical Information Service  
U.S. Department of Commerce  
5285 Port Royal Road  
Springfield, Virginia 22151

Massachusetts Institute of Technology  
Department of Civil Engineering  
Constructed Facilities Division  
Cambridge, Massachusetts 02139

NONLINEAR DYNAMIC RESPONSE OF REINFORCED CONCRETE FRAMES

by

KENNETH MUN SUNG MARK

Supervised by

José M. Roesset

August 1976

Sponsored by National Science Foundation  
Division of Advanced Environmental Research and Technology  
Grant GI-43106

ABSTRACTNONLINEAR DYNAMIC RESPONSE OF REINFORCED CONCRETE FRAMES

The purpose of this study is to investigate the applicability of a fiber model to the determination of the nonlinear dynamic response of frames. In this model the stress and strain are monitored through time at each fiber of several cross sections along each member. The tangent moduli for the steel and concrete resulting from the assumed nonlinear stress-strain relationships are then used to assemble a tangent stiffness matrix for the structure at each step. The dynamic analysis is carried using a central difference formula to advance the solution in time.

Several models for the concrete and the steel are first reviewed and compared. The effect of these models on the moment curvature relationship for a cross section is investigated and results are compared to experimental data. The process is repeated for simple members under static cyclic loading. Finally the fiber model is used to study the dynamic response of a single-bay one-story frame under sinusoidal and earthquake excitation. Results are again compared to experimental data and to those of simpler models.

The fiber model reproduces well the qualitative behavior of a reinforced concrete section or member and explains the effect of constant or variable axial loads. A point by point agreement with experimental data cannot be, however, obtained. Results for the frame are somewhat better than those provided by other, simpler models, but the model is mainly of academic interest, because of the cost of computations. Several refinements are suggested.

PREFACE

The work described in this report is based on the thesis by Kenneth Mun Sung Mark, presented to the Civil Engineering Department of M.I.T. in partial fulfillment of the requirements for the degree of Doctor of Philosophy. The research was supervised by Professor José M. Roesset and was made possible through Grant GI-43106 of the National Science Foundation, Division of Advanced Environmental Research and Technology.

This is the second of a series of reports published under this grant. The first report was:

Research Report R76-37, by Tarek S. Aziz: "Inelastic Dynamic Analysis of Building Frames."

Any opinions, findings, conclusions  
or recommendations expressed in this  
publication are those of the author(s)  
and do not necessarily reflect the views  
of the National Science Foundation.

## TABLE OF CONTENTS

	Page
Title Page	1
Abstract	2
Acknowledgements	3
Table of Contents	4
List of Figures, Tables, Symbols	7
Chapter I INTRODUCTION	12
1.1 Scope	12
1.2 Thesis Organization	13
Chapter 2 BEHAVIOR OF CONCRETE IN A REINFORCED CONCRETE MEMBER	15
2.1 Introduction	15
2.2 Plain Concrete, Monotonic Loading	16
2.3 Effect of Confinement on the Stress-Strain Curve	18
2.4 Behavior of Concrete under Cyclic Loading	21
2.5 Comparison of Various Models for Concrete Fiber Behavior	25
2.6 Conclusions	44
Chapter 3 BEHAVIOR OF REINFORCING STEEL	46
3.1 Introduction	46
3.2 Analytic Formulations for Reinforcing Steel	48
3.2.1 Elasto-Plastic Formulation	48
3.2.2 Singh, Gerstle, Tulin (SGT) Formulation	48
3.2.3 Improved SGT Formulation	51
3.2.4 Brown's Formulation	52
3.2.5 Kent's Formulation	54
3.2.6 Aktan, Karlsson, Sozen (AKS) Formulation	55
3.2.7 Strain Hardening	58
3.3 Comparisons of the Analytic Formulations for Steel	60
3.3.1 Kent Steel #8 Data	60
3.3.2 Kent Steel #17 Data	65
3.3.3 AKS Steel #3 Data	72
3.3.4 AKS Steel #5 Data	77
3.4 Conclusions	82

Chapter 4	CROSS-SECTION STUDY: MOMENT-CURVATURE RELATIONS	84
4.1	Introduction	84
4.2	Cross-Section Properties and Their Effect on the Moment-Curvature Relations	85
4.3	Incremental Stiffness Approach for Moment-Curvature	90
4.4	Effect of Increment Size	93
4.5	Characteristics of the Moment-Curvature Relationship	100
4.6	Effect of Axial Force on Cyclic Loading	105
4.6.1	Constant Axial Force	105
4.6.2	Axial Force Proportional to Moment	118
4.6.3	Constant Axial Force Combined with an Axial Force that Varies with Moment	128
4.6.4	Effect of Concrete Tensile Capacity on Moment-Curvature Relations with Axial Forces	136
4.7	Effect of Slippage between Concrete and the Steel Reinforcement	143
4.8	Comparison of Moment-Curvature Relations for Different Analytical Formulations	145
4.8.1	Aoyama's Beam A2	147
4.8.2	Agrawal, Tulin, Gerstle Beam #2	152
4.8.3	Kent's Beam #24	157
4.8.4	Kent's Beam #27	162
4.9	Conclusions	167
Chapter 5	MEMBER STUDY	168
5.1	Introduction	168
5.2	Incremental Stiffness Analysis	168
5.2.1	Solution Scheme	168
5.2.2	Nonlinear Effects	171
5.2.3	Limitations of the Incremental Approach for the Member Study	172
5.3	Simply Supported Beam Study	176
5.3.1	Kent's Beam #24	176
5.3.2	Burns and Siess Beam J12	180
5.4	Cantilever Beam Study	184
5.4.1	Brown's Cantilever Beam 86-35-RV10	184
5.4.2	Popov, Bertero, Krawinkler's Cantilever Beam	191
5.5	Frame Study, Gulkan's Frame FS1	195
5.6	Conclusions and Recommendations	201

Chapter 6	DYNAMIC ANALYSIS	203
6.1	Introduction	203
6.2	Dynamic Analysis with the Fiber Model	203
6.2.1	Analytic Formulation	203
6.2.2	Behavior of the Fiber Model under Sinu- soidal Base Motion	207
6.2.3	Behavior of the Fiber Model under Earth- quake Base Motion	223
6.3	Comparison of Simple Models for Frame Behavior	231
6.3.1	Behavior of Simple Models to Sinusoidal Base Motion	234
6.3.2	Behavior of Simple Models to Earthquake Base Motion	247
6.4	CONCLUSIONS	247
Chapter 7	CONCLUSIONS AND RECOMMENDATIONS	249
References		251
Biography		255
Appendix A	Formulation of the Member Incremental Stiffness Matrix	256
Appendix B	Semi-Rigid Joints to Account for Rotations due to Slip of Anchorage Reinforcement	260

## LIST OF FIGURES

<u>Fig. No.</u>	<u>Title</u>	<u>Page</u>
2-1	HOGNESTAD'S STRESS-STRAIN CURVE FOR CONCRETE	17
2-2	BROWN'S FORMULATION FOR CONFINED CONCRETE	17
2-3	KENT'S FORMULATION FOR CONFINED CONCRETE	19
2-4	EXPERIMENTAL CURVE FOR CONCRETE UNDER CYCLIC LOADING	19
2-5	RELOADING ASSUMPTIONS FOR CONCRETE FIBER BEHAVIOR	26
2-6	ENVELOPE FOR CONCRETE STRESS-STRAIN RELATIONSHIP	26
2-7	COMPARISON OF UNLOADING AND LOADING CURVES FOR CONCRETE	29
2-8	COMPARISON OF MOMENT-CURVATURE CURVES AND STRESS DISTRIBUTION FOR DIFFERENT CONCRETE FORMULATIONS	33
2-9	COMPARISON OF MOMENT-CURVATURE CURVES AND STRESS DISTRIBUTION FOR DIFFERENT CONCRETE FORMULATIONS	39
3-1	TYPICAL BEHAVIOR OF REINFORCING STEEL UNDER CYCLIC LOADINGS	47
3-2	ELASTO-PLASTIC FORMULATION FOR STEEL	48
3-3	SINGH, GERSTLE, TULIN FORMULATION FOR STEEL	50
3-4	EXPERIMENTAL STRESS-STRAIN CURVES FOR STEEL	50
3-5	BROWN'S FORMULATION FOR STEEL	53
3-6	KENT'S FORMULATION FOR STEEL	53
3-7	AKTAN, KARLSSON, SOZEN FORMULATION FOR STEEL	57
3-8	GENERAL STRAIN-HARDENING CURVES FOR MILD STEEL	57
3-9	STEEL FORMULATIONS (KENT #8 DATA)	61
3-10	STEEL FORMULATIONS (KENT #17 DATA)	67
3-11	STEEL FORMULATIONS (AKS #3 DATA)	73
3-12	STEEL FORMULATIONS (AKS #5 DATA)	78
4-1	EFFECT OF A VARIATION OF SECTION PROPERTIES ON MOMENT-CURVATURE RELATIONS	87
4-2	EFFECT OF A VARIATION OF SECTION PROPERTIES ON YIELD MOMENT	89

<u>Fig. No.</u>	<u>Title</u>	<u>Page</u>
4-3	TYPICAL REINFORCED CONCRETE CROSS-SECTION	91
4-4	STRAIN DISTRIBUTION FOR A CROSS-SECTION	91
4-5	INCREMENTAL STIFFNESS APPROACH FOR MOMENT-CURVATURE	94
4-6	EFFECT OF INCREMENT SIZE ON THE MOMENT-CURVATURE RELATIONS	96
4-7	MOMENT-CURVATURE COMPARISONS TO DETERMINE INCREMENT SIZE	101
4-8	CHARACTERISTICS OF THE MOMENT-CURVATURE RELATIONSHIP	103
4-9	INTERACTION DIAGRAM (MOMENT VS. AXIAL FORCE)	106
4-10	MOMENT VS. CURVATURE FOR VARYING AXIAL FORCES	107
4-11	MOMENT VS. CURVATURE FOR VARYING AXIAL FORCES	108
4-12	CYCLIC MOMENT-CURVATURE RELATIONS WITH AN AXIAL FORCE	110
4-13	MOMENT VS. AXIAL STRAIN WITH AN AXIAL FORCE	113
4-14	CYCLIC MOMENT-CURVATURE RELATIONS WITH AN AXIAL FORCE	115
4-15	EXPERIMENTAL MOMENT-CURVATURE RELATIONSHIP WITH AN AXIAL FORCE	117
4-16	CYCLIC MOMENT-CURVATURE RELATIONS WITH A TENSILE AXIAL FORCE	119
4-17	MOMENT-CURVATURE RELATIONS FOR AN AXIAL FORCE THAT VARIES WITH MOMENT	120
4-18	MOMENT-CURVATURE RELATIONS WITH AN AXIAL FORCE THAT VARIES WITH MOMENT	123
4-19	MOMENT VS. AXIAL STRAIN FOR CYCLIC LOADING WITH AN AXIAL FORCE THAT VARIES WITH MOMENT	127
4-20	CYCLIC MOMENT-CURVATURE RELATIONS WITH AXIAL FORCE PROPORTIONAL TO MOMENT; VARY CURVATURE LIMITS	130
4-21	CYCLIC MOMENT-CURVATURE RELATIONS WITH AN AXIAL FORCE THAT VARIES WITH MOMENT	131
4-22	CYCLIC MOMENT-CURVATURE RELATIONS WITH A CONSTANT AXIAL FORCE PLUS AXIAL FORCE WHICH VARIES WITH MOMENT	133
4-23	CYCLIC MOMENT-CURVATURE RELATIONS WITH A CONSTANT AXIAL FORCE PLUS AXIAL FORCE WHICH VARIES WITH MOMENT	137
4.24	CYCLIC MOMENT-CURVATURE WITH AXIAL FORCE AND TENSILE CAPACITY IN CONCRETE	140

<u>Fig. No.</u>	<u>Title</u>	<u>Page</u>
4-25	MOMENT-CURVATURE COMPARISONS FOR AOYAMA'S BEAM A2	147
4-26	MOMENT-CURVATURE COMPARISONS FOR AGRAWAL, TULIN, GERSTLE'S BEAM #2	153
4-27	MOMENT-CURVATURE COMPARISONS FOR KENT'S BEAM #24	158
4-28	MOMENT-CURVATURE COMPARISONS FOR KENT'S BEAM #27	163
5-1	COMPARISON OF ASSUMPTIONS ON M- $\theta$ CURVES	175
5-2	LOAD-DEFLECTION BEHAVIOR OF KENT'S BEAM #24	177
5-3	LOAD-DEFLECTION BEHAVIOR FOR BURNS & SIESS BEAM J12	181
5-4	LOAD-DEFLECTION BEHAVIOR FOR BROWN'S CANTILEVER BEAM	185
5-5	LOAD-DEFLECTION BEHAVIOR FOR POPOV, BERTERO, KRAWIN- KLER'S CANTILEVER BEAM	192
5-6	LOAD-DEFLECTION BEHAVIOR OF GULKAN'S FRAME FSI	196
6-1	BASE MOTIONS IN THE DYNAMIC ANALYSIS	208
6-2	DISPLACEMENT-TIME RESPONSE FOR THE FIBER MODEL UNDER SINUSOIDAL BASE MOTION	210
6-3	TYPICAL MOMENT-CURVATURE RELATIONS FOR THE COLUMNS	216
6-4	LOAD-DEFLECTION RELATIONSHIPS	220
6-5	VARIATION OF LATERAL STIFFNESS	221
6-6	EXPERIMENTAL RESPONSE OF FRAME FDI TO STEADY-STATE BASE MOTION	224
6-7	RESPONSE OF FIBER MODEL TO STEADY-STATE BASE MOTION	225
6-8	EXPERIMENTAL RESPONSE OF FRAME HE1 TO EL CENTRO EARTHQUAKE	227
6-9	RESPONSE OF FIBER MODEL TO EL CENTRO EARTHQUAKE	228
6-10	RESPONSE OF SIMPLE MODELS TO STEADY-STATE BASE MOTION	236
6-11	RESPONSE OF SIMPLE MODELS TO EL CENTRO EARTHQUAKE	242

LIST OF TABLES

<u>Table No.</u>	<u>Title</u>	<u>Page</u>
4-1	INCREMENT SIZE COMPARISON	95
4-2	COMPARISON OF MAXIMUM MOMENTS WITH AN AXIAL FORCE WHICH VARIES WITH MOMENT	129
4-3	COMPARISON OF MAXIMUM MOMENTS FOR INCREMENTAL AXIAL FORCES IN ADDITION TO A CONSTANT AXIAL FORCE	129
4-4	PROPERTIES OF MEMBERS USED FOR MOMENT-CURVATURE COMPARISON IN SECTION 4-8	146
6-1	COMPARISON OF PEAK DISPLACEMENTS FOR FIBER MODEL UNDER SINUSOIDAL BASE MOTION	222
6-2	COMPARISON OF MODELS FOR MODIFIED SINUSOIDAL LOADINGS	234

List of Symbols

$a_{ij}$	stiffness coefficients at a cross-section
$c$	coefficient relating $\Delta M/\Delta N$
$\epsilon$	strain
$f$	stress
$f'_c$	concrete cylinder strength
$f_y$	steel yield stress
$\phi$	curvature
$K$	stiffness matrix
$M$	moment
$N$	axial force
$t$	time
$TM$	tangent modulus
$u$	axial displacement
$v$	lateral displacement
$U$	relative displacement vector
$\ddot{U}$	relative acceleration vector
$\ddot{U}_c$	ground acceleration vector

## CHAPTER 1 - INTRODUCTION

1.1 SCOPE

In order to study the nonlinear dynamic response of reinforced concrete frames, a fiber model using the incremental stiffness approach is developed. The effectiveness and limitations of this model are demonstrated by parameter studies and comparisons with experimental data.

Reinforced concrete behavior is complex and particularly hard to quantify. Formulations for the nonlinear behavior of both the reinforcing steel and concrete are derived, but the complete generality of these is not assumed. Of the two materials, steel has been shown to have a much greater effect on the reinforced concrete member behavior.

It is common to use a fiber model in moment-curvature studies. Several studies have even applied it to predict the load-deflection behavior of simple members such as cantilever beams. This is as far as it went, for to obtain deflections curvatures were integrated across the member and were determined by iteration for equilibrium at each cross-section. This type of analysis became prohibitively time (computer) consuming. Using the incremental stiffness approach to advance the solution, studies of members and even frames is feasible. However, the incremental stiffness is sensitive to increment size and subject to error propagation.

To study the dynamic response of frames there have been several approaches. In some cases springs which represent the stiffness degradation in the cyclic loading are used to represent members of the frame or the whole frame. There are intermediate models where the moment rotation curves for a member are specified and "hinges" are assumed to occur at the ends of each member. The fiber model is very complex, because of all the parameters that must be monitored. However, the fiber model is theoretically a consistent approach, which carries the formulation from the stress-strain behavior of the individual fibers of concrete and steel, through the cross-section behavior, and finally to the behavior of structures under static and dynamic loadings.

## 1.2 THESIS ORGANIZATION

Chapter 2 studies the behavior of both plain concrete and concrete in a reinforced member. A simple formulation for the stress-strain relationship, which includes the effect of cyclic unloading and reloading, is proposed. Comparisons are made to show the effect of various concrete formulations on the moment-curvature behavior.

Reinforcing steel which exhibits a distinctly nonlinear behavior (the Bauschinger effect) is discussed in Chapter 3. Under a variety of loading conditions, various steel formulations are compared, and the best curvilinear formulation is selected for subsequent studies.

At the cross-section level, member behavior is studied through the moment-curvature relationship. This study is carried out in Chapter 4, where the incremental stiffness is presented, and effects such as axial force, concrete tensile capacity, and slippage of the reinforcement are discussed.

In Chapter 5 the model is used to represent the load-deflection behavior of members under cyclic loading. Effects such as slippage at the joints and shear deformation are discussed.

Finally, Chapter 6 covers the use of the fiber model and the incremental stiffness approach to study the dynamic response of simple reinforced concrete frames. Comparisons are made with experimental values and also with simpler models.

## CHAPTER 2 - BEHAVIOR OF CONCRETE IN A REINFORCED CONCRETE MEMBER

### 2.1 INTRODUCTION

In order to investigate the effect of material properties as far as the concrete is concerned, an analytic model will be used, where the concrete at each cross section is represented by fibers distributed in layers and related by an assumed linear strain distribution. Each fiber has a stress-strain relationship which is strongly dependent upon its previous loading history.

Most of the information available on the behavior of plain concrete has been obtained from standard cylinder tests where the specimen is loaded in compression to failure. However, the stress conditions for a fiber in a reinforced concrete member may be significantly different. At a cross-section there are the presence of a strain gradient<sup>(8,9)</sup> and corresponding differences in straining rates.<sup>(2)</sup> Web reinforcement provides confining action for the concrete fibers in the core. Tensile strains and the occurrence of finite cracks along the member complicate further the problem.

Several analytic formulations for the behavior of concrete fibers which have been proposed by other authors will be compared. A suitable model will be selected by determining how the various features of the stress-strain relation affect member behavior, and how sophisticated a model is required.

## 2.2 PLAIN CONCRETE, MONOTONIC LOADING

There have been many analytical expressions for concrete's stress-strain curve under monotonic loading to failure. Results based on cylinder tests show, however, a great scatter. This variability can be attributed to such diverse factors as mix proportions, quality control, age of the specimen and to the testing procedure itself.

The nonlinear stress-strain relation has an ascending portion to the maximum stress,  $f_{c \max}$ , then a descending branch to failure, as shown in Fig. 2-1. The most widely used formulation is due to Hognestad and it has a second order parabola for the ascending branch and a straight line for the descending branch.

Ascending relation

$$f_c = f_{c \max} \left[ \frac{2\epsilon_c}{\epsilon_{c0}} - \left( \frac{\epsilon_c}{\epsilon_{c0}} \right)^2 \right]$$

Descending relation

(2.1)

$$f_c = f_{c \max} \left[ 1 - .15 \frac{\epsilon_c - \epsilon_{c0}}{\epsilon_{cu} - \epsilon_{c0}} \right]$$

where  $\epsilon_{c0}$  is the strain at which the maximum stress occurs, and  $\epsilon_{cu}$  is the ultimate strain.

Popovics<sup>(1)</sup> has tabulated many such formulations from a variety of researchers. In addition he has collected expressions relating

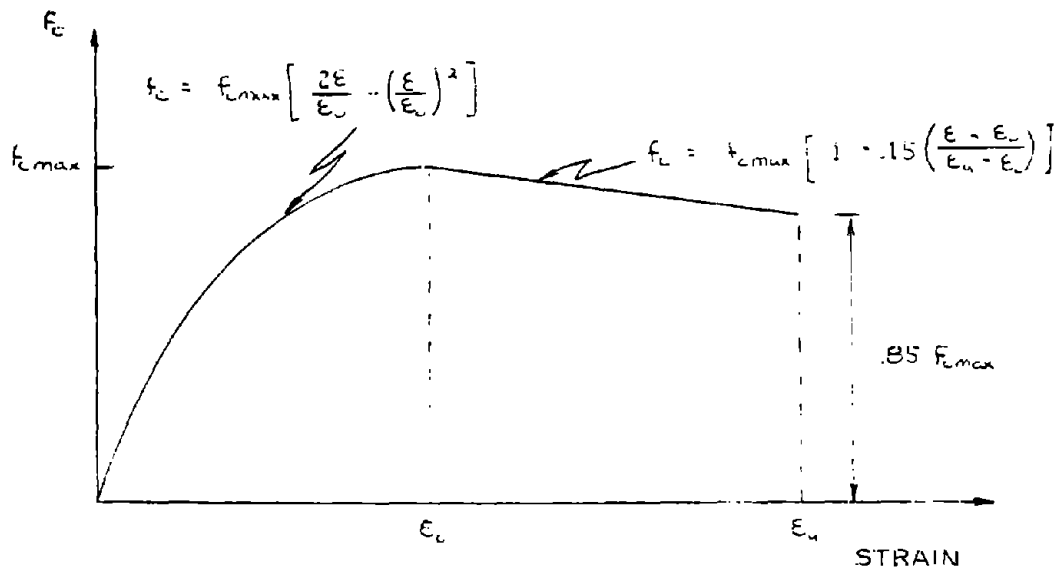


FIG. 2-1 - HOGNESTAD'S STRESS-STRAIN CURVE FOR CONCRETE

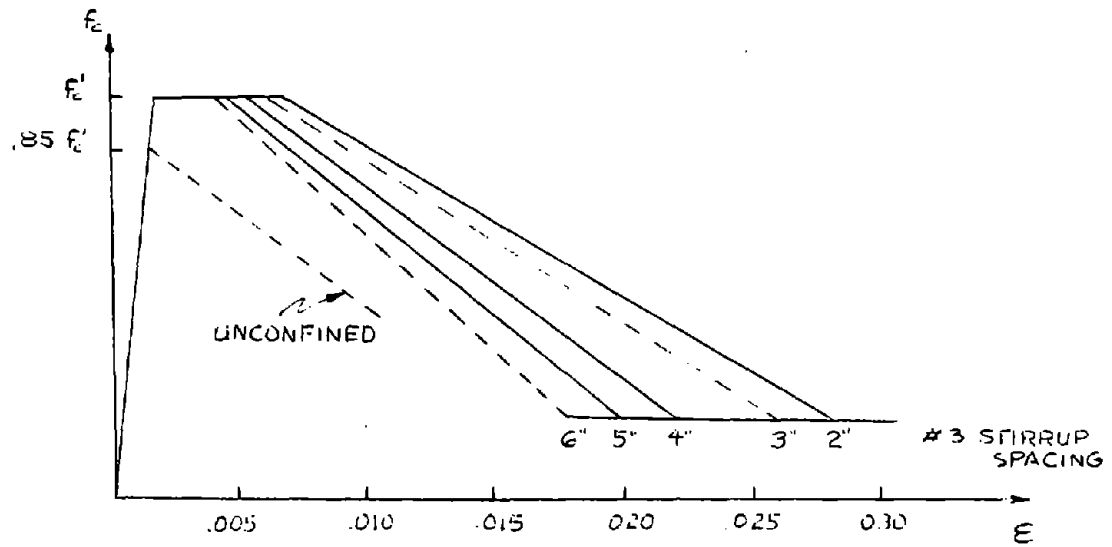


FIG. 2-2 - BROWN'S FORMULATION FOR CONFINED CONCRETE

$\epsilon_{CO}$  and  $E_{CO}$  with  $f'_C$  max. These expressions show that both  $\epsilon_{CO}$  and  $E_{CO}$  increase with concrete cylinder strength,  $f'_C$ .

### 2.3 EFFECT OF CONFINEMENT ON THE STRESS-STRAIN CURVE

Unlike the standard concrete cylinder, the concrete in the core of a reinforced concrete member is usually confined by web reinforcement. Increasing the web reinforcement (i.e., decreasing the stirrup spacing) has the primary effect of reducing the slope of the descending branch of the stress-strain curve. There is then additional ductility, since the concrete can accommodate larger strains and has less strength reduction for a given strain increment. This confining action was considered by both Brown<sup>(16)</sup> and Kent<sup>(18)</sup> in their concrete formulations.

Brown's relationship, shown in Fig. 2-2, extrapolates from Yamashiro's data to obtain a variation in the slope of the descending portion with different spacings of #3 rectangular stirrups. Brown has also indicated an increase in the maximum concrete stress in a member from  $.85 f'_C$  to  $f'_C$ , and attributes this increase to the effect of confinement.

As shown in Fig. 2-3, Kent has proposed a more general formulation. The slope of the descending branch is related to the binding ratio,  $p^*$ .

$$p^* = \frac{A_s^* (b^* + d^*)}{b^* d^* s} \quad (2.2a)$$

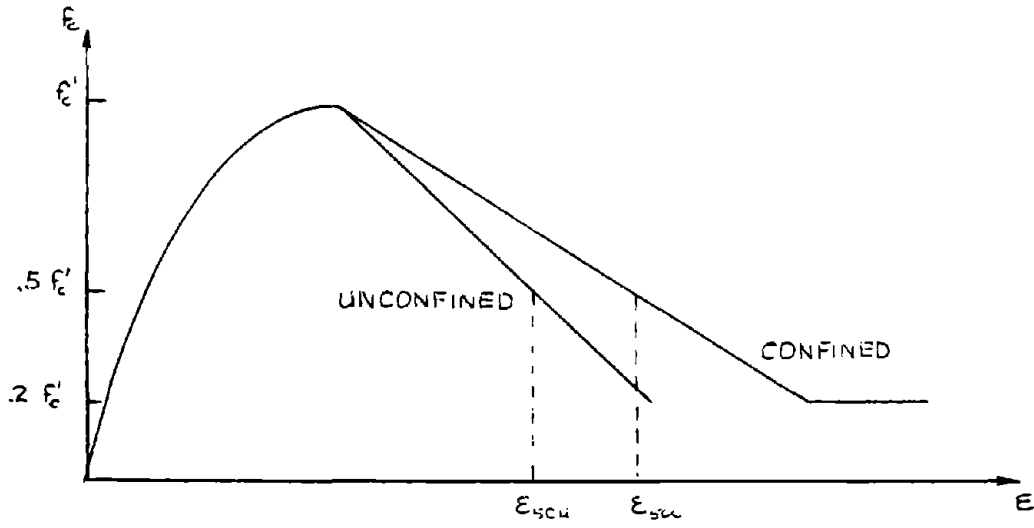


FIG. 2-3 - KENT'S FORMULATION FOR CONFINED CONCRETE

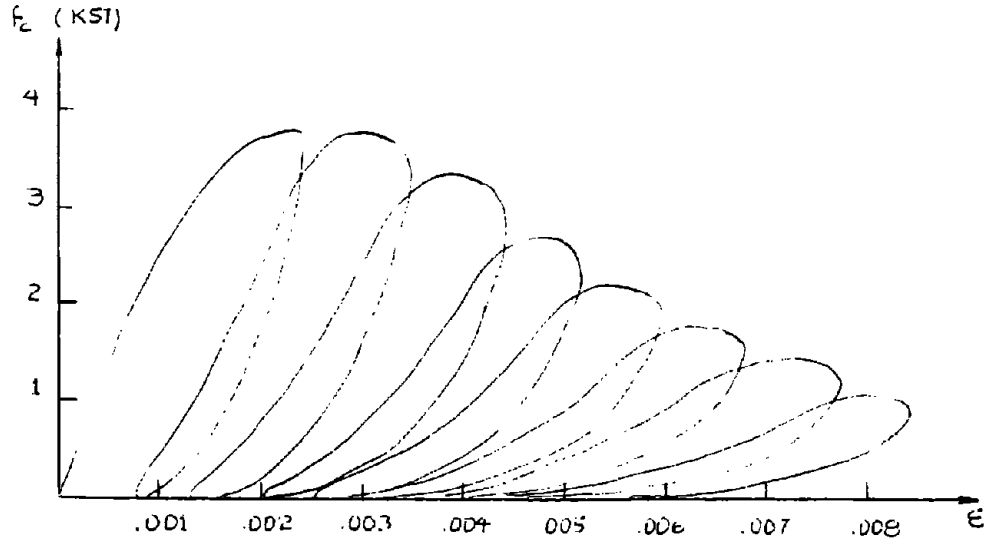


FIG. 2-4 - EXPERIMENTAL CURVE FOR CONCRETE UNDER CYCLIC LOADING (SGT)

where  $A_s^*$  is the area of a rectangular stirrup and  $b^*$  and  $d^*$  are the dimensions of the confined core.  $s$  is the stirrup spacing in inches. Kent identifies the strain at which the stress in the descending branch is half the maximum stress as  $\epsilon_{50}$ :

$$\epsilon_{50} = \frac{3 + .002 f'_c}{f'_c - 1000} + \frac{3}{4} p^* \sqrt{\frac{b^*}{s}} \quad (f'_c \text{ in psi}) \quad (2.2b)$$

The descending branch is represented by a straight line from  $(f'_{c \max}, \epsilon_{c0})$  through  $(f'_{c \max}/2, \epsilon_{50})$ . In the expression for  $\epsilon_{50}$ , the first term is the strain for unconfined concrete and the second term represents the effect of confinement. The negative slope of the descending branch then decreases with increasing confinement as indicated by the proportionality of the second term to  $p^*/\sqrt{s}$ .

Kent states that  $f'_c$  should be the maximum stress for both confined and unconfined concrete. He argues that the  $.85 f'_c$  normally used is based on column tests and that tests where a strain gradient is imposed, as in Sturman, Shah, and Winter's studies,<sup>(9)</sup> indicate that the use of  $f'_c$  is conservative. In this thesis,  $f'_c$  will be used as the maximum stress in the concrete stress-strain relationship.

The effect of the slope of the descending branch can be shown by considering the moment curvature relations. In the initial loading cycle, the moment curvature curve has a plateau with a slight positive slope after the tension steel has yielded. If the curvature continues to increase, eventually the extreme concrete fiber will

reach the descending branch of the stress-strain curve. From this point the moment curvature curve will start to bend downward as additional fibers reach the descending branch. This effect will be more pronounced when the section is singly reinforced or when there is an axial force imposed on the cross-section.

In the subsequent unloading cycle, the curvature begins to decrease and the concrete fibers unload. The unloading continues until concrete contributes nothing to the stiffness; later fibers on the opposite side of the neutral axis will provide compressive strength. If the extreme concrete fibers had reached the descending branch, then the zero contribution point on the unloading curve will be reached sooner. Other characteristics of the moment-curvature curve will be discussed in greater detail in Chapter 4.

#### 2.4 BEHAVIOR OF CONCRETE UNDER CYCLIC LOADING

Under dynamic, earthquake-type loading, the individual concrete fibers are subjected to cyclic loading where there may be severe strain reversals. Concrete's inability to take significant tension and the formation of cracks make the cyclic behavior complex.

Shina, Gerstle and Tulin<sup>(11)</sup> cyclically tested 24 standard cylinders with 2000, 3750, and 4000 psi concrete. A typical set of experimental curves for one test is shown in Fig. 2-4. Generally the slope of the reloading and unloading curves decreased as the maximum strain in the cycle increased. The limiting or envelope curve,

which the reloading curves reach and then follow, was found to be slightly higher than the monotonic loading curve. These authors proposed the following relationships to represent the family of unloading and reloading curves:

Unloading

$$f_c = \frac{J}{X} (\epsilon_c - X)^2 - H \quad (2.3)$$

$$X = \epsilon_{c1} + \frac{f_{c1} + H}{2J} - \sqrt{\left(\epsilon_{c1} + \frac{f_{c1} + H}{2J}\right)^2 - \epsilon_{c1}^2}$$

Reloading

$$f_c = Y (\epsilon_c + L) - K$$

$$Y = \frac{f_{c1} + K}{\epsilon_{c1} + L}$$

where  $(f_{c1}, \epsilon_{c1})$  is the end point of the previous cycle and H, J, K, L are parameters which are specified for given cylinder strengths (i.e., for 3000, 3750, 4000 psi concrete only).

The form of these equations and the variation of the parameters with  $f_c'$  make it difficult to extend the relations for other than the concrete strengths tested.

Shina, Gerstle, Tulin considered each unloading and reloading curve to be independent of the previous loading history. In their formulation one point uniquely specified the unloading or reloading curve passing through it.

Karson and Jirsa<sup>(7)</sup> used 46 - 3" x 5" rectangular columns in their cyclic loading tests. Their experimental results were essentially the same as those of the previous researchers. The unloading and reloading curves were shown to be dependent on the maximum stress and strain in the previous cycle. The analytical formulation consists of equations which determine three points through which a second order parabola is passed. The points are: one on the envelope curve, one on the zero stress axis, and a common point, defined as the point where the reloading curve crosses the previous unloading curve.

Envelope curve

$$F_E = .85 S_E e^{(1-S_E)} \quad (2.49)$$

Common point curve

$$F_C = \beta \frac{S_C}{.315 + .77\beta} e^{(1 - \frac{S_C}{.315 + .77\beta})}$$

The location of the common point is determined by the peak of the previous load cycle. If the peak is above the common point limit,  $\beta = .75$ . If it is between the common point and the stability limit,  $\beta$  varies between .76 and .62. If the peak is below the stability limit, then the peak becomes the common point and a closed hysteresis loop is formed. Thus the stability limit curve defines the points below which stable closed hysteresis loops occur.

Zero stress point

$$S_p = (1.76 - \beta) (.160 S_c^2 + .133 S_c)$$

For reloading zero stress point

$$S_p = .093 S_E^2 + .091 S_E \quad (2.4b)$$

For unloading zero stress point

$$S_p = .145 S_E^2 + .13 S_E$$

where  $F = \frac{f_c}{f_T}$  and  $S = \frac{\epsilon_c}{\epsilon_{co}}$

The procedure in both of these experimental programs was to load, then unload the specimens. No tensile force was exerted. However, in a flexural member with loading reversals, some fibers are subjected to tensile stress. Discrete cracks occur when the tensile stress exceeds the limiting tensile strength, usually taken to be  $f_r$ , the modulus of rupture, and with cracking there is a redistribution of stress. Once the fiber has cracked, it can never take tensile stress again.

In the analytic model that will be used, the location of cracks will not be precisely determined since this requires a much more sophisticated analysis. Using the "plane-sections-remain-plane" assumption at each cross-section, "average" tensile strains are defined. With this type of averaging, finite cracks are crudely accounted for; this is usually adequate for obtaining overall behavior of the member. These tensile strains then must be considered in the

analytic behavior of the individual concrete fibers.

It will be assumed that the concrete fiber cannot supply compressive strength until the crack closes; that is, until the tensile strain is recovered. In the situation where the fiber has incurred significant plastic deformation before unloading, the fiber will crack upon load reversal with an unrecoverable strain. Point A in Fig. 2-5 is such a point if no tensile capacity is assumed or if the fiber has previously cracked. With additional unloading there would be straining without any stress contribution to points such as B or C. If reloading were to proceed from one of these points, it is consistent to assume that the strain must exceed  $\epsilon_A$  before any compressive stress can be supplied by the fiber. Sozen<sup>(12)</sup> has pointed out that the reloading would probably follow a path like the dashed line beginning at  $\epsilon_B$ . Physically this can be explained by the roughness and irregularity of cracks providing partial contact as the crack closes. An extreme assumption would be to assume that at the reloading point, full stiffness is obtained. In the next section these assumptions on concrete behavior will be compared for their effect on the moment-curvature relations and on the concrete stress distribution in a section.

## 2.5 COMPARISON OF VARIOUS MODELS FOR CONCRETE FIBER BEHAVIOR

In order to understand how the various formulations for the unloading and reloading of the concrete fibers compare, a simple tri-

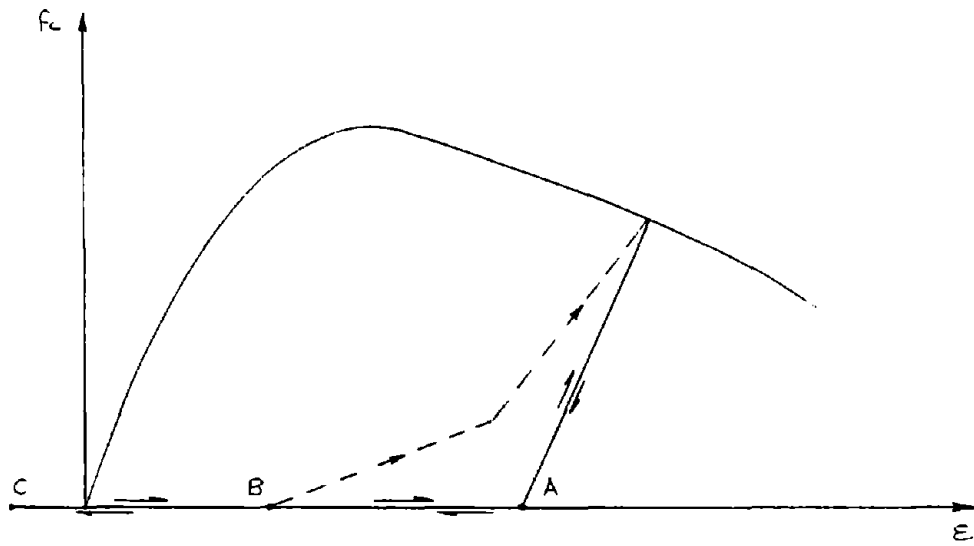


FIG. 2-5 - RELOADING ASSUMPTIONS FOR CONCRETE FIBER BEHAVIOR

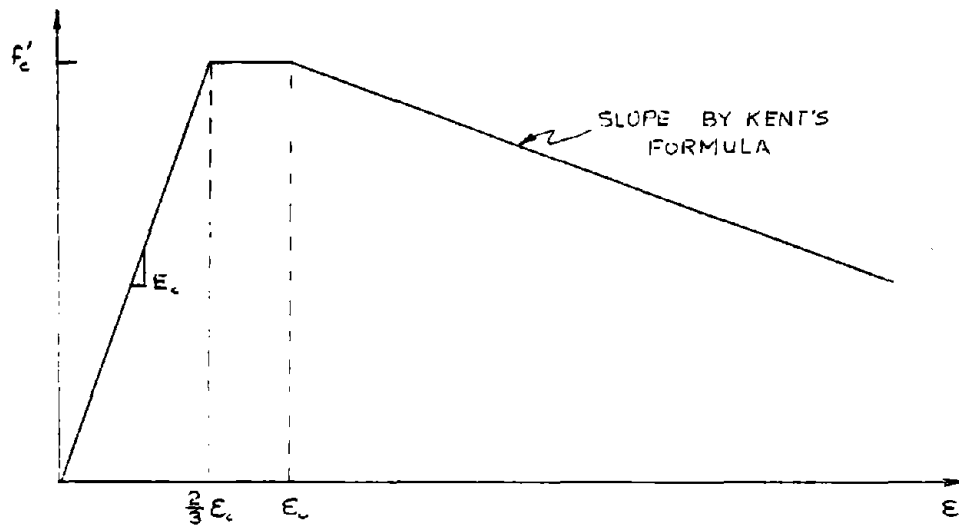


FIG. 2-6 - ENVELOPE FOR CONCRETE STRESS-STRAIN RELATIONSHIP

linear envelope was used for all the formulations (Fig. 2-6) and the following schemes were considered:

a) LINEAR1 FORMULATION

Unloading and reloading linearly with slope  $E_c$ , the initial loading slope. Reloading beginning at the reversal point (i.e., the crack doesn't have to close before compressive strength is supplied).

b) LINEAR2 FORMULATION

Unloading and reloading linearly with slope  $E_c$ . The crack must close before compressive stress can be supplied by the fiber. (Strain must return to  $\epsilon_A$  in Fig. 2-5 before reloading. The strain where the unloading curve intersects this zero stress axis will subsequently be called  $\epsilon_{rev}$ ).

The remaining formulations will follow this reloading procedure of returning to  $\epsilon_{rev}$ .

c) SGT FORMULATION

Unloading and reloading according to Shina, Gerstle, Tulin's formulation where the relationship at any point is uniquely specified.

d) KJ FORMULATION

Unloading and reloading according to the general Karson, Jirsa formulation, which depends upon the previous loading history.

3) LINEAR3 FORMULATION

Unloading and reloading linearly with a slope which varies with the maximum strain in the previous cycle. Karson, Jirsa's equation for unloading  $S_p$  will be used to determine this step. (Eqn. 2-4b)

a) In Fig. 2-7 (A to F), these five formulations are compared. Each of the analytic results were obtained for the same strain limits in each cycle. The loading and unloading cycles are numbered and arrows indicate the direction of loading. In this test conducted by Shina, Gerstle, Tulin, the specimen was loaded, then unloaded; no tensile stress was applied to the specimen.

In LINEAR1, the stiffness in unloading initially fits well, but the experimental curve becomes much softer as most of the load is removed. In reloading the stiffness is larger to begin with and gets closer to the experimental value as the envelope is approached. This formulation supplies a loop for unloading and reloading which is significantly larger than the one experimentally observed.

The same general comments apply for LINEAR2, but the loops are now smaller. It should be noticed that the unloading and reloading curves should coincide in this model, but the zero stress point  $(0, \epsilon_{rev})$  is determined with one increment delay.

The SGT and KJ formulations used here are modifications of the original models because of the manner in which tensile strains are handled. In both of them the unloading curve provides good agreement. Reloading is better than in the previous two formulations, but the agreement decreases with larger strains. Overall, the KJ formulation gives the best fit.

LINEAR3 does reflect the change of unloading and reloading slopes with increasing strains. For this simple model there is a

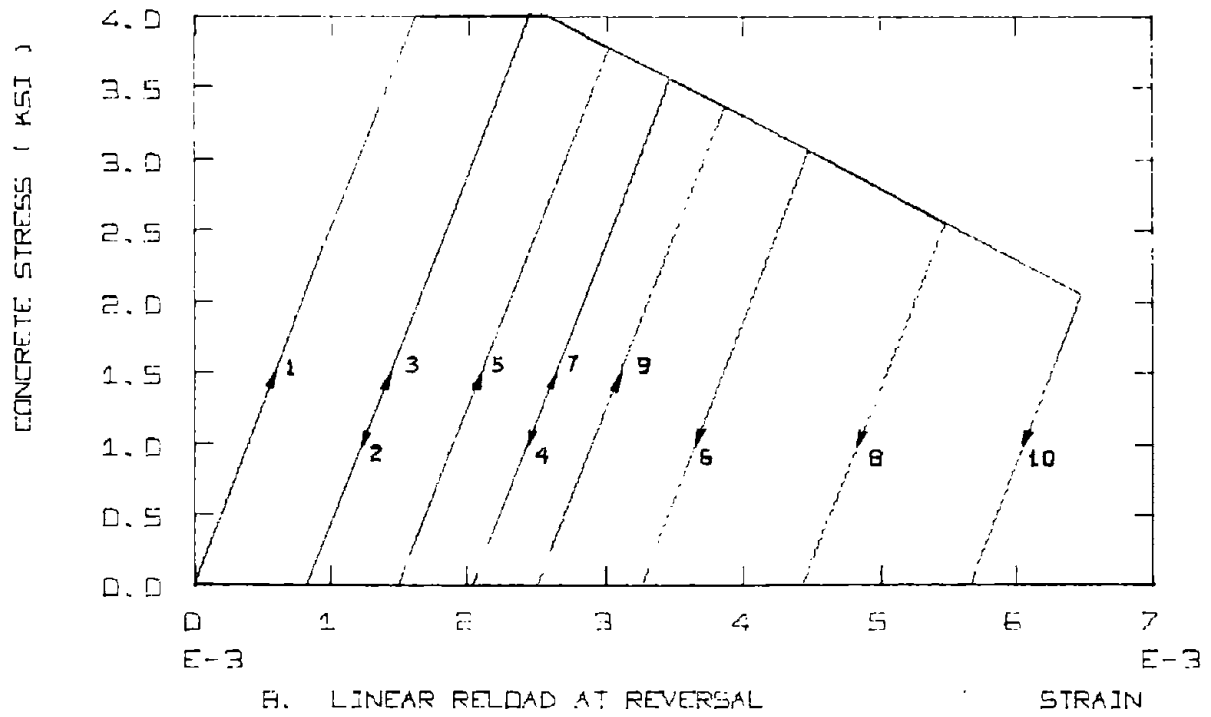
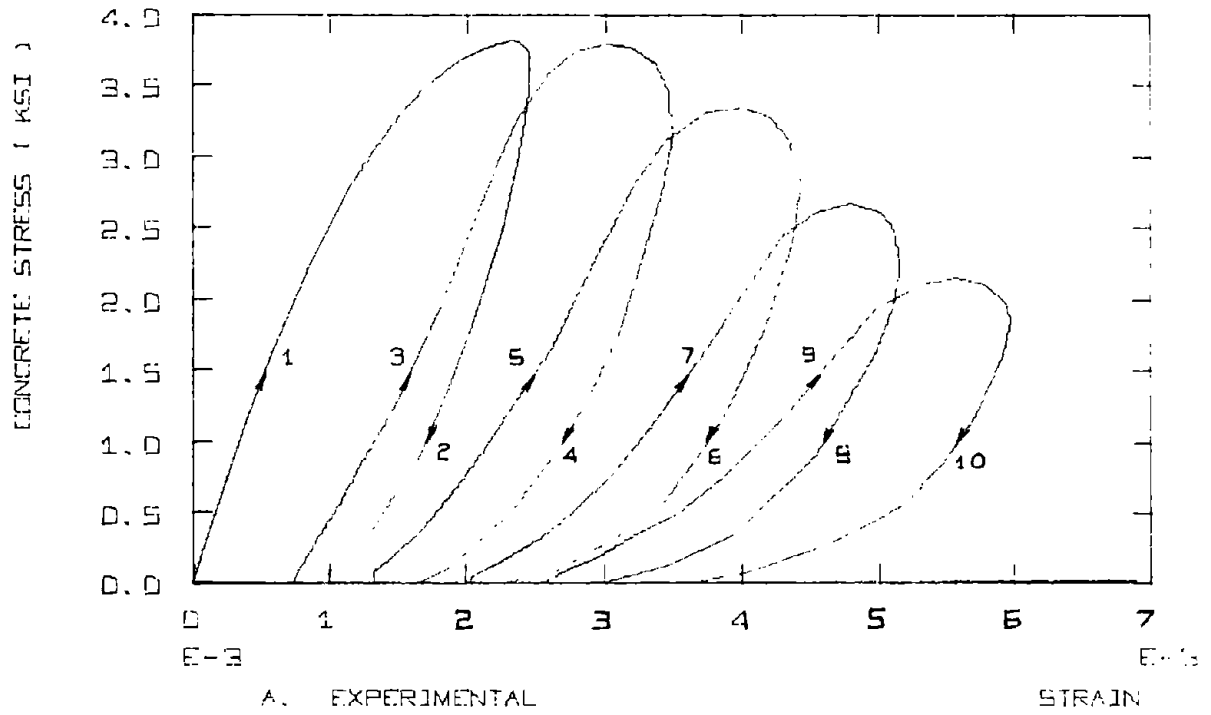


FIG. 2-7 - COMPARISON OF UNLOADING AND RELOADING CURVES FOR CONCRETE

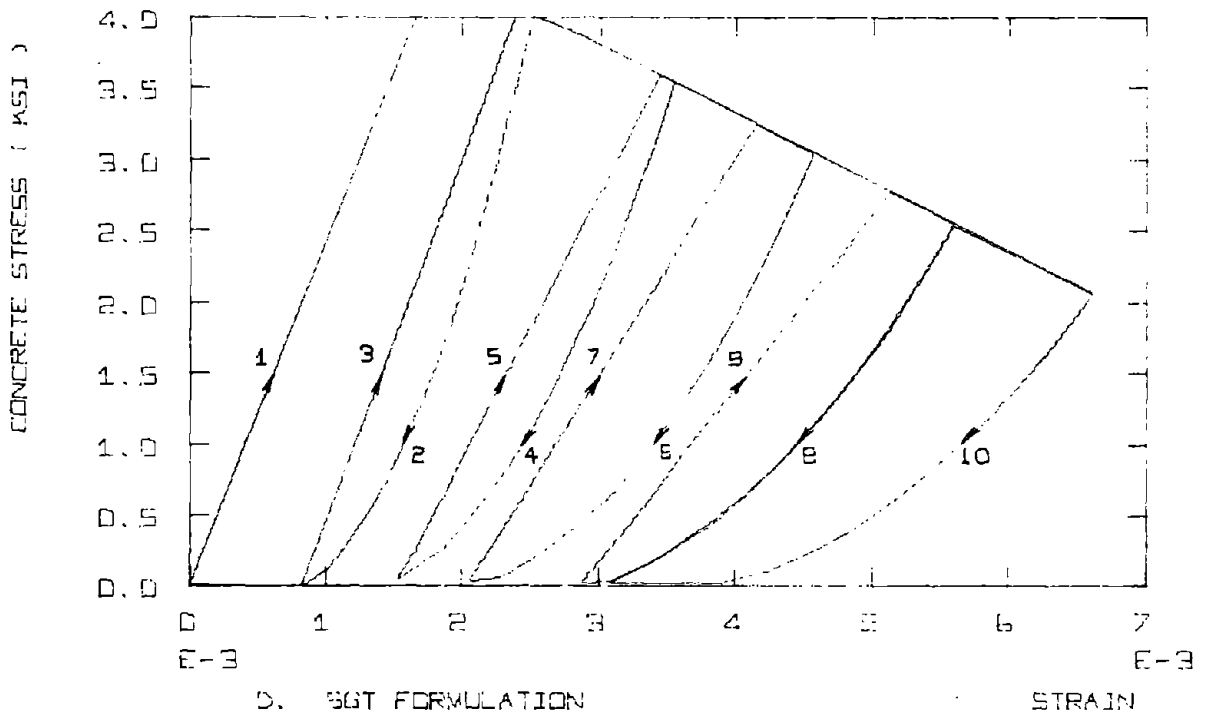
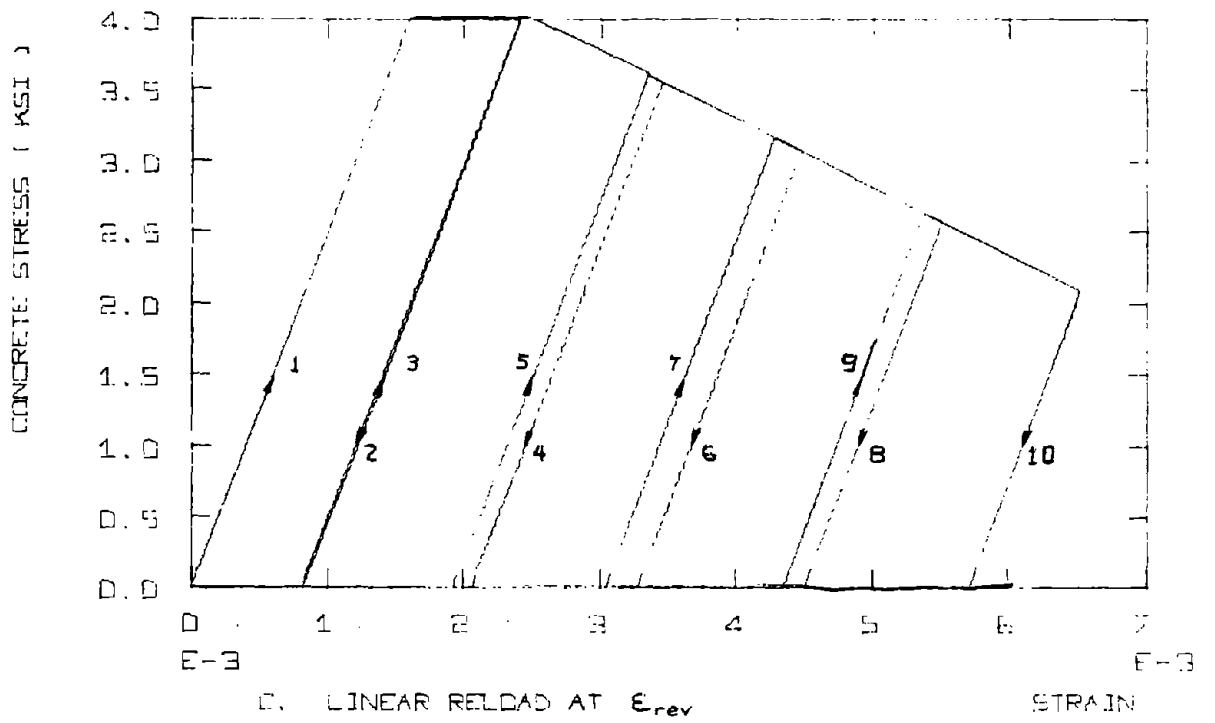


FIG. 2-7 (Continued)

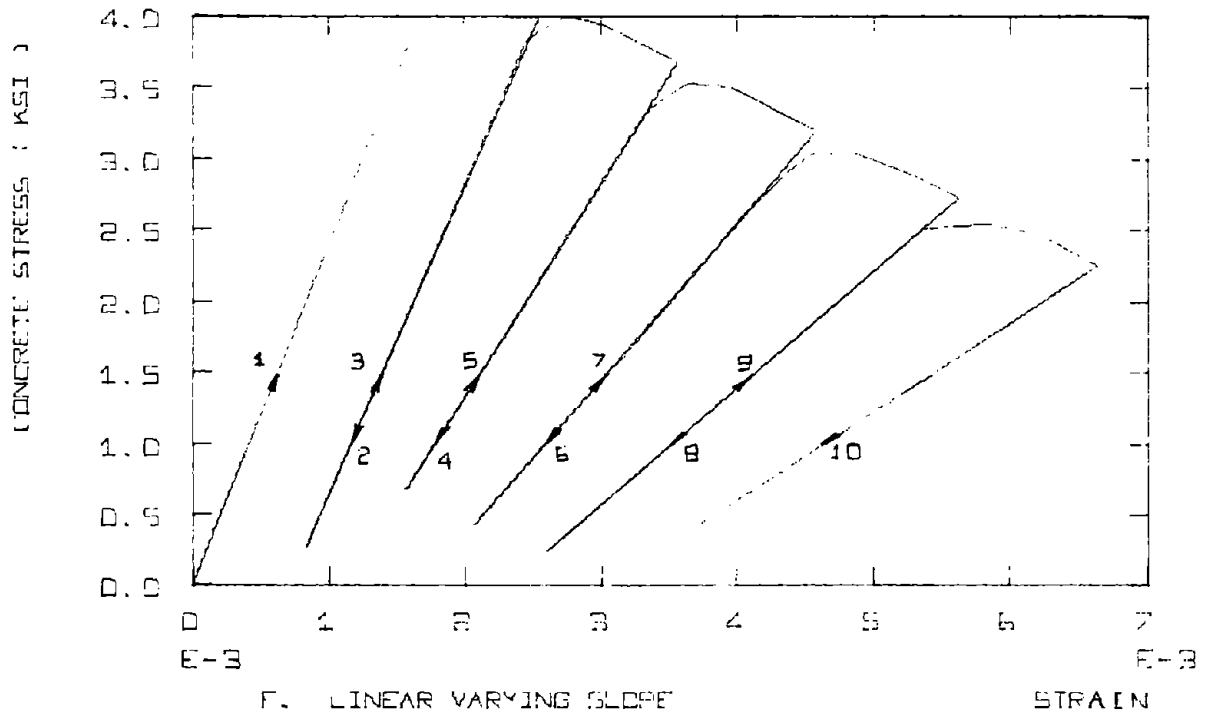
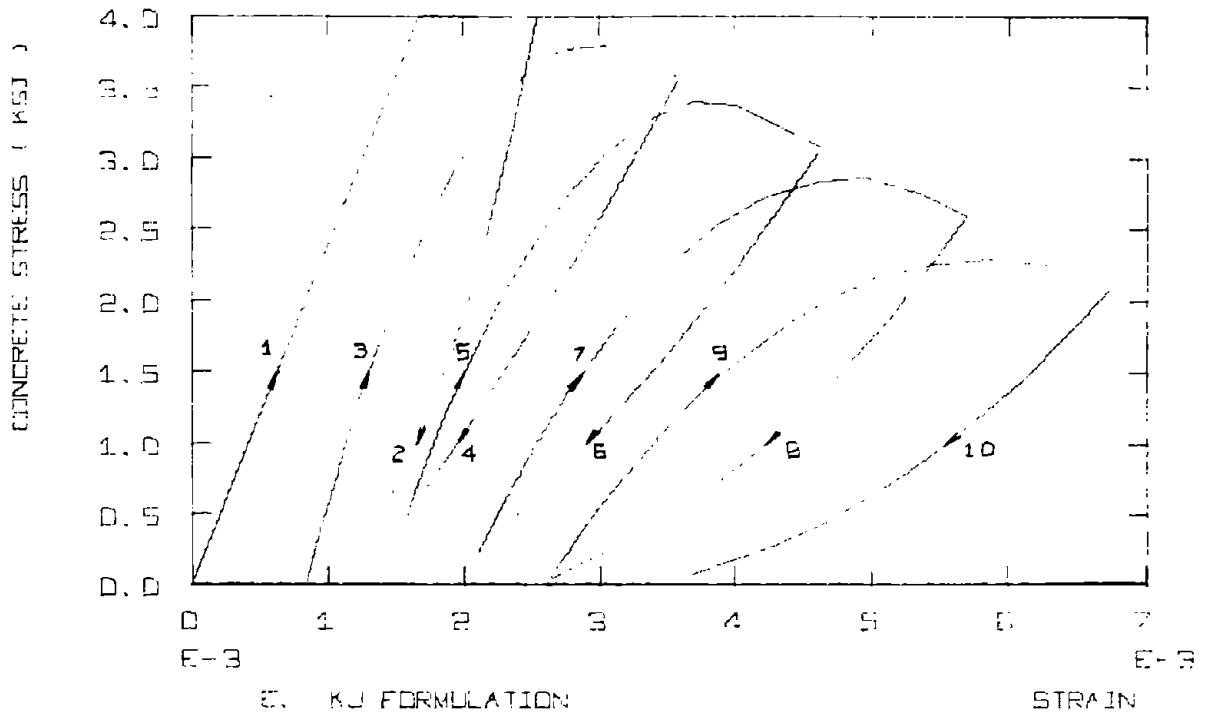


FIG. 2-7 - (Continued)

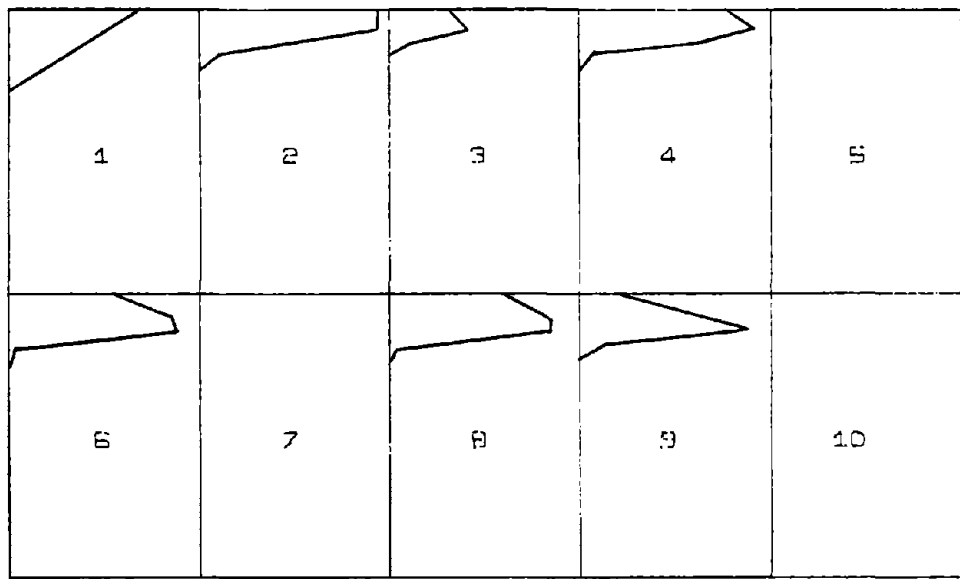
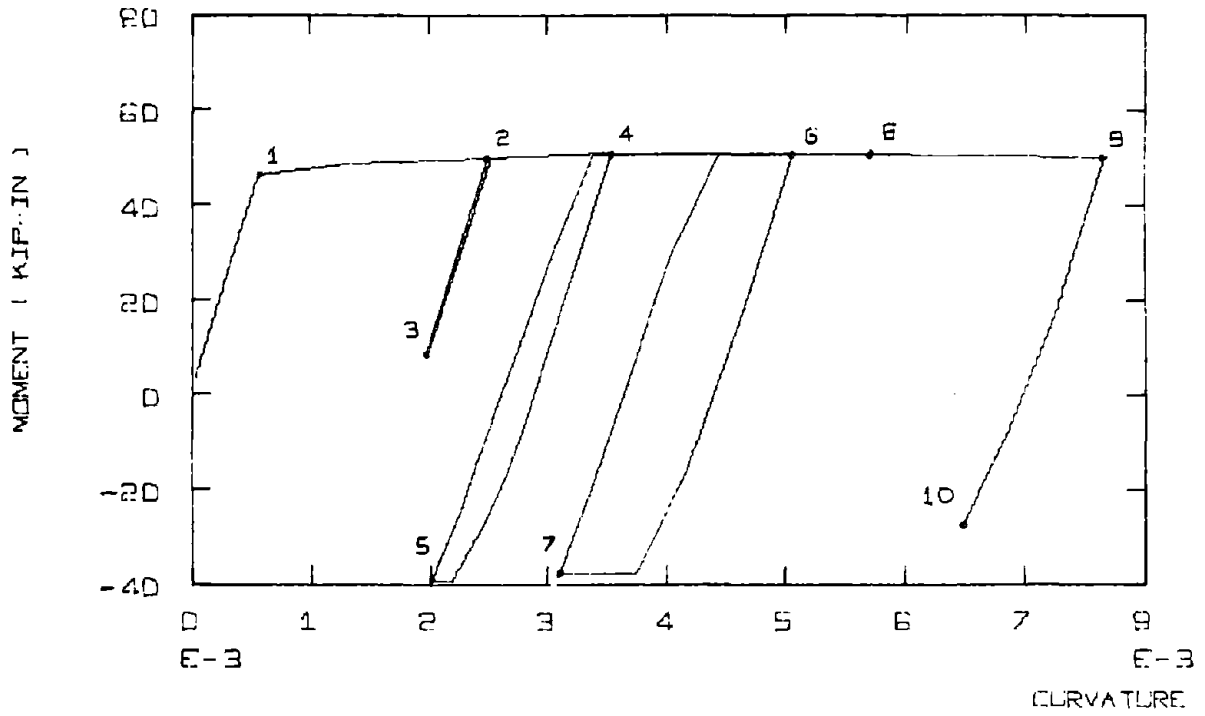
good fit as far as the end points of the unloading curves are concerned, although the variation in stiffness between these points is not correctly reproduced.

b) More important perhaps is to see how these unloading and re-loading formulations affect member behavior. To investigate this effect analytic moment-curvature curves were obtained using each of these formulations. A simple elasto-plastic steel was used for these studies in order to make comparisons easier. In addition, the concrete stresses for the cross-section were compared at selected points of the moment-curvature diagram.

In Figs. 2-8 (A to E), the loading sequence used provides a condition where the curvature is always positive and there is little yielding for the negative moments. This loading sequence and cross-section corresponds to an experiment by Agrawal, Tulin, and Gerstle which will be again used for comparison in Chapter 4.

The LINEAR1 formulation differs from the others in the initial reloading stiffness (i.e., beginning at points 5 and 7). At these points there is immediate concrete participation in this model, indicated by a reloading branch with the same slope as the initial unloading branch. In all other formulations the concrete does not participate until additional reversal of curvature has occurred.

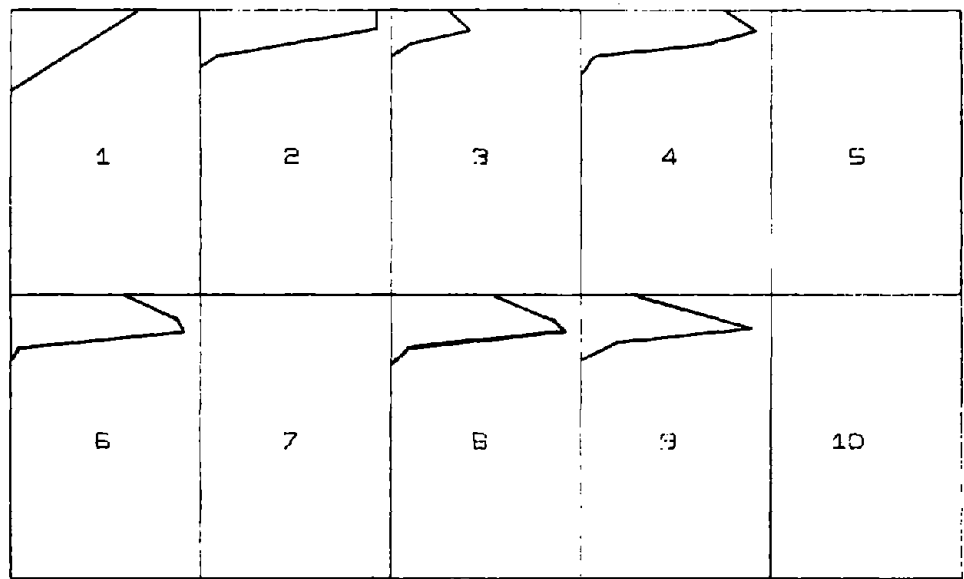
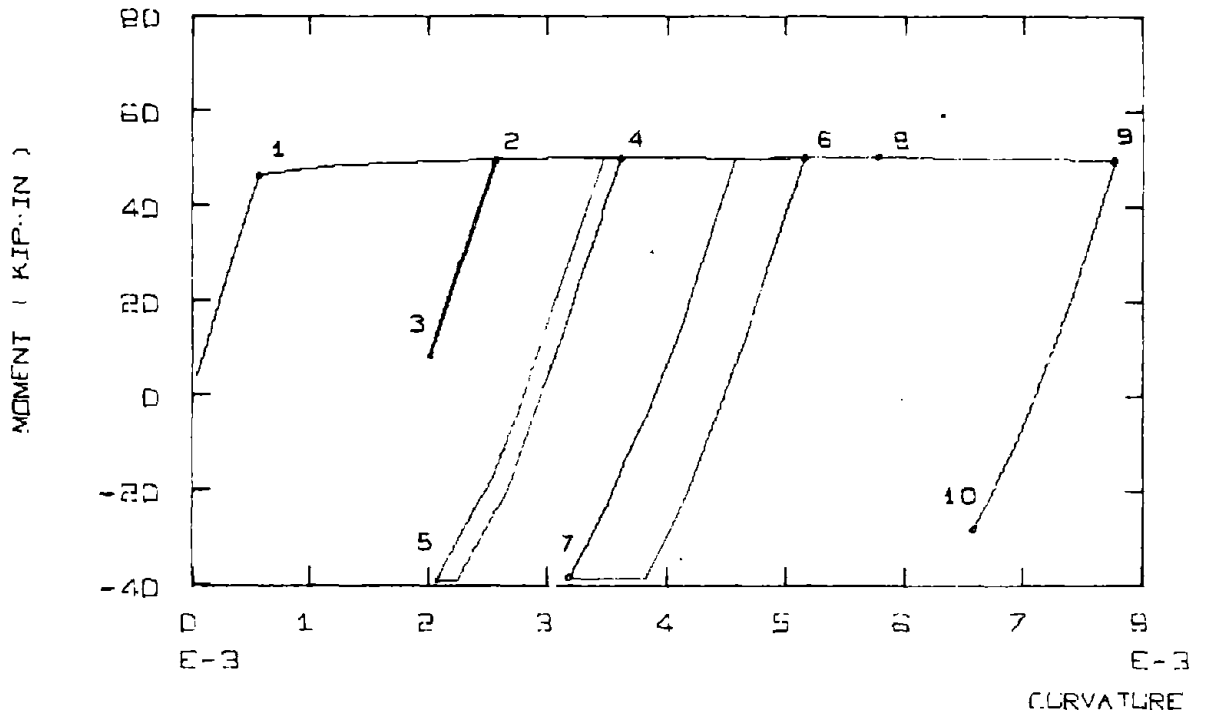
The SGT and KJ models, which both have separate formulations for loading and unloading, produce jumps in the yield moment plateau which are not observed experimentally. This results because both are stiffer in reloading than unloading.



STRESS DISTRIBUTION

A. CONCRETE: LINEAR RELOAD AT REVERSAL POINT

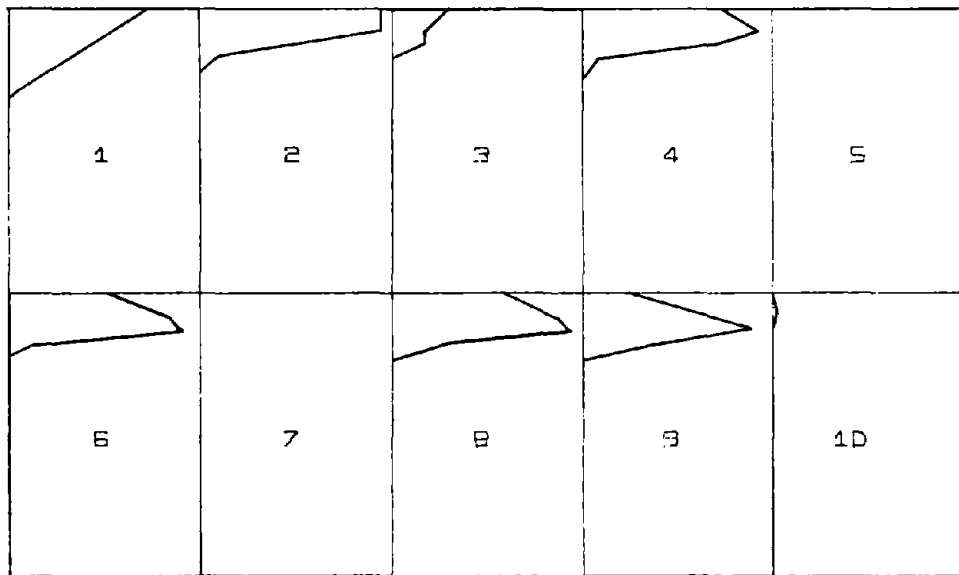
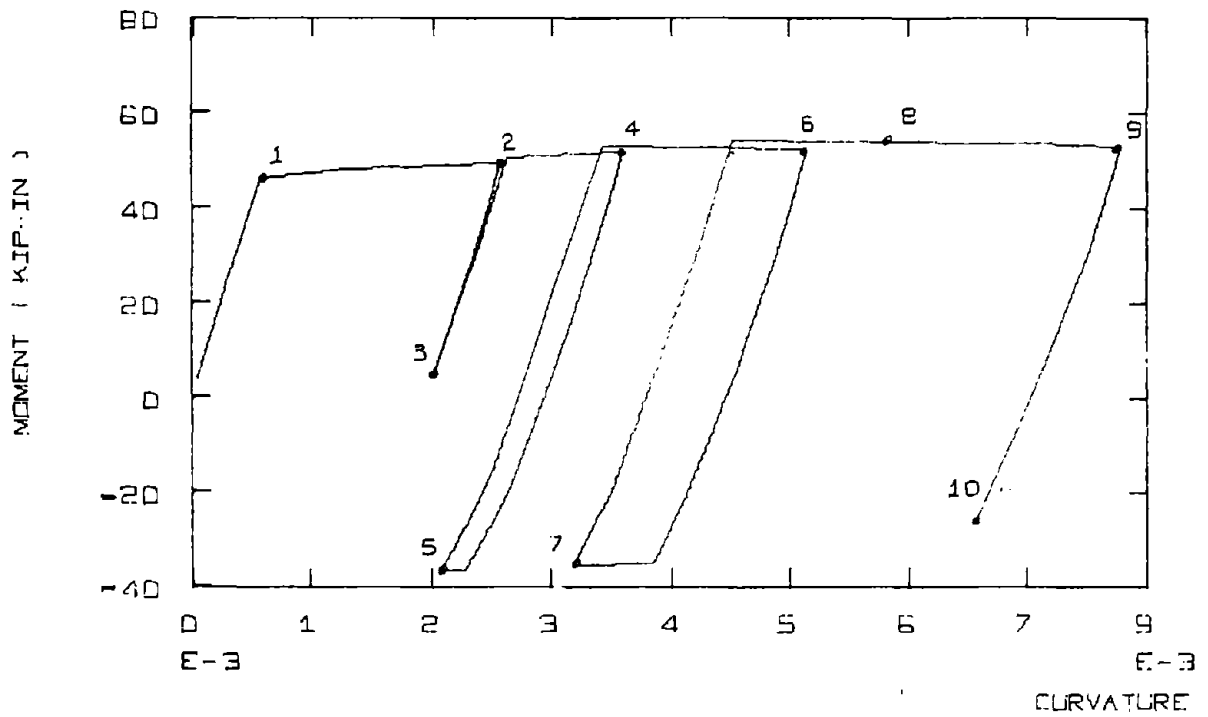
FIG. 2-8 - COMPARISON OF MOMENT-CURVATURE CURVES AND STRESS DISTRIBUTION FOR DIFFERENT CONCRETE FORMULATIONS



STRESS DISTRIBUTION

9. CONCRETE, LINEAR RELOAD AT  $\epsilon_{rev}$

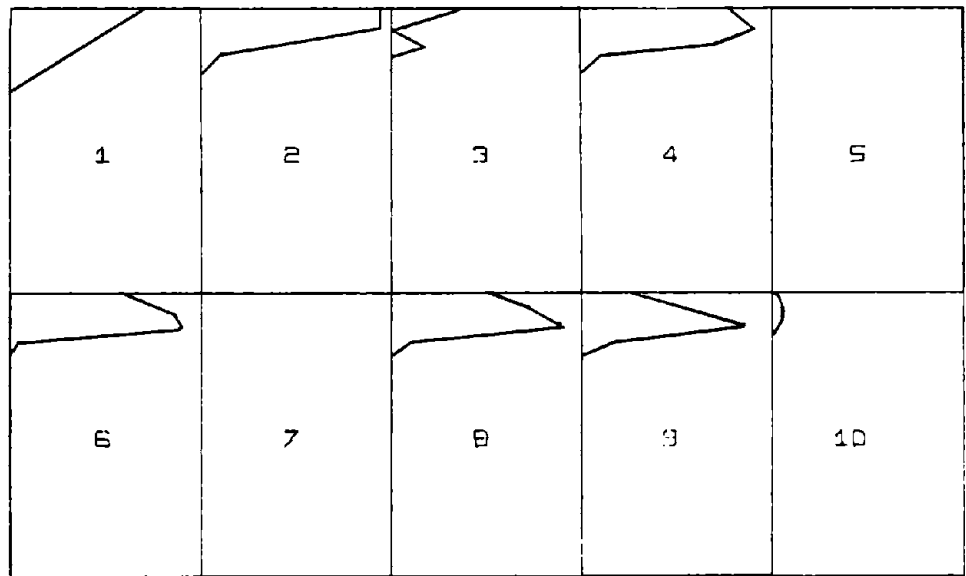
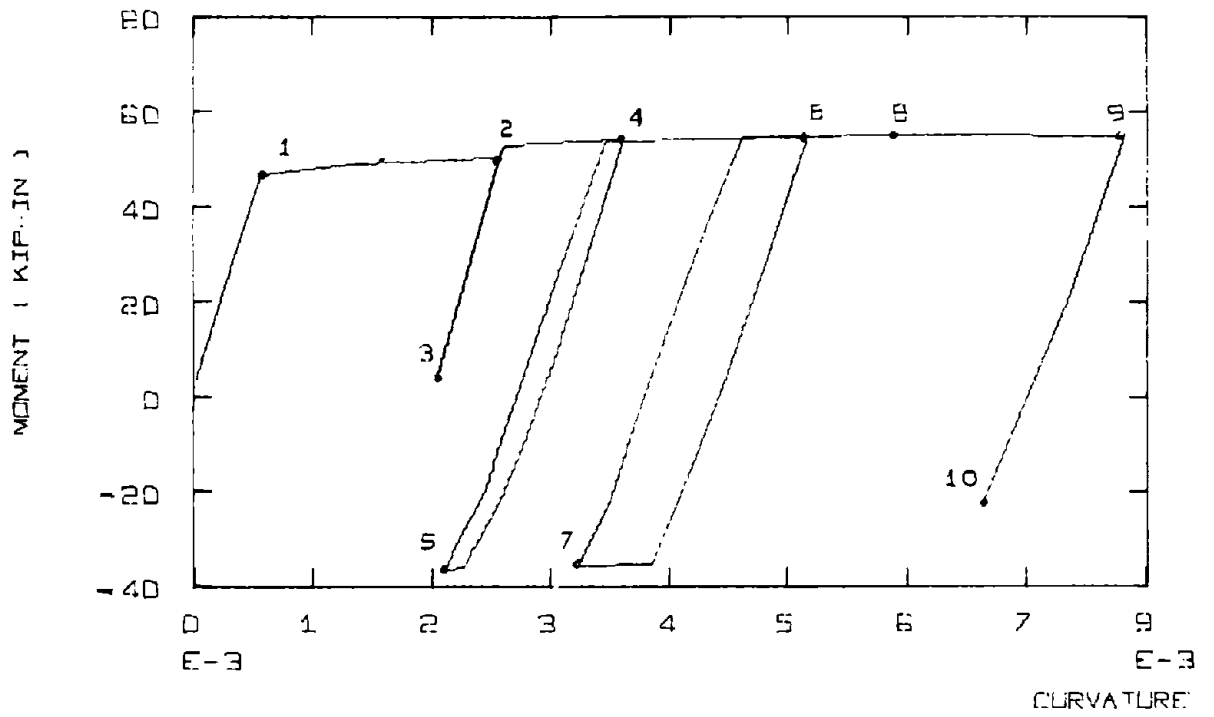
FIG. 2-8 (Continued)



STRESS DISTRIBUTION

C. CONCRETE. SGT FORMULATION

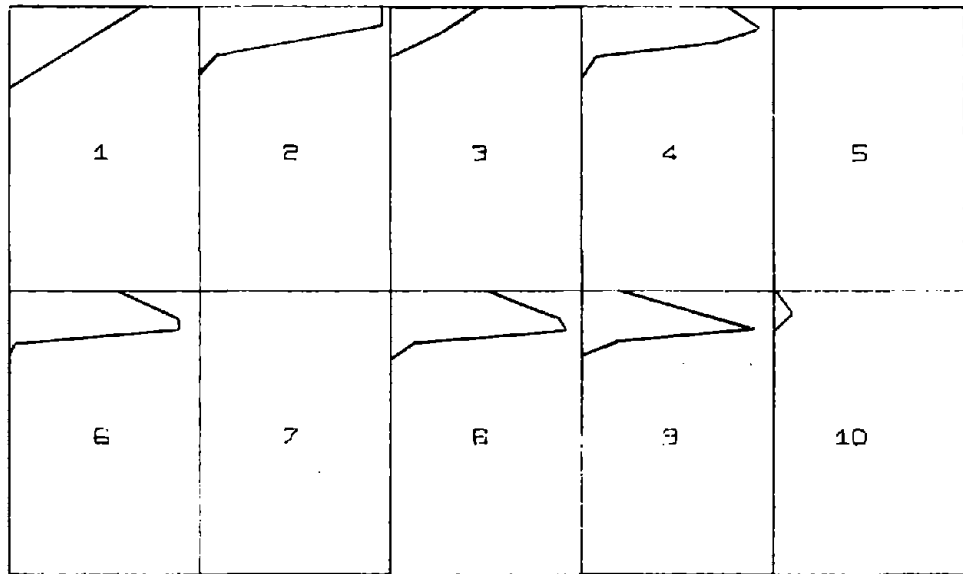
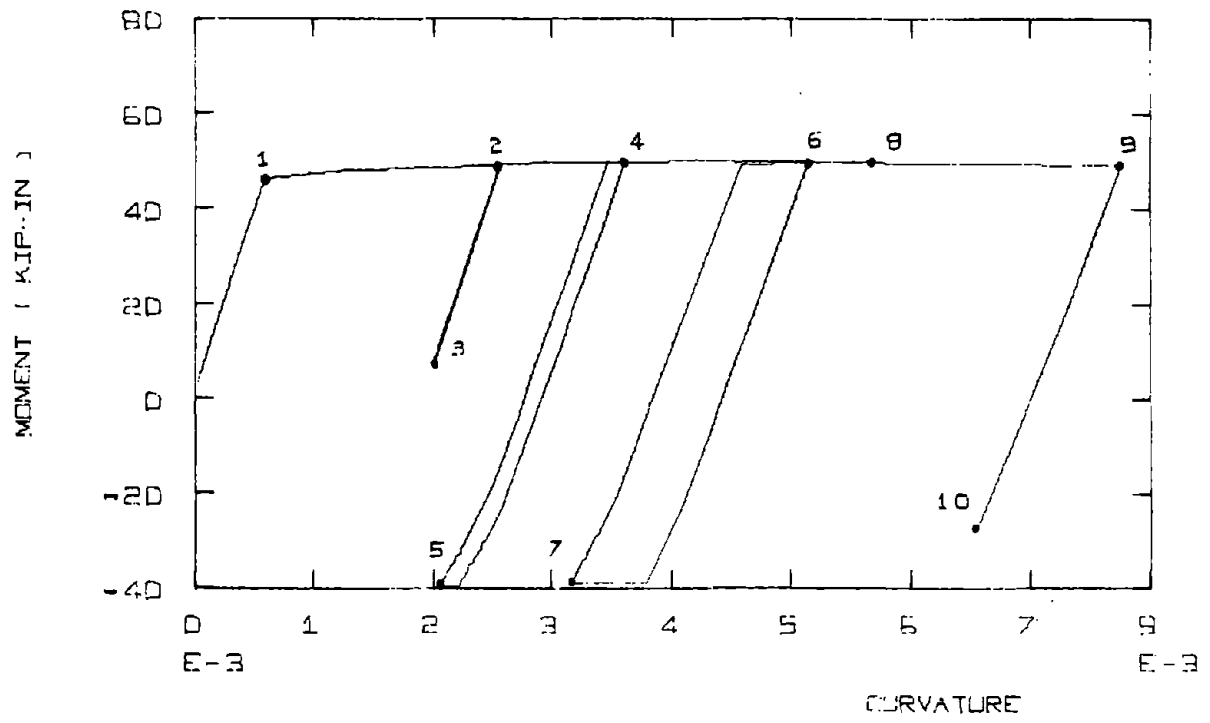
FIG. 2-8 (Continued)



STRESS DISTRIBUTION

D. CONCRETE, KJ FORMULATION

FIG. 2-8 (Continued)



E. CONCRETE, LINEAR WITH VARYING SLOPE

FIG. 2-8 (Continued)

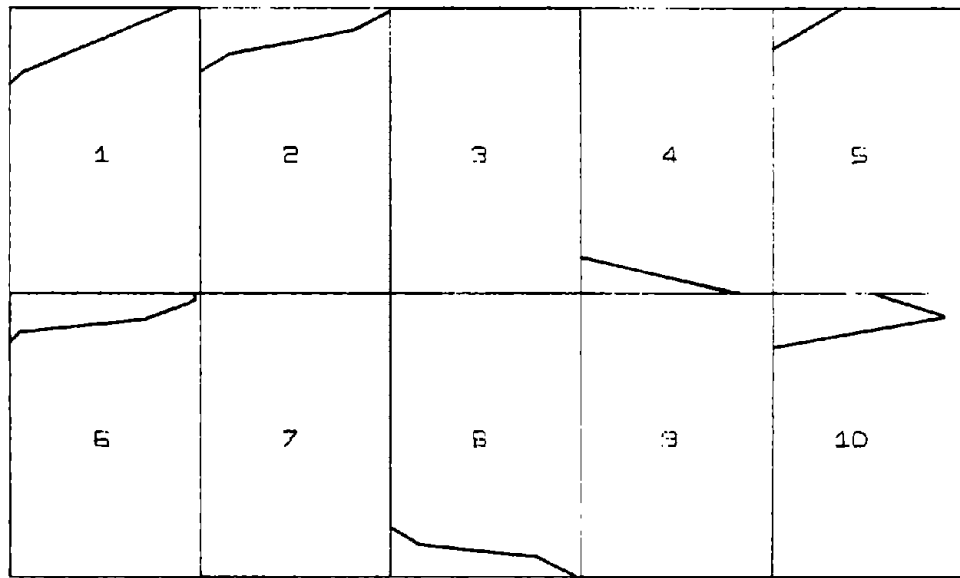
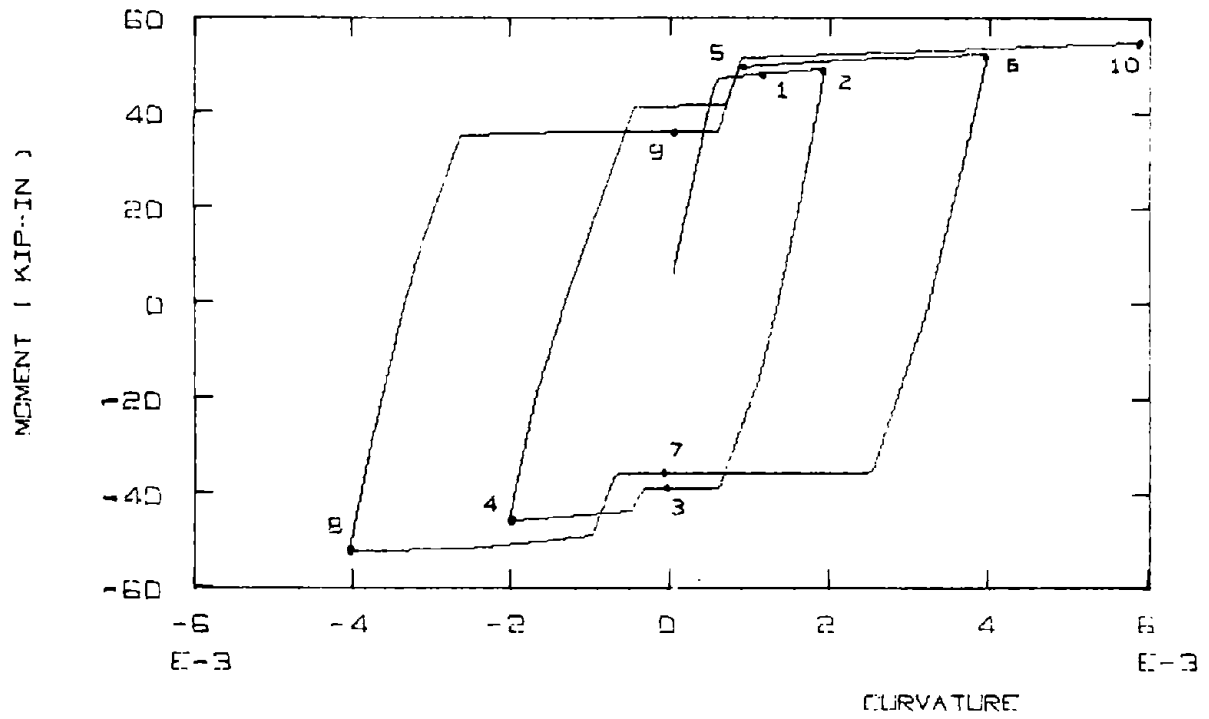
LINEAR2 and LINEAR3 produce moment-curvature relations which are essentially identical.

In all of the formulations there is little change in the maximum moment capacity. Only LINEAR1 shows a significant difference in the tangent stiffness.

In comparing the concrete stress diagrams for the specified points in the cycle, stresses are determined at the midpoints of each fiber and straight lines connect these points. Points 1 and 2 are exactly the same for all formulations since unloading has not begun. At point 3 SGT and KJ formulations produce results that are significantly different from the others. The difference is in the stress of the extreme fibers. There are only slight differences at the remaining points, except for point 10, where SGT, KJ, LINEAR3 show stress and the others do not. The primary differences are then at the ends of the unloading cycles, but they do not seem to affect the ensuing behavior.

c) In Fig. 2-9 (A to E) the moment-curvature relationship used for the concrete comparison is cyclic with curvatures at the ends of the cycles equidistant from the zero point. This cross-section is the same as used in Fig. 2-8, but these cyclic loadings are arbitrarily chosen to demonstrate a different loading condition.

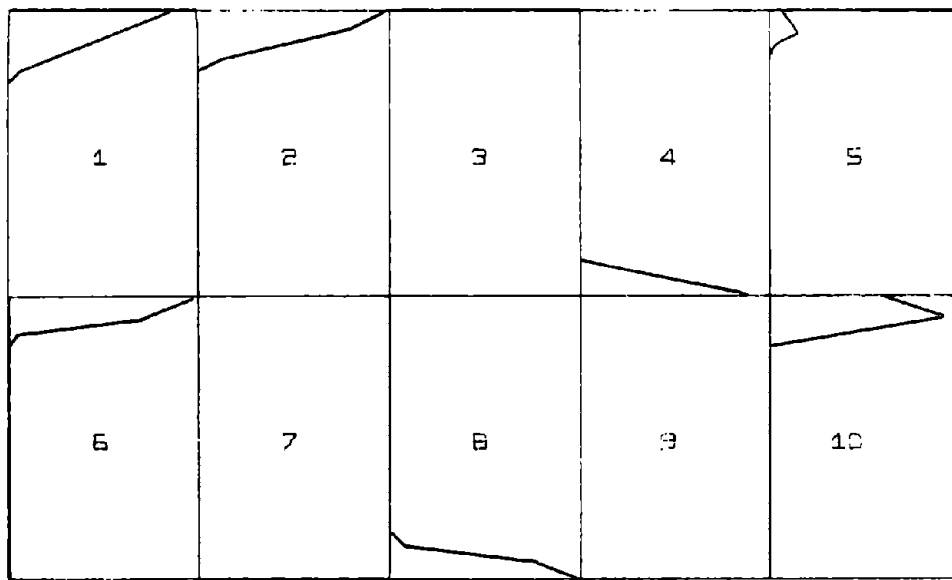
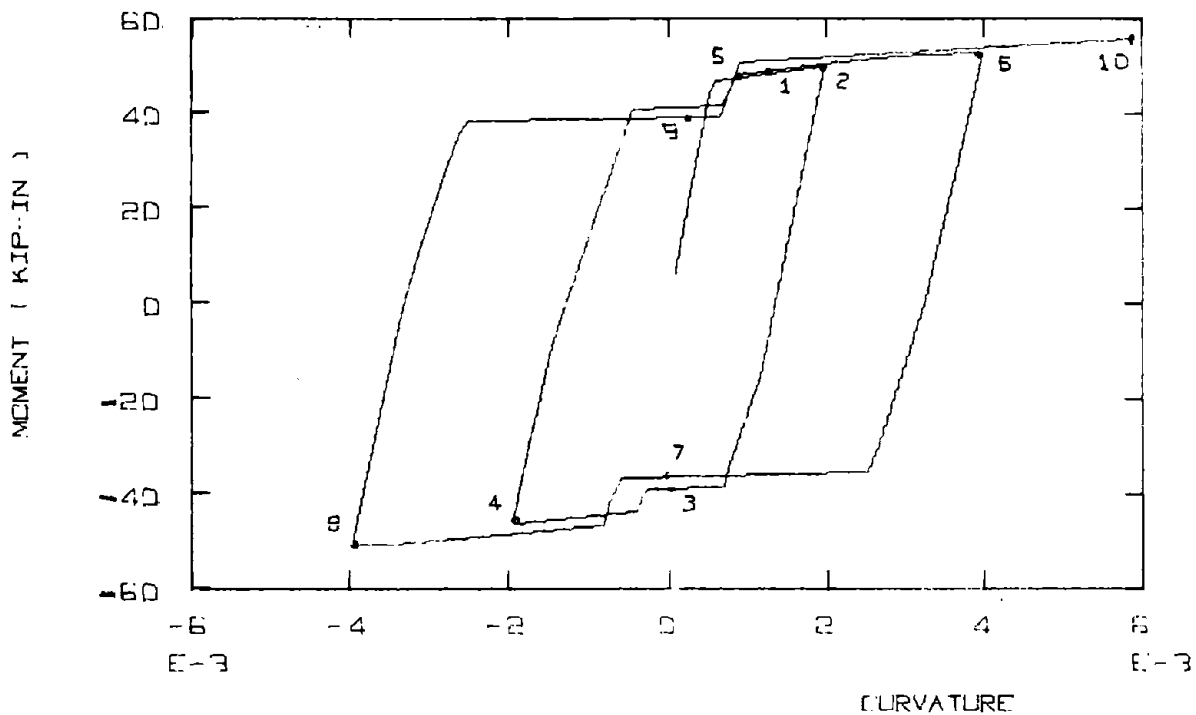
The SGT formulation provides positive and negative maximum moment that is larger than any of the others. The KJ formulation produces the loops which are most stable with respect to increasing



STRESS DISTRIBUTION

A. CONCRETE: LINEAR RELOAD AT REVERSAL POINT

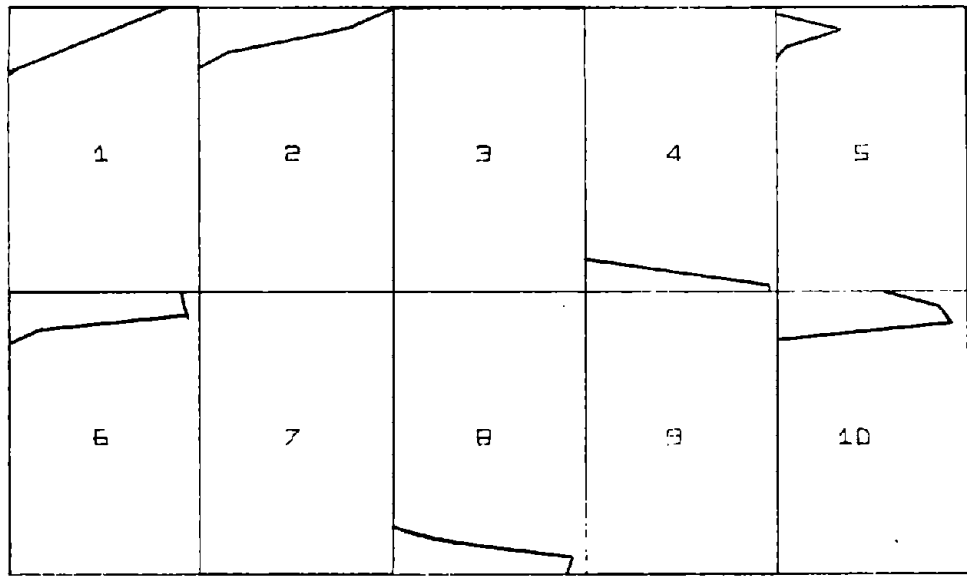
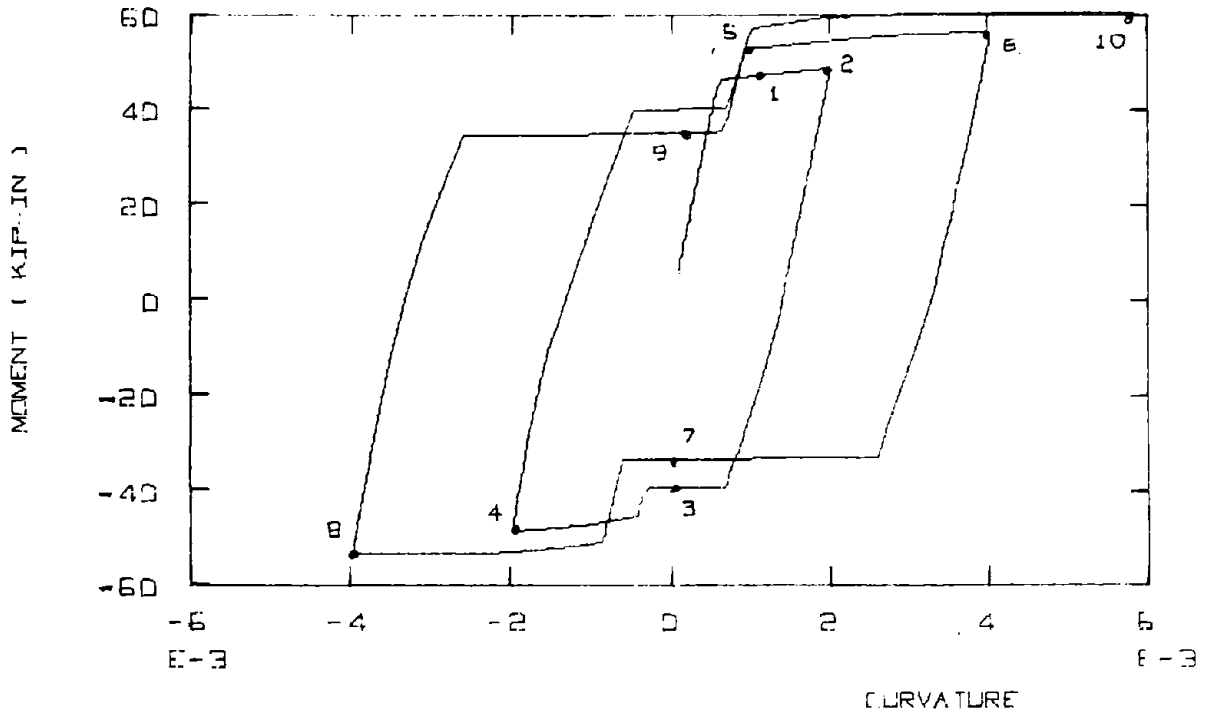
FIG. 2-9 - COMPARISON OF MOMENT-CURVATURE CURVES AND STRESS DISTRIBUTION FOR DIFFERENT CONCRETE FORMULATIONS



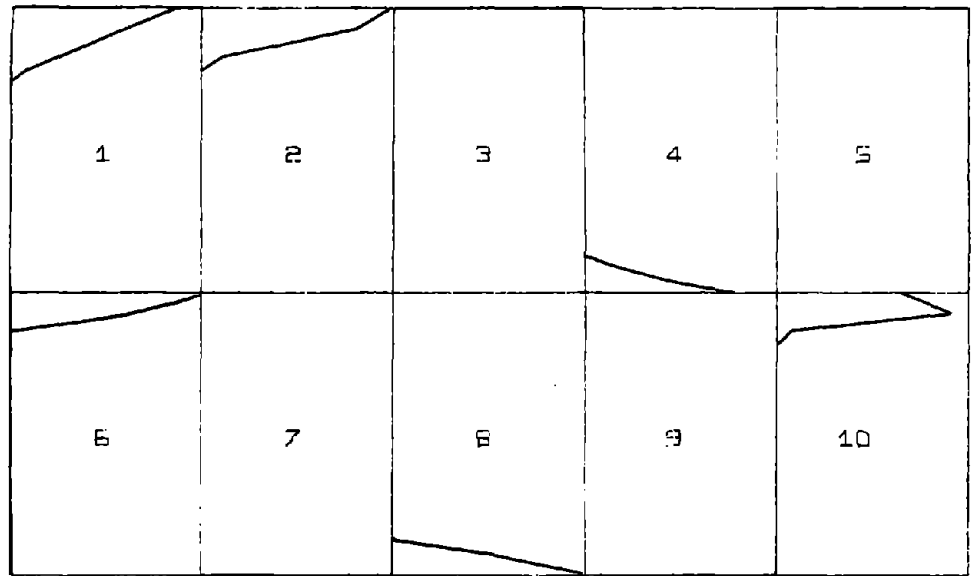
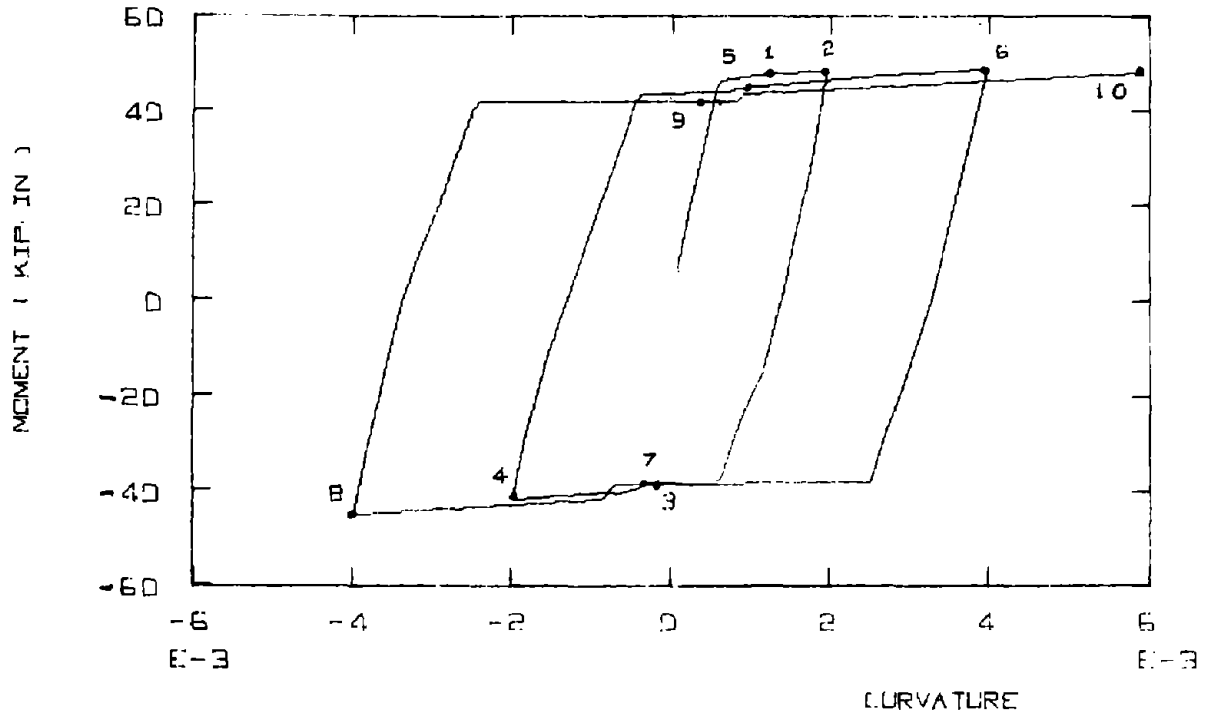
STRESS DISTRIBUTION

9. CONCRETE: LINEAR RELOAD AT  $\epsilon_{rev}$

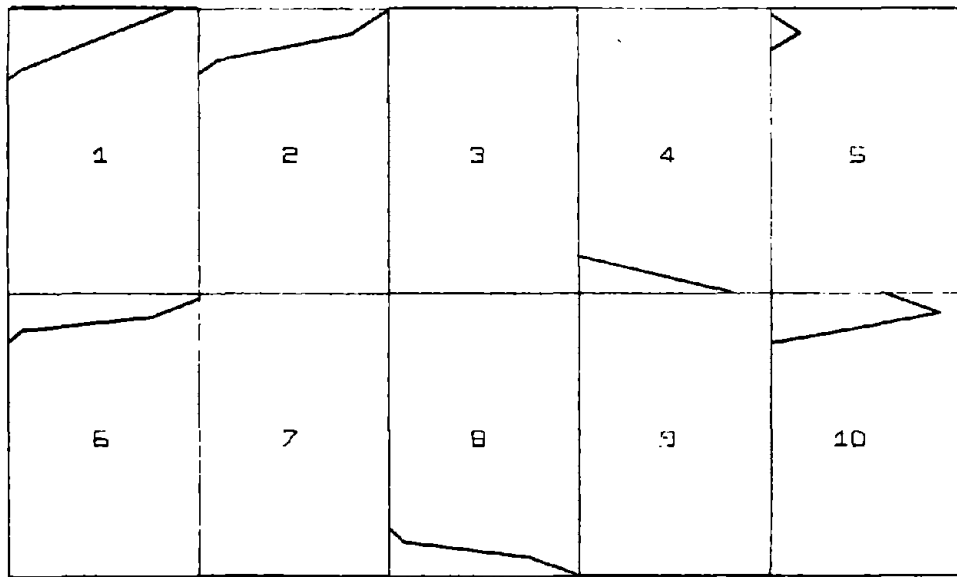
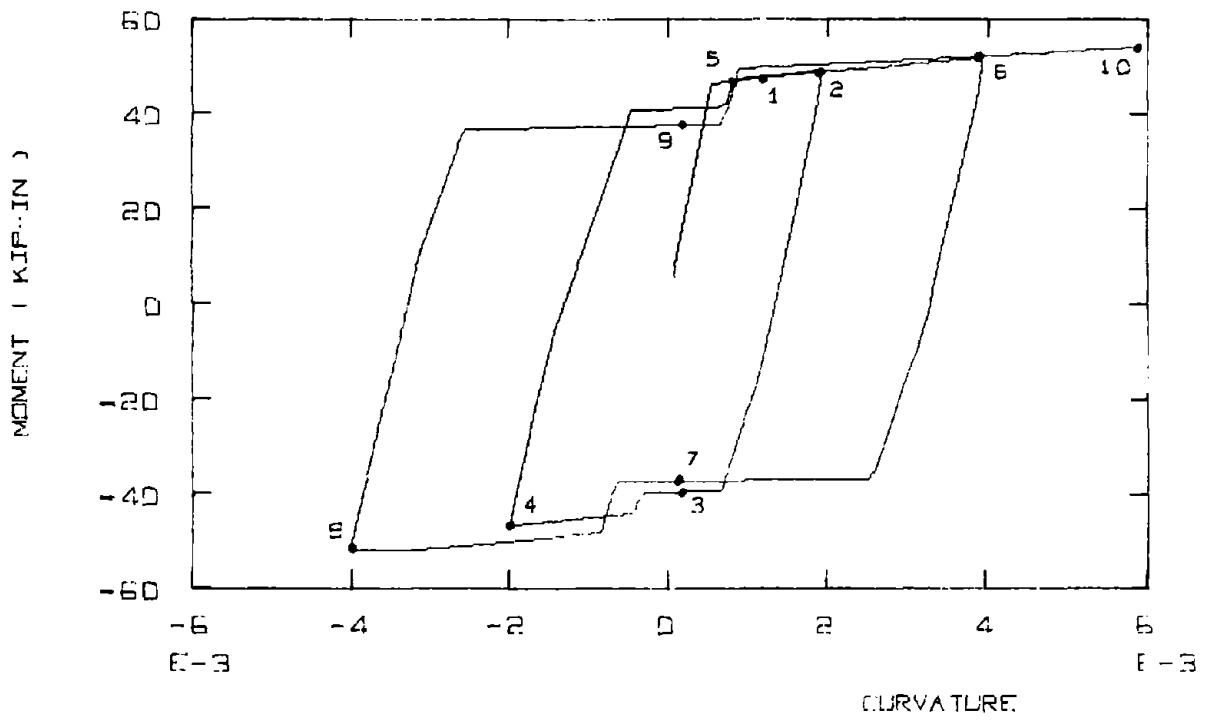
FIG. 2-9 (Continued)



C. CONCRETE. SGT FORMULATION  
 FIG. 2-9 (Continued)



D. CONCRETE; KJ FORMULATION  
 FIG. 2-9 (Continued)



E. CONCRETE: LINEAR WITH VARYING SLOPE

FIG. 2-9 (Continued)

maximum moment with number of cycles. LINEAR2 and LINEAR3 are essentially the same.

In the stress comparison, there is no difference in the first four points. At point 5, which is at the middle of the first reloading cycle, a large variation of stress distribution exists. LINEAR1 and SGT have the most stress contribution, while KJ supplies none. The differences at points 6, 7 and 8 are minor. For this loading, fibers on both the top and bottom of the section participate.

In selecting an analytic formulation as simple a model as possible should be used, since increased complexity means additional parameters which must be kept track of. The KJ formulation is the most complex and requires four additional variables per fiber to describe its behavior. The differences in both the moment curvature and stress distribution is, on the other hand, slight. In normal loading these differences will occur only in the extreme fibers, since most of the section will remain in the "elastic" range of the stress-strain curve.

It is felt that a simple model like LINEAR3 is adequate and reasonably reflects the contribution of the concrete to member behavior.

## 2.6 CONCLUSIONS

From the comparative studies carried out in this chapter, it would seem that the details of the concrete model do not affect signif-

icantly the section behavior. As a result, the concrete model that will be used in subsequent chapters consists of the envelope shown in Fig. 2-6, with  $f_c'$  as the maximum stress. The slope of the descending branch will be determined by Kent's relationship for  $\epsilon_{50}$  and  $p^*$ . Unloading and reloading will proceed linearly, with a slope such that the zero stress point satisfies Karson, Jirsa's relation for unloading  $S_p$ . Reloading must recover the strain up to  $\epsilon_{rev}$  before the concrete fiber can supply compressive strength.

## CHAPTER 3 - BEHAVIOR OF REINFORCING STEEL

3.1 INTRODUCTION

The behavior of reinforcing steel under monotonic loading to failure is well understood. The stress-strain curve is essentially bilinear, with an initial slope of 29,000,000 psi and a slope of nearly zero after reaching the yield point ( $\epsilon_y, f_y$ ). For higher strength steel there may be no distinct yield point, but rather a roundhouse curve. After significant yielding, the steel is able to provide additional strength through strain hardening.

However, under cyclic loading where the steel is subjected to both tension and compression, the stress-strain curve becomes distinctly nonlinear. For the initial loading cycle, it is essentially elasto-plastic. Unloading from a point such as A in Fig. 3.1, it proceeds along a straight line with approximately the same slope as the original loading curve. Once the stress is reversed the stress-strain relation is nonlinear and the tangent modulus continually decreases. This phenomenon has been called the Bauschinger effect. In subsequent cycles the behavior is always nonlinear whenever the stress changes sign and the steel behavior is strongly dependent on the previous strain history.

In this chapter six different analytical formulations for the behavior of the reinforcing steel under cyclic loading will be compared. Experimentally, there have been three significant studies by

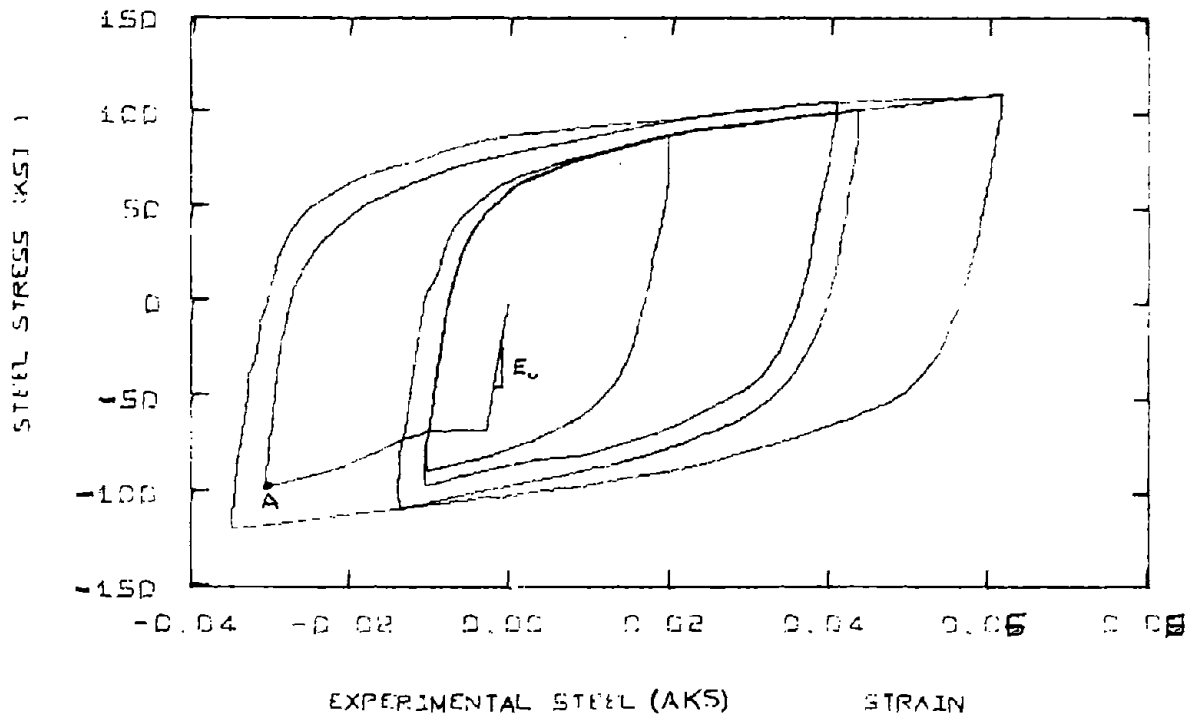


FIG. 3-1 - TYPICAL BEHAVIOR OF REINFORCING STEEL UNDER CYCLIC LOADINGS

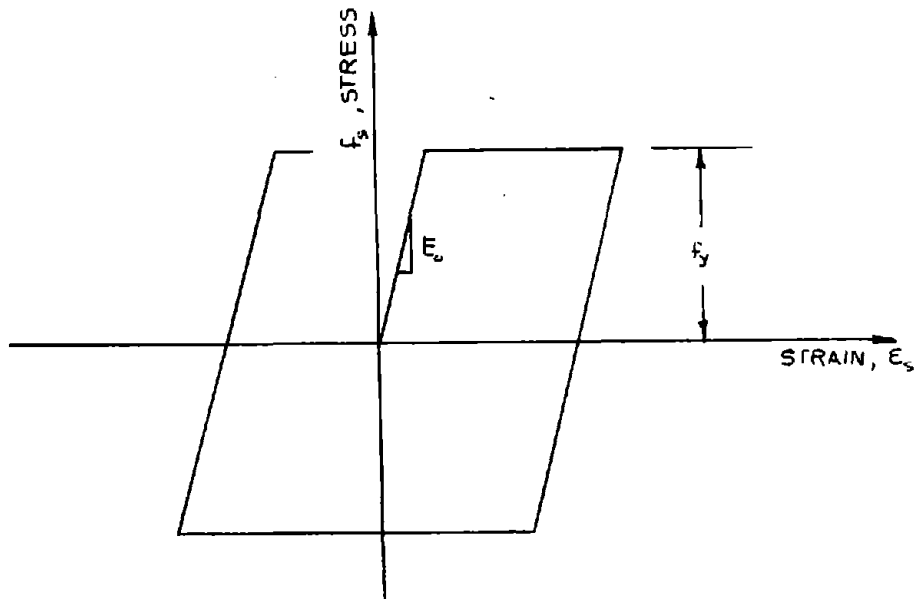


FIG. 3-2 - ELASTO-PLASTIC FORMULATION FOR STEEL

Singh, Gerstle, and Tulin (1965);<sup>(15)</sup> Kent, Park (1971);<sup>(18)</sup> and by Akton, Karlsson, and Sozen (1973).<sup>(20)</sup> Each of these groups proposed an analytic model. In addition, the simple elasto-plastic model, a model by Brown,<sup>(16)</sup> and an improvement on the Singh, Gerstle, and Tulin model will be discussed.

In subsequent discussions the terms reloading and unloading will be used in an experimental context. That is, reloading will signify adding load (tension or compression) to the specimen, and unloading will mean decreasing the load.

### 3.2 ANALYTIC FORMULATIONS FOR REINFORCING STEEL

#### 3.2.1 Elasto-Plastic Formulation

The elasto-plastic formulation shown in Fig. 3-2 is the simplest, but it does not reproduce the observed Bauschinger effect in cyclic loading. Unloading and reloading are assumed to take place along a line having the initial slope, 29,000,000 psi. Further straining will continue along this line until  $|f_s|$  reaches the yield stress,  $f_y$ . The stress-strain relationship then follows a line with zero slope, and the steel becomes "plastic" since additional straining is possible without a corresponding increase in stress.

#### 3.2.2 Singh, Gerstle, Tulin (SGT) Formulation

These researchers carried out tests on hard-grade reinforcing steel specimens machined from the same batch. The steel had an aver-

age yield strength of 52 ksi. Each specimen was cycled between prescribed strain limits, and these limits were varied to study the effect of initial plastic strain (defined as the strain where the initial stress reversal took place). As the initial plastic strain increases, the stiffness in the first load reversal (e.g., segment  $\overline{BC}$  in Fig. 3-3 decreases at a greater rate. The curve becomes flatter, as shown in Fig. 3-4.

The following expression for the nonlinear portions, such as  $\overline{BC}$  and  $\overline{EF}$ , was proposed:

$$|f_s| = 64.5 - 52.7 (.838)^{1000 \epsilon_s} \quad (\text{ksi}) \quad (2.1)$$

where  $\epsilon$  is the strain measured from the point where the unloading curve crosses the strain axis (e.g. from point A). Singh, Gerstle, and Tulin (SGT) felt that one expression was sufficient to represent the whole family of such curves. This curve corresponds to an initial plastic strain of .004.

Unloading proceeds linearly, with slope  $E_0$ , until intersecting the nonlinear curve given by the preceding expression. For a yield stress of 52 ksi, there is a jump in the tangent modulus from 29,000 to 8,750 (ksi). In the incremental stiffness method, where the tangent modulus and not the actual stress is important, a more gradual transition is desirable.

To apply this formulation to steels with different yield strengths, the expression for the nonlinear curve was scaled with

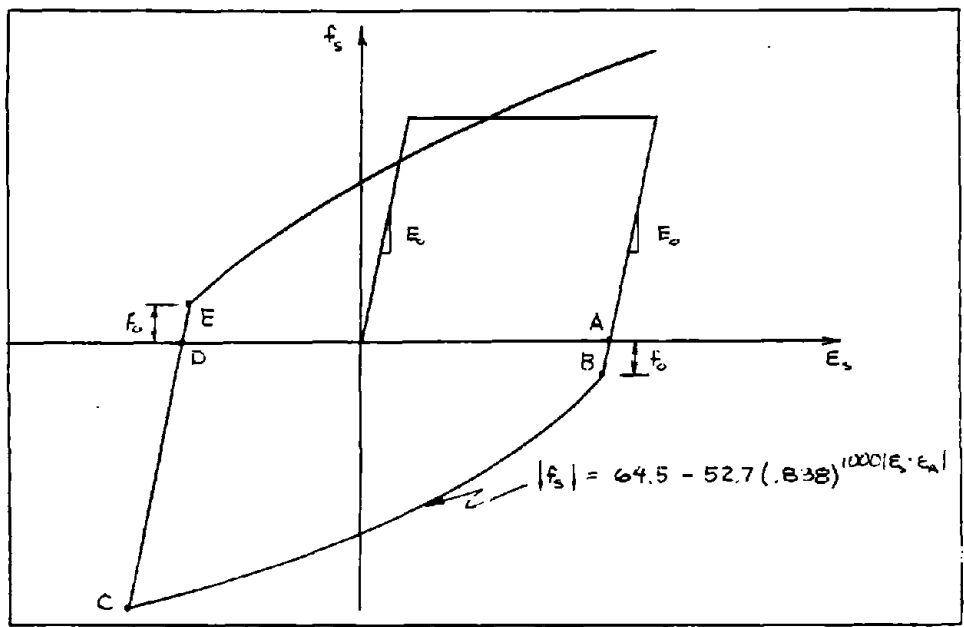


FIG. 3-3 - SINGH, GERSTLE, TULIN FORMULATION FOR STEEL

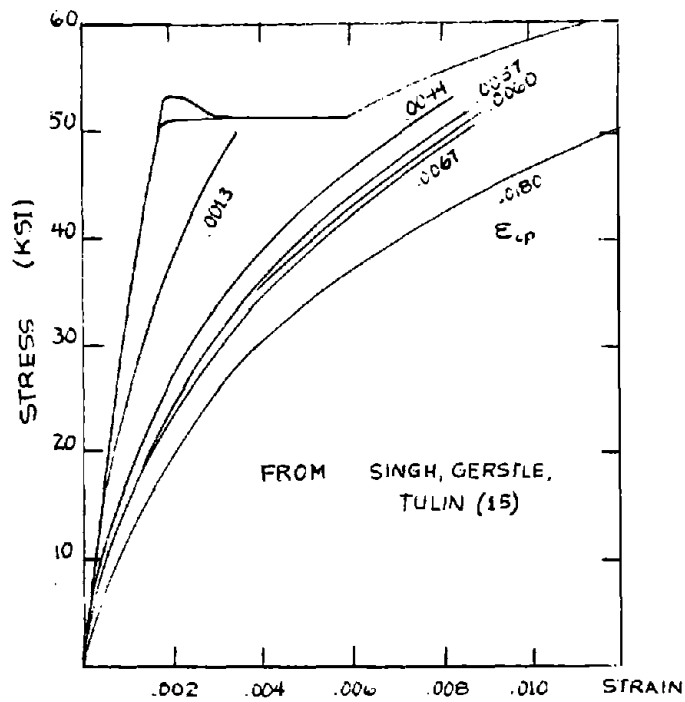


FIG. 3-4 - EXPERIMENTAL STRESS-STRAIN CURVES FOR STEEL

respect to  $f_y$  and new junction points were determined.

### 3.2.3 Improved SGT Formulation

This formulation extends the SGT expression to include the change in the nonlinear relation with the variation of initial plastic strain. The definition of initial plastic strain is interpreted to be the strain between successive zero stress points (e.g., between A and D for curve  $\overline{EF}$  in Fig. 3-3).

The nonlinear relationship can be expressed in the form

$$|f_s| = A + B \log_e (1000 \epsilon_s) \quad (\text{ksi}) \quad (2.2a)$$

This expression is obtained by plotting the SGT reloading data (Fig. 3-4) on semi-log paper. From the resulting straight lines, parameters A and B are evaluated. Both A and B vary with the initial plastic strain, and the following expressions were found by curve fitting:

$$A = 12.4 - .450 (1000 \epsilon_{ip} - 4.0) \quad (2.2b)$$

$$B = (25.5 - .177 (1000 \epsilon_{ip} - 4.0)) / (.602 \times 2.3)$$

where  $\epsilon_{ip}$  is the initial plastic strain.

This relationship is valid for  $(1000 \epsilon) > 1$ . Unloading is initially linear with slope  $E_0$ , and a transition curve with a linearly varying tangent modulus is necessary to connect the nonlinear portion to the zero stress point. For a strain of .001 from the zero stress

point the tangent modulus changes from 29,000 (ksi) to B. For the non-linear segment the tangent modulus is simply

$$TM = B/(1000 \epsilon_s) \quad (2.2c)$$

A scale factor proportional to the yield strength was used for steels with different  $f_y$ .

### 3.2.4 Brown's Formulation (16,17)

The steel stress-strain relationship proposed by Brown is shown in Fig. 3-5 and is also based on SGT data.

Although most tests have shown that unloading proceeds linearly with slope  $E_0$ , Brown introduces stiffness degradation into his formulation by varying this slope. In an apparently arbitrary manner, the slope is adjusted so that  $\epsilon_{ip}$ , the initial plastic strain, is equal to 80% of the peak strain in that half cycle. Comparison with the experimental data of Kent and Aktan show this is not a valid assumption for the behavior of steel, and in subsequent comparisons this assumption will not be implemented.

Brown includes the change in curvature with additional straining by having one of his parameters be a function of  $\epsilon_{ip}$ . The expression for the nonlinear reloading portion is

$$|f_s| = f_y \left[ 1 - \exp \left( \frac{-2.06\epsilon_s}{\epsilon_{sh}} + \frac{.129}{\epsilon_{sh}} \right) \right] \quad (2.3)$$

$$\text{and} \quad \epsilon'_{sh} = \frac{\epsilon_{sh}}{1.38} \log_e \frac{\epsilon_{ip}}{\epsilon_y}$$

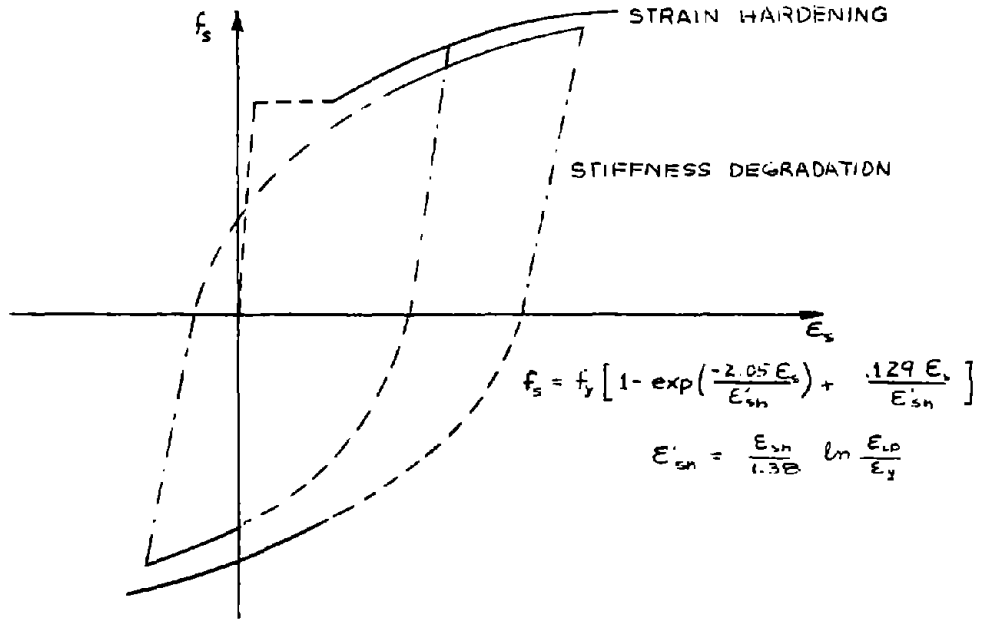


FIG. 3-5 - BROWN'S FORMULATION FOR STEEL

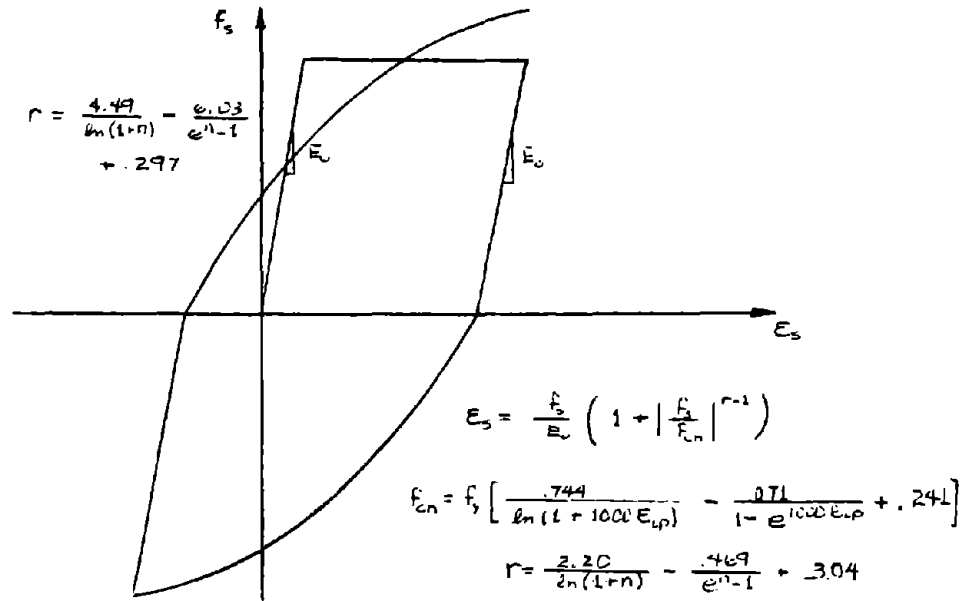


FIG. 3-6 - KENT'S FORMULATION FOR STEEL

where  $\epsilon_{sh}$  is the strain at which strain hardening begins.  $\epsilon_{sh}$  is thus another parameter that must be specified and the nonlinear relation was found to be very sensitive to its specification.

Whenever the absolute value of the stress exceeds  $f_y$ , Brown reverts back to a strain hardening relation proposed by Burns. (14)

Brown's formulation has the advantage of having a smoothly varying tangent modulus, unlike the previous ones.

### 3.2.5 Kent's Formulation (18,19)

Kent tested 11 specimens with an average yield stress of 45 ksi and based his analytic model on these tests. The specimens were of different bar sizes and from different batches of steel. The loadings were varied to create earthquake-type behavior and several of his results will be used to compare the analytic formulations.

The primary difference in this formulation is in the nonlinear reloading curve where Kent uses a Ramberg-Osgood\* type model. The important parameters are  $E_0$ , a characteristic stress,  $f_{ch}$ , and an exponent  $r$ .

$$\epsilon_s = \frac{f_s}{E_s} \left[ 1 + \frac{f_s}{f_{ch}}^{r-1} \right] \quad (2.4)$$

where  $f_{ch} = f_y \left[ \frac{.744}{\log_e(1 + 1000 \epsilon_{ip})} - \frac{.071}{1 - e^{-1000 \epsilon_{ip}}} + .241 \right]$

---

\* W. Ramberg and W. R. Osgood (13) formulated an expression to describe a nonlinear stress-strain curve in terms of three parameters.

and

$$r = \frac{4.49}{\log_e(1+n)} - \frac{6.03}{e^{n-1}} + .297 \quad \text{for odd numbered runs (from tension)}$$

$$r = \frac{2.20}{\log_e(1+n)} - \frac{.462}{e^{n-1}} + 3.04 \quad \text{for even numbered runs (from compression)}$$

The nonlinear stress-strain equation must be solved by an iterative procedure such as Newton's method. The effect of plastic deformation on the curvature is taken care of by the  $\epsilon_{ip}$  term in the expression for  $f_{ch}$ .  $f_{ch}$  decreases with increasing  $\epsilon_{ip}$  and thus the curve becomes flatter.

Kent's data showed that  $r$  was different for compression and tension, and that  $r$  decreased with an increasing number of cycles. A decrease in  $r$  means an increase in stiffness. This coincides with Singh, Gerstle, Tulin's observation that the stiffness increases with the number of cycles. However, this applies when cycling is carried out between the same fixed limits, and this may not be the general behavior for loadings where the limits are varied.

Kent also uses a slope  $E_0$  for unloading and reverts back to a modified Burns' equation for strain hardening.

### 3.2.6 Aktan, Karlsson, Sozen (AKS) Formulation (20)

A series of 9 coupon tests on reinforcing steel with an average yield stress of 69 ksi was carried out with large strain reversals. This was by far the most extensive and thorough study of rein-

forcing steel under "earthquake type loading. Whereas previous investigators had used strain ranges of approximately -.01 to .03, these authors used a range of -.05 to .08.

Aktan, Karlsson, Sozen propose an analytic model using a Ramberg Osgood function for the complete cycle, rather than only for the nonlinear portion as Kent did. Again a cyclic procedure like Newton's method must be used to obtain specific values. Fig. 3-7 shows the AKS formulation:

$$\frac{\epsilon_s - \epsilon_{s1}}{\epsilon_0} = \frac{f_s - f_{s1}}{f_0} + \left( \frac{f_s - f_{s1}}{f_0} \right)^r \quad (2.5a)$$

where  $(\epsilon_{s1}, f_{s1})$  is an end point of the cycle and  $\epsilon_0, f_0$  are characteristic parameters given by:

$$\frac{f_0}{\epsilon_0} = 29,000 \quad (\text{ksi}) \quad (2.5b)$$

$$f_0 = 47.628 + .51723 (f_{\max} - f_{\min})$$

for cycles starting from compression

$$f_0 = 46.410 + .47989 (f_{\max} - f_{\min})$$

for cycles starting from tension

$(f_{\max} - f_{\min})$  is the difference between the maximum tensile stress and the maximum compressive stress reached prior to the half cycle under consideration.

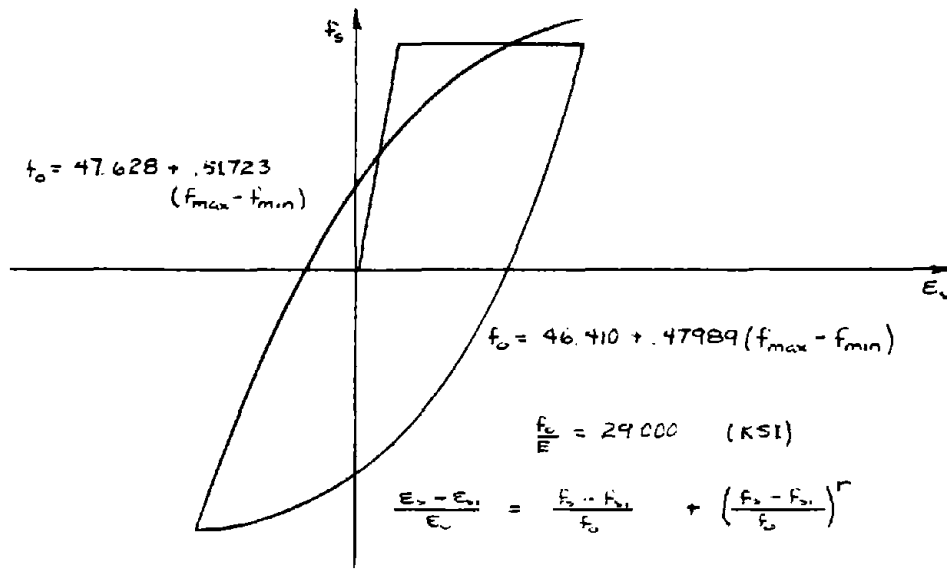


FIG. 3-7 - AKTAN, KARLSSON, SOZEN FORMULATION FOR STEEL

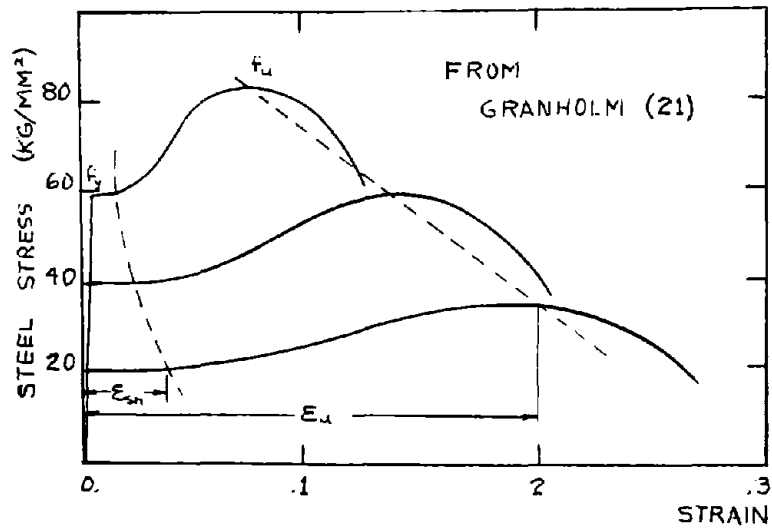


FIG. 3-8 - GENERAL STRAIN-HARDENING CURVES FOR MILD STEEL

In applying this formulation, an initial elasto-plastic branch is assumed. If the loading in this portion continues until  $\epsilon_s > 4.2447 \epsilon_y$ , then a strain hardening curve is used. In subsequent cycles the nonlinear relation is used with the exception that in the first unloading,  $(f_{\max} - f_{\min}) = 2f_{\max}$ .

AKS obtained these relationships by curve fitting techniques. The exponent,  $r$ , is determined by assuming  $|f_s|$  will be 110 ksi at a strain  $\epsilon_{s1} \pm .09$ . As pointed out by the authors, the parameters specified in this formulation were developed specifically for the reinforcing steel studied (i.e.,  $f_y = 59$  and  $f_u = 110$  ksi), and there was no attempt to generalize them for other steels other than factoring out  $f_y$ .

### 3.2.7 Strain Hardening

To consider the additional strength produced by strain hardening, several authors, e.g. Kent and Brown, use the following formula from Burns:<sup>(14)</sup>

$$f_s = f_y \left[ \frac{112(\epsilon_s - \epsilon_{sh}) + 2}{60(\epsilon_s - \epsilon_{sh}) + 2} + \frac{(\epsilon_s - \epsilon_{sh})}{(\epsilon_u - \epsilon_{sh})} \left( \frac{f_u}{f_y} - 1.7 \right) \right] \quad (2.6)$$

where  $\epsilon_{sh}$  = strain at which strain hardening begins

$f_u$  = ultimate strength

$\epsilon_u$  = strain at which  $f_u$  occurs.

These are three additional parameters over the normal  $f_y$  and  $E_o$ . They may be obtained from a standard tensile test on a reinforc-

ing steel specimen. However, these tests are not always carried out for the steel in a reinforced concrete member, and it is desirable to have some guidelines to estimate them.

The change of the steel stress-strain curve with increasing yield strength can be seen in Fig. 3-8, which indicates representative curves for mild steel. The yield plateau,  $\epsilon_{sh} - \epsilon_y$ , decreases while the ratio  $f_u/f_y$  also decreases, with increasing  $f_y$ . Grandholm,<sup>(21)</sup> from whose book this figure is taken, states that the range on  $f_u/f_y$  is normally 1.5 to 1.8, but may be as extreme as 1.3 to 2.0.

Several crude approximations were obtained from this figure, and no generality is presumed.

$$\frac{\epsilon_{sh}}{\epsilon_y} = \frac{7070}{f_y^{1.77}}$$

$$\frac{f_u}{f_y} = 2.26 e^{-.00408 f_y} \quad (2.7)$$

$$\frac{\epsilon_u}{\epsilon_y} = 2.94 e^{-.0363 f_y}$$

where  $f_y$  is the yield strength in ksi.

These ratios will be used whenever more accurate information is unavailable.

### 3.3 COMPARISONS OF THE ANALYTIC FORMULATIONS FOR STEEL

Computer programs were written for each of the six steel formulations. The cyclic loading data used for comparison were taken from the work of Kent and AKS. Although only four such comparisons were made, they represent four different "earthquake-type" loading conditions.

#### 3.3.1 Kent Steel #8 Data, Fig. 3-9

In this test, the specimen was loaded into tension, then into compression with larger strains in the second cycle. Strains range from  $-.0028$  to  $.0211$ . Even though there is considerable straining, no strain hardening is apparent.

At the end points of the cycles, the Elasto-Plastic steel fits well, but it does not represent adequately the nonlinear behavior in between these points.

The SGT model has only one shape for the nonlinear reloading curve. For segments  $\overline{BC}$  and  $\overline{DE}$ , the model is too soft, but in  $\overline{FG}$  the fit is good.

For the Improved SGT, the same general comments apply. In  $\overline{DE}$ , this model is initially better than SGT, but it becomes too stiff with increasing strain. Here the analytic model should have been more plastic. The "kink" at point F is due to the crude transition between the linear unloading curve and the nonlinear reloading curve.

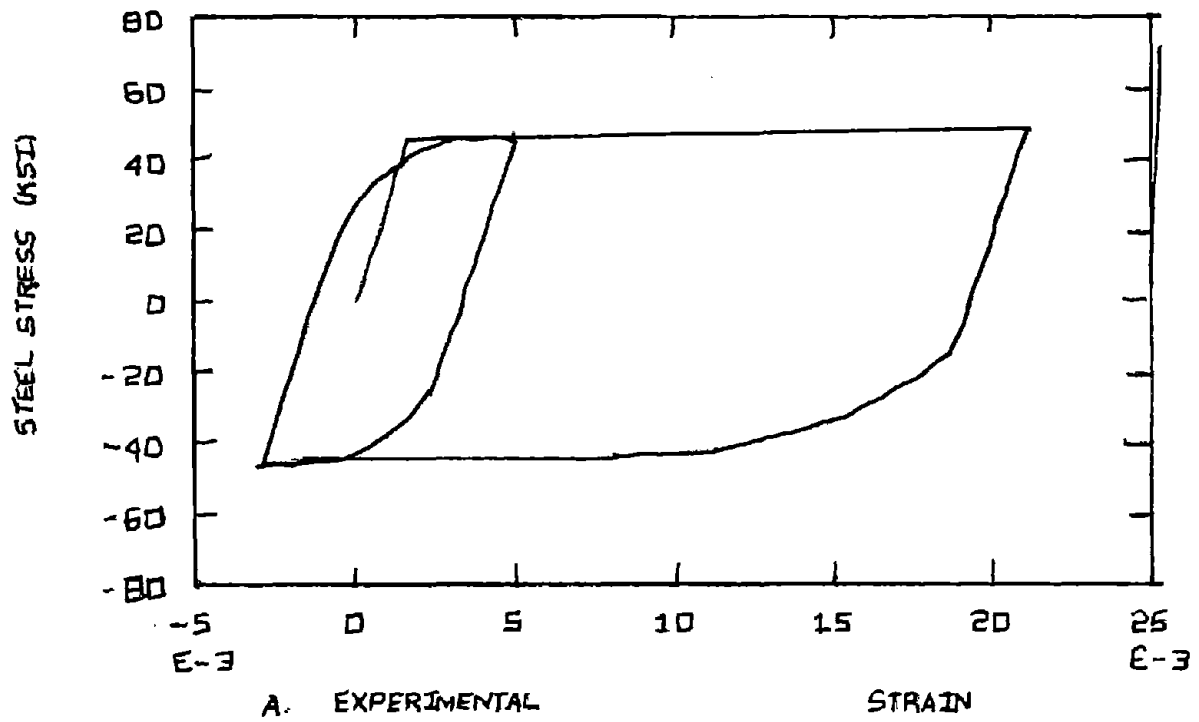


FIG. 3-9 - STEEL FORMULATIONS (KENT #8 DATA)

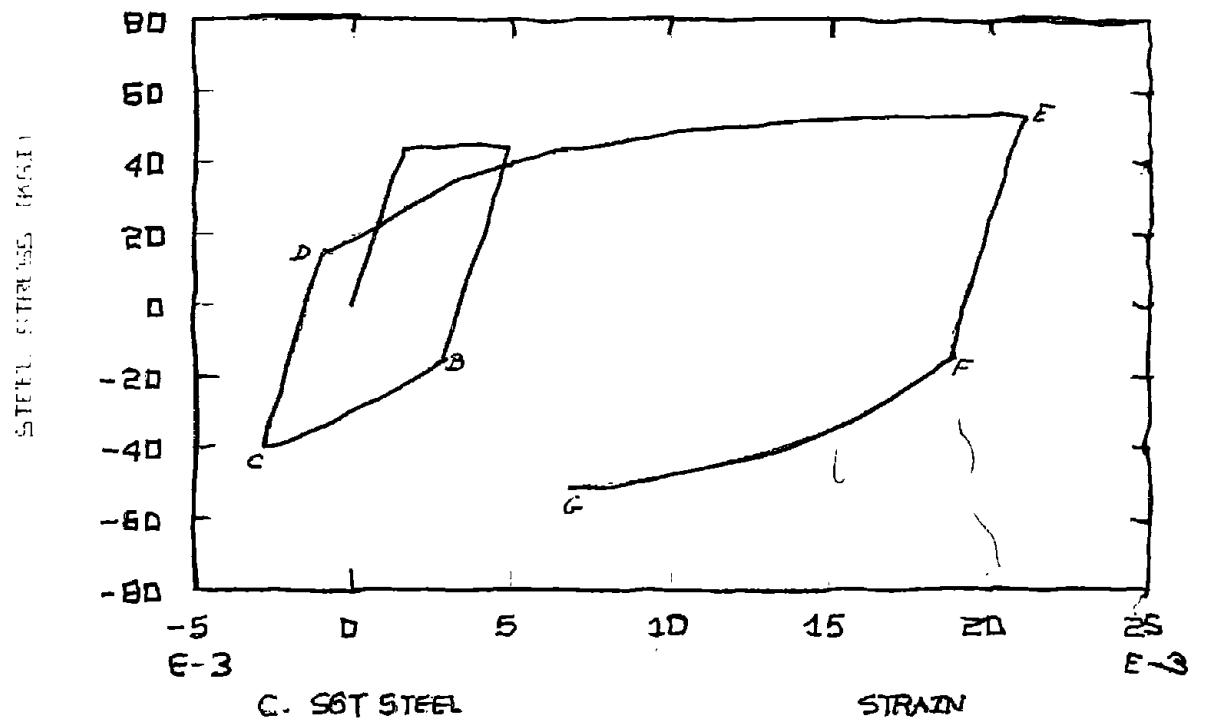
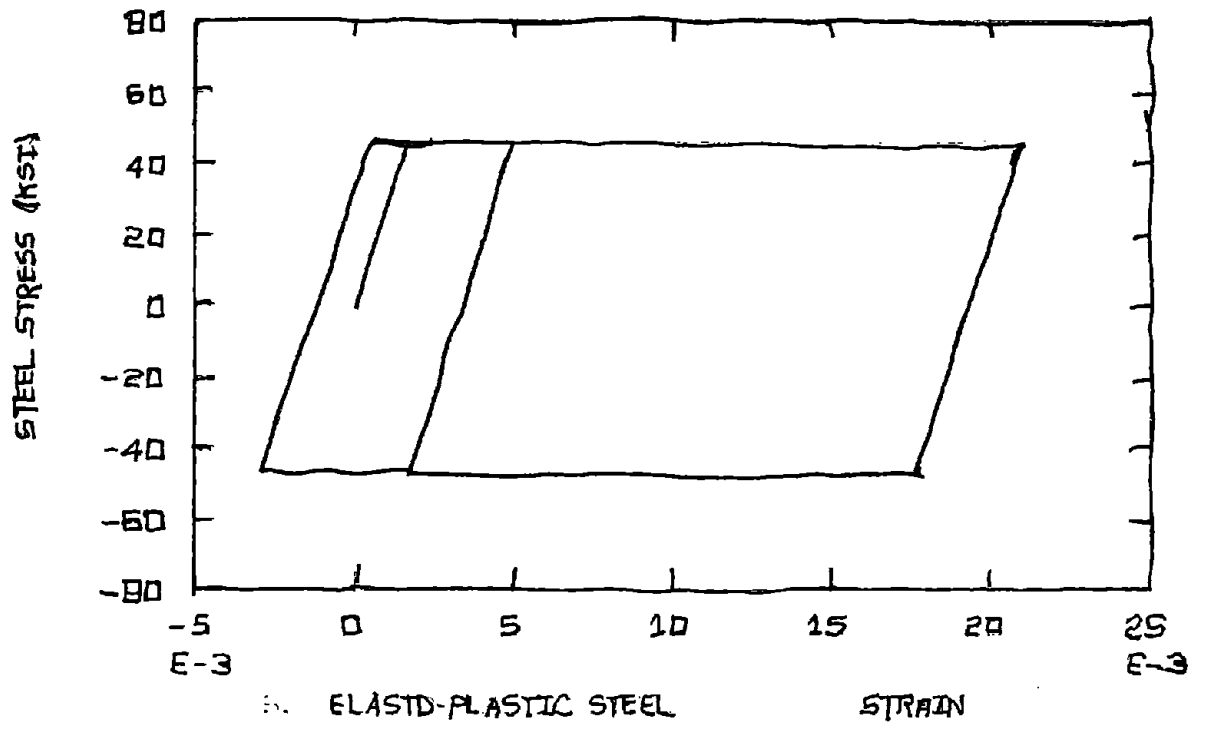


FIG. 3-9 (Continued)

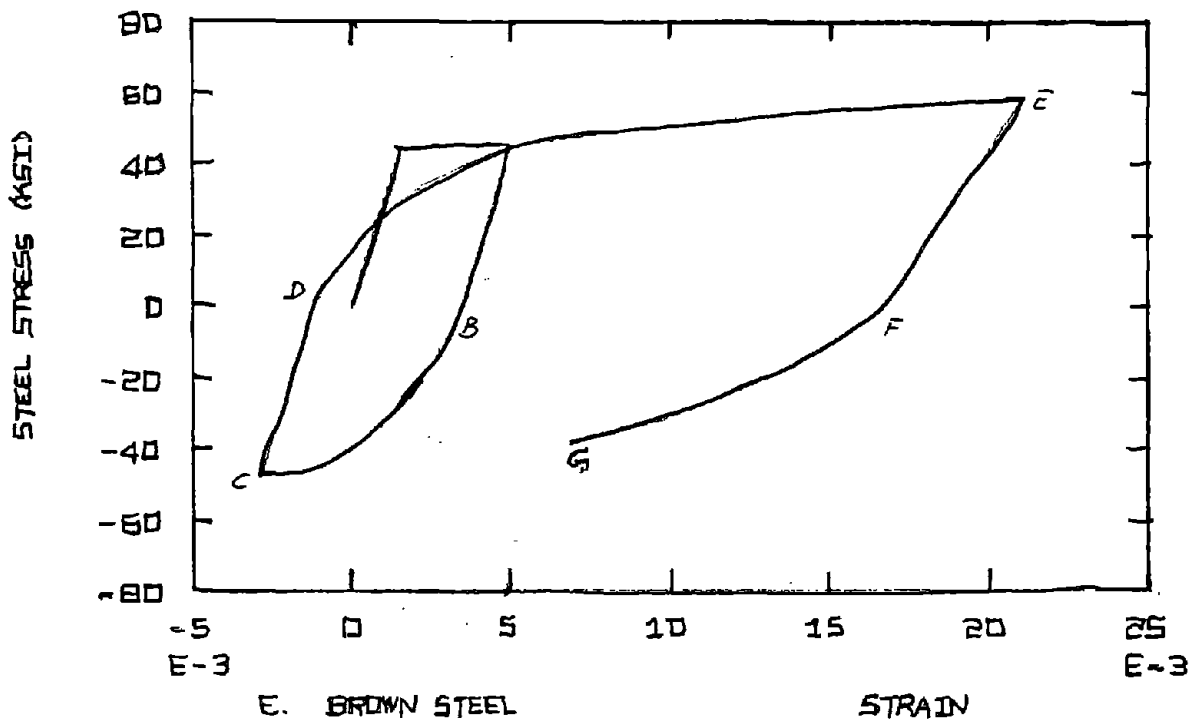
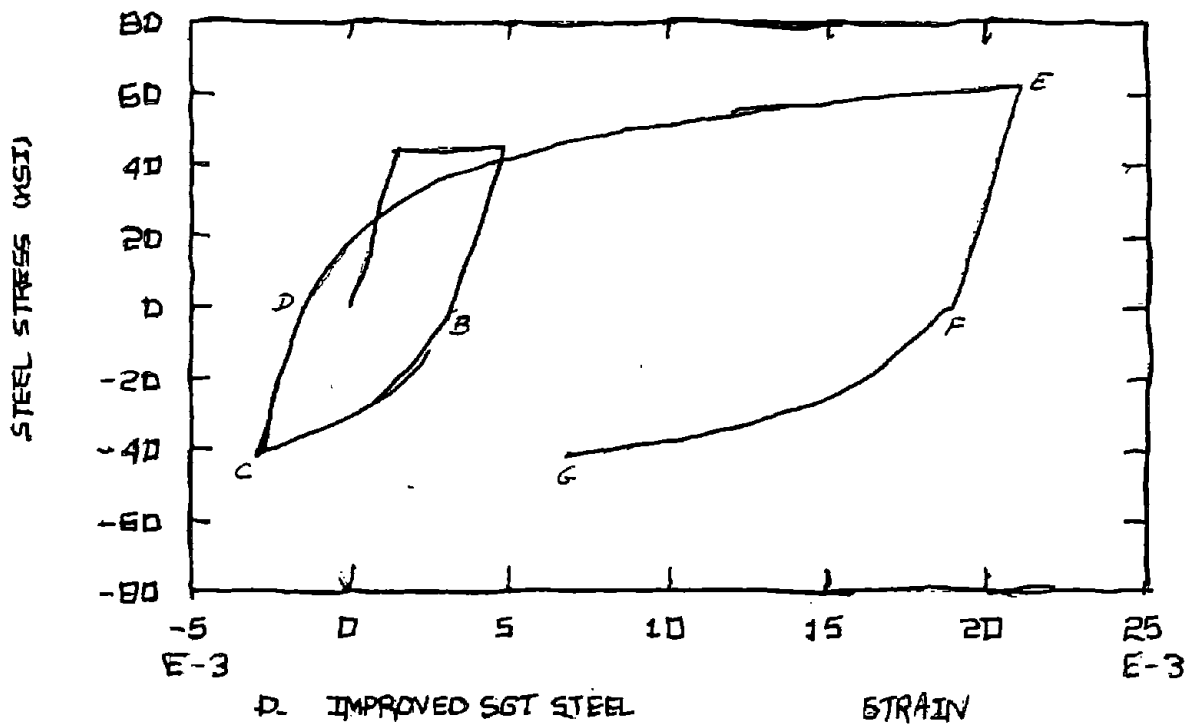


FIG. 3-9 (Continued)

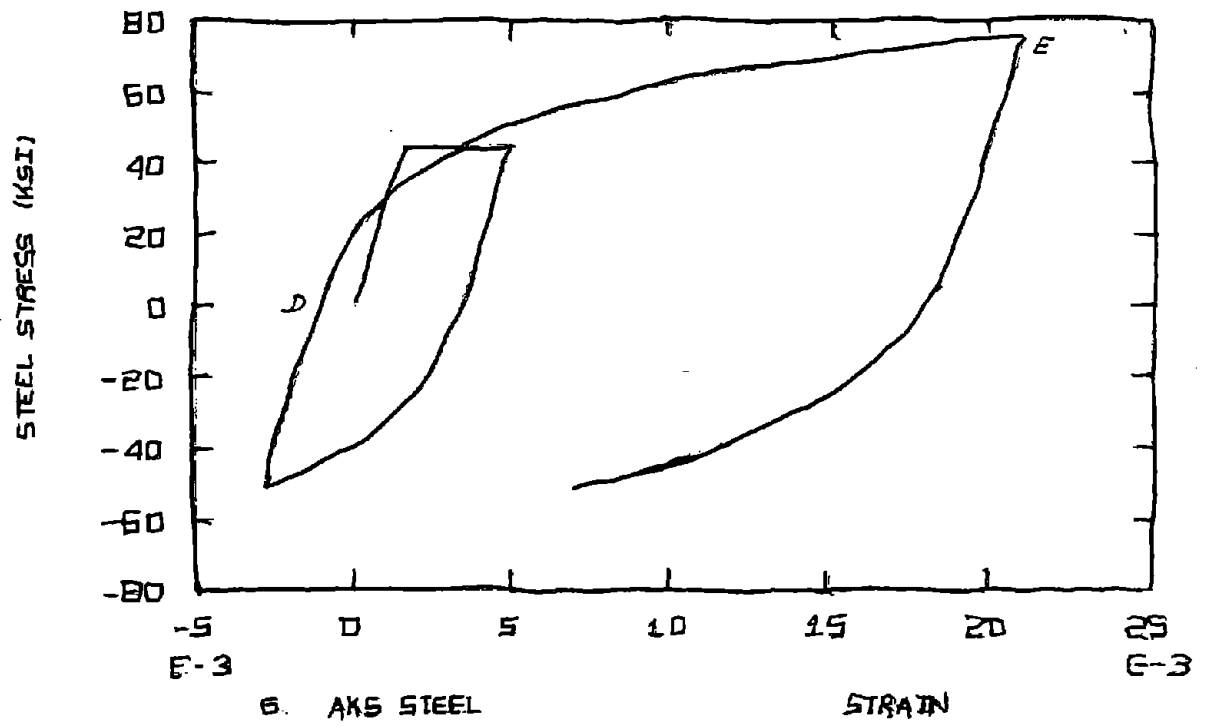
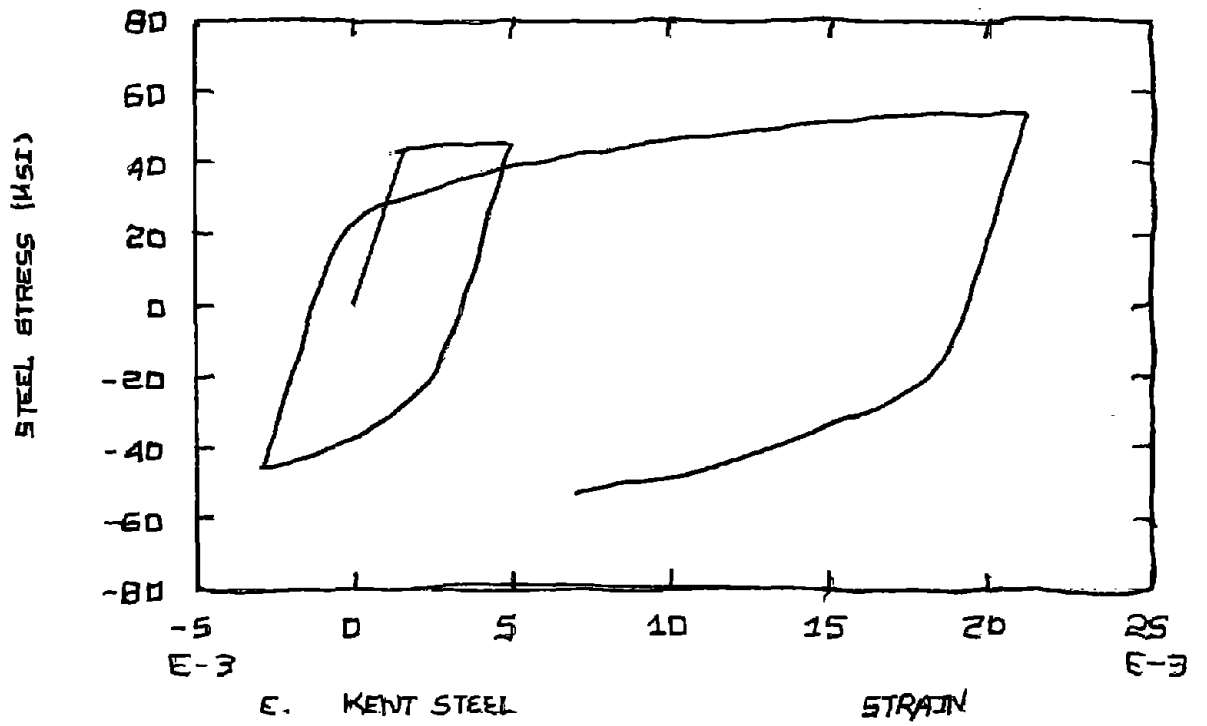


FIG. 3-9 (Continued)

Of the models based on SGT data, Brown's is the best up to point D. It should be noticed, however, that there is no stiffness degradation in the experimental results. As a consequence Brown's formulation deviates significantly in the segment  $\overline{EFG}$ .

Kent's relationship fits best over all, but it must be remembered that it was derived specifically for this data.

The AKS model behaves very well up to the first third of segment  $\overline{DE}$ . After this it becomes much too stiff and predicts a strength 50% higher than the observed one. This occurs because the AKS model was formulated for a steel with a much higher yield strength than this one.

It seems that all curvilinear models have the same trend: too much softening initially and too stiff later. The experimental result is somewhat between the Elasto-Plastic steel and the Improved SGT (such as the average of both) for this experiment.

### 3.3.2 Kent Steel #17 Data, Fig. 3-10

In this test the steel bar is loaded to yielding in tension, then the load is reversed four times to a compressive stress that is half the yield stress. There is no compressive strain, and the maximum tensile strain is .01272. In reloading to tension, the curve takes a very sharp bend to the "plastic" plateau. There is no distinct strain hardening point.

Except for providing a compressive stress 70% higher, the Elasto-Plastic model gives a good representation of this type of loading.

For the SGT and Improved SGT models, the reloading curves, both to tension and to compression, are much too soft. The loops then are too wide. Even though there is agreement with the experimental data for the maximum compressive stress, the reloading to tension produces a tensile stress much lower than observed. Brown's steel provides a closer agreement, but the loops are still wide and the tensile stress low.

Of course Kent's model seems to fit the data best. However, it becomes too stiff in the last reloading cycle. The AKS model was not suited again to reproduce with this set of data. For this type of loading condition it is too stiff in reloading to tension and the error seems to propagate. The AKS formulation assumes an ultimate strength of 110 ksi, and this is very high for Kent's intermediate grade steel. An attempt to use a more realistic  $f_y$  and strain hardening point led to an unstable formulation as the exponent  $r$  became negative.

Since this type of loading does not cause significant straining upon reversal of loading direction, the Bauschinger effect is slight. In reloading to tension, the behavior is essentially elasto-plastic. To consider situations such as this, the steel will be considered to be elasto-plastic if this initial plastic strain is less than  $\epsilon_y$ . Fig. 3-10H shows the effect of this when applied to the Improved SGT formulation. The loops are still wider than observed, but the maximum tensile stresses are now in agreement.

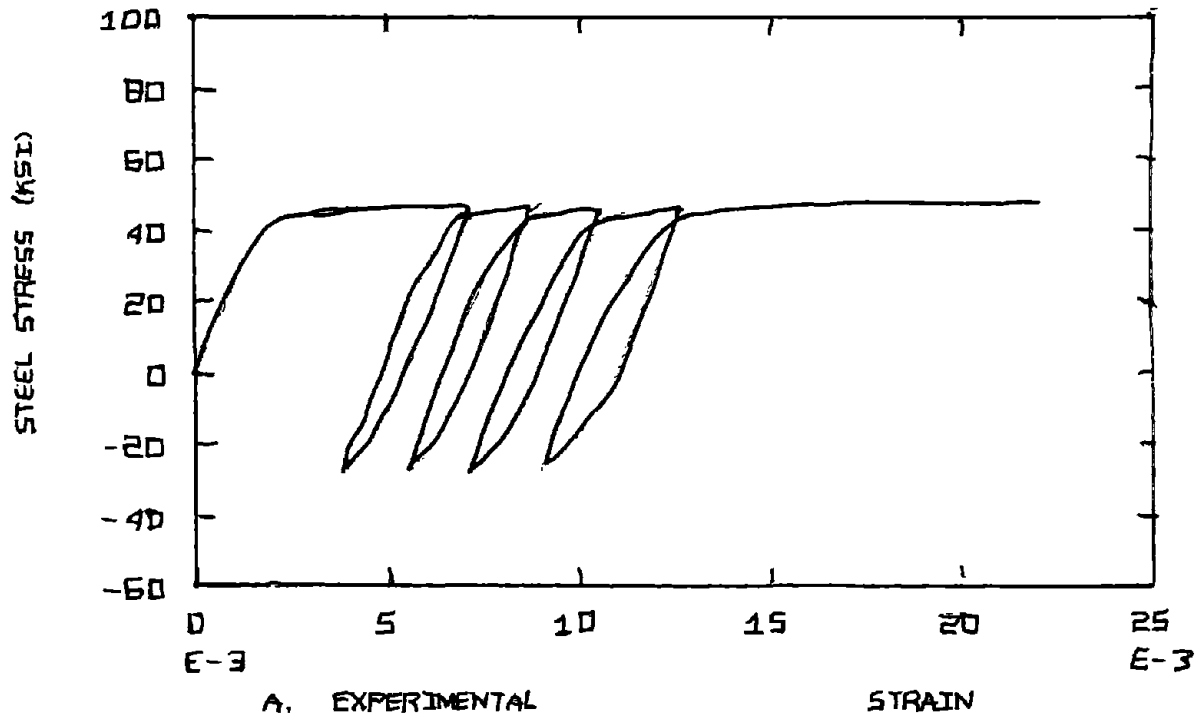


FIG. 3-10 - STEEL FORMULATIONS (KENT #17 DATA)

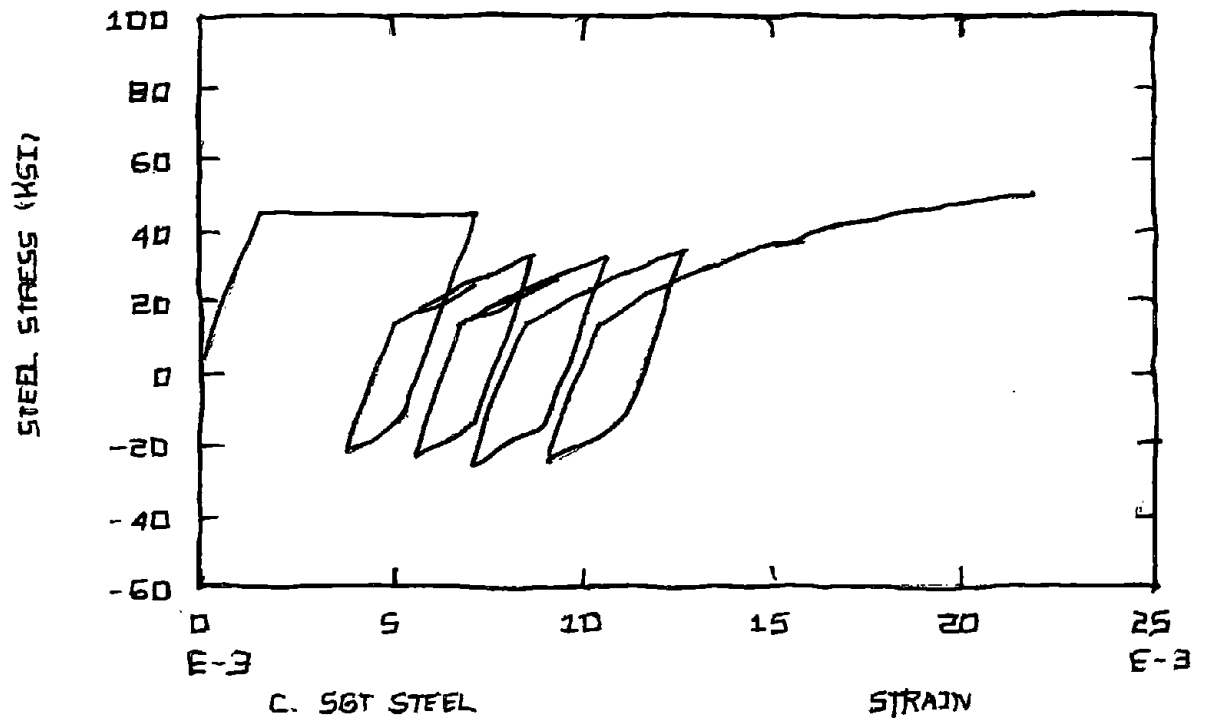
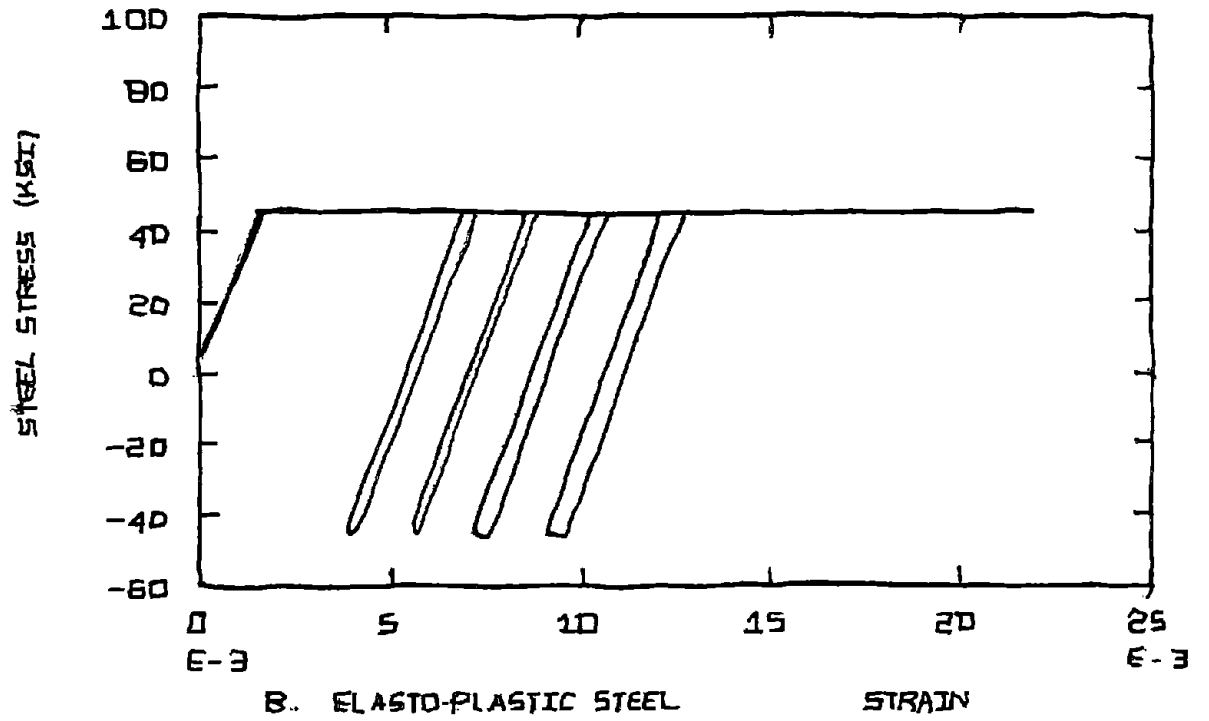


FIG. 3-10 (Continued)

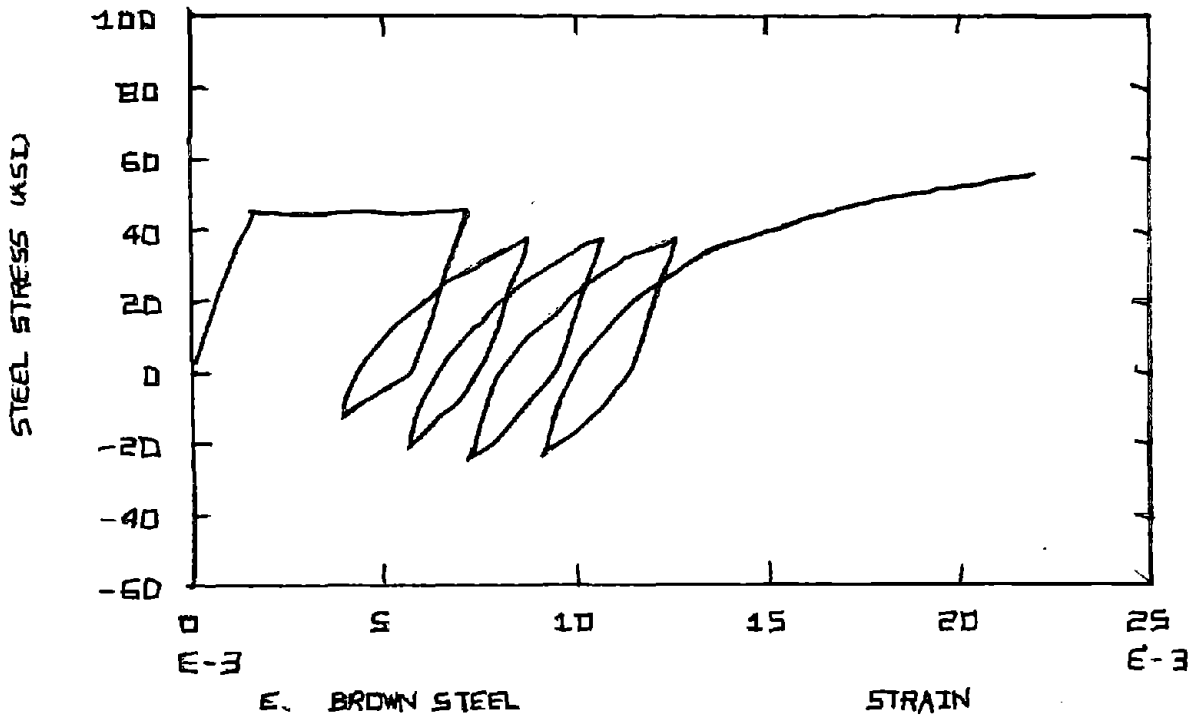
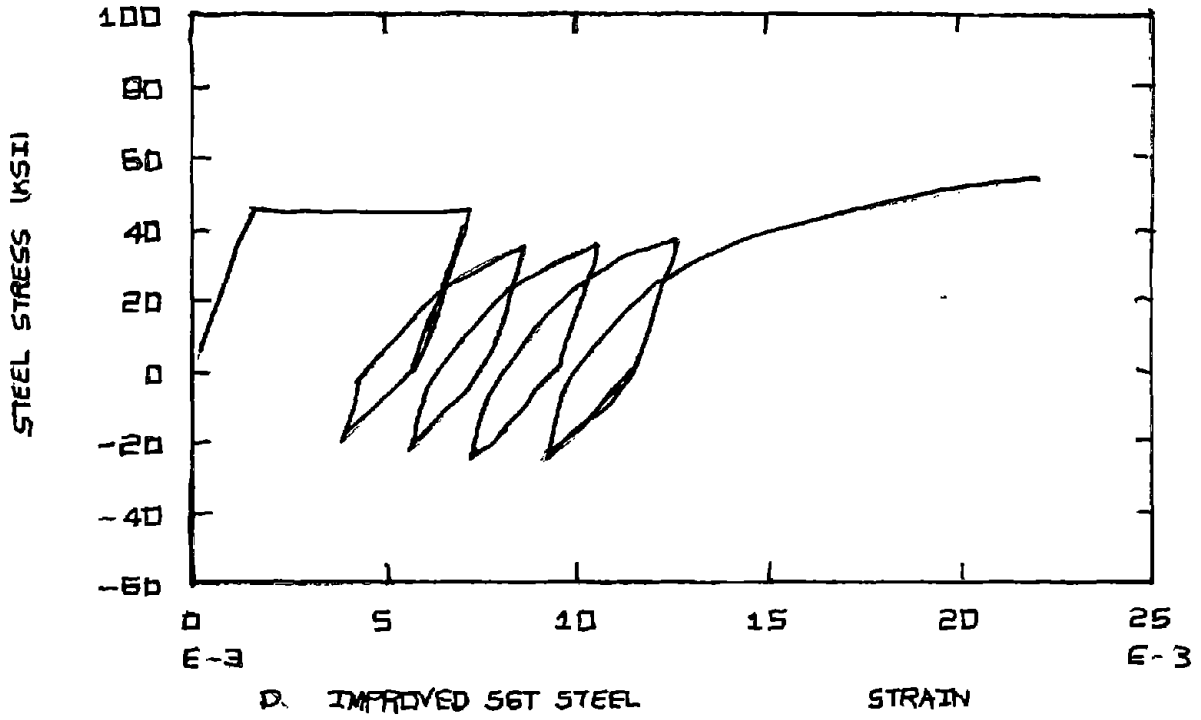


FIG. 3-10 (Continued)

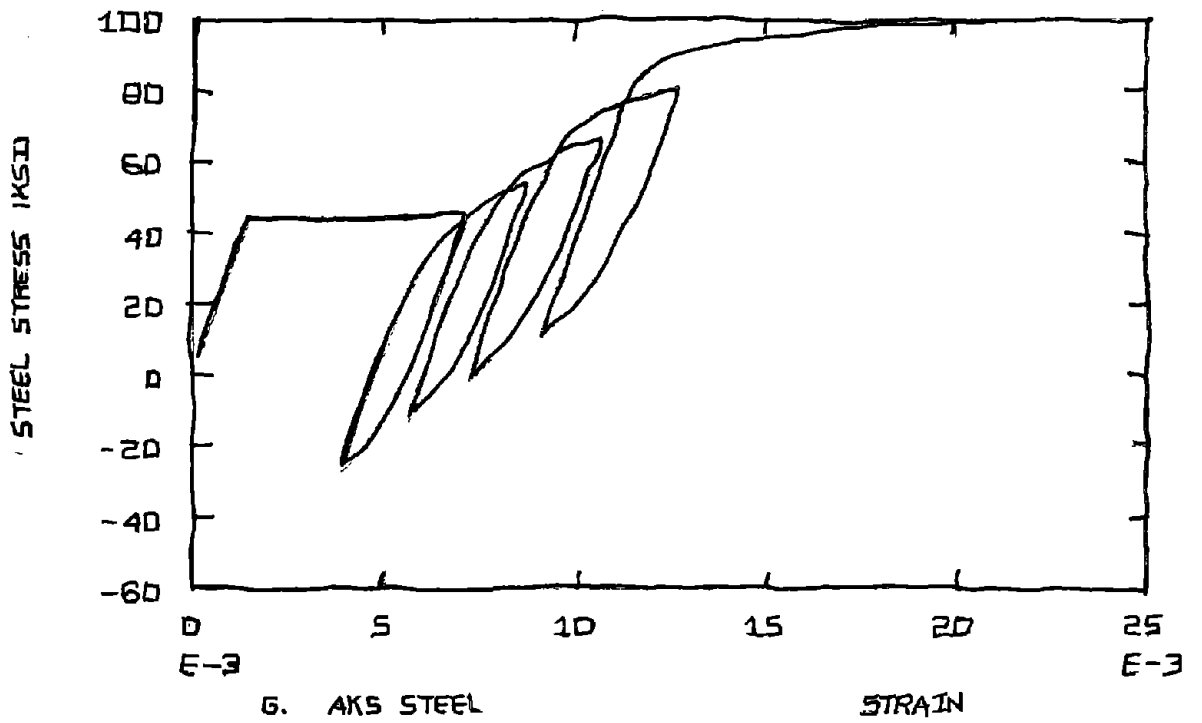
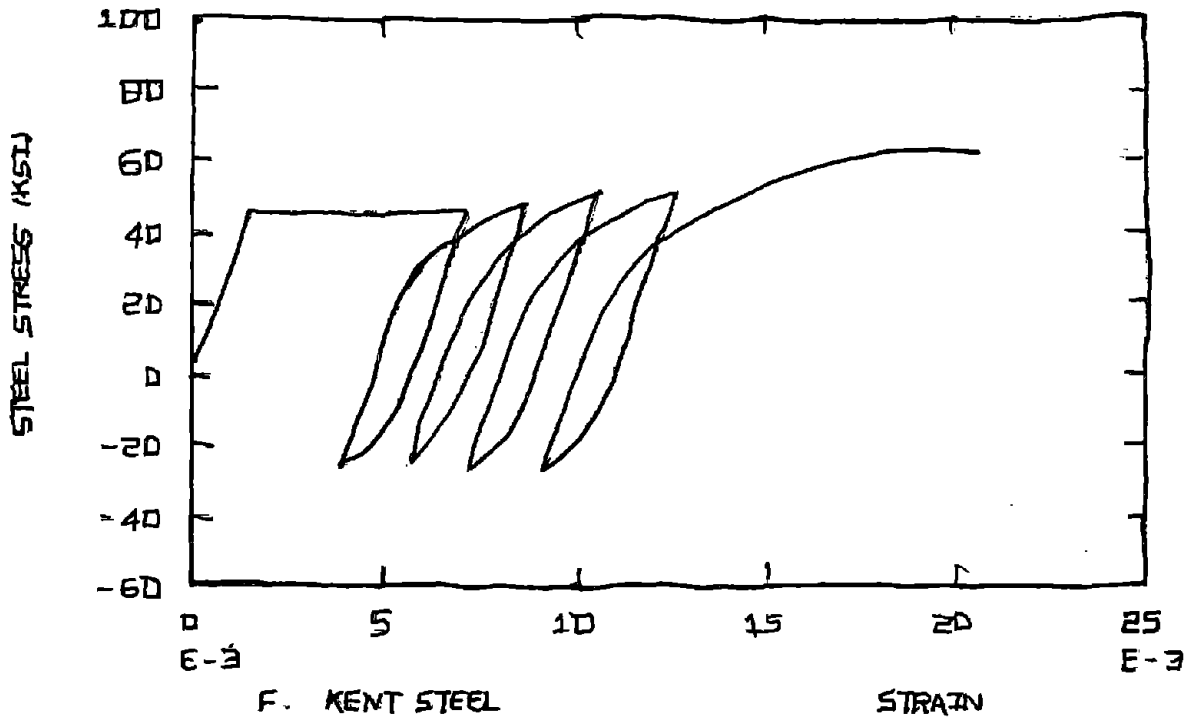


FIG. 3-10 (Continued)

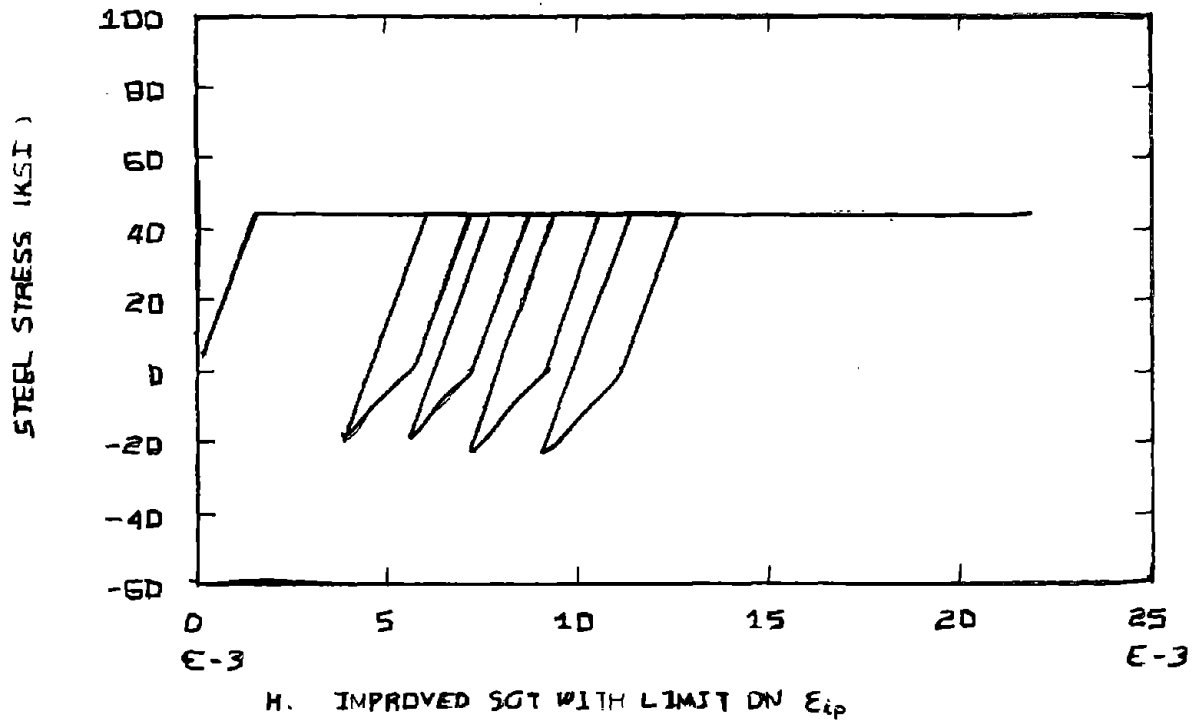


FIG. 3-10 (Continued)

### 3.3.3 AKS Steel #3 Data, Fig. 3-11

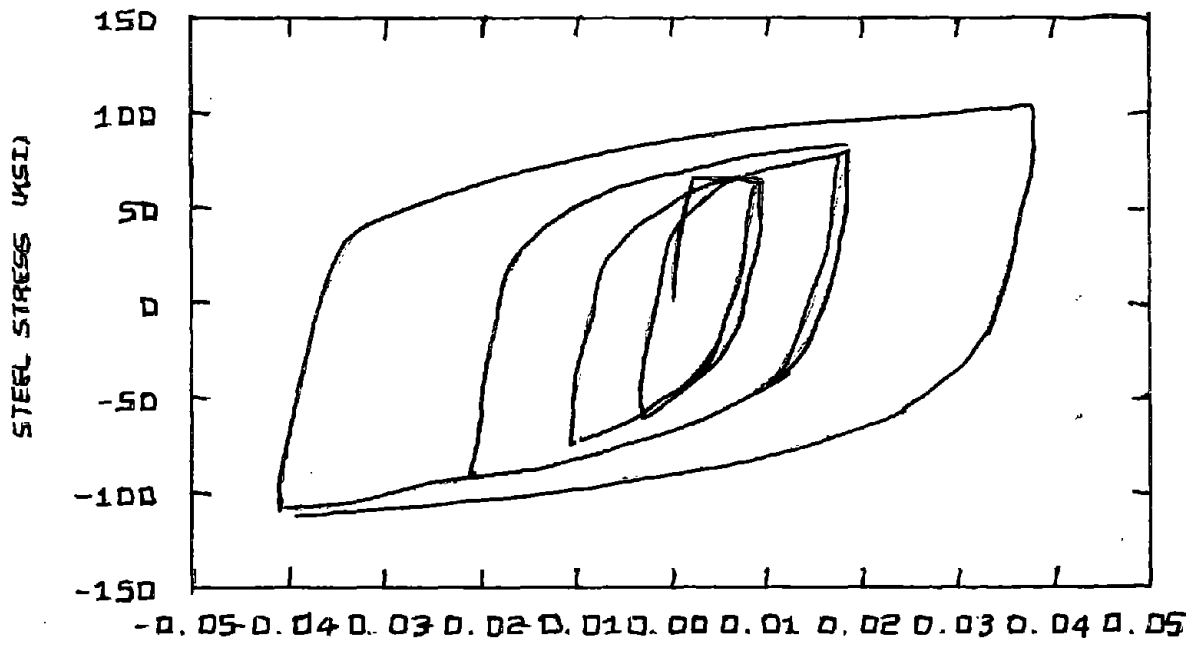
In this test, the specimen was subjected to cyclic loading in tension and compression between strain limits that gradually increase in magnitude. Generally the maximum strain in compression was the same as the strain in tension, and the maximum strain range was  $-.0412$  to  $.0382$ .

The Elasto-Plastic model compares very poorly because it does not represent the nonlinearity and any increase in strength due to the strain hardening phenomenon. At the end of the largest strain cycle the tensile stress is 60% of that observed.

The SGT model, with its unique curve formulation, has a fixed limiting stress and thus has a maximum stress that is 75% of the observed stress. Generally the nonlinear portion is stiffer than the experimental results.

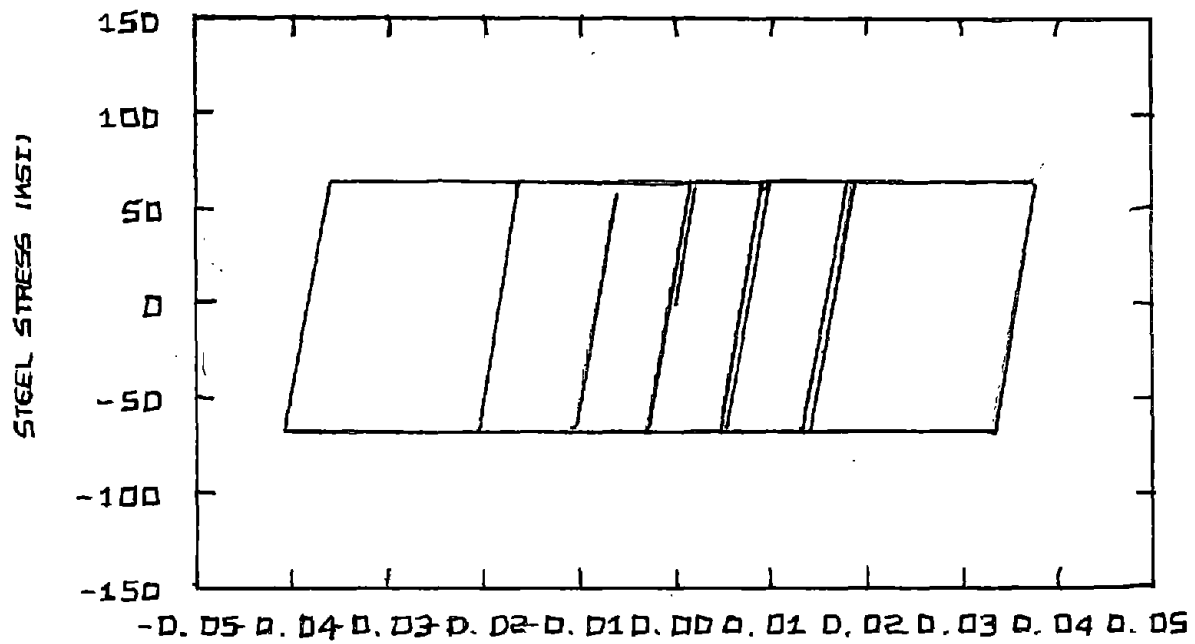
Very good agreement is found with the Improved SGT formula throughout most of the cycles. The maximum stress at strain  $-.04$  and  $+.04$  corresponds well to the experimental value. Again the slight kinks are due to the transition from linear unloading to nonlinear reloading curves.

Brown's model with the stiffness degradation in the unloading portion has very little resemblance to the observed curves. Brown's model without stiffness degradation and without resorting to the strain hardening curve after  $f_y$  is reached was also run, and this will be referred to as the Modified Brown formulation. The



A. EXPERIMENTAL

STRAIN



B. ELASTO-PLASTIC STEEL

STRAIN

FIG. 3-11 - STEEL FORMULATIONS (AKS #3 DATA)

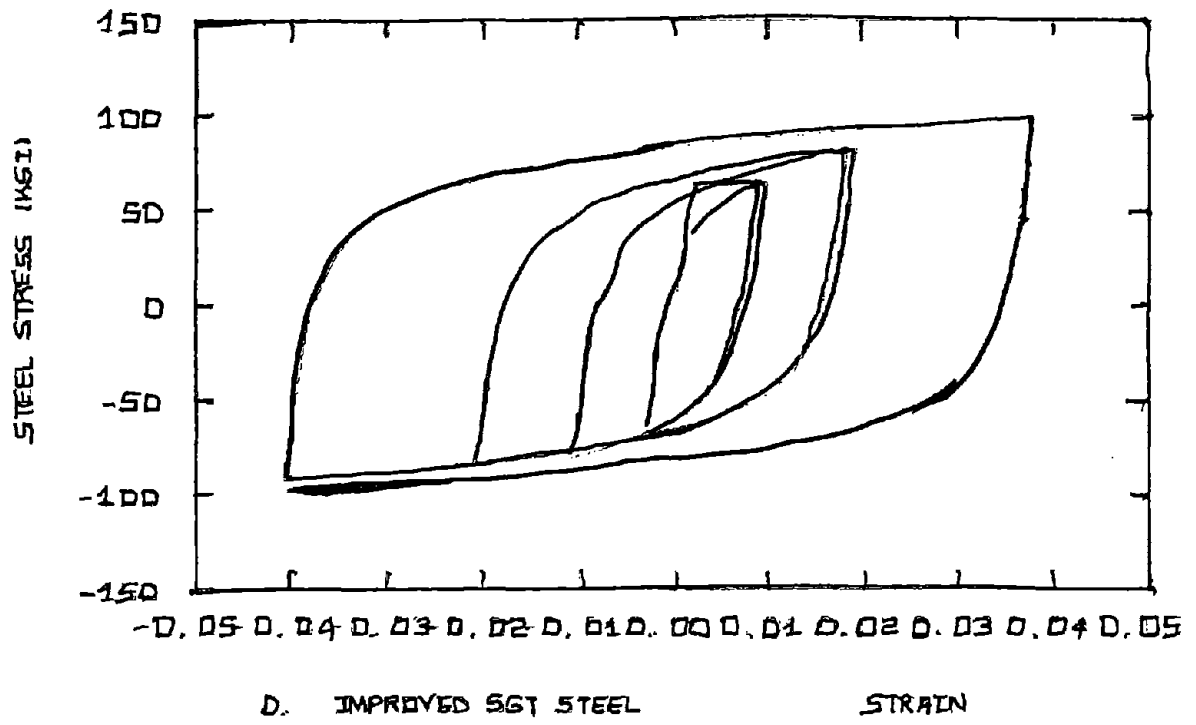
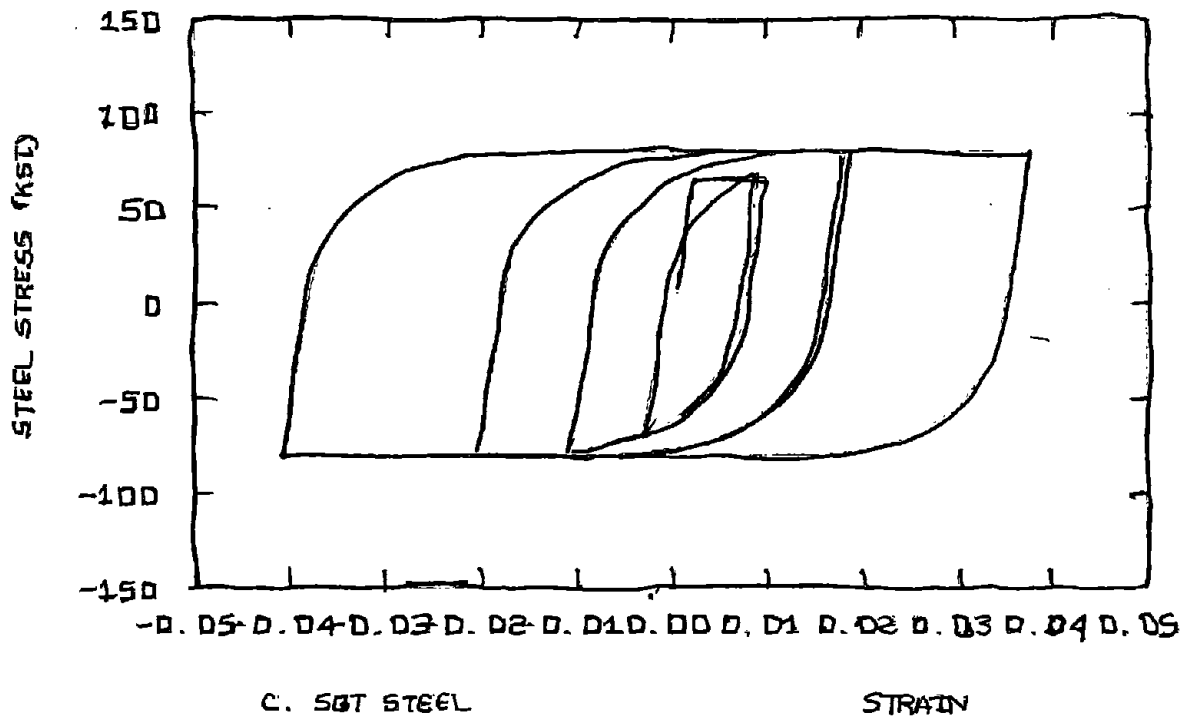


FIG. 3-11 (Continued)

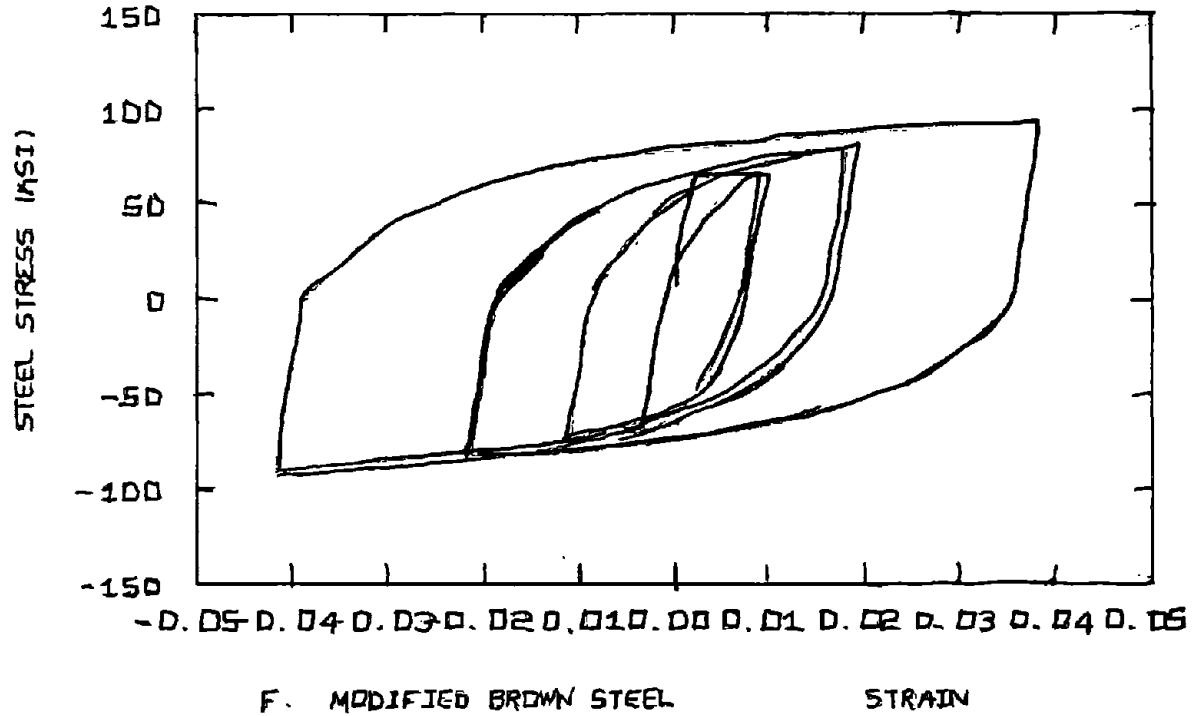
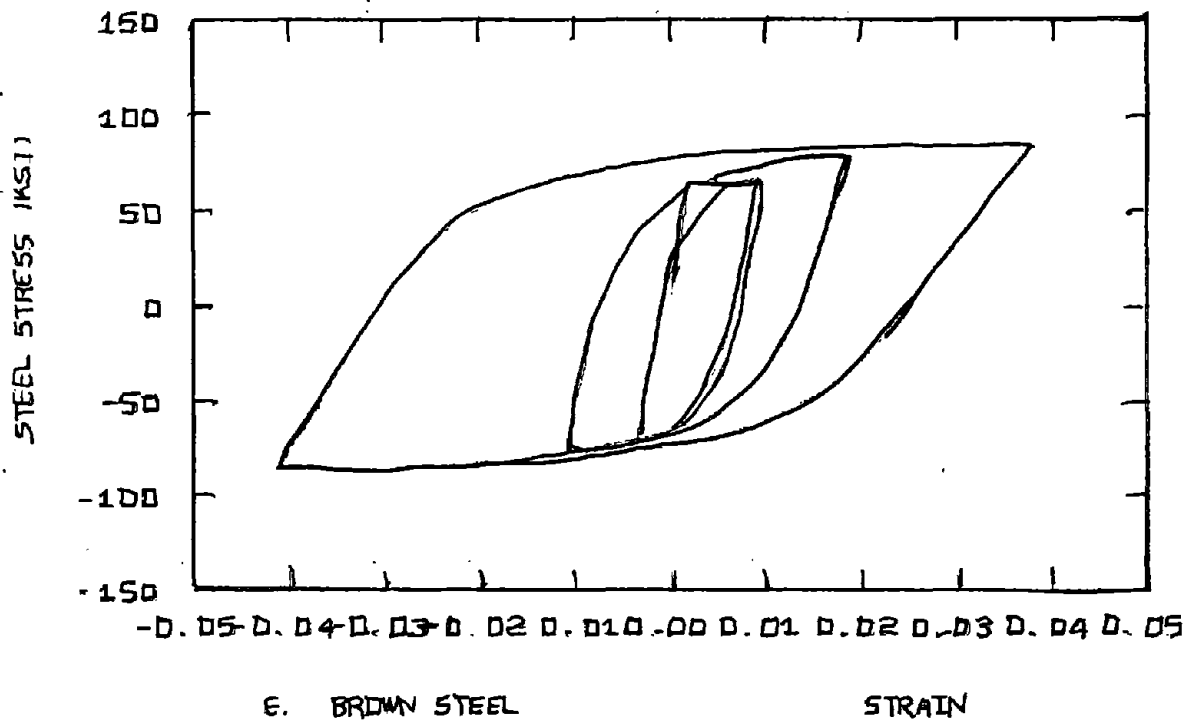
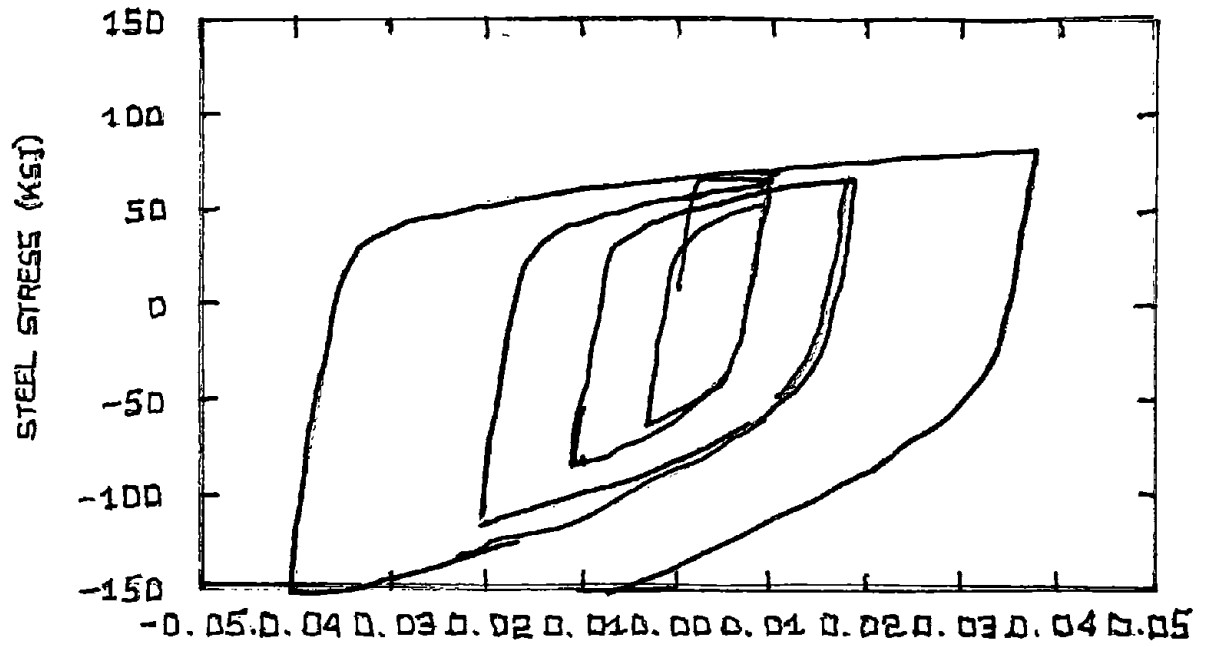
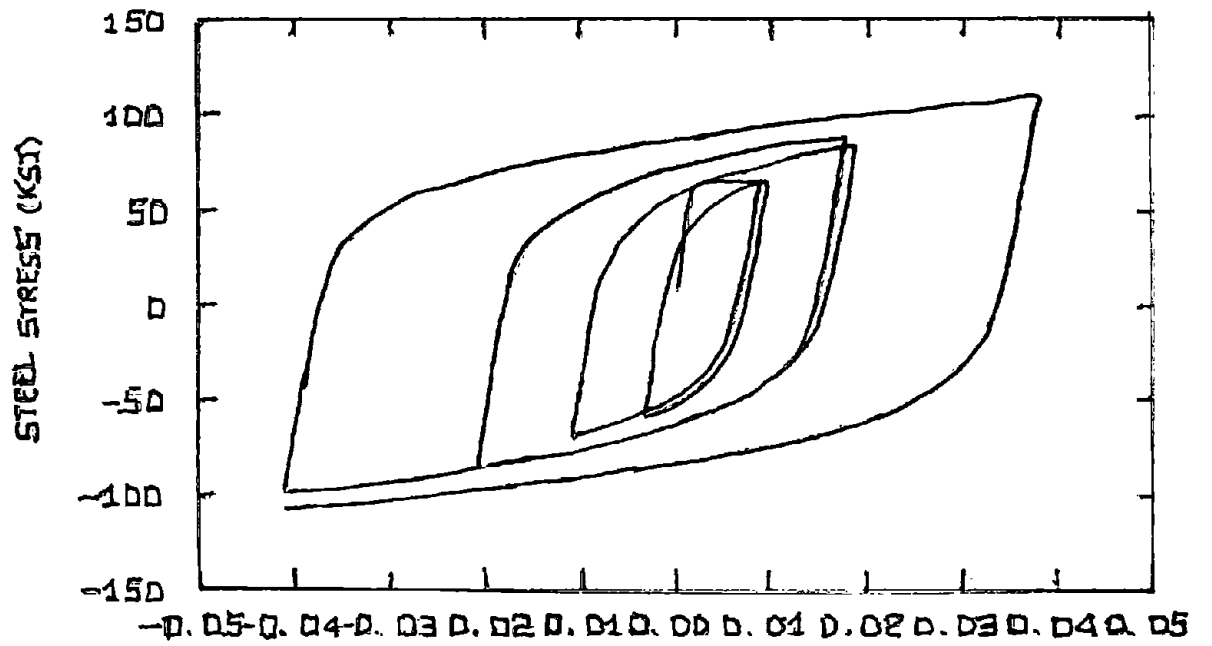


FIG. 3-11 (Continued)



G. KENT STEEL

STRAIN



H. AKG STEEL

STRAIN

FIG. 3-11 (Continued)

fit now is more reasonable, except that there are sharp jumps in the tangent modulus at the transition point. Apparently the stiffness degradation provided a better transition to the non-linear curve.

Kent's formulation does poorly, especially in reloading to compression, where it is significantly stiffer than the experimental results would indicate. The fact that Kent has a different formulation for the nonlinear portion, depending on whether the reloading started from tension or compression, is obvious. The increase in stiffness with the number of cycles is shown to make the agreement increasingly worse.

The AKS formulation matches the data very well, since the formulation is based, in part, on this data.

#### 3.3.4 AKS Steel #5 Data, Fig. 3-12

The cyclic loading in this test was similar to the previous one, except that the strain limits in the cycles were skewed to the tensile strain side. The range of strains were from  $-.0351$  to  $.0631$ . The specimen was initially loaded to strain hardening in compression.

The comments for Elasto-Plastic and SGT models that were made for the previous comparison still apply. Again the Improved SGT fits very well in both the stiffness and maximum stress. The Modified Brown also matches well.

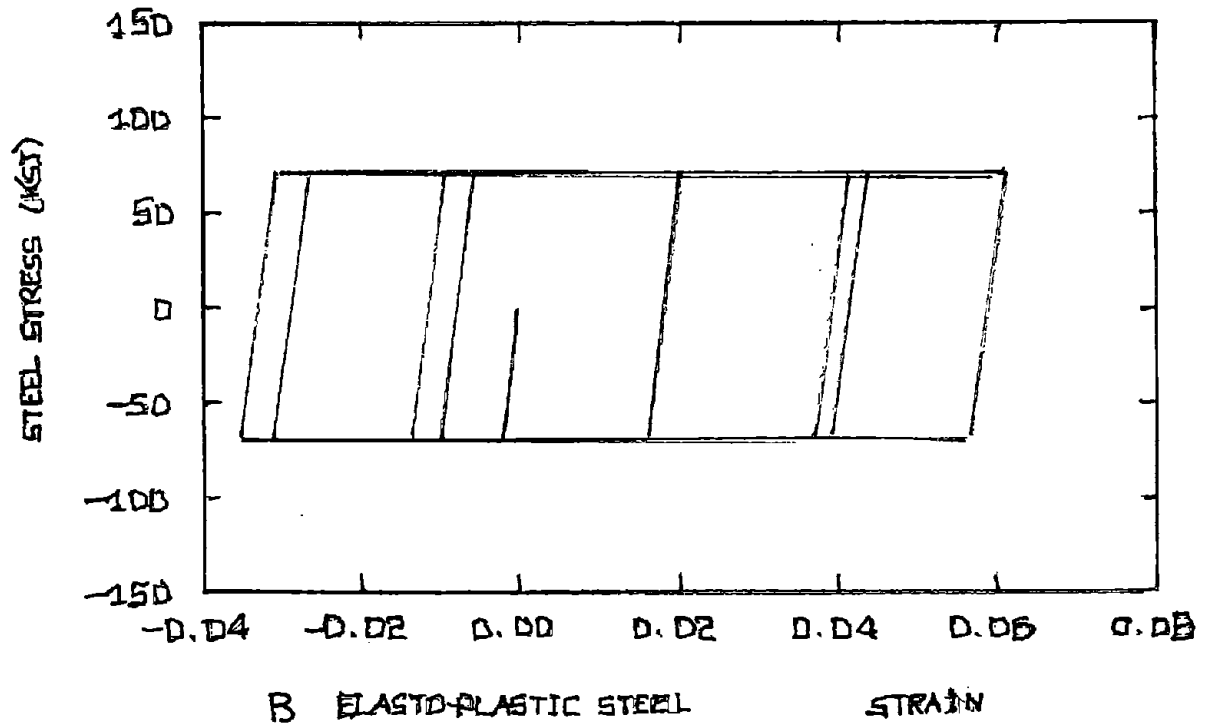
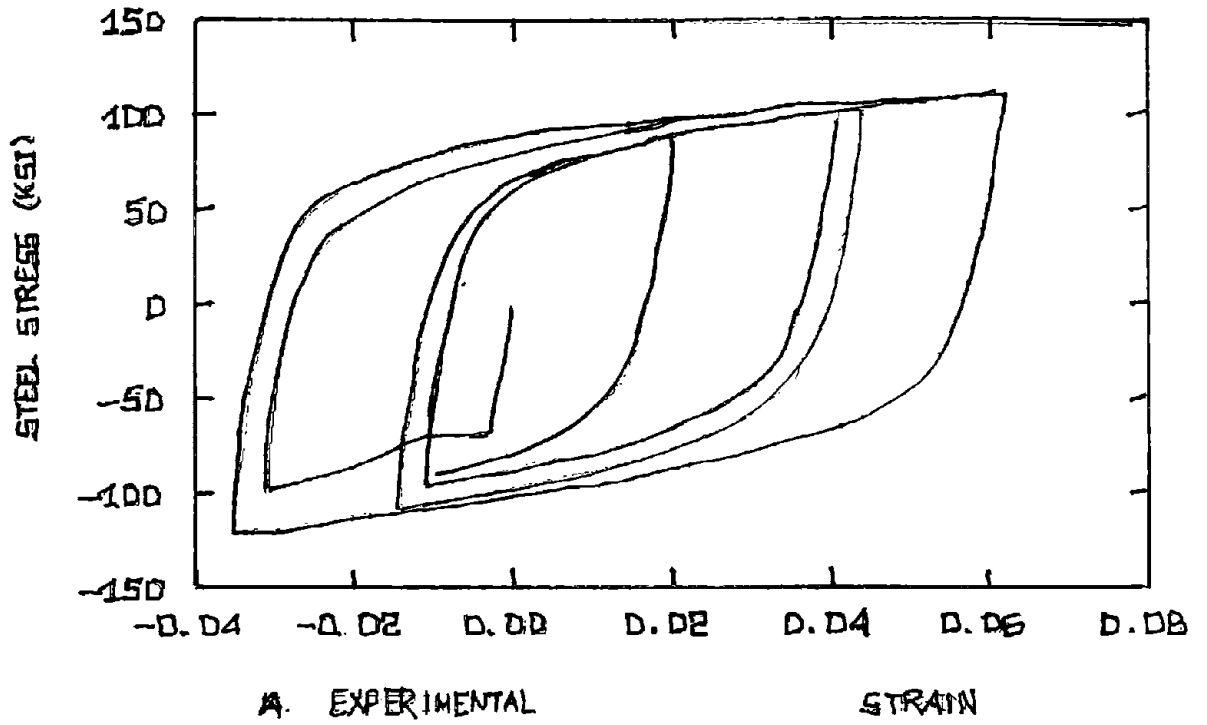


FIG. 3-12 - STEEL FORMULATIONS (AKS #5 DATA)

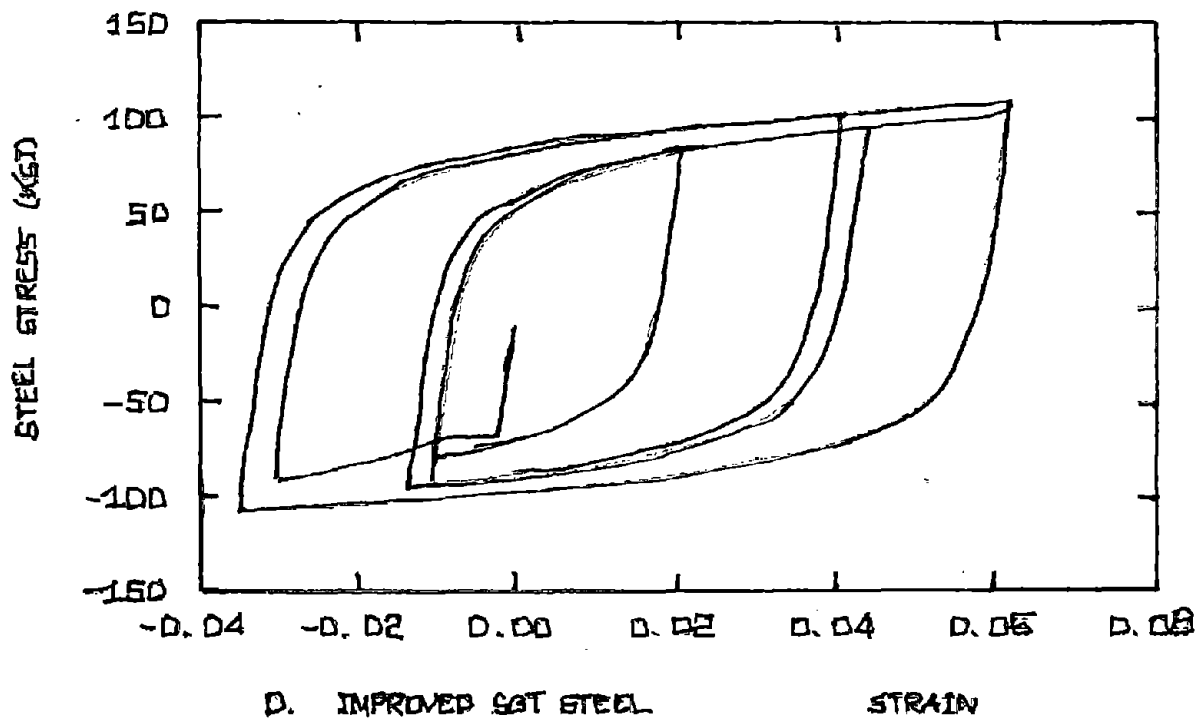
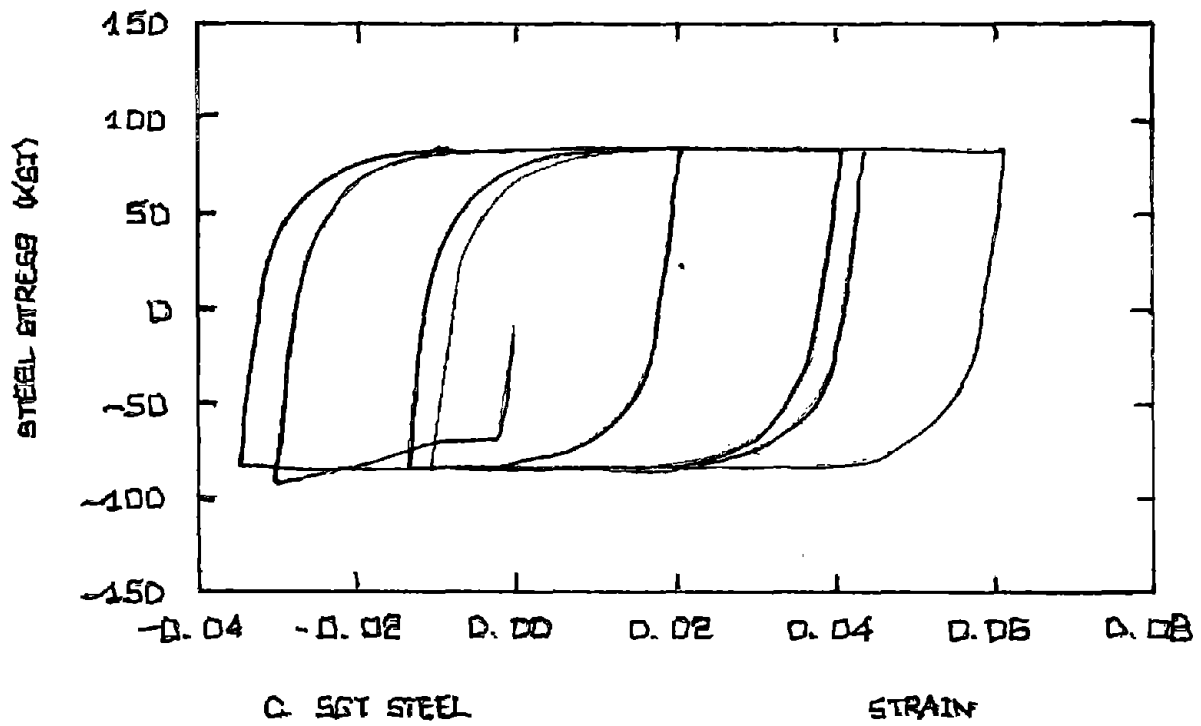


FIG. 3-12 (Continued)

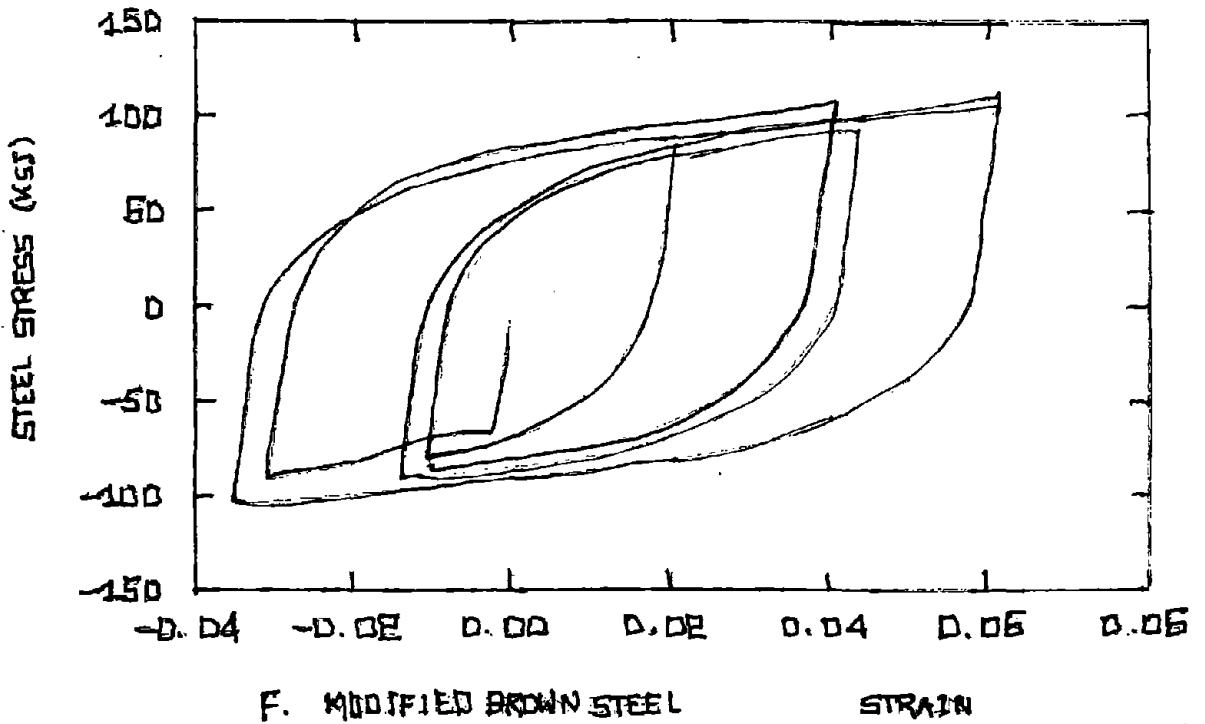
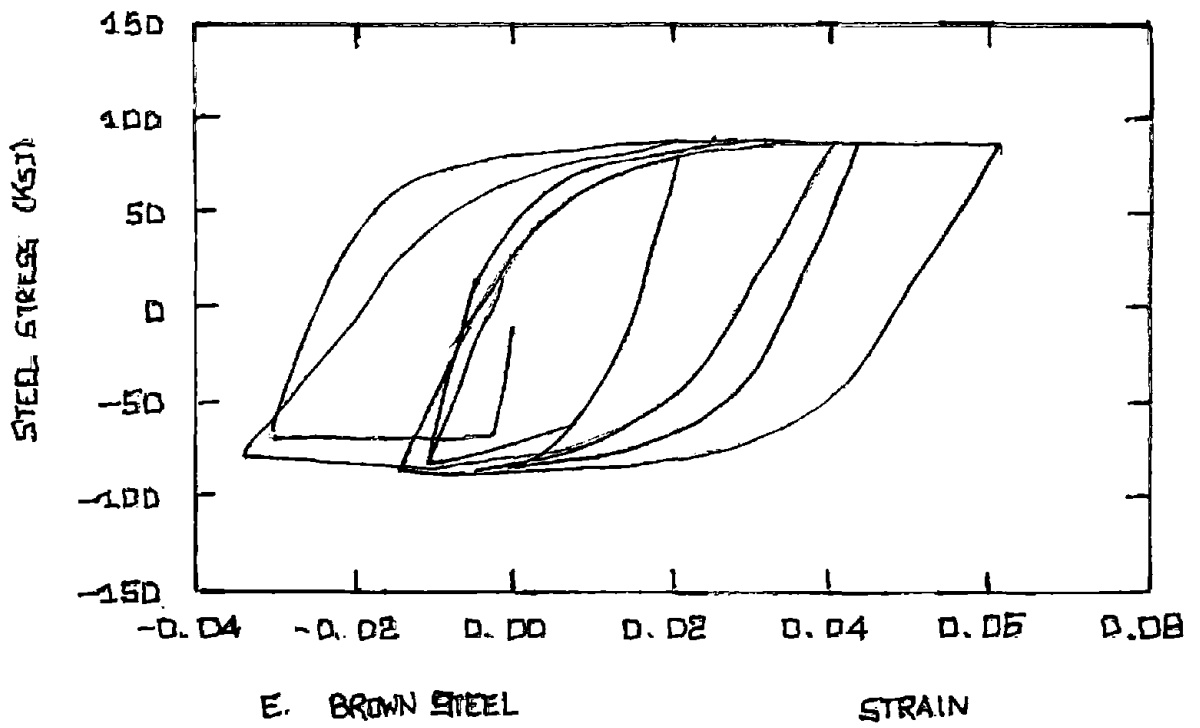


FIG. 3-12 (Continued)

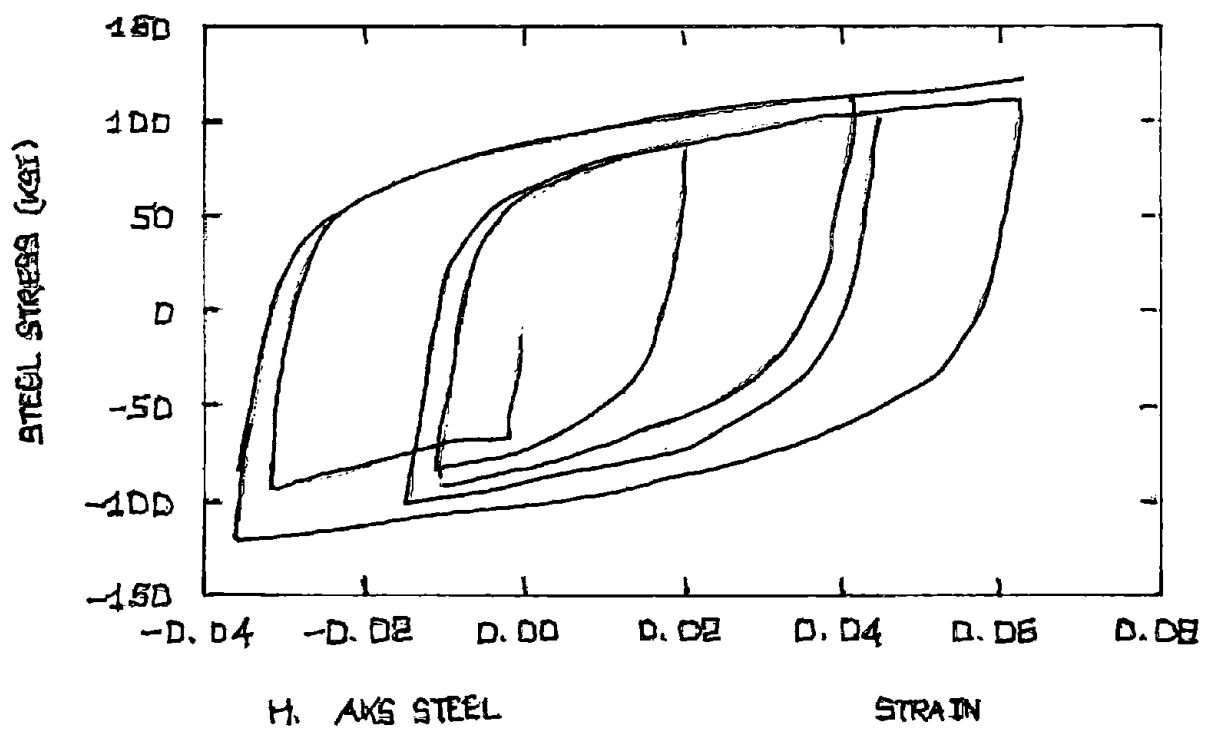
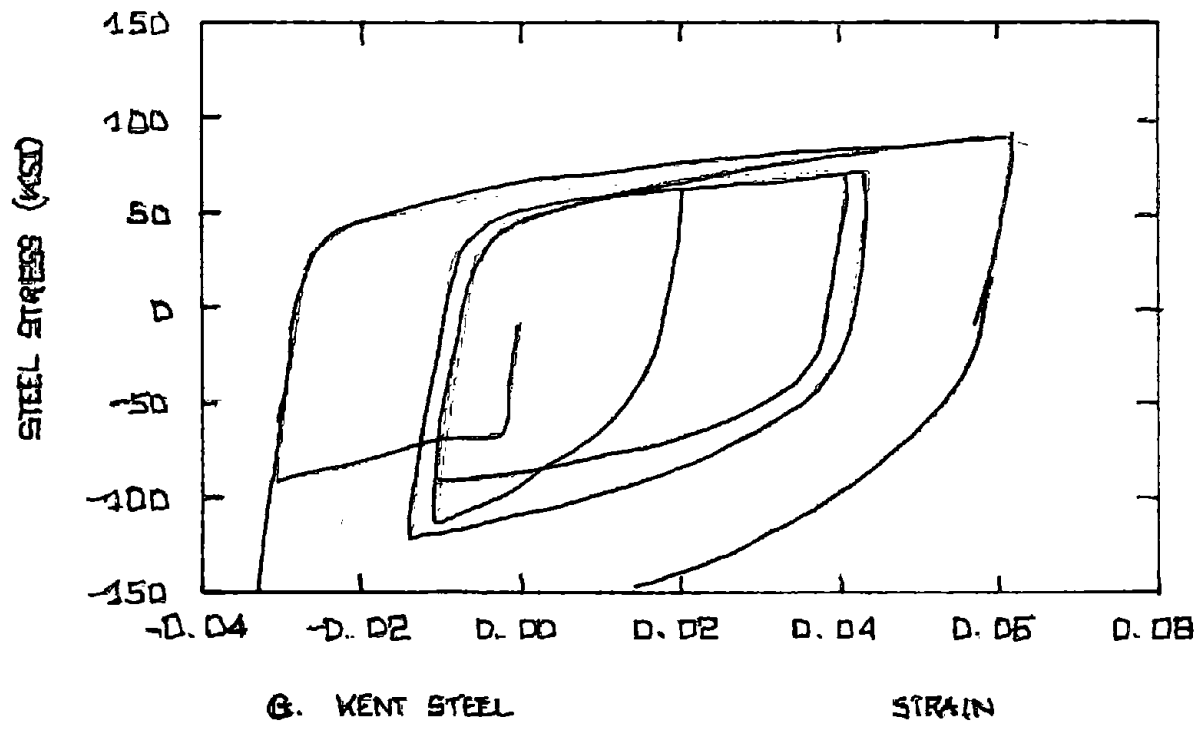


FIG. 3-12 (Continued)

Kent's formulation is obviously the poorest for this experimental data. In particular the reloading to compression greatly overestimates the compressive stress. The AKS formulation gives the best agreement, and is a very smooth curve with no jumps at transition points.

### 3.4 CONCLUSIONS

The Elasto-Plastic model does well for conditions where the strains are small and reversal of stress is not accompanied by significant straining. This type of behavior comes close to repeated loading without stress reversal, which is very much Elasto-Plastic. For cyclic loading with a large range of strain, it is poor.

The SGT is an attempt to provide some nonlinearity. With its single curve, it does not compare favorably with any of the experimental results.

The two Ramberg-Osgood type formulations, Kent's and AKS, have limited applicability. They represent well the data for which they are formulated, but do poorly in comparison with other experimental results with different types of steel and different loading conditions. These formulations require more parameters than the others, and consequently are harder to implement.

The intermediate models, Improved SGT and Modified Brown, give a better overall representation. Both these formulations are

based on the work of Singh, Gerstle, and Tulin, which was an early study. Even though the Modified Brown is slightly better for small strains, the Improved SGT is better for the large strain limits in the AKS data. The Improved SGT will be subsequently used in this thesis, although further comparison of the six steel formulations will be made on the cross-section level in the next chapter on moment curvature behavior.

## CHAPTER 4 - CROSS-SECTION STUDY: MOMENT-CURVATURE RELATIONS

4.1 INTRODUCTION

The behavior of a reinforced concrete member is studied at the cross-section level through the moment-curvature relations. To obtain these relationships analytically, an incremental stiffness approach and the fiber model will be used. Experimentally moment-curvature curves result from tests on simply supported beams or sometimes cantilever beams which simulate beam-column behavior. Of particular interest is behavior under cyclic loading where there are load reversals.

The analytic model used in this part of the study consists of fibers of concrete and steel which are related by an assumed linear variation of strain across the cross-section. Analytic formulations for moment-curvature studies have been proposed by Shina, Gerstle, Tulin;<sup>(23)</sup> Aoyama;<sup>(26)</sup> Kent, Park;<sup>(18)</sup> and by Brown, Jirsa.<sup>(16)</sup> These models differ in two important respects. The first is the difference in the assumed stress-strain curves and the second is the use of an iteration for equilibrium technique to obtain the moment-curvature relation. In this approach the extreme fiber strain is varied for a given curvature until the computed stresses satisfy equilibrium. In the incremental stiffness approach used here, the tangent stiffness of the previously computed moment and curvature is used to approximate the moment at the desired curvature, without

correction for equilibrium. Small errors will thus be introduced at each step. It is part of the purpose of this study to investigate the magnitude of these errors and how they propagate, since a fiber type model with cyclic correction at each step would be prohibitively expensive for dynamic studies.

#### 4.2 CROSS-SECTION PROPERTIES AND THEIR EFFECT ON THE MOMENT-CURVATURE RELATIONS

The following parameters are standard in reinforced concrete design and will be used here:

$b, t$	width and depth of cross section
$d$	distance to centroid of the tensile (bottom) reinforcement measured from the extreme compressive fiber
$d'$	distance to centroid of the compressive (top) reinforcement, similarly measured
$A_s, A_s'$	steel areas
$f_y$	yield strength of steel
$f_c'$	concrete strength from standard cylinder tests.

In the course of this study comparisons will be made between experimental results and the predictions of various analytical models. It is important to realize, however, that experimental results are also subject to uncertainties due to: 1) variation in material prop-

erties from those assumed; 2) differences in dimensions and configuration due to construction tolerances; 3) accuracy of measurements. Proper comparison of any analytic model with different sets of experimental data requires that the parameters listed above be accurately known. But the degree of certainty depends on the quality control of the construction and the accuracy of measurement.

For example, in some cases the analytic model provides a good prediction of the yield and ultimate moments consistent with the assumptions, but even for these simple measures the agreement may be very poor in other cases. It is thus important to keep in mind how a variation in each of these parameters affects the moment-curvature relationship.

In Figure 4-1 the moment-curvature relations are drawn with a 50% increase in the parameter indicated. (b and t were not varied, because of all the parameters these should be most accurately known.) For each of these analytic curves, failure is defined as the point where the strain in the extreme concrete fiber reaches .006. The section used for comparison is Kent's Beam #24, which has the same reinforcement ratio for the top and bottom steel.

Increasing d has the greatest effect; while an increase of 50% is exaggerated, it illustrates the point. Varying  $f_y$  and  $A_s$  (for both top & bottom steel) had an effect that was approximately proportional to their increase. The initial part (up to yield) of the curves for 1.5d and 1.5  $A_s$  are stiffer than the original curve,

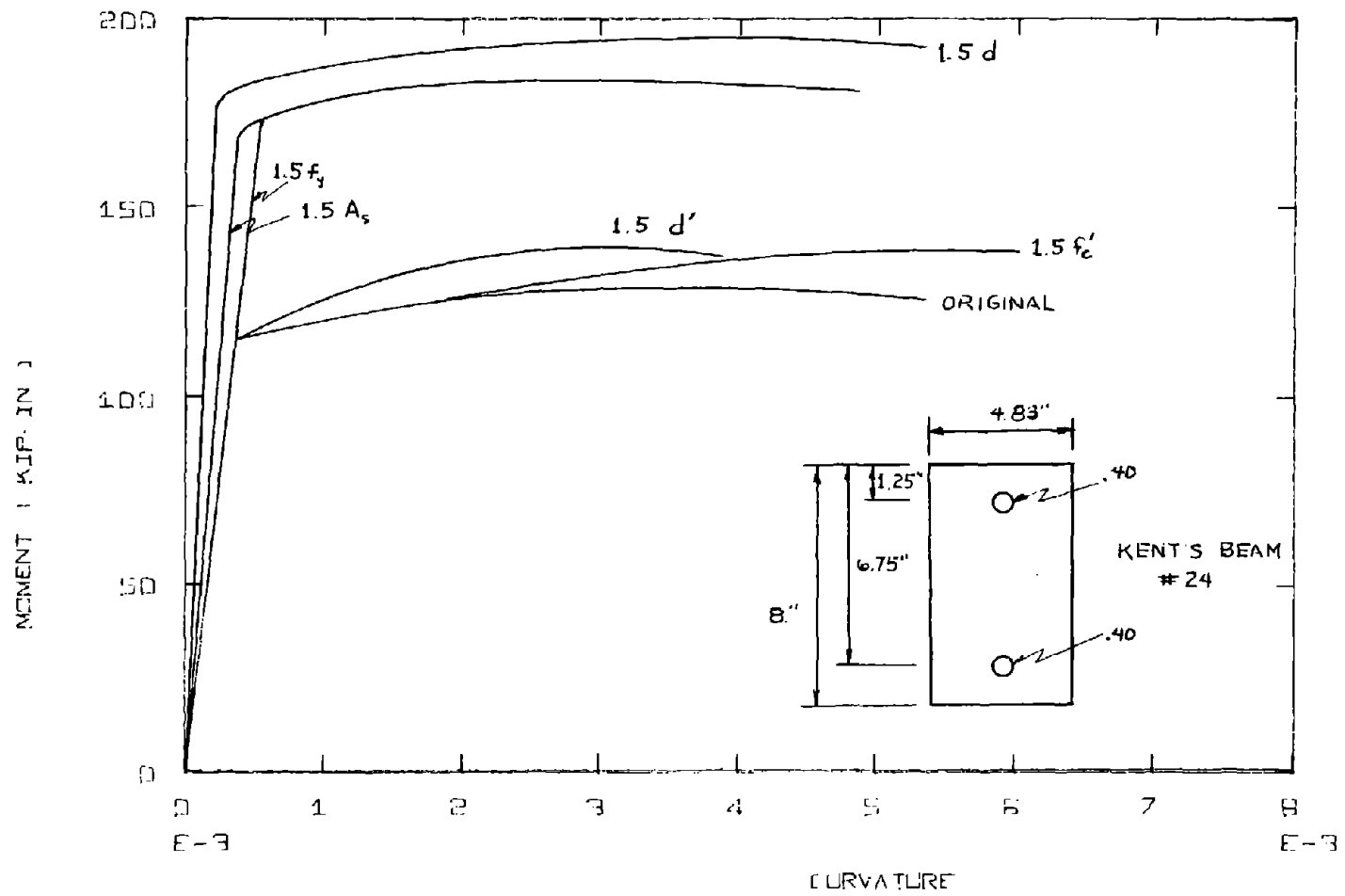


FIG. 4-1 - EFFECT OF A VARIATION OF SECTION PROPERTIES  
ON MOMENT-CURVATURE RELATIONS

while the 1.5  $f_y$  curve maintains the original stiffness. The increase in  $d$  causes an increase in ultimate curvature, while the increase in  $A_s$  and  $f_y$  decreases the curvature.

Changing  $d'$  and  $f'_c$  does not seem to affect the initial stiffness nor the yield moment, but there is a slight increase in moment capacity. Increasing  $f'_c$  leads to a larger ultimate curvature, while increasing  $d'$  leads to a smaller one.

In Fig. 4-2 the variation of yield moment is drawn as a function of these parameters. The parameters are varied from .5 to 1.5 times the original value (the intersection point in this figure). Variations in  $d$ ,  $A_s$ ,  $f_y$  provide nearly linear relationships with approximately the same slope, while  $f'_c$  and  $d'$  have a relatively small effect.

In any experimental program  $f'_c$  is obtained as an average of several standard cylinder tests. This value of concrete cylinder strength may vary from the strength of the concrete in the member because of differences in curing conditions and differences in loading. The steel strength usually reported comes from tests of the reinforcing steel bars that are used in the members, but sometimes only the supplier's designated strength is indicated.

The largest variation probably occurs in the location of the steel. In the pouring and vibrating of the concrete, there can be considerable movement of the steel, both laterally and vertically. Unfortunately, it has been shown that this is critical as far as the

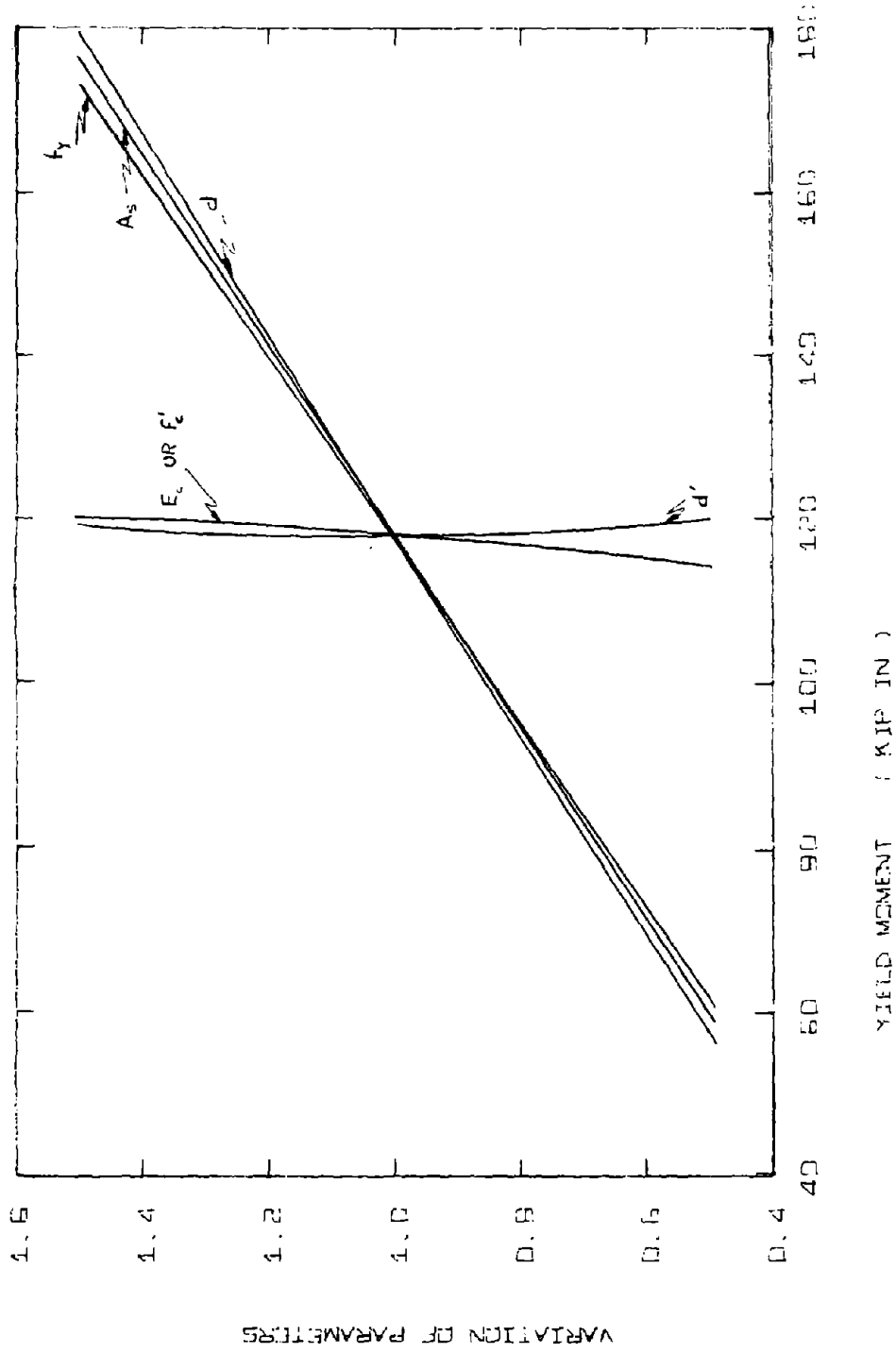


FIG. 4-2 - EFFECT OF A VARIATION OF SECTION PROPERTIES ON YIELD MOMENT

moment capacity of the section is concerned. In this analysis  $d$  (and  $d'$ ) will be adjusted to provide a reasonable fit for the yield moment.

#### 4.3 INCREMENTAL STIFFNESS APPROACH FOR MOMENT-CURVATURE

Figure 4-3 shows the typical reinforced concrete cross-section divided up into concrete and steel fibers. Typical strain and stress distributions are also shown.

The strain in each of these fibers is determined from the assumption that plane sections remain plane. While only an approximation, this assumption is usually valid; Figure 4-4 shows the actual distribution of strain for a member with increasing load. However, when significant cracking occurs under cyclic load, the assumption becomes less valid since there may be considerable slippage between the reinforcing steel and the adjacent concrete.

Given the centroidal strain,  $\epsilon_0$ , and the curvature,  $\phi$ , the strain in the  $i^{\text{th}}$  fiber is computed as

$$\epsilon_i = \epsilon_0 + y_i \phi \quad (4.1)$$

The sign convention is such that compressive strain is positive, and positive curvature causes compression on the top fiber of the beam. The corresponding convention for moment,  $M$ , and axial force,  $N$ , are also shown in Figure 4-3.

In the incremental stiffness approach, the moment curvature relationship is obtained stepwise with the values at the  $(i+1)^{\text{th}}$  step

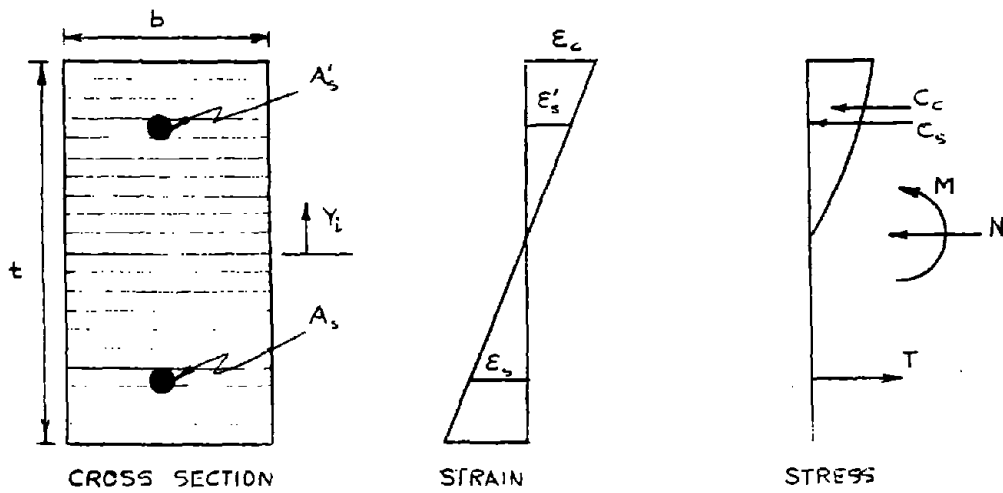


FIG. 4-3 - TYPICAL REINFORCED CONCRETE CROSS-SECTION

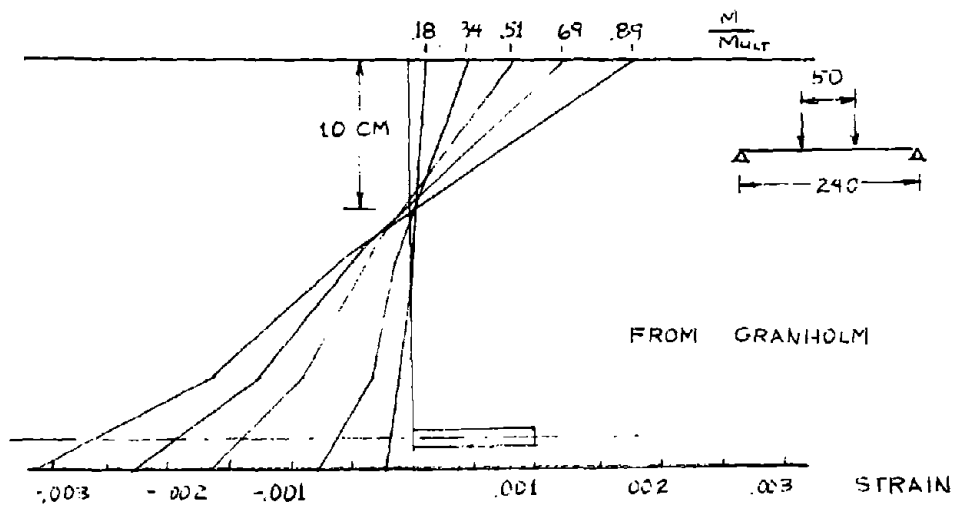


FIG. 4-4 - STRAIN DISTRIBUTION FOR A CROSS-SECTION

obtained from the properties at the  $(i)^{\text{th}}$  step.

At any step the incremental axial force,  $\Delta N$ , and moment,  $\Delta M$ , are related to the incremental centroidal strain and curvature,  $\Delta \epsilon$  and  $\Delta \phi$ , respectively, by the following expressions:

$$\begin{aligned}\Delta N &= a_{11} \Delta \epsilon + a_{12} \Delta \phi \\ \Delta M &= a_{21} \Delta \epsilon + a_{22} \Delta \phi\end{aligned}\tag{4.2}$$

where  $a_{ij}$  are the stiffness coefficients for the cross-section defined as:

$$\begin{aligned}a_{11} &= \sum_{i=1}^n b_i t_i E_i \\ a_{12} &= a_{21} = \sum_{i=1}^n y_i b_i t_i E_i \\ a_{22} &= \sum_{i=1}^n y_i^2 b_i t_i E_i\end{aligned}\tag{4.3}$$

where

- $b_i t_i$  is the area of the  $i^{\text{th}}$  fiber
- $y_i$  is the distance from the centroid of the cross-section to the centroid of the  $i^{\text{th}}$  fiber
- $E_i$  is the tangent modulus of the  $i^{\text{th}}$  fiber

For the moment-curvature study it is assumed that the axial force does not change value. (The case when axial force varies will be considered in a subsequent section.)

$$\begin{aligned} \Delta N = 0 \rightarrow \Delta \epsilon &= -\frac{a_{12}}{a_{11}} \Delta \phi \\ \text{so } \Delta M &= \left( a_{22} - \frac{a_{12} a_{21}}{a_{11}} \right) \Delta \phi \\ &= k^i \Delta \phi \end{aligned} \quad (4.4)$$

where  $k^i$  is then the tangent stiffness for rotation at the  $(i)^{\text{th}}$  step.

To proceed from step  $(i)$  to step  $(i+1)$  (Fig. 4-5),  $k^i$  is evaluated and it is assumed to be constant in the interval. In the Euler method the stiffness coefficients  $a_{ij}$  and thus  $k^i$  are evaluated at step  $(i)$  from the tangent moduli of the fibers. In the Modified Euler method  $k^i$  is evaluated at the midpoint of the interval, i.e., at  $(i+1/2)$ , and this stiffness is used for the interval. Both of these methods will be used and compared.

#### 4.4 EFFECT OF INCREMENT SIZE

To obtain the analytic moment-curvature relation, curvature is incremented and the resulting change in moment is determined. The results provided by the incremental stiffness approach will be sensitive to the size of the applied increment. To illustrate this effect and to determine an appropriate increment size, an analytic moment-curvature relationship (Kent's beam #24, Elasto-Plastic steel) is run with varying increment sizes. In Fig. 4-6 (A to D)  $\Delta \phi$  varies from approximately  $\phi_y/10$  to  $\phi_y/80$ . In addition, Table 4-1 summarizes the results of this comparison.

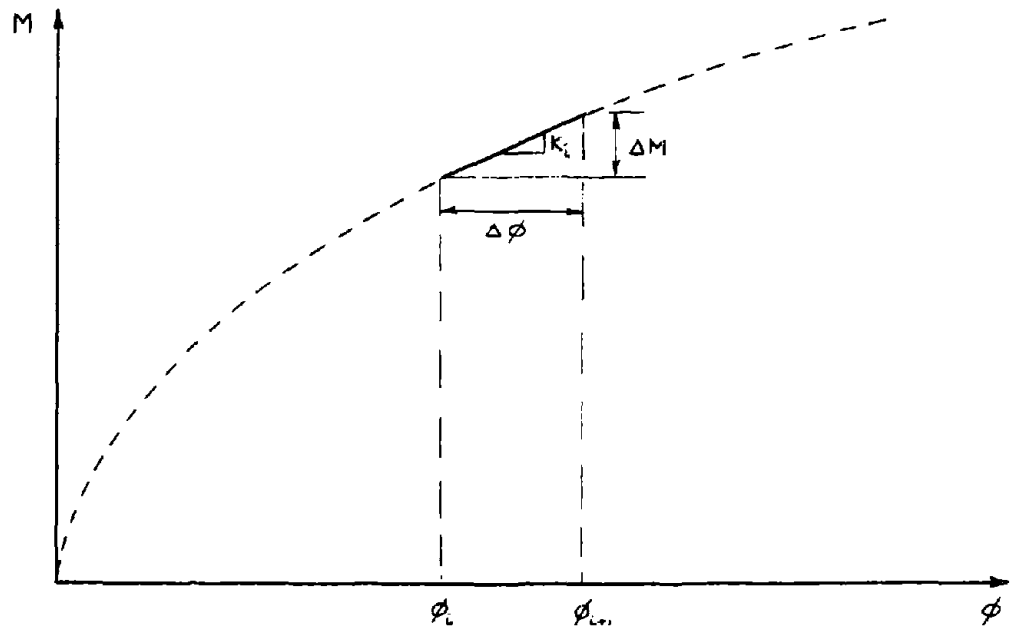


FIG. 4-5 - INCREMENTAL STIFFNESS APPROACH  
FOR MOMENT-CURVATURE

TABLE 4-1 - INCREMENT SIZE COMPARISON FOR KENT'S BEAM #24

Cycle	Curvature at end of cycle	Exper. M <sup>+</sup>	M ( $\Delta\phi \sim \frac{\phi_y}{10}$ )	M ( $\Delta\phi \sim \frac{\phi_y}{20}$ )	M ( $\Delta\phi \sim \frac{\phi_y}{40}$ )	M ( $\Delta\phi \sim \frac{\phi_y}{80}$ )	M Modified Euler ( $\Delta\phi \sim \frac{\phi_y}{20}$ )
7	.000230	79.5	76.6	75.9	75.6	72.5	75.3
8	-.000230	-75.5	-19.0	-88.6	-82.0	-76.1	-75.9
9	.0001225	108.0	194.1	145.5	134.0	129.7	129.4
10	-.000790	-96.0	-220.2	-147.6	-130.2	-123.0	-111.3
11	.001870	108.0	223.9	148.1	130.2	124.6	125.1
12	-.001555	-100.0	-258.3	-164.0	-136.6	-126.4	-118.5
13	.0000135	81.0	21.9	62.2	88.2	95.6	102.2
Fig.		4-27A	4-6A	4-6B	4-6C	4-6C	4-6E

<sup>+</sup>Moments in kip-in.

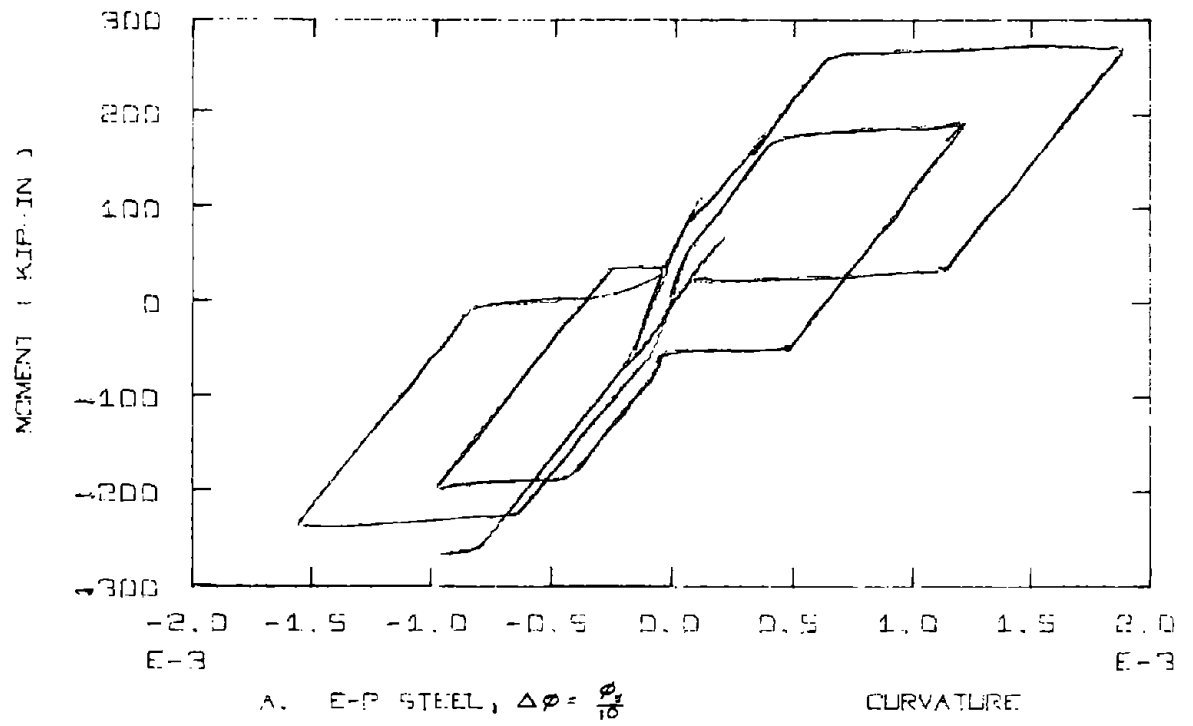


FIG. 4-6 - EFFECT OF INCREMENT SIZE ON THE  
MOMENT-CURVATURE RELATIONS

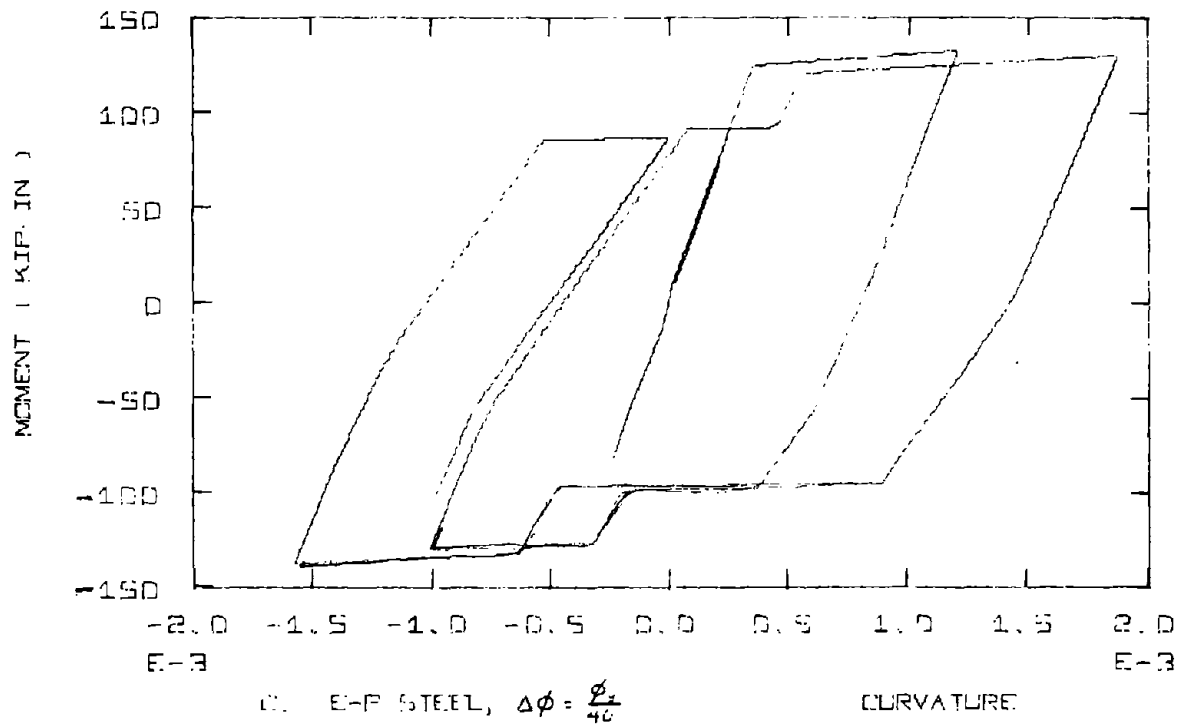
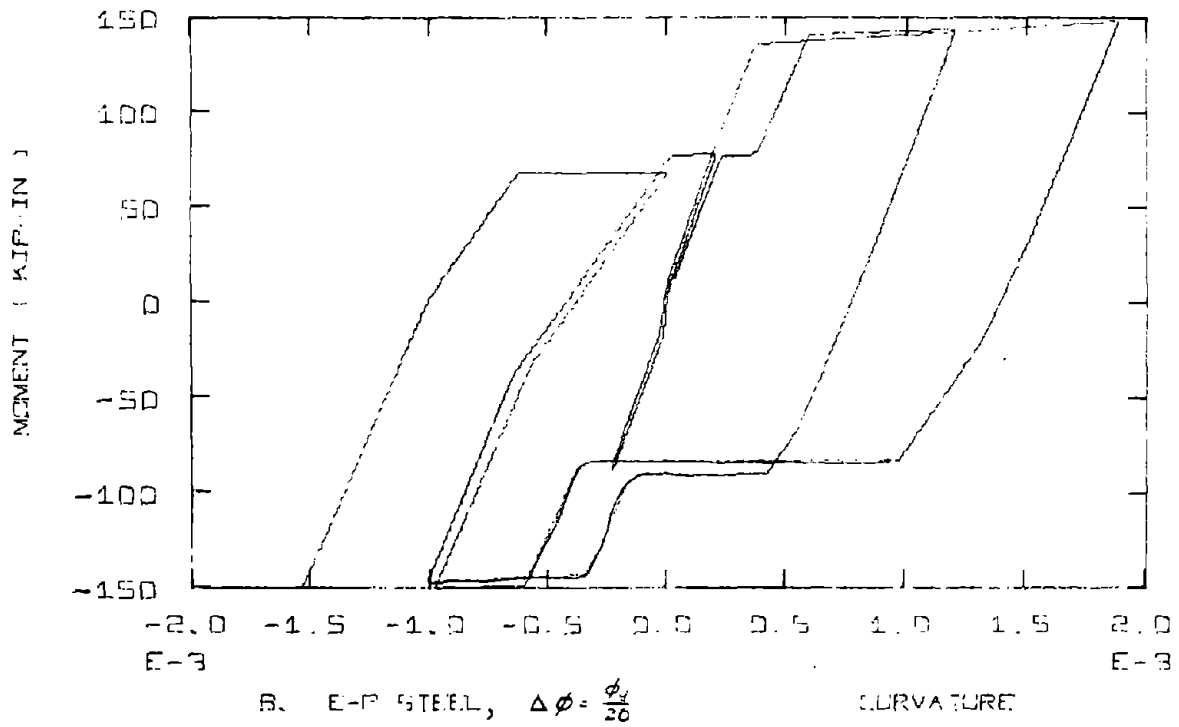


FIG. 4-6 (Continued)

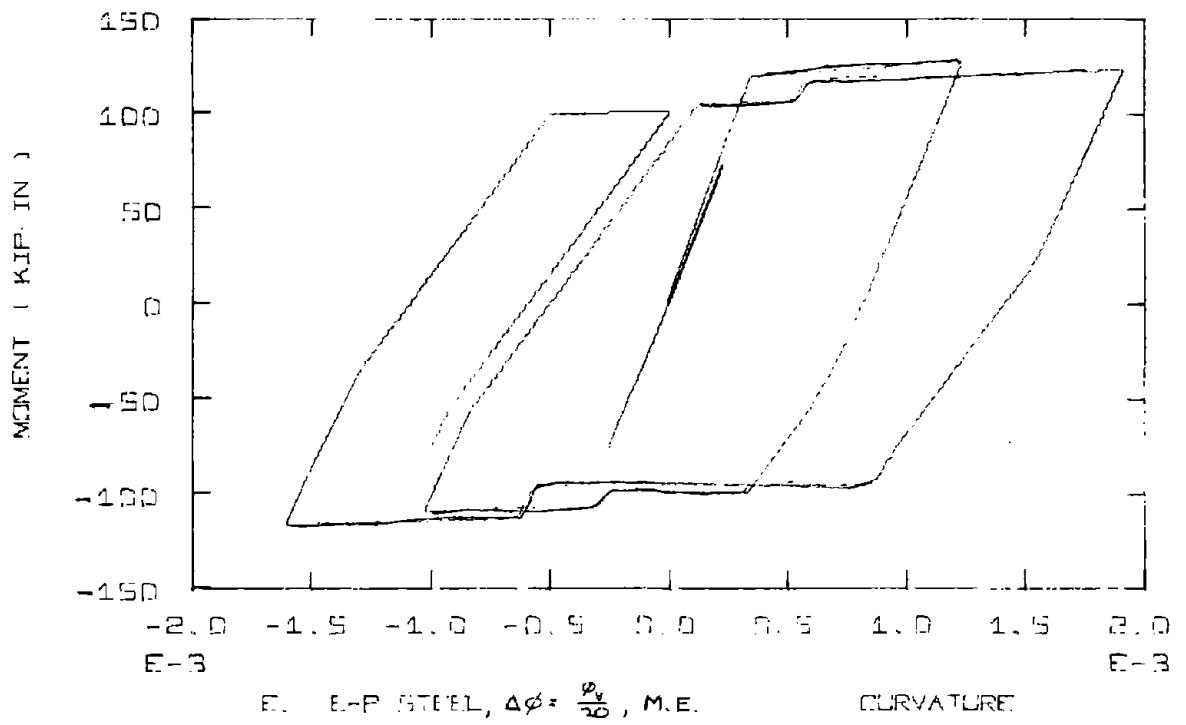
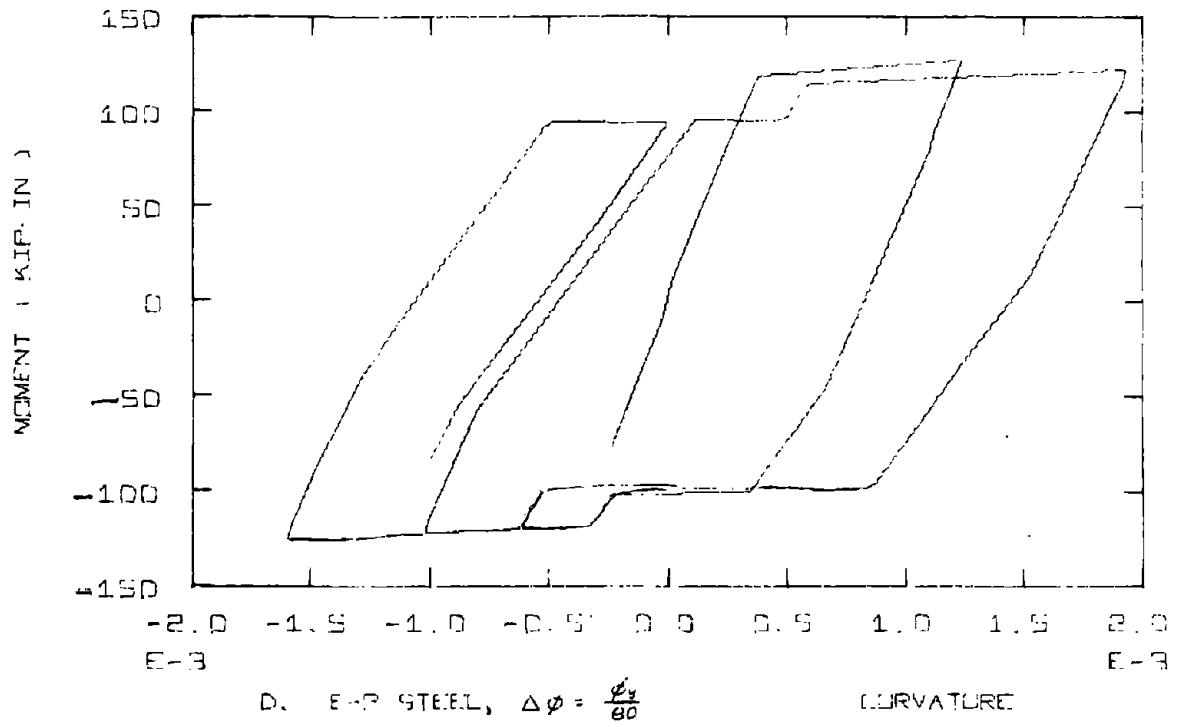


FIG. 4-6 (Continued)

At  $\phi_y/10$  the maximum moments are greatly overestimated. There is clearly an increase in moment capacity with the number of cycles and this reflects the accumulation of error. As the increment size is decreased, the maximum moments approach the experimental value. For increment sizes  $\phi_y/40$  and  $\phi_y/80$  the analytical results are close to each other.

The Modified Euler method, being a second-order formulation, provides results which stabilize at a larger increment size. In Fig. 4-6 E, the Modified Euler method is used with an increment size of  $\phi_y/20$ .

If the stiffness of the cross-section were constant, then for any choice of increment size the computed yield moment would be off by at most  $k\Delta\phi$ . However, the reinforced concrete section has a stiffness which continually varies. It is initially very stiff, since all concrete fibers are participating. But each fiber has little tensile capacity, and upon cracking, it no longer contributes to the section stiffness. In addition, the nonlinear stress-strain behavior of both steel and concrete fibers causes the stiffness to vary.

In the initial loading the stiffness is decreasing, so the Euler method will overestimate the moment until there is a direction change. This truncation<sup>\*</sup> error is the result of dropping higher order terms (i.e.,  $d^2M/dx^2 + \dots$ ) from the Taylor series represen-

---

\* Crandall (28)

tation of the moment. At the same time, roundoff error occurs because the number of significant figures retained in the computations is limited. For example, in single precision computer calculations, there are approximately 7 significant figures. As the increment size is decreased, the truncation error decreases, but the roundoff error increases. Decreasing the increment size indefinitely is therefore not the solution.

In this  $M-\phi$  study a comparison under monotonic loading was used to select an appropriate increment size. The standard of comparison was a formulation where equilibrium was enforced by iteration. The third curve is the moment-curvature relation obtained from the stress distribution at the points determined by the incremental stiffness approach. Figure 4-7(A to C) show examples of this comparison.  $\Delta\phi = \phi_y/80$  seemed to provide reasonable agreement for this example.

#### 4.5 CHARACTERISTICS OF THE MOMENT-CURVATURE RELATIONSHIP

The moment-curvature relationship is a function of the nonlinear behavior of both reinforcing steel and concrete and their interaction. To point out the typical characteristics of a doubly reinforced section under cyclic loading, an elasto-plastic steel and a linearized concrete model will be initially used.

Abrupt changes in the slope of the moment-curvature curve occur whenever the steel yields either in tension or compression,

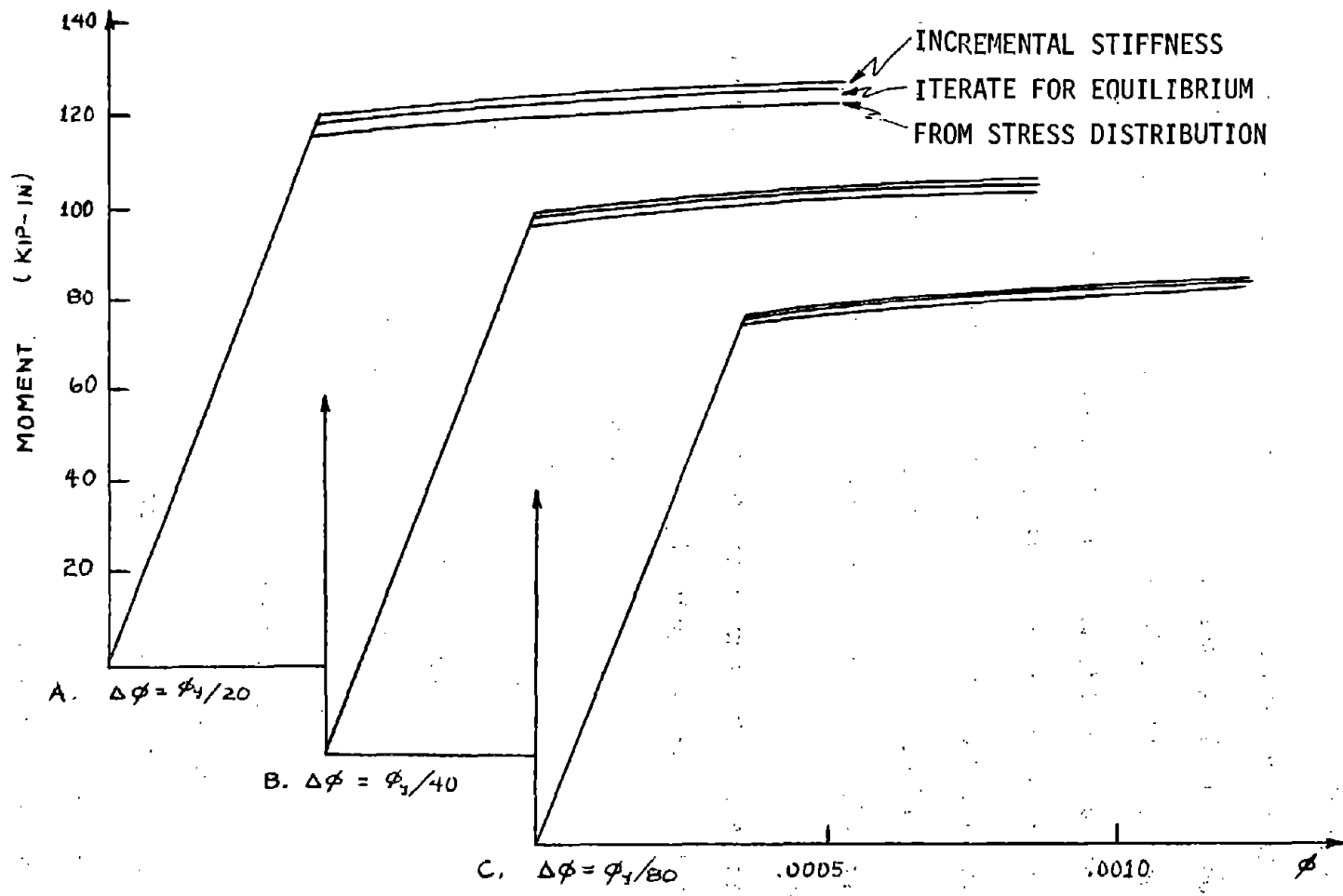


FIG. 4-7 - MOMENT-CURVATURE COMPARISONS TO DETERMINE INCREMENT SIZE

because most of the section stiffness is contributed by the reinforcement. Small curvature limits are used in Fig. 4-8 A and the  $M-\phi$  relationship reflects the reinforcing steel behavior as far as the occurrence of yield plateaus. At points A and E the tensile reinforcement has yielded, causing the corresponding drastic change in stiffness in the  $M-\phi$  curve. Between points C and D, the reduced stiffness is caused by the lack of concrete fibers contributing to the section stiffness. The fibers of the top of the beam have completely unloaded, while the bottom fibers have yet to come into compression.

In Fig. 4-8 B the same cross-section is subjected to a larger curvature before reversal (point B) takes place. There is a "kink" in the unloading branch at point D, a result of the bottom steel yielding in compression. At point B the bottom steel had incurred considerable straining in tension, and after an unloading strain of  $2\epsilon_y$ , it yielded in compression. Between points C and D no concrete participates. At E the fibers at the bottom begin to supply compressive strength and the stiffness of the cross-section increases substantially. Finally, the top steel yields in tension at point F and a yield plateau exists until reversal.

Approximate strain distributions corresponding to points B, D, E, F are shown in Fig. 4-8 C. For this symmetrically reinforced cross-section the yield moments in both directions are approximately the same. In the case of the reloading beginning at G, similar comments are applicable.

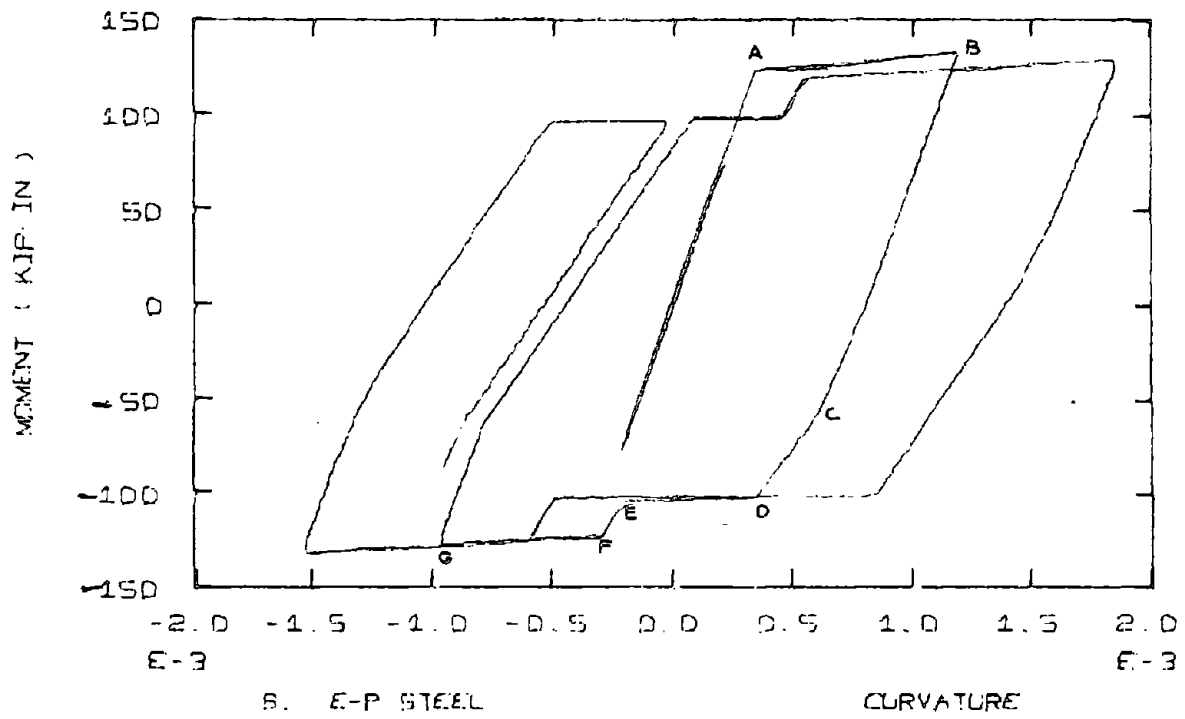
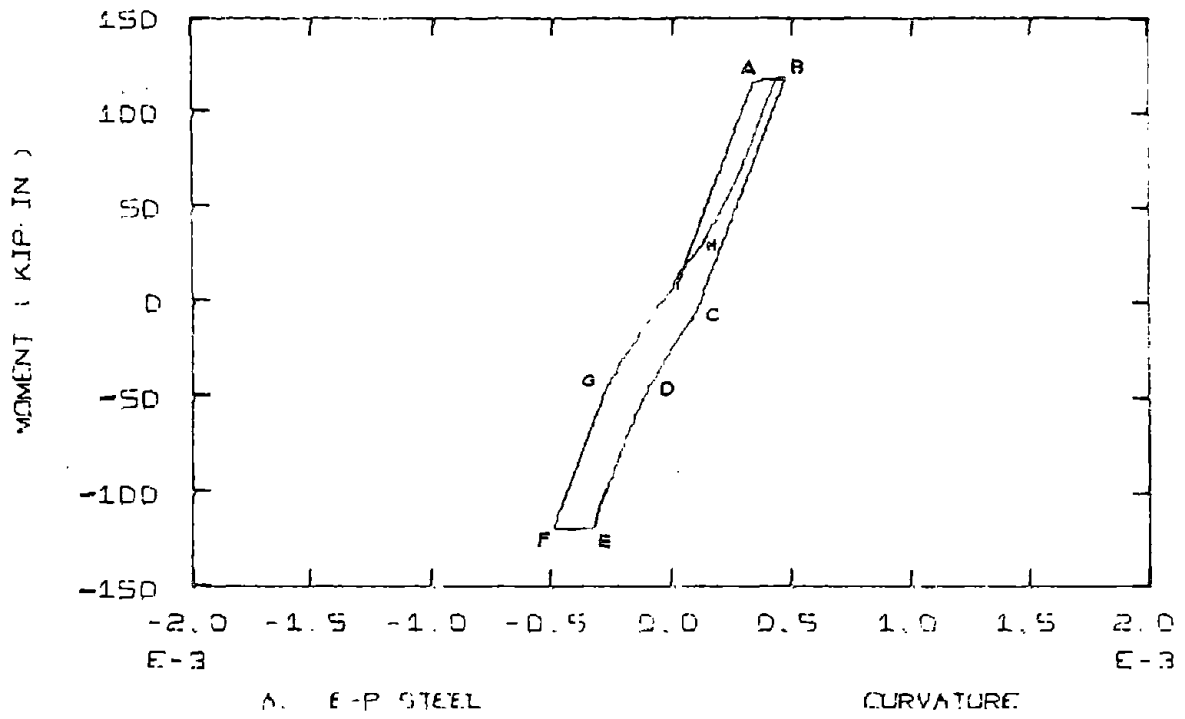
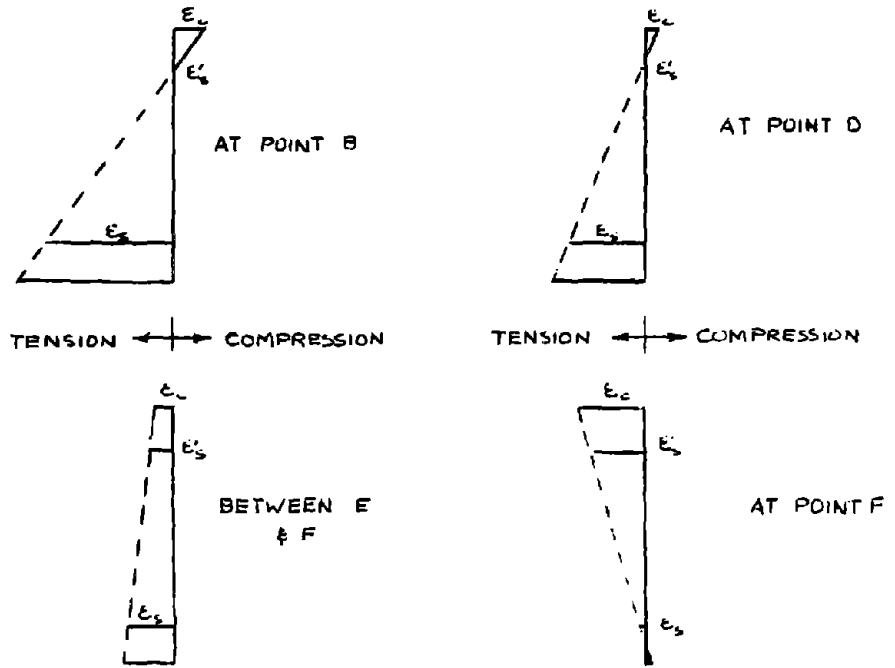


FIG. 4-8 - CHARACTERISTICS OF THE MOMENT-CURVATURE RELATIONSHIP



C. STRAIN DISTRIBUTION

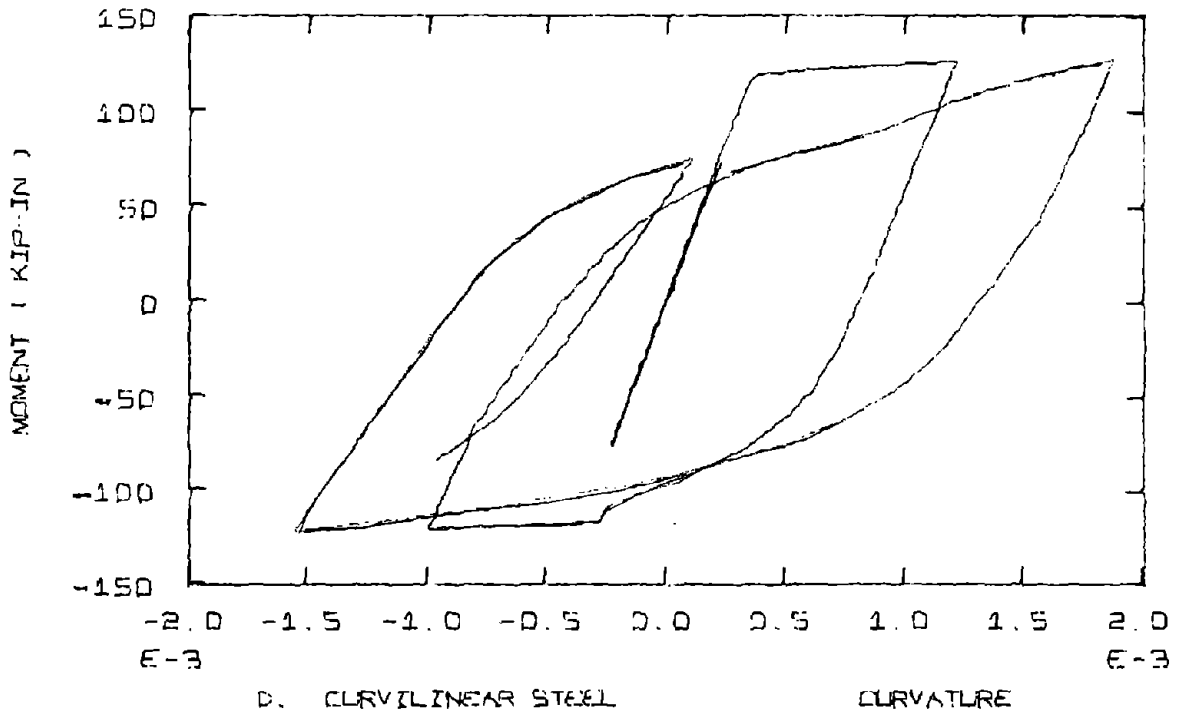


FIG. 4-8 (Continued)

When a steel formulation with the Bauschinger effect (Fig. 4-8 D) is used, these  $M-\phi$  transition points will not be so distinct. In particular, except for the initial yielding, yield plateaus will not occur.

#### 4.6 EFFECT OF AXIAL FORCE ON CYCLIC LOADING

##### 4.6.1 Constant Axial Force

The fiber model with the incremental stiffness approach is used in this section to study the effect on a cross section of combined bending and axial deformation. The formulation automatically takes into consideration the coupling between moment and axial force.

Figure 4-9 is an interaction diagram relating the axial force to the moment capacity of the cross-section. An excellent discussion of interaction diagrams and moment-curvature behavior for monotonic loading is given by Pfrang, Siess, Sozen<sup>(22)</sup>. From the moment-curvature curves, Figs. 4-10 and 4-11, each corresponding to a particular axial force, the maximum moment and the applied axial force, are obtained, and they represent a point on the interaction diagram. The long descending branches on the moment-curvature curves reflect the descending branch assumed for the concrete stress-strain curve.

With an axial force there are two distinct types of behavior for monotonic loading. The first is characterized by significant ductility due to the yielding of the tensile reinforcement. The

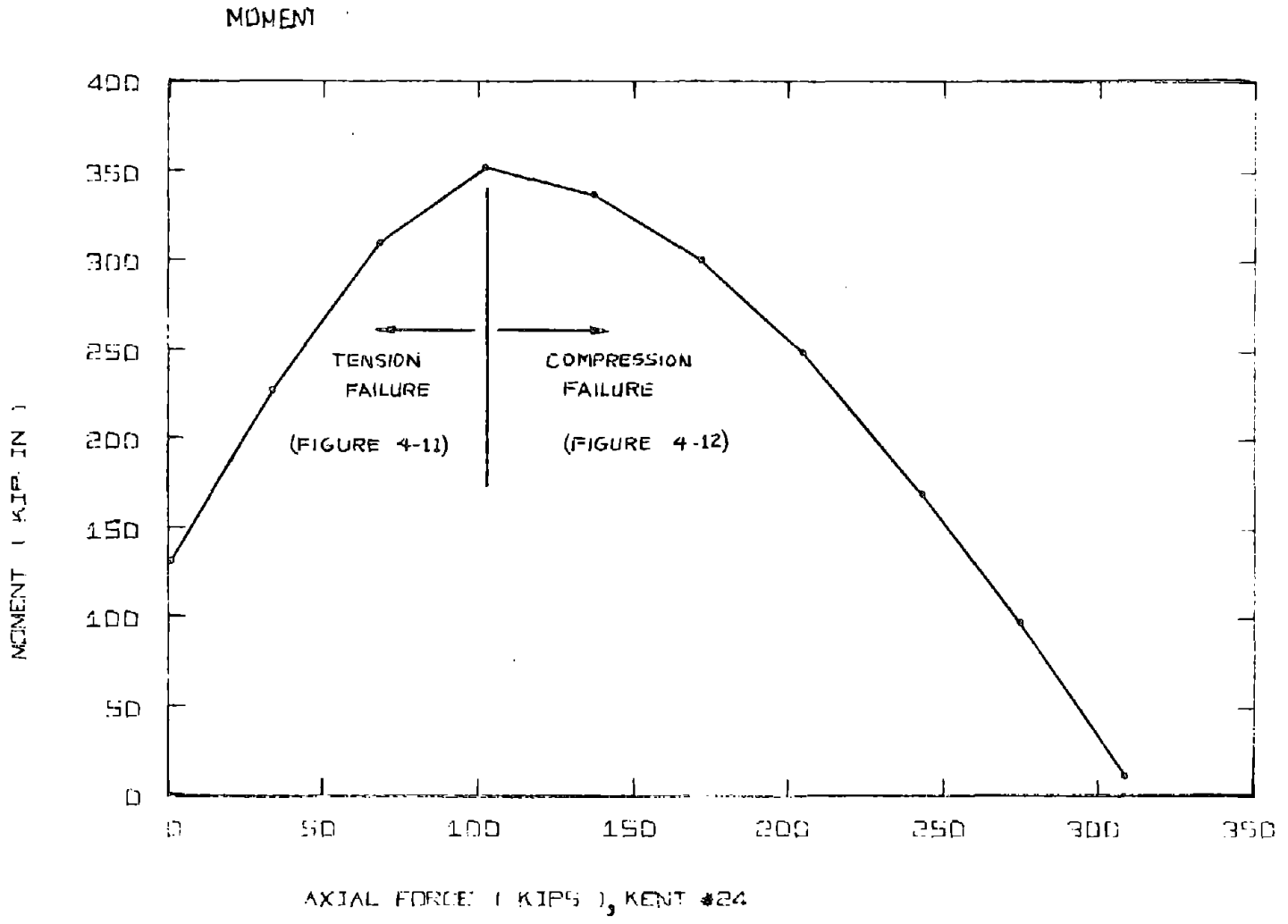


FIG. 4-9 - INTERACTION DIAGRAM (MOMENT VS. AXIAL FORCE)

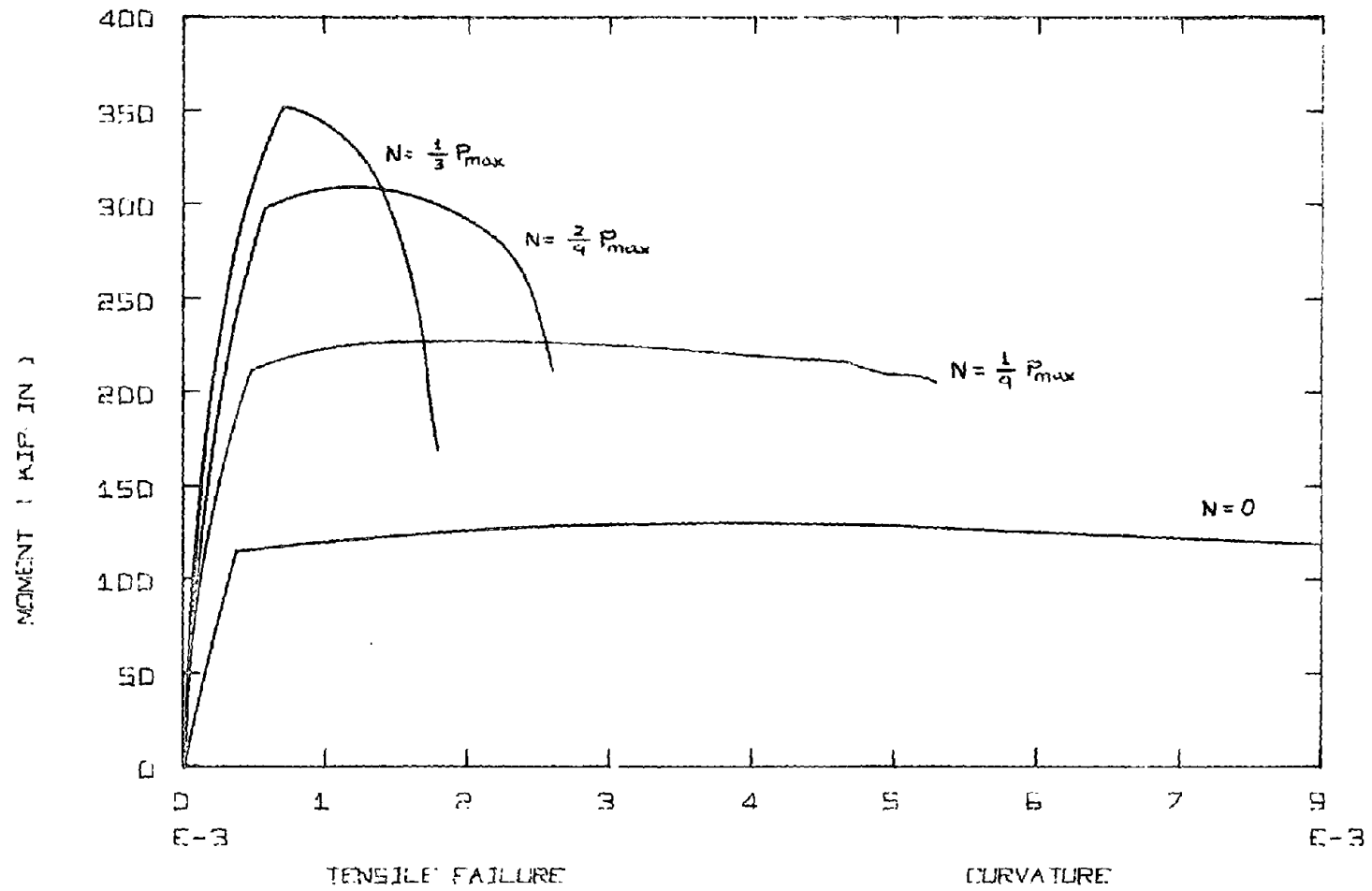


FIG. 4-10 - MOMENT VS. CURVATURE FOR VARYING AXIAL FORCES

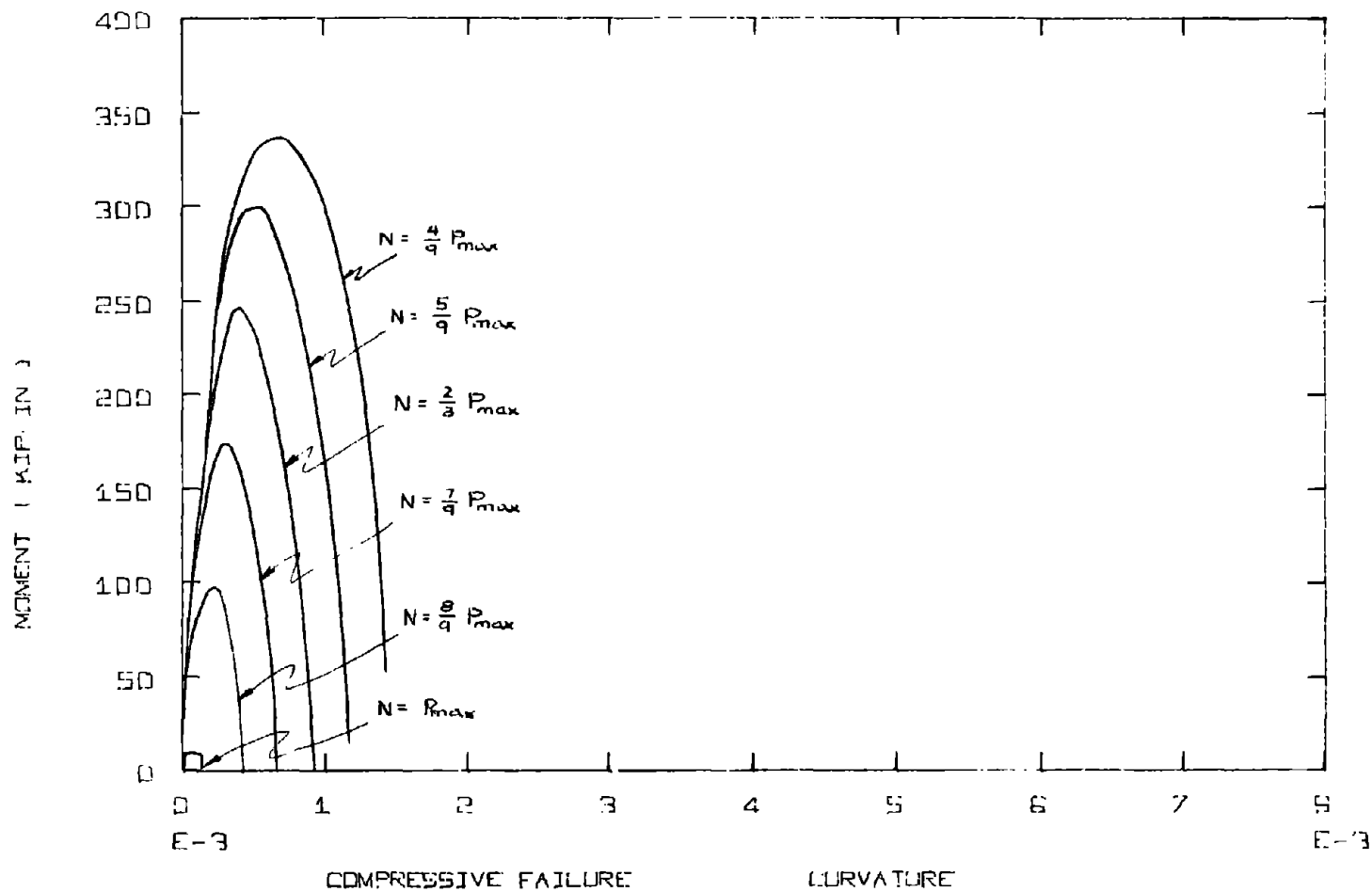


FIG. 4-11 - MOMENT VS. CURVATURE FOR VARYING AXIAL FORCES

doubly reinforced section with no axial force can sustain a large curvature before the extreme concrete fibers fail in compression. As the axial force is increased, the initial stiffness and the maximum moment capacity increase, while ductility decreases. Eventually a point is reached where the tensile reinforcement just yields as the extreme concrete fiber reaches its descending branch. This is the balance point which separates the tensile mode of failure from the compressive mode. With additional axial force, the moment capacity decreases and is limited by the strength of the concrete. Failure then occurs due to crushing of the concrete fibers before the tensile steel can yield.

Figure 4-12 (A to D) shows the effect of constant axial force on cyclic loading using an elasto-plastic steel. The applied axial force varies from 0. to  $\frac{2}{9} P_{\max}$ , where  $P_{\max}$  is the maximum short column load the section can take with no bending moment. The section is again Kent's beam #24, and curvature limits were arbitrarily set at  $\pm .0012$  for this example. An increment size of  $\Delta\phi \approx \phi_y/80$  was used.

In Fig. 4-12 A, no axial force is applied. The initial loading and unloading branches are stiffer than those in subsequent cycles. In addition, the moment capacity is slightly larger in the first loading cycle. These effects are due to the greater participation of the concrete fibers.

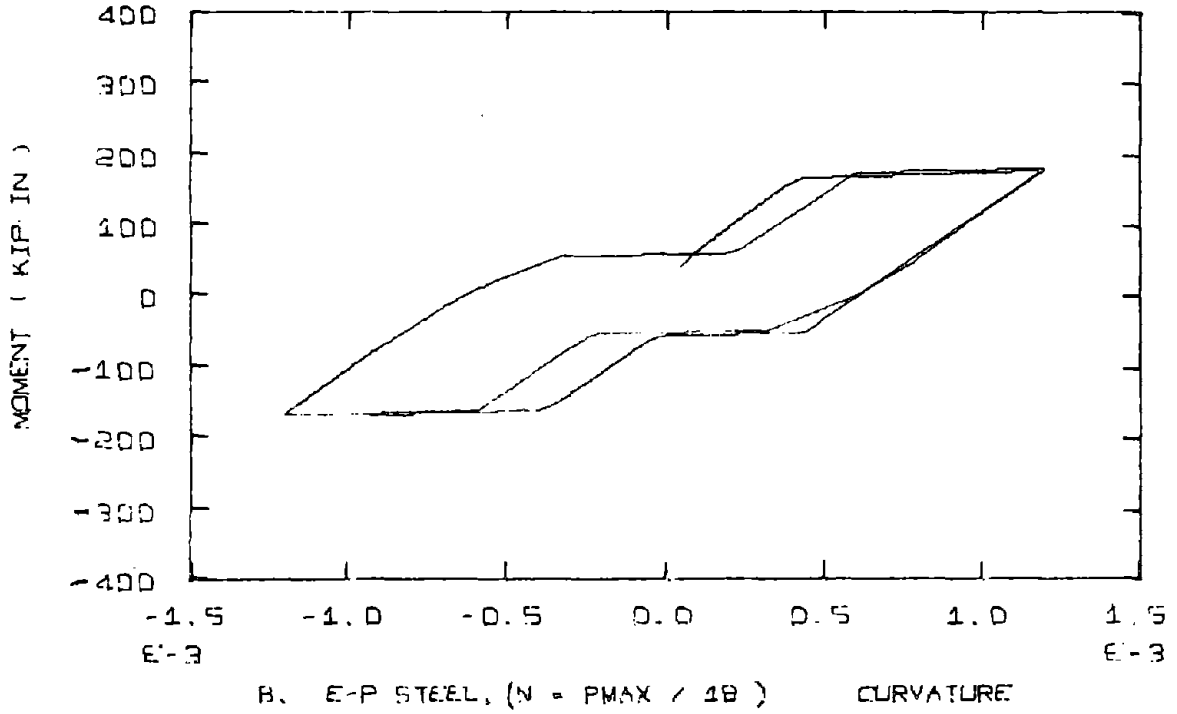
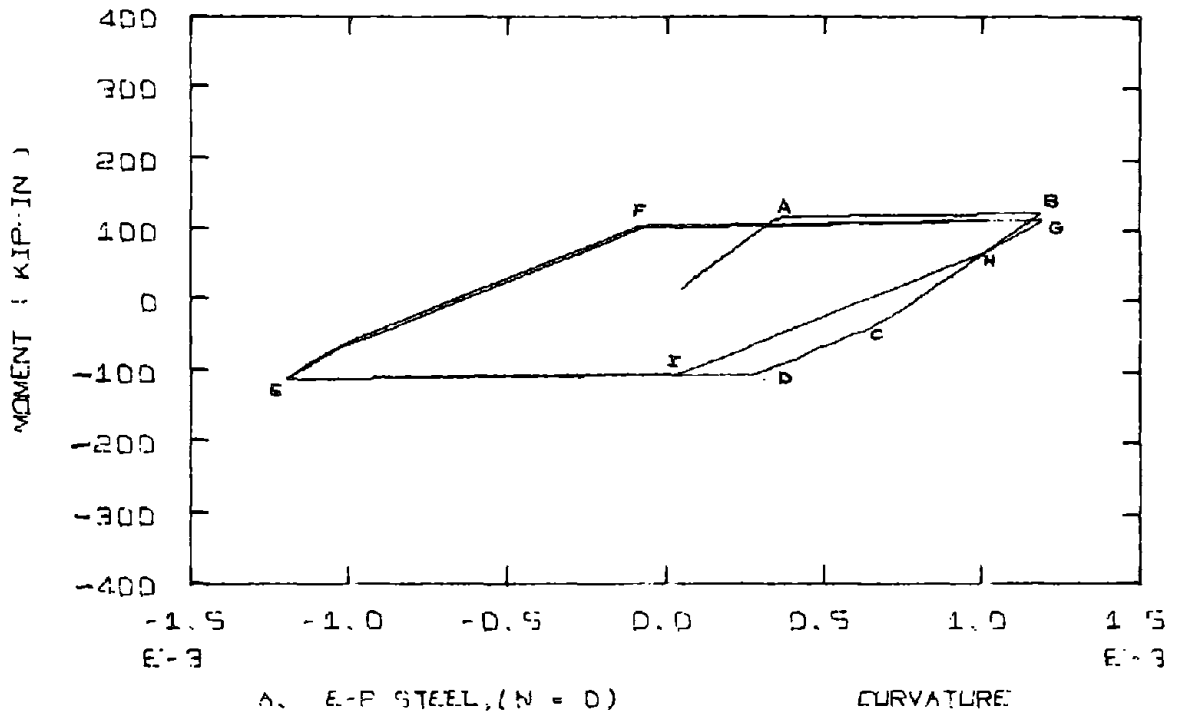


FIG. 4-12 - CYCLIC MOMENT-CURVATURE RELATIONS WITH AN AXIAL FORCE

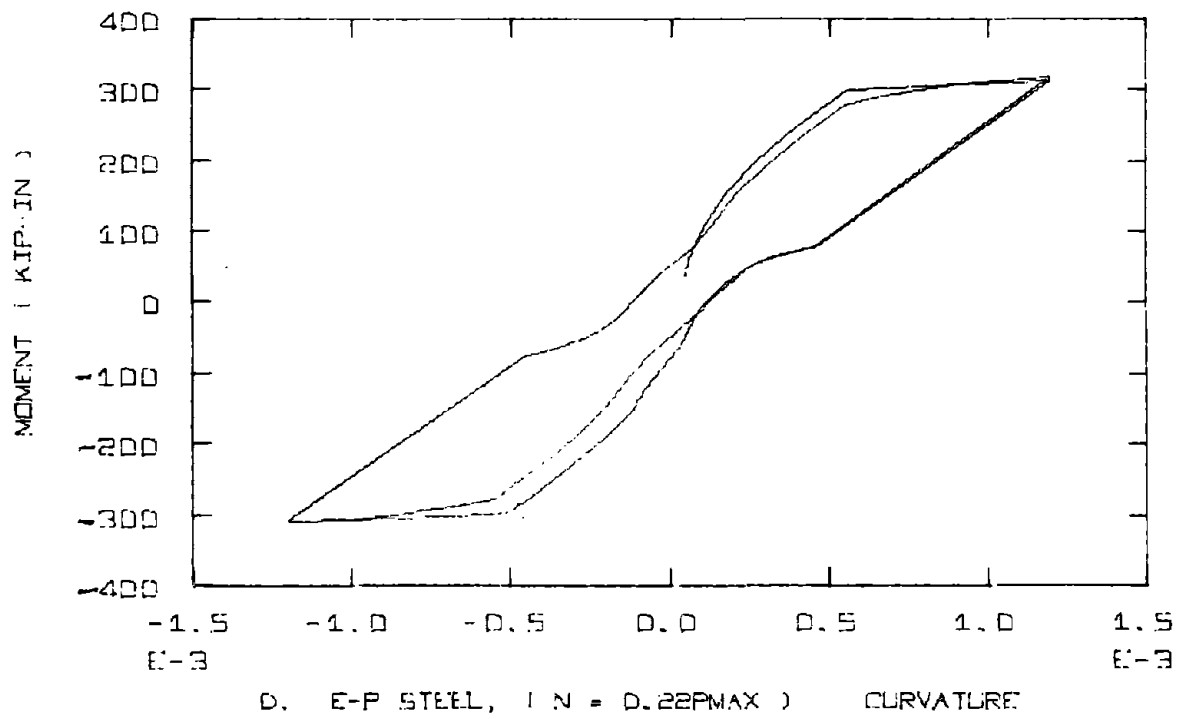
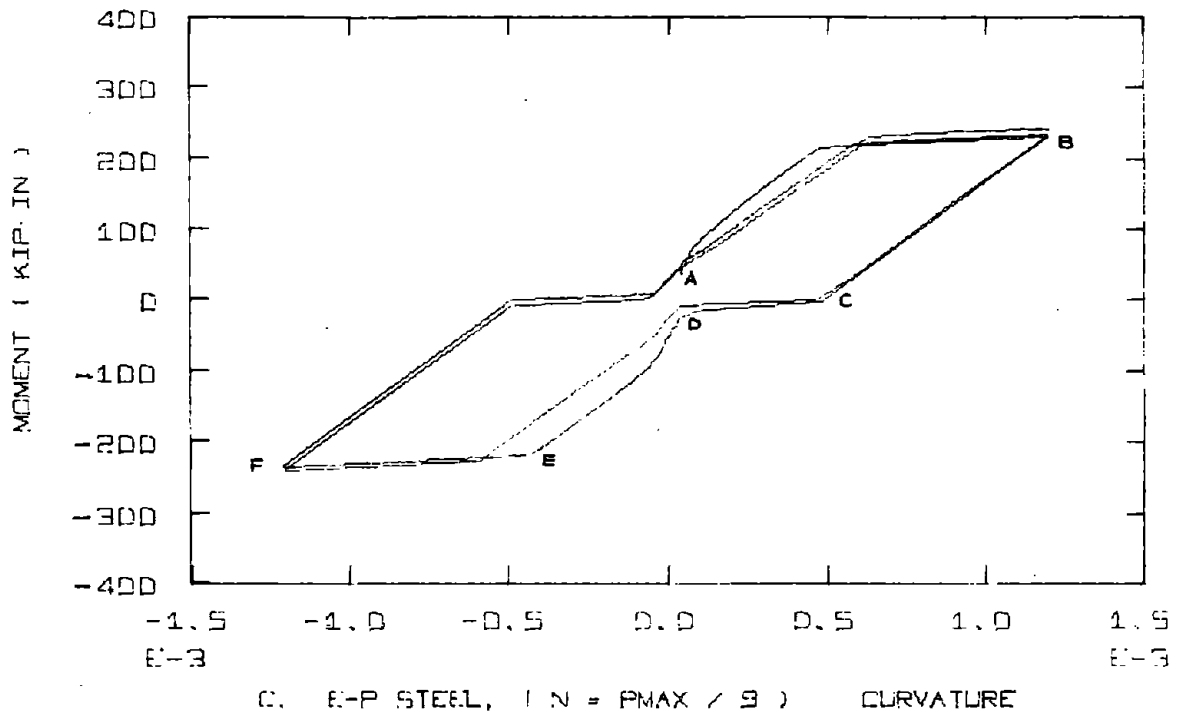


FIG. 4-12 (Continued)

Figures 4-12 (B to D) show moment-curvature relations for axial forces that still allowed some ductility in the section. The predominant effects of the axial force are the increase in moment capacity and the "squeezing-in" of the middle of the loops. The latter occurs when the reinforcement which previously yielded in tension now yields in compression. This is followed by the participation of the cracked concrete fibers as the crack closes.

As the axial force is increased, the pinching effect increases, and the hysteresis loop resembles the number "8". With further increase in axial force up to  $\frac{2}{9} P_{\max}$ , the concrete fibers begin to reach their descending branches and the moment-curvature relationship becomes curved rather than always reflecting the elasto-plastic steel used.

Another aspect of the cross-section behavior is the variation of the centroidal strain with the cyclic loading. In Fig. 4-13 A a plot of moment vs. strain is shown for cyclic loading with no axial force (corresponding to the moment-curvature curve in Fig. 4-12 A). The letters indicate corresponding points on both figures. In the initial loading, the strain becomes increasingly tensile. For the unloading cycle  $\overline{BCDE}$ , the tensile strain decreases up to  $D^*$ , then increases to point E. At point D the bottom steel which had previously yielded in tension yields in compression; the section is now behaving as a singly reinforced section. When the top steel finally yields at  $D^*$  the sign of the  $a_{12}$  stiffness coefficient will change.

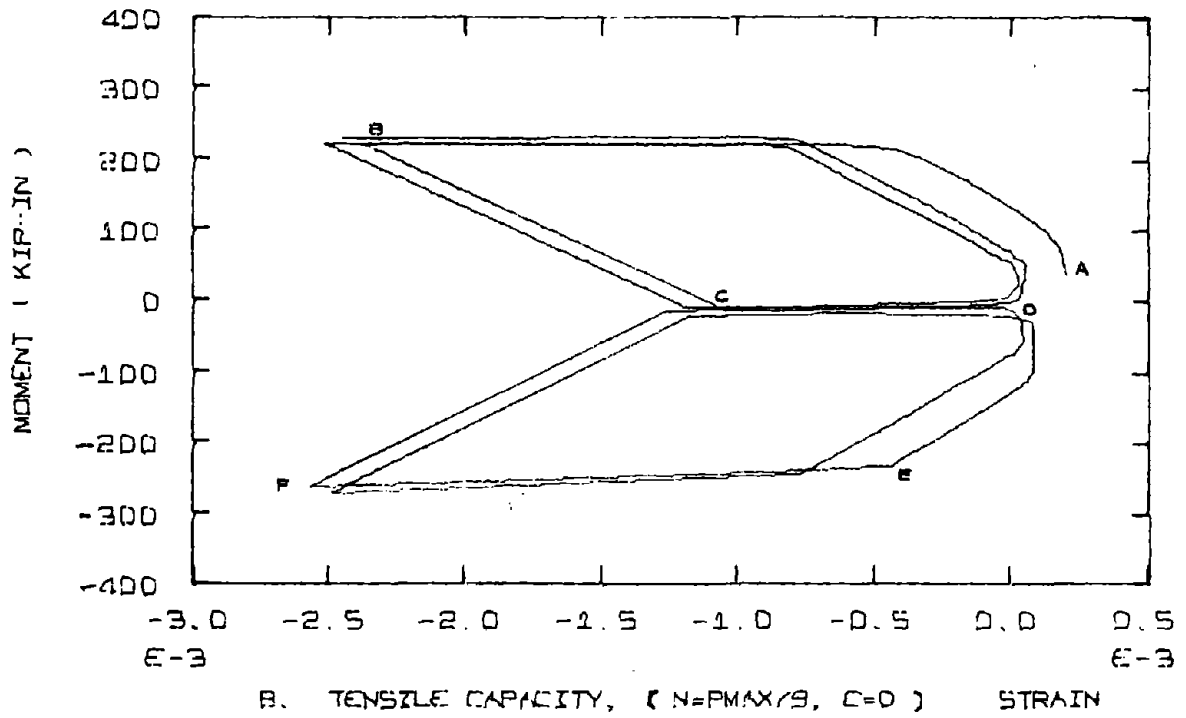
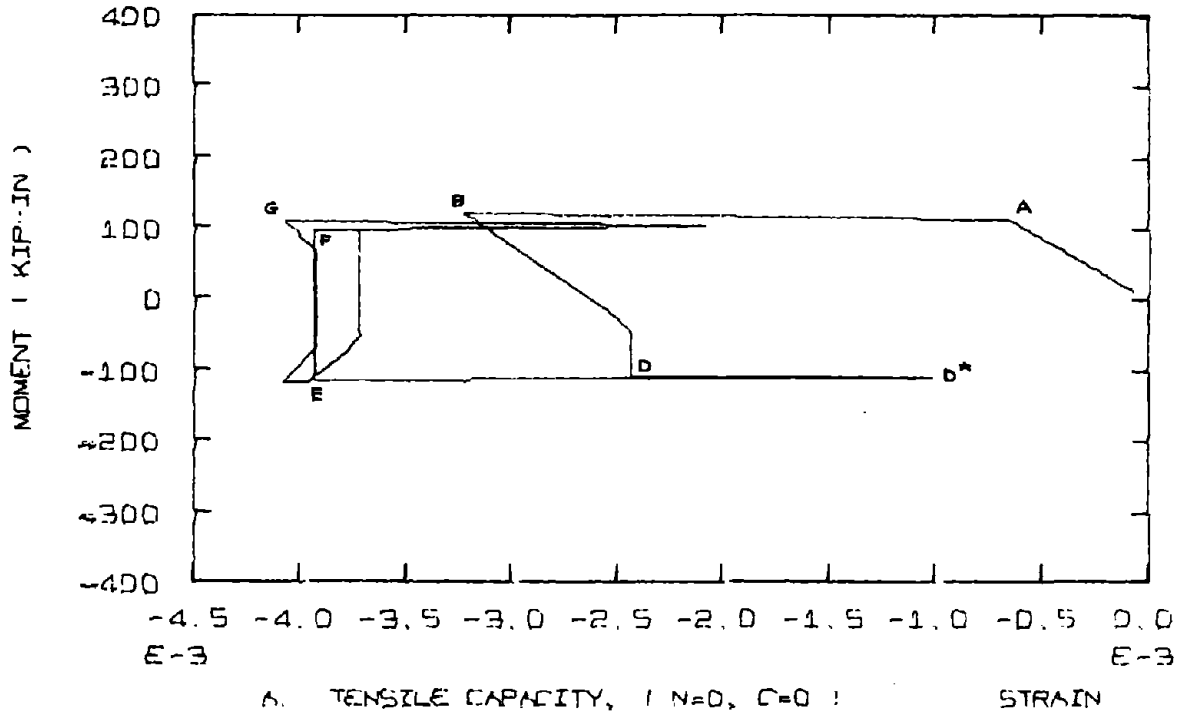


FIG. 4-13 - MOMENT VS. AXIAL STRAIN WITH AN AXIAL FORCE

Since  $\Delta\varepsilon = (-a_{12}/a_{11})\Delta\phi$ , and  $\Delta\phi$  and  $a_{11}$  retain the same sign, the centroidal strain now begins to change direction.

Figure 4-13 B illustrates the situation when an axial force,  $P_{\max}/9$ , is applied (corresponding to the moment-curvature curve in Fig. 4-12 C.) The strain is initially compressive because of the axial force, but becomes tensile in the first loading cycle. The loading and unloading moment-strain path has taken the shape of an "S" and can be followed by observing the segment  $\overline{ABCDEF}$ .

The effect of using a more realistic, curvilinear steel for the moment-curvature relations with axial force is shown in Fig. 4-14 (A to D). The Improved SGT steel is used and those curves more closely resemble the experimental ones.

One of the few experimental studies on moment-curvature behavior with axial loads was carried out by Parducci and Ferretti.<sup>(27)</sup> An example of their experimental results is shown in Fig. 4-15 (A to F). The general shape agrees with the analytical studies carried out in this thesis. Unfortunately this paper did not contain sufficient information on the steel and concrete strengths to be able to analytically duplicate their results. The larger stiffness of this initial cycle has been accounted for in the analytic model as was the stability of subsequent cycles when an axial force is applied. Parducci & Ferretti showed that with axial force the moment capacity decreases significantly with the number of cycles. To account for this, the analytic model should have a failure criteria for the concrete, and

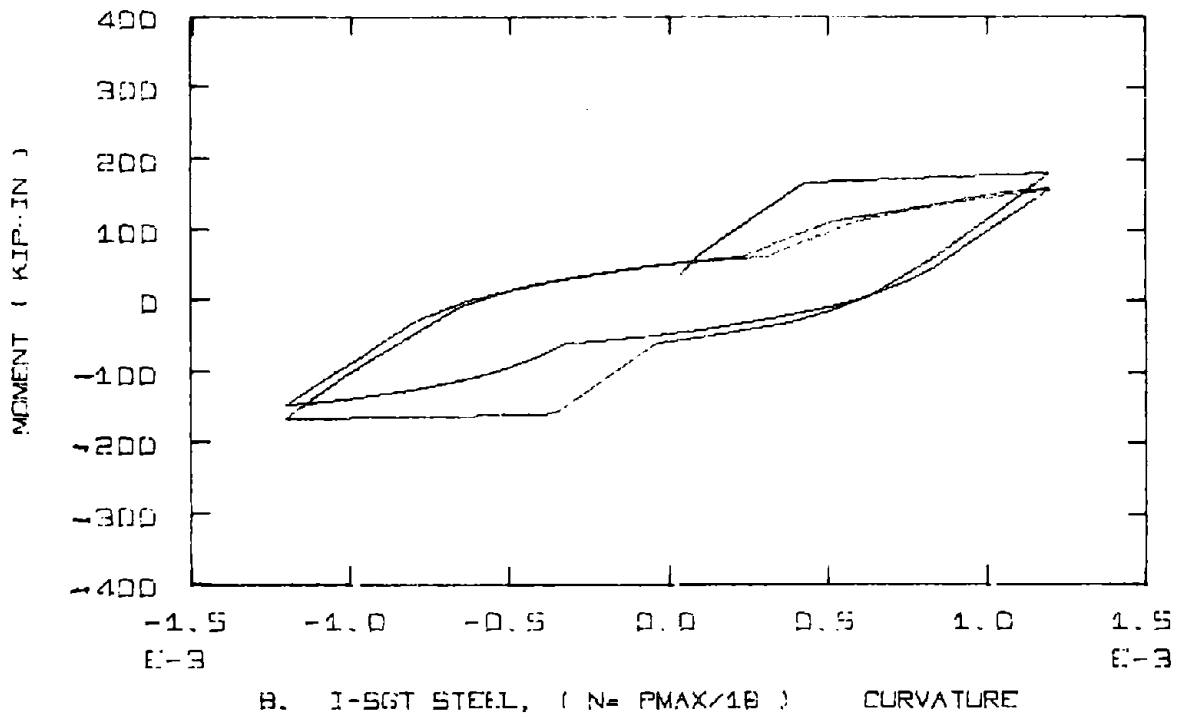
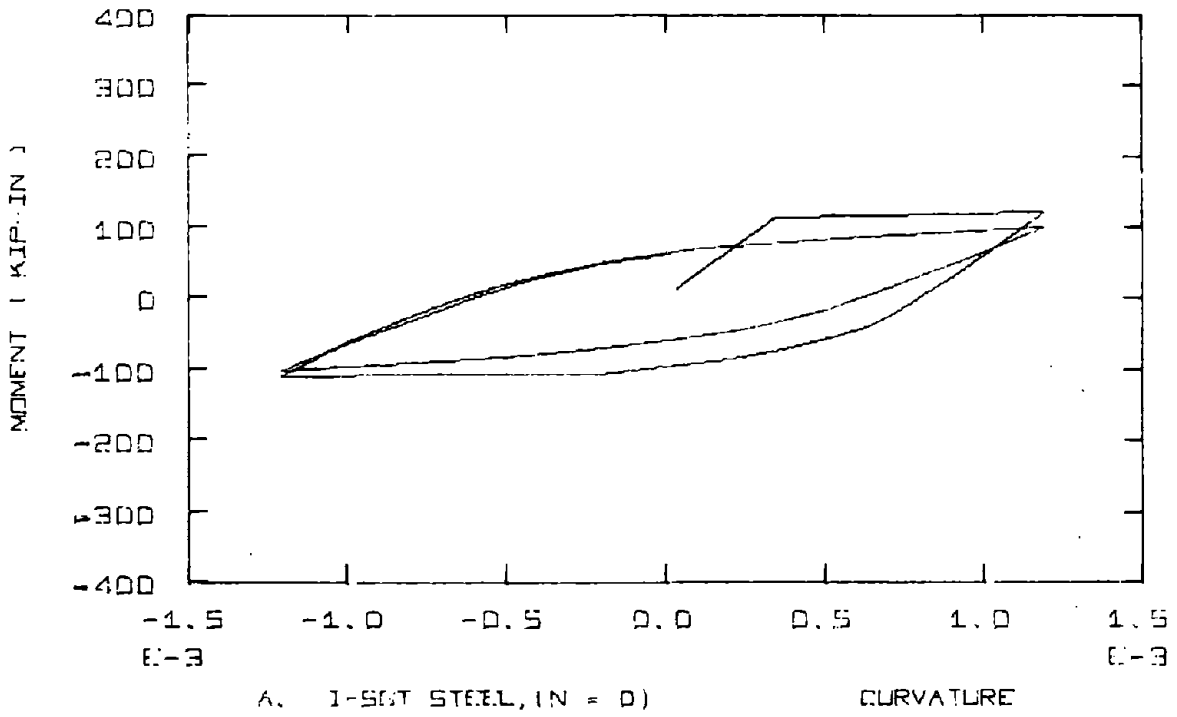


FIG. 4-14 - CYCLIC MOMENT-CURVATURE RELATIONS WITH AN AXIAL FORCE

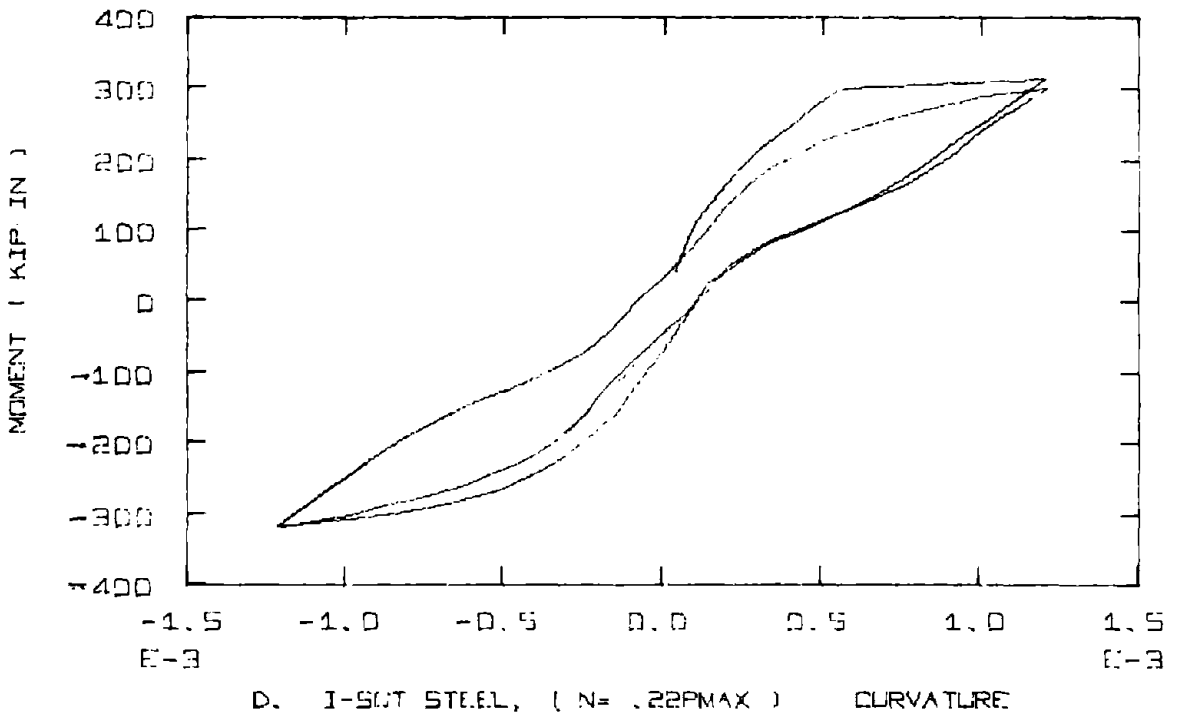
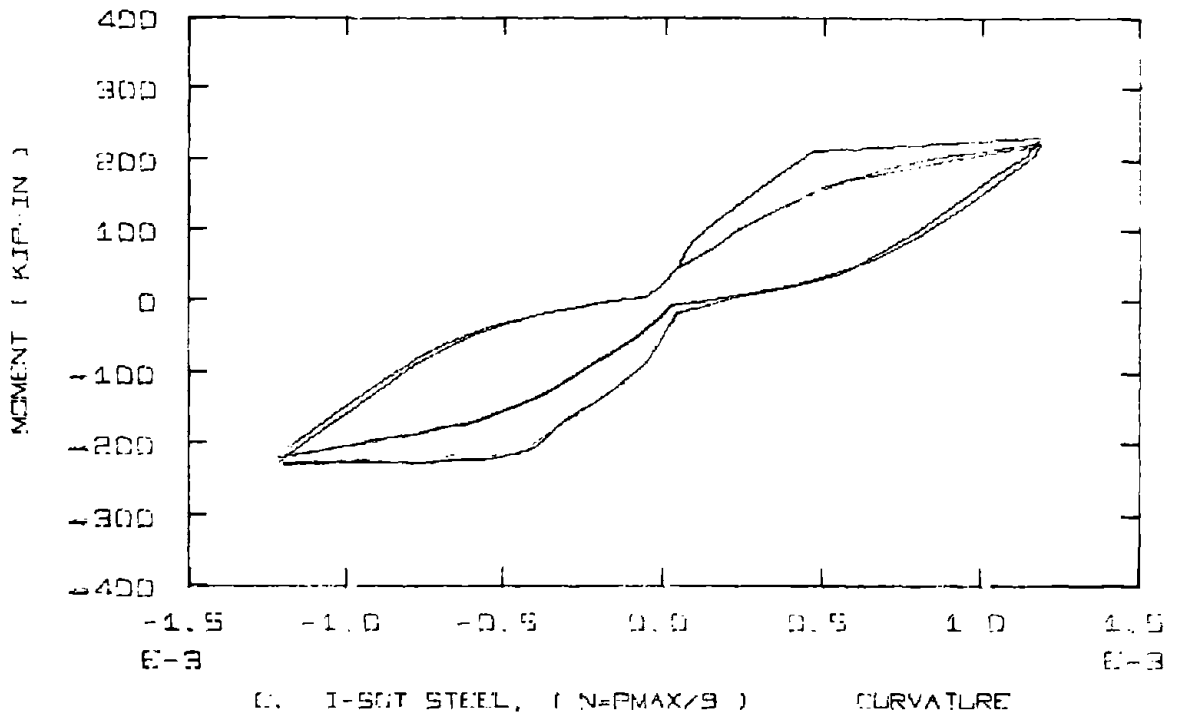


FIG. 4-14 (Continued)

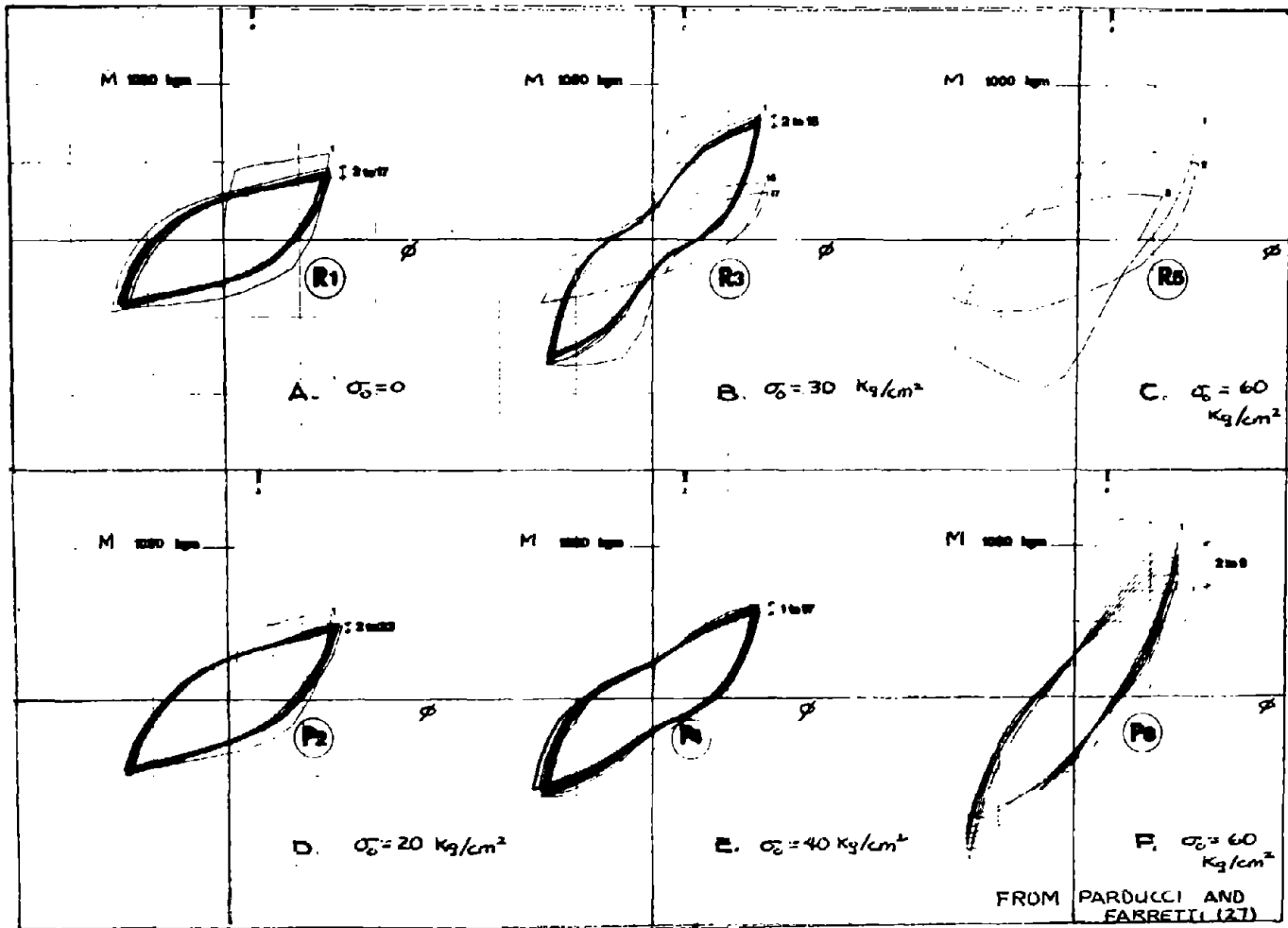


FIG. 4-15 - EXPERIMENTAL MOMENT-CURVATURE RELATIONSHIP WITH AN AXIAL FORCE

consider buckling of the compressive reinforcement when the surrounding concrete has spalled.

Finally, Fig. 4-16 (A and B) illustrate the effect of an axial force that is tensile. There is concrete participation in the first loading and unloading cycles, but thereafter the section becomes a steel couple.

#### 4.6.2 Axial Force Proportional to the Moment

In a typical frame, Fig. 4-17A, the columns will have a constant axial force  $V_0$ , and a smaller distributed axial force due to the dead load. When the frame is laterally loaded, additional axial forces will develop in the columns; tension in one and compression in the other. For many practical cases,  $V_0$  will be much larger than the laterally-induced axial forces, and the behavior of the frame will be essentially the same as the constant axial force case. However, this may not be true for tall slender frames. In addition, many experimental tests are carried out without large loads in the columns and the axial forces resulting from the lateral loading can significantly affect the behavior.

For a particular incremental lateral load or displacement, incremental axial forces and moments will be induced at each cross-section. The incremental axial force will be approximately proportional to the incremental moment, although the ratio may not be constant as the behavior becomes significantly nonlinear. To con-

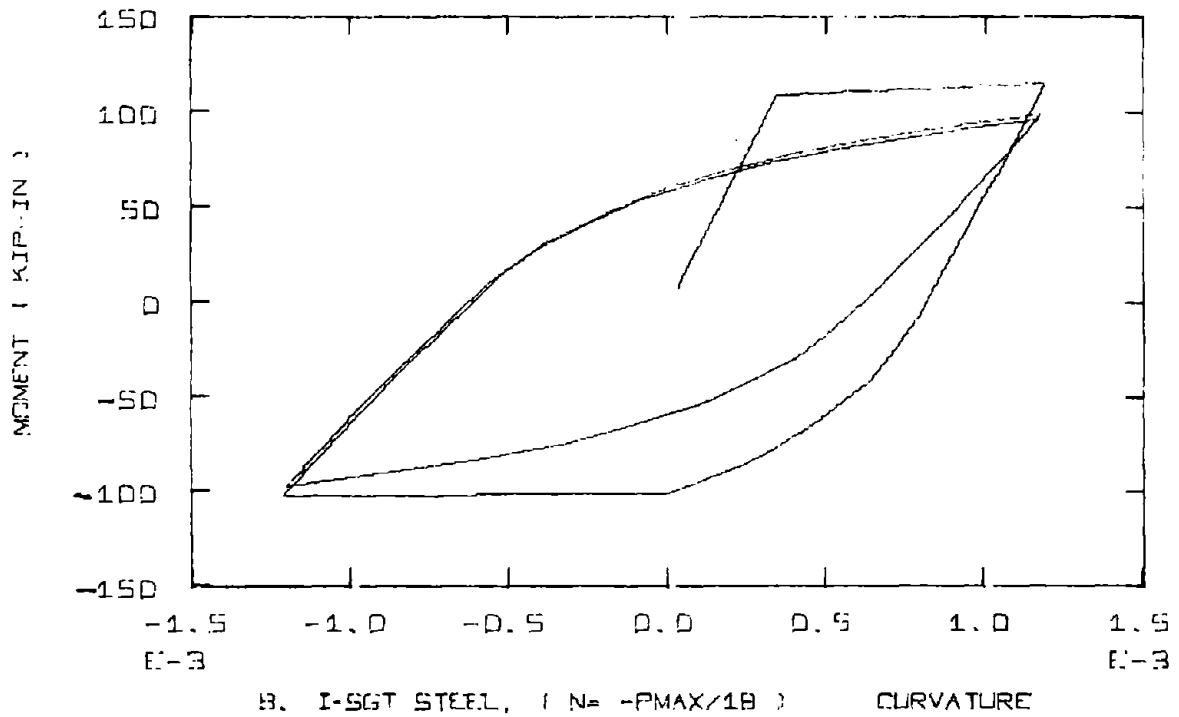
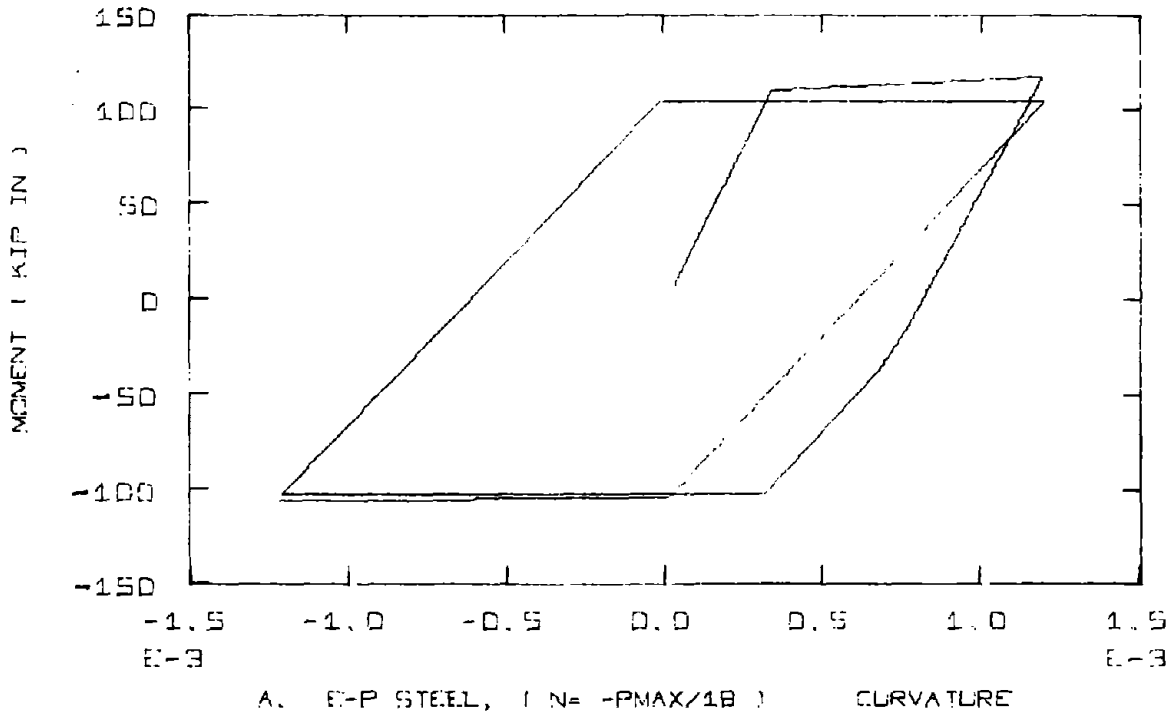


FIG. 4-16 - CYCLIC MOMENT-CURVATURE RELATIONS WITH A TENSILE AXIAL FORCE

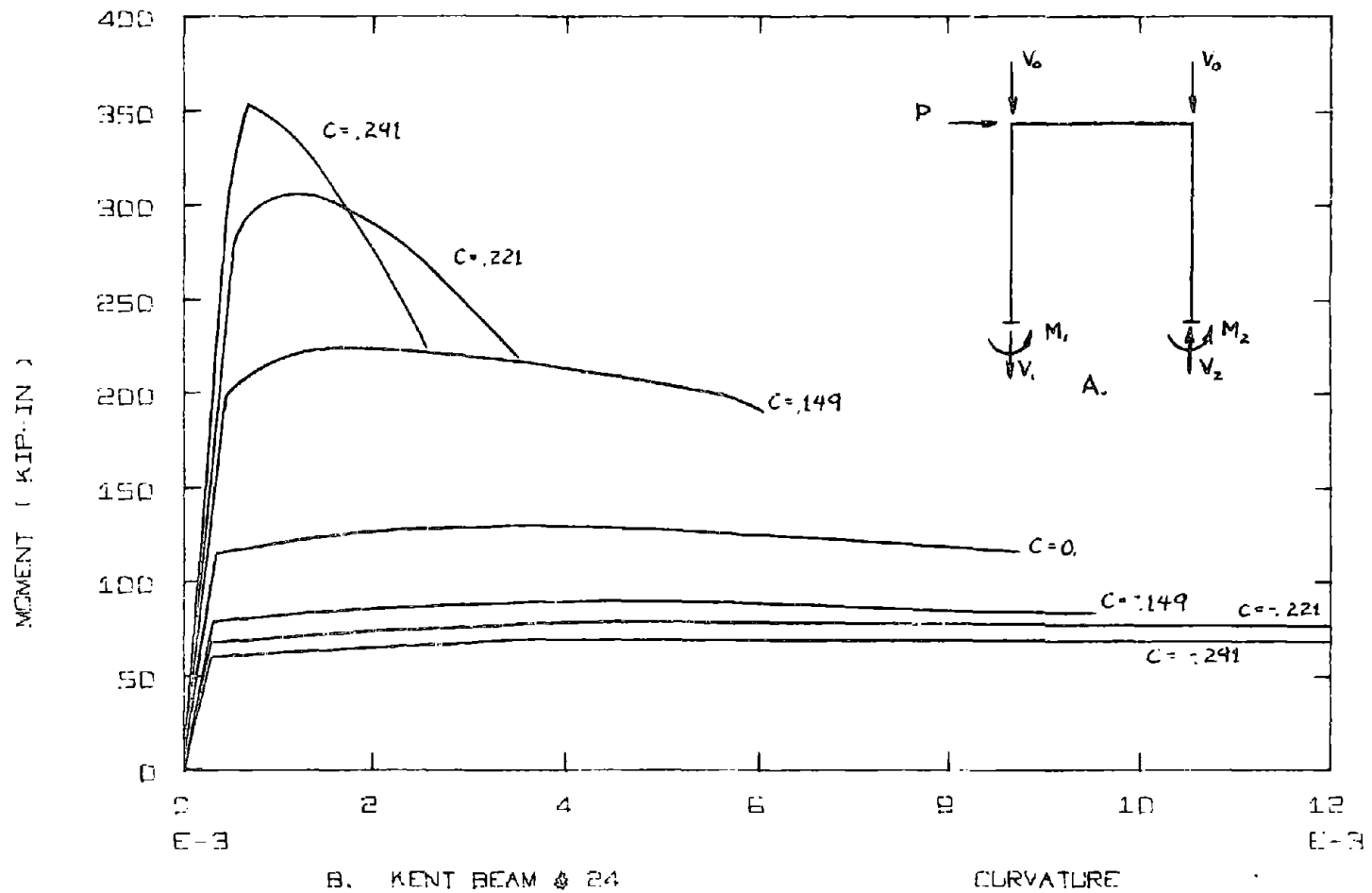


FIG. 4-17 - MOMENT-CURVATURE RELATION FOR AN AXIAL FORCE THAT VARIES WITH MOMENT

sider the situation when axial force is proportional to moment, the following equation is used:

$$\Delta N = c \Delta M \quad (4.5)$$

where  $c$  is a constant of proportionality which has the units of  $\text{length}^{-1}$ . The parameter  $c$  can be positive or negative. A positive  $c$  will mean that when moment increases, an incremental compressive axial force is applied.

For any cross-section in the frame, the value of  $c$  would depend on the location of the cross-section, the dimensions of the structure, and the support conditions.

Substitution of the above equation results in:

$$\begin{aligned} c\Delta M &= a_{11} \Delta \epsilon + a_{12} \Delta \phi \\ \Delta M &= a_{12} \Delta \epsilon + a_{22} \Delta \phi \end{aligned} \quad (4.6)$$

In order to obtain the moment-curvature,  $\Delta \phi$  is specified and  $\Delta M$  and  $\Delta \epsilon$  are computed from the stiffness coefficients. Solving for  $\Delta M$ ,  $\Delta \epsilon$  :

$$\begin{aligned} \Delta M &= \frac{a_{22} a_{11} - a_{12} a_{12}}{a_{11} - a_{12} c} \Delta \phi \\ \Delta \epsilon &= \frac{a_{22} c - a_{12}}{a_{11} - a_{12} c} \Delta \phi \end{aligned} \quad (4.7)$$

If  $c = 0$ , these equations revert back to the incremental stiffness equation of Section 4.3 (Eqn. 4.2).

In Fig. 4-17 moment-curvature relations for tensile failure modes are shown for different values of  $c$ . The values of  $c$  were chosen such that when the maximum moment occurred, the cross-section would have the same  $N/M_{\max}$  ratios as the curves in Fig. 4-10, in which the axial force is constant. For example,  $c = .149$  corresponds to the case where  $N = P_{\max}/9$ .

In comparing the moment-curvature curves for these two figures, the moment capacities have not changed for corresponding curves. However, there are slight differences in the descending branches. For the varying axial force case, the axial force is also decreasing in this range, since it is proportional to the moment. The varying axial forces provide slightly greater ultimate curvatures. For negative values of  $c$ , the moment capacity decreases and ductility increases. With larger negative  $c$  values, the doubly reinforced cross-section may become a steel couple.

The effect of cyclic loading is shown in Fig. 4-18 (A to E), where the parameter  $c$  ranges from .221 to .010. In the loading and reloading stages, incremental compressive forces are applied, while in unloading, incremental tensile forces are applied. The compressive axial force increases the positive moment, while a tensile one decreases the negative moment capacity.

The primary effect of an axial force which varies with moment is a significant decrease in the area enclosed by the hysteresis loops. In Fig. 4-18 A, for example, there is a long yield plateau,

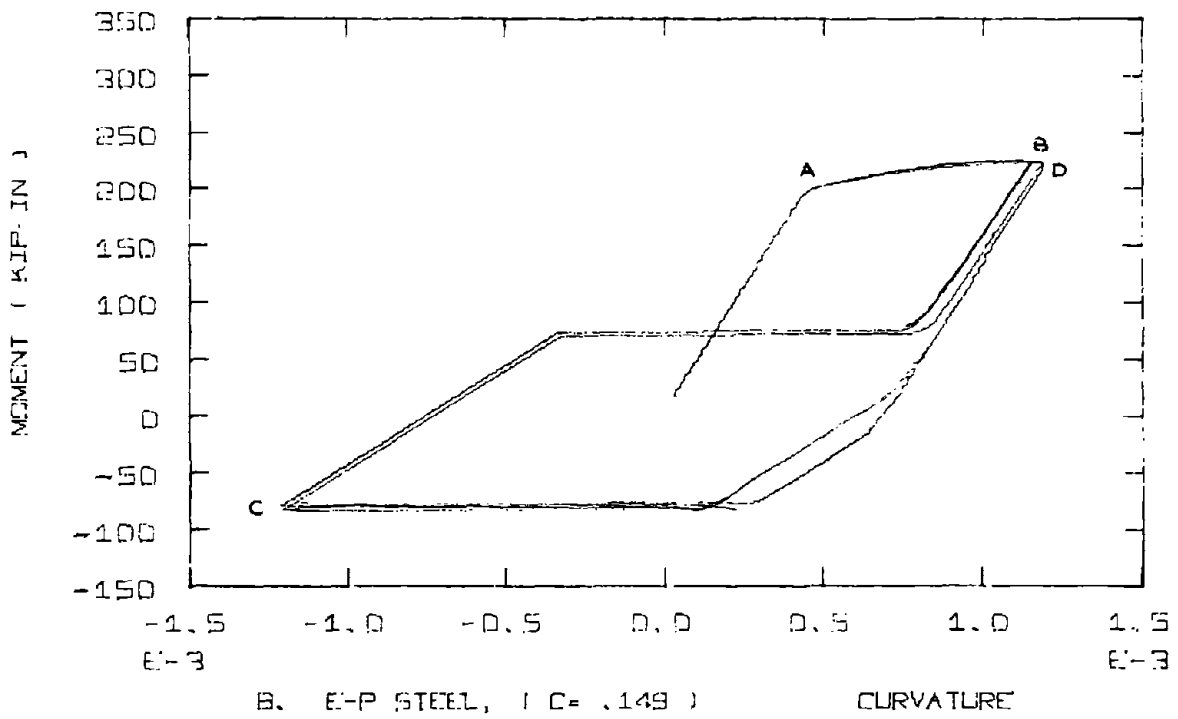
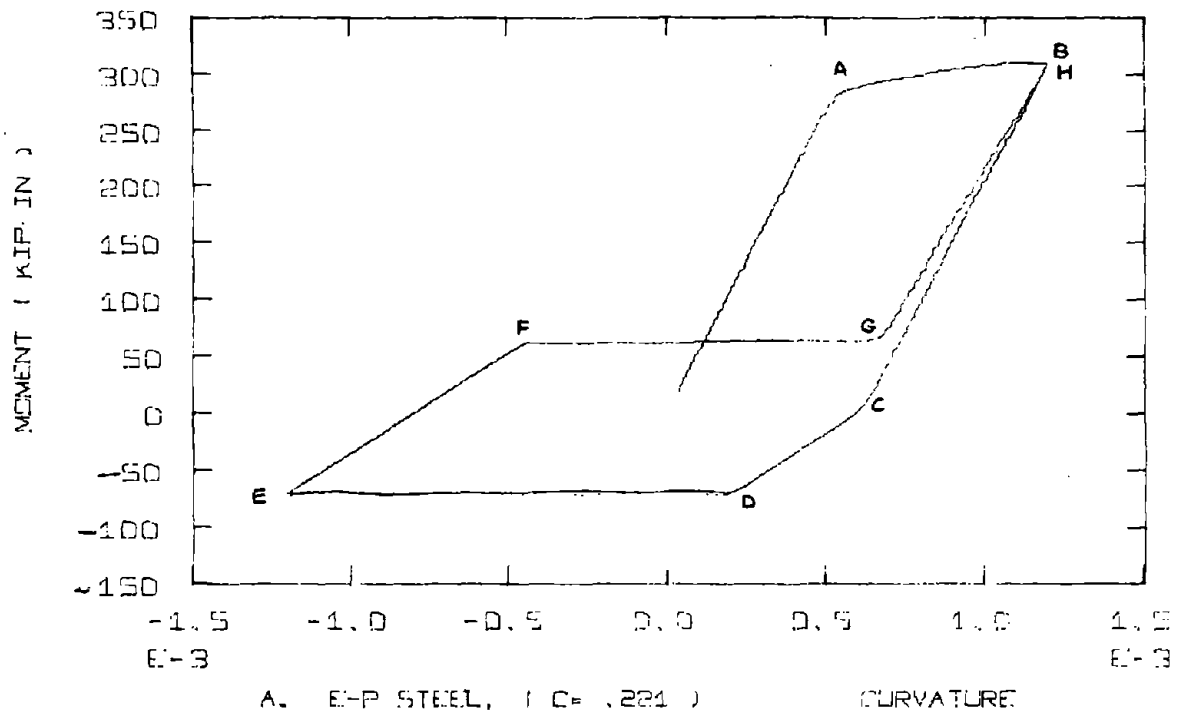


FIG. 4-18 - MOMENT-CURVATURE RELATIONS WITH AN AXIAL FORCE THAT VARIES WITH MOMENT

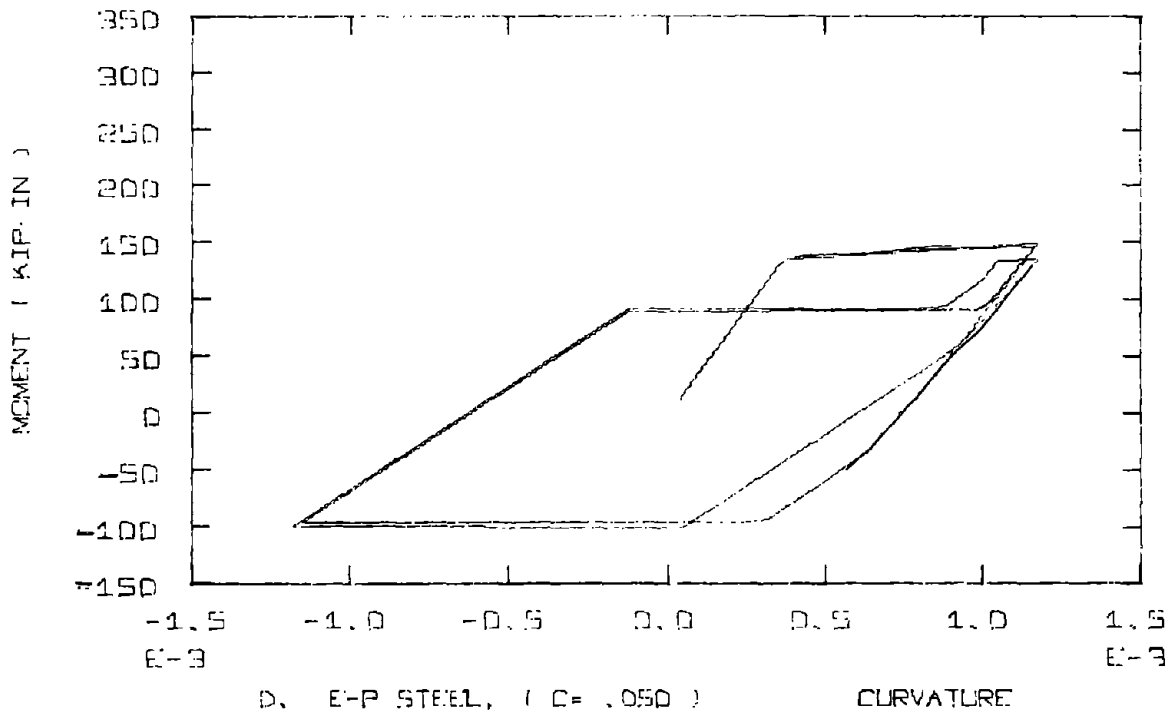
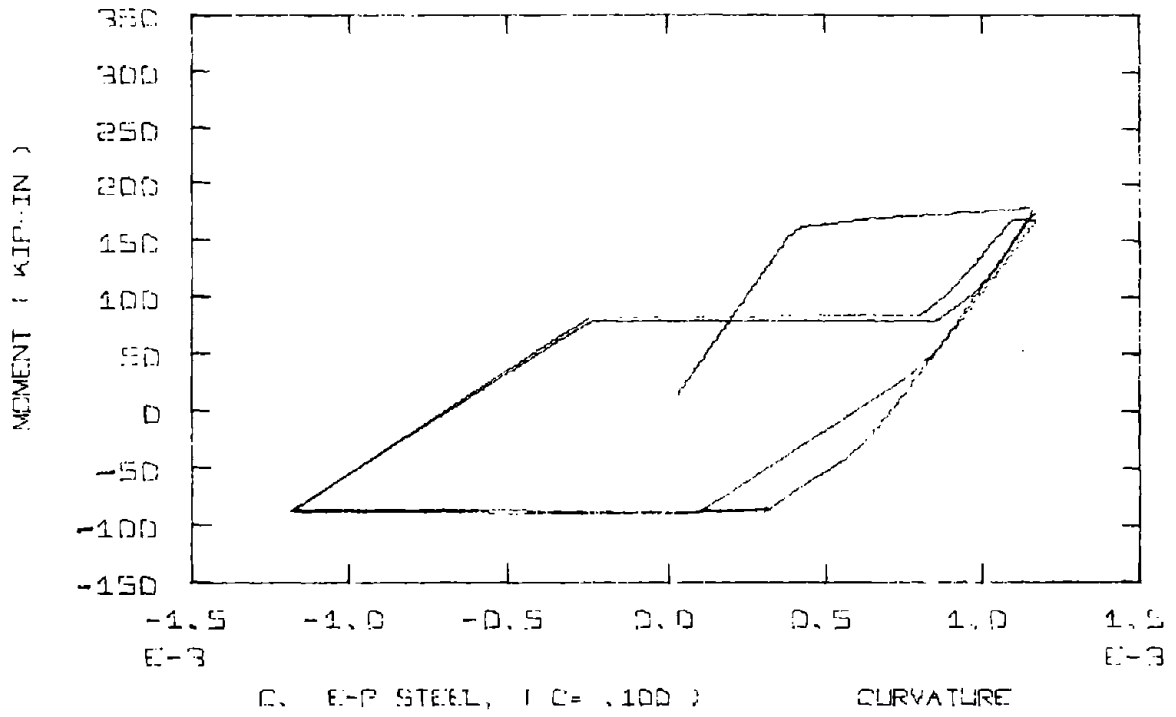


FIG. 4-18 (Continued)

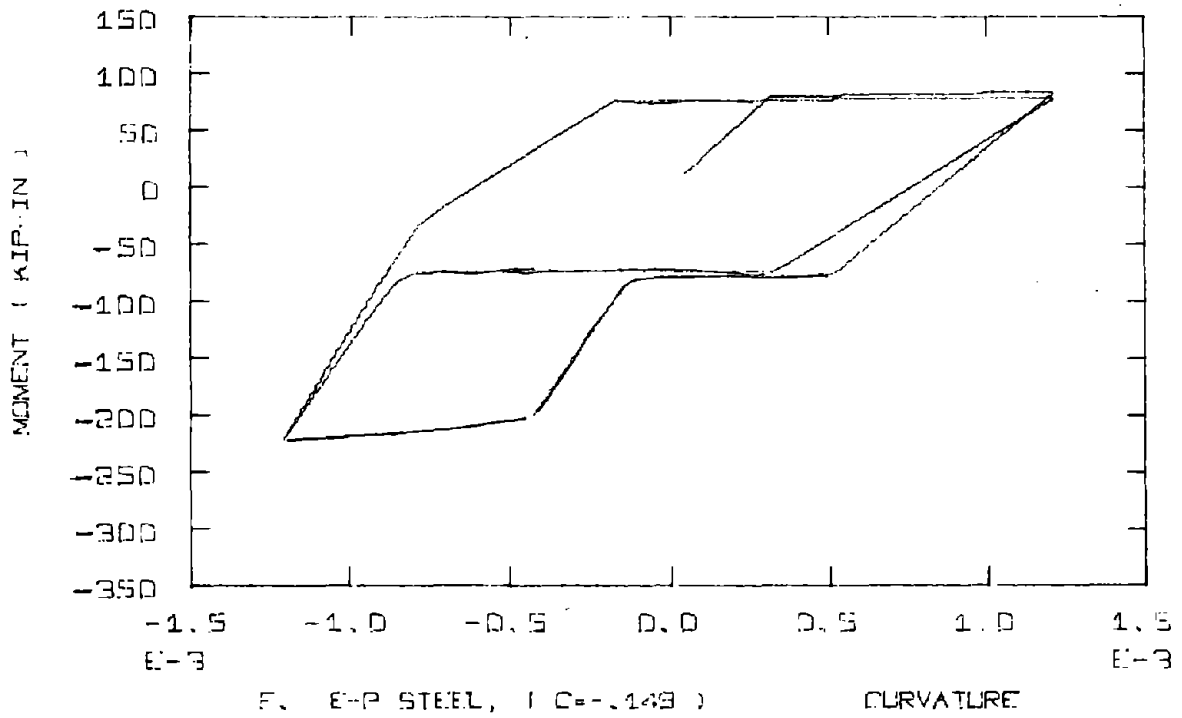
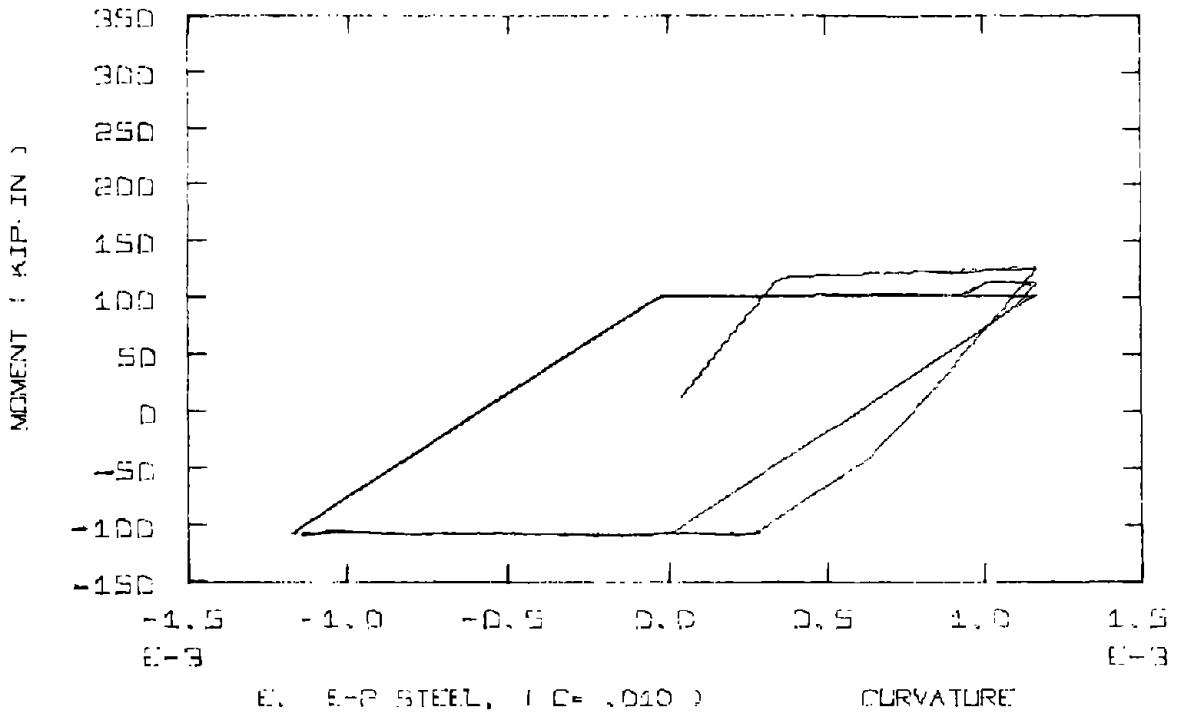


FIG. 4-18 (Continued)

$\overline{FG}$ , formed in reloading when the top steel yields in compression. The top steel had previously yielded in tension at point D. Because of the tensile stress imposed on the section, the concrete fibers at the top must recover this additional tensile strain before supplying compressive strength. At point G the concrete fibers are participating again after making no contribution in  $\overline{CDEFG}$ . The bottom steel barely yields before the loading direction is changed and a "spike" has occurred. The delay in picking up compressive strength from the concrete has caused this reduction in the area of the hysteresis loop.

Although the section is symmetrically reinforced, the resulting moment-curvature relationship is no longer symmetric. As  $c$  decreases, symmetry returns. In unloading, the incremental tensile axial force prevents compression from developing in the bottom concrete fibers; as a consequence the reloading (up to point G, Fig. 4-18A) proceeds with only the stiffness supplied by the steel. This effect takes place even when  $c$  is as small as .010.

The behavior of the centroidal strain under cyclic loading with axial force varying is shown in Fig. 4-19, where  $c = .149$ . The corresponding moment-curvature curve is that of Fig. 4-18B. Here the strain is always tensile. When concrete fibers are participating, the ratio  $\Delta\epsilon/\Delta\phi$  is negative, but when only the steel contributes to the stiffness it is positive.

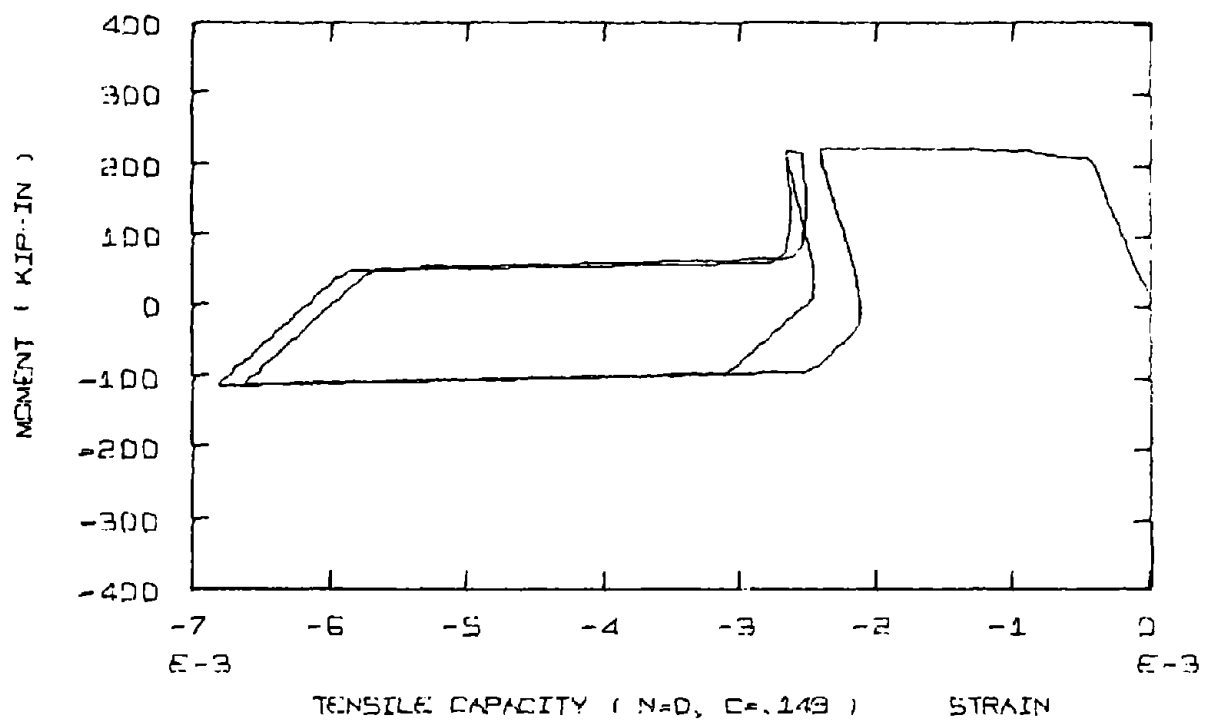


FIG. 4-19 - MOMENT VS. AXIAL STRAIN FOR CYCLIC LOADING  
WITH AN AXIAL FORCE THAT VARIES WITH MOMENT

In Fig. 4-18F,  $c$  is negative; so as moment is increased, an incremental tensile force is applied. Essentially the moment-curvature relation has been flipped over an axis parallel to the curvature axis. In Fig. 4-20 (A and B) the strain limits were varied for the case  $c = .149$ . Changing these limits did not alter the behavior, especially the long yield plateau and resulting "spikes" in the moment-curvature relation.

Fig. 4-21 (A to D) are comparable to Fig. 4-18 (A to D), except the Improved SGT steel formulation was used to provide a more realistic relationship.

#### 4.6.3 Constant Axial Force Combined with an Axial Force that Varies with Moment

A constant axial force,  $N$ , merely applies an initial compressive stress and therefore a compressive strain to the cross-section. Previously, in Fig. 4-12c, the case of a constant axial force was considered where  $N/M_{\max}$  was approximately .15. To provide visual comparison (Fig. 4-22 A to F) of the effect of the constant axial force plus an incremental force that varies with moment,  $c$  has the values  $\pm .15$ ,  $\pm .10$ ,  $\pm .05$  and  $N = P_{\max}/9$ .

With positive  $c$  the maximum positive moment is increased and the negative moment decreased (Table 4-3 compares the maximum moments). As should be expected, when  $c$  is small in relation to  $N/\max$ , the varying axial force is less important. The "flipping" of the moment-curvature relationship with a change in the sign of

TABLE 4-2 - COMPARISON OF MAXIMUM MOMENTS WITH AN AXIAL FORCE WHICH VARIES WITH MOMENT				
C*	Curvature Limits		M <sub>+</sub> (kip-in)	M <sub>-</sub> (kip-in)
.221	-.0012	.0012	306.1	-67.8
.149	-.0012	.0012	220.7	-77.1
.100	-.0012	.0012	177.0	-85.5
.050	-.0012	.0012	146.1	-95.1
.010	-.0012	.0012	126.7	-105.0
-.149	-.0012	.0012	83.1	-220.0
.149	-.0012	.0018	224.0	-77.0
.149	-.0018	.0018	224.0	-77.0
* C = N/M			For Kent Beam #24	

TABLE 4-3 - COMPARISON OF MAXIMUM MOMENTS FOR INCREMENTAL AXIAL FORCES IN ADDITION TO AN AXIAL CONSTANT FORCE				
C	Elasto-Plastic		Improved SGT	
	M <sub>+</sub>	M <sub>-</sub>	M <sub>+</sub>	M <sub>-</sub>
0	226.8	-228.1	226.8	-228.1
.05	260.0	-197.2	260.0	-197.2
.10	300.4	-172.1	300.4	-188.5
.15	334.8	-152.7	334.8	-171.7
-.05	199.4	-268.1	199.4	263.1
-.10	176.6	-302.0	176.6	-303.1
-.15	158.7	-334.9	158.7	-340.2
N = P <sub>max</sub> /9			For Kent Beam #24	

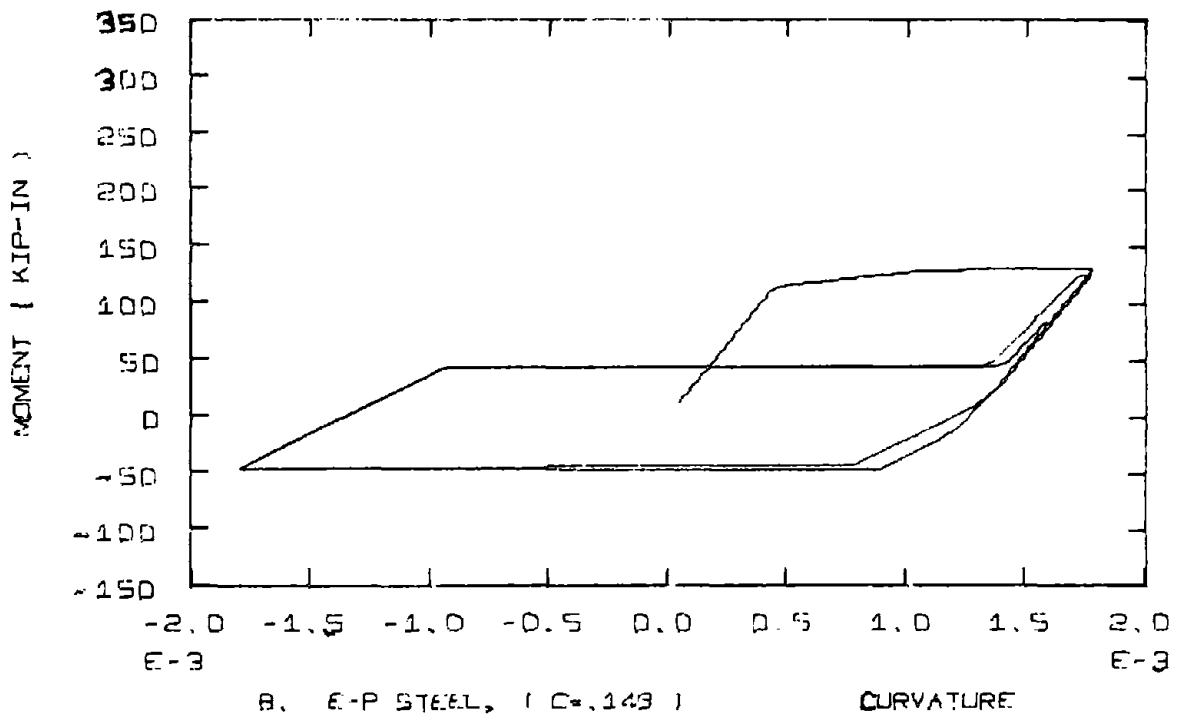
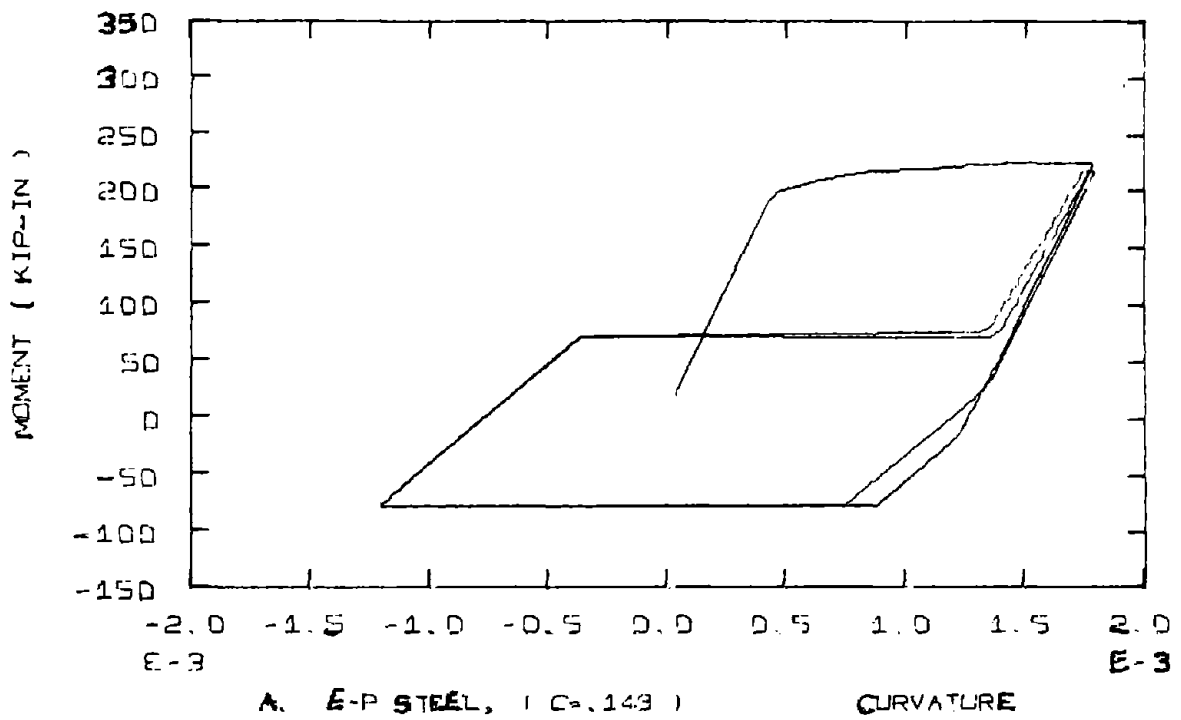


FIG. 4-20 - CYCLIC MOMENT-CURVATURE RELATIONS WITH AXIAL FORCE PROPORTIONAL TO MOMENT; VARY CURVATURE LIMITS

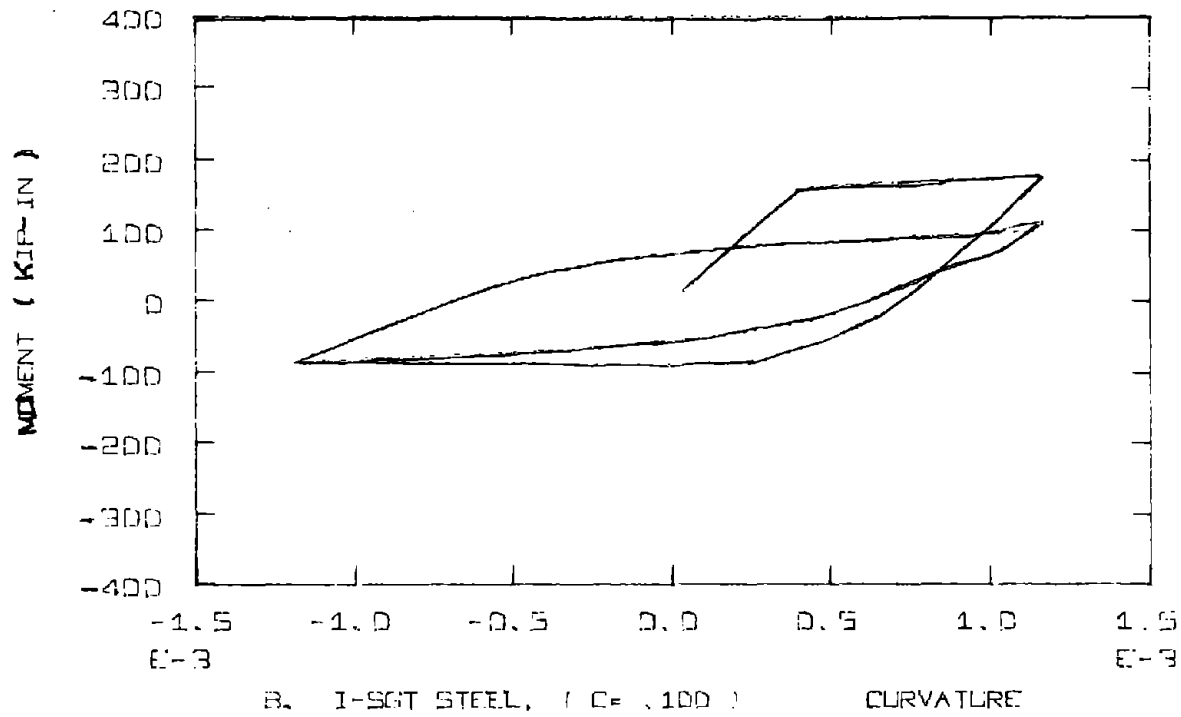
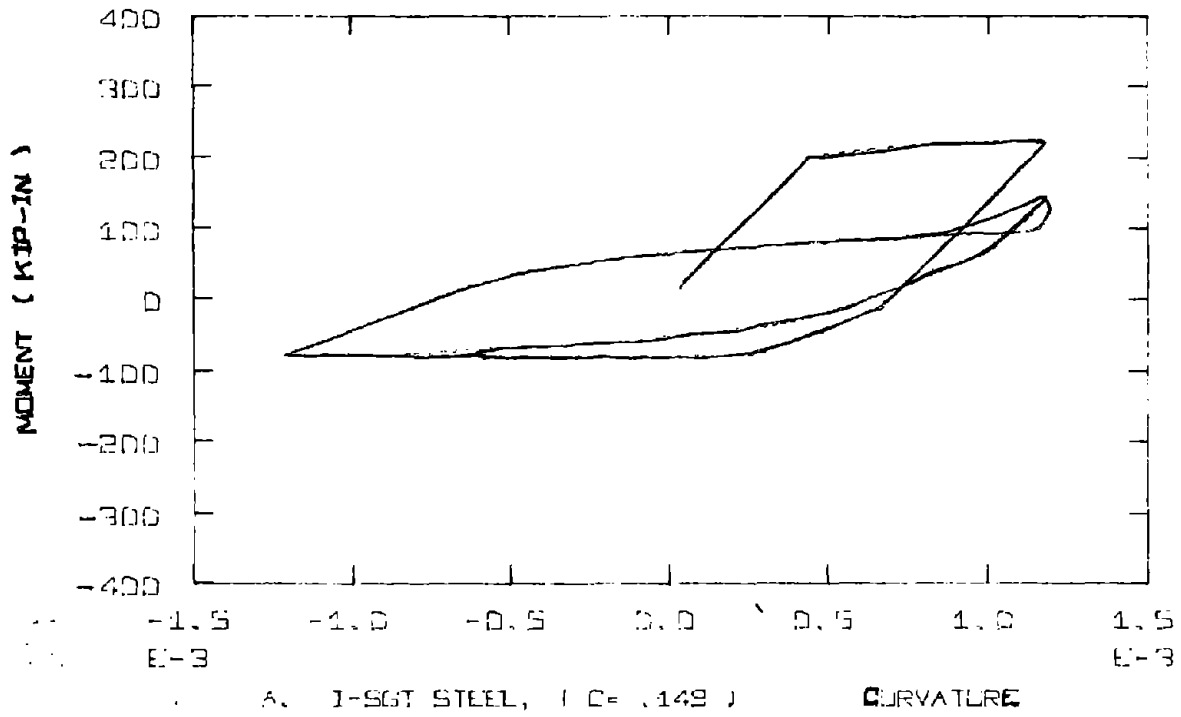


FIG. 4-21 - CYCLIC MOMENT-CURVATURE RELATIONS WITH AN AXIAL FORCE THAT VARIES WITH MOMENT

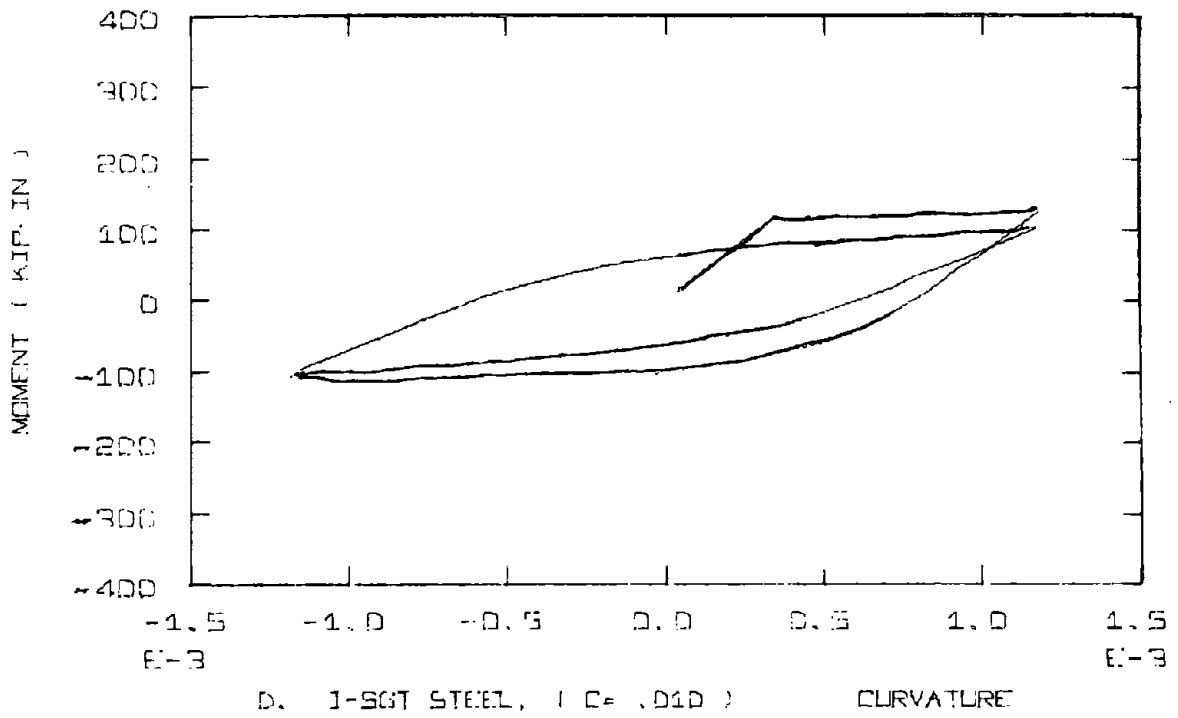
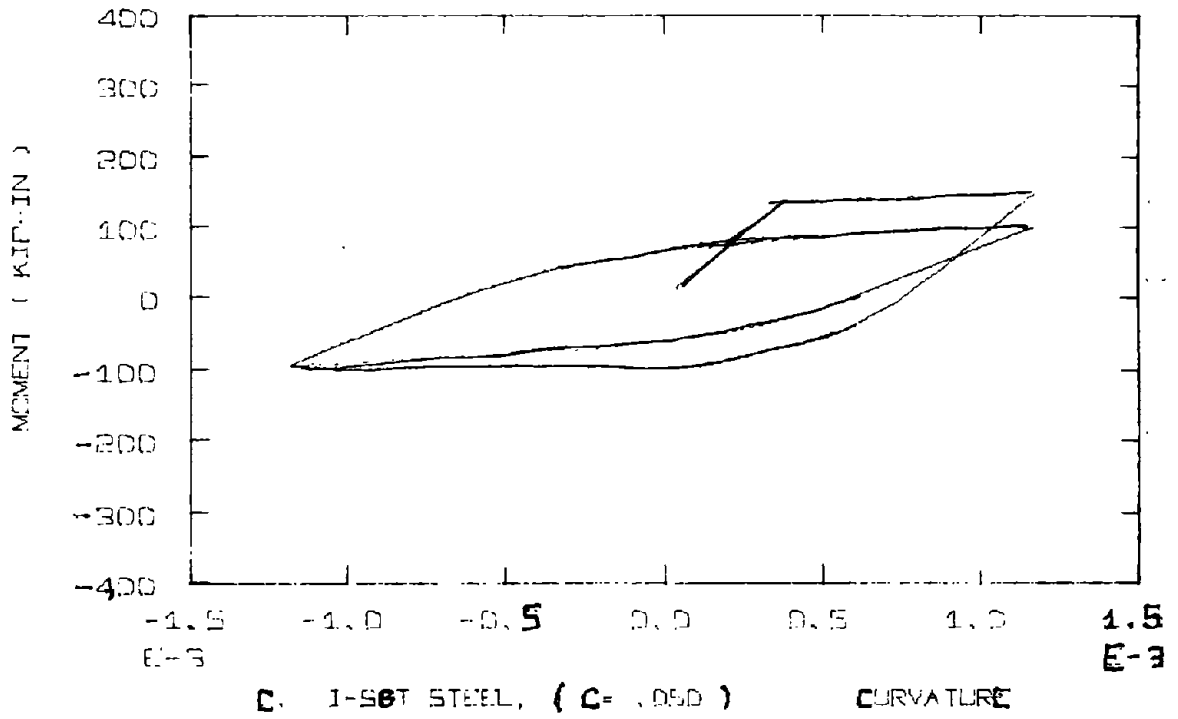


FIG. 4-21 (Continued)

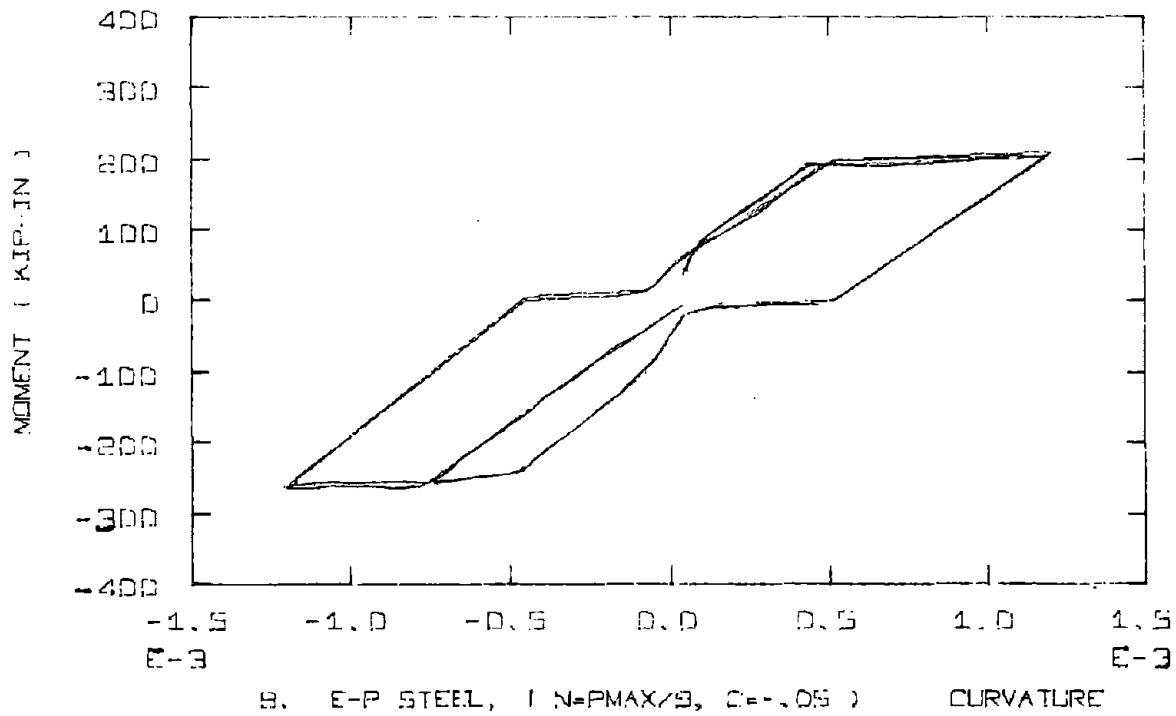
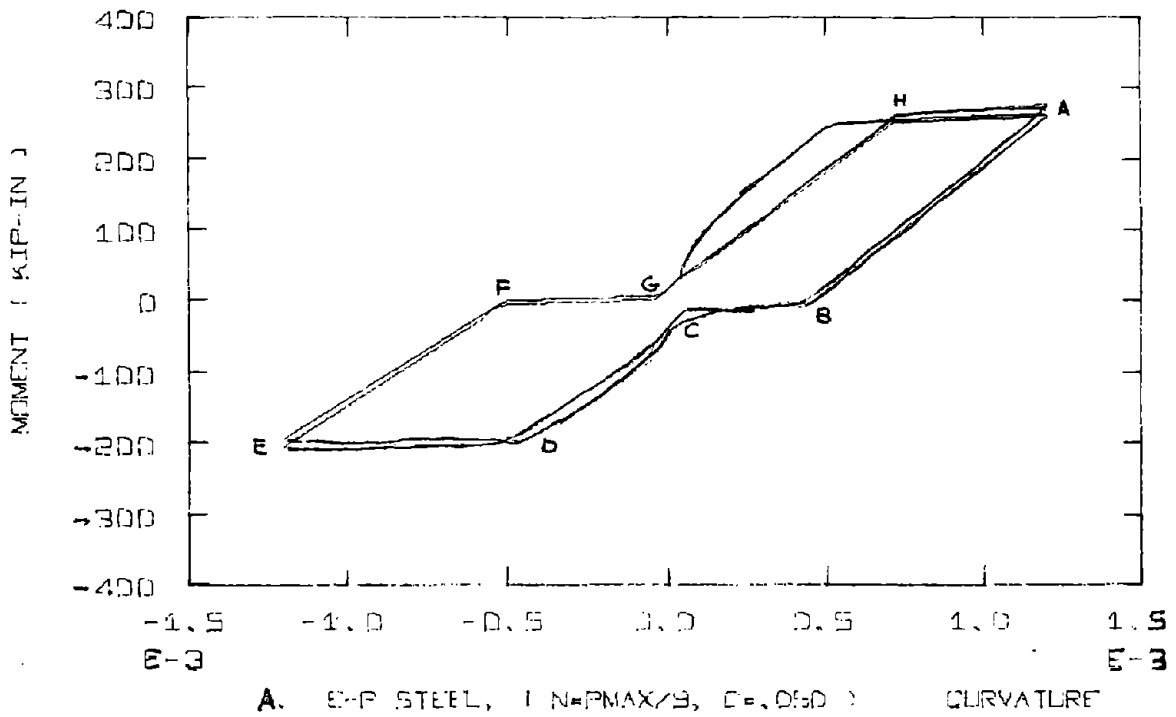


FIG. 4-22 - CYCLIC MOMENT-CURVATURE RELATIONS WITH A CONSTANT AXIAL FORCE PLUS AXIAL FORCE WHICH VARIES WITH MOMENT

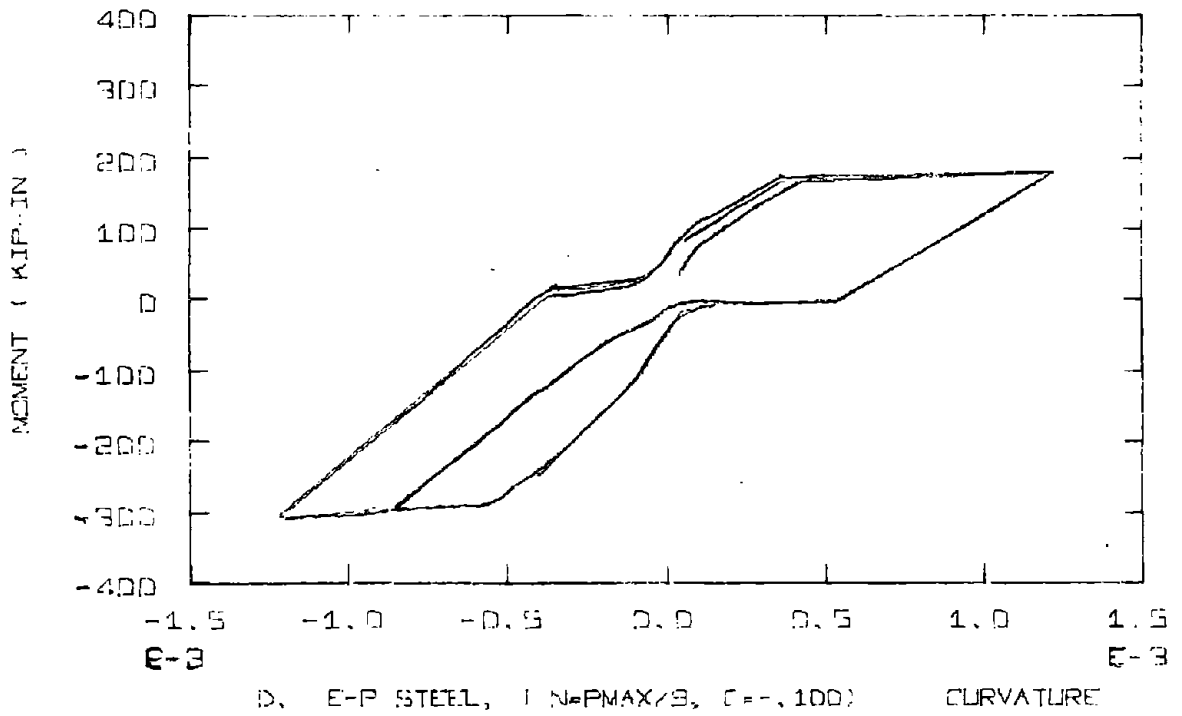
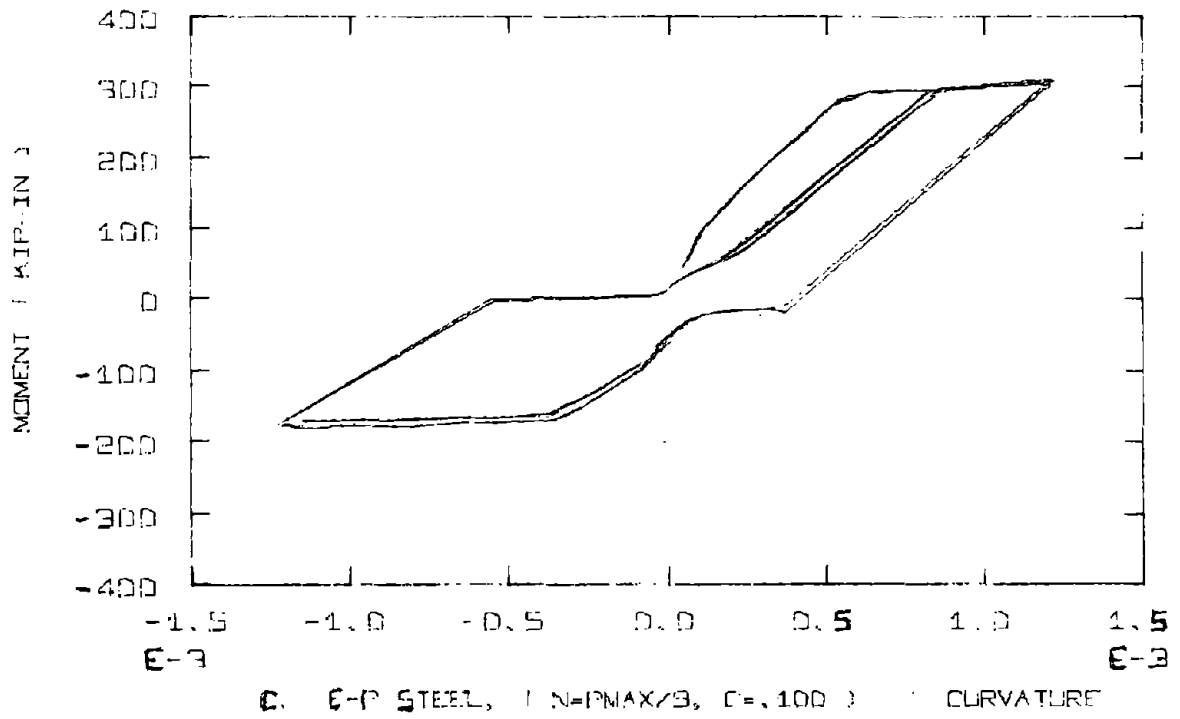


FIG. 4-22 (Continued)

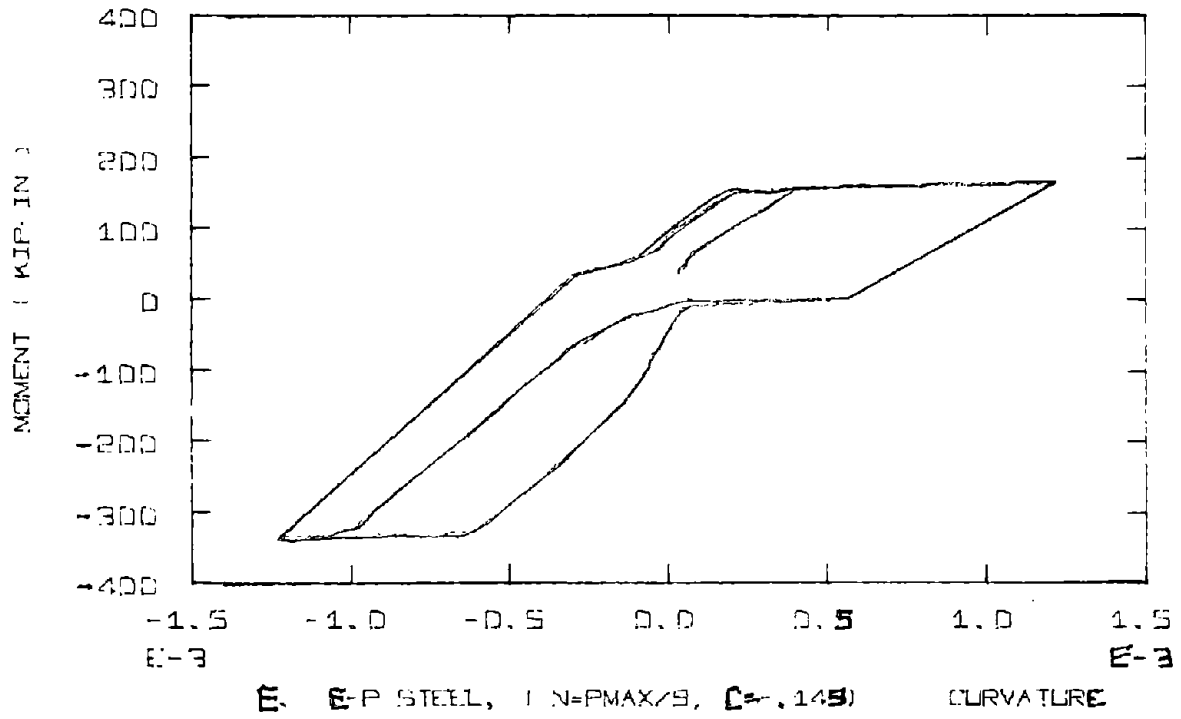
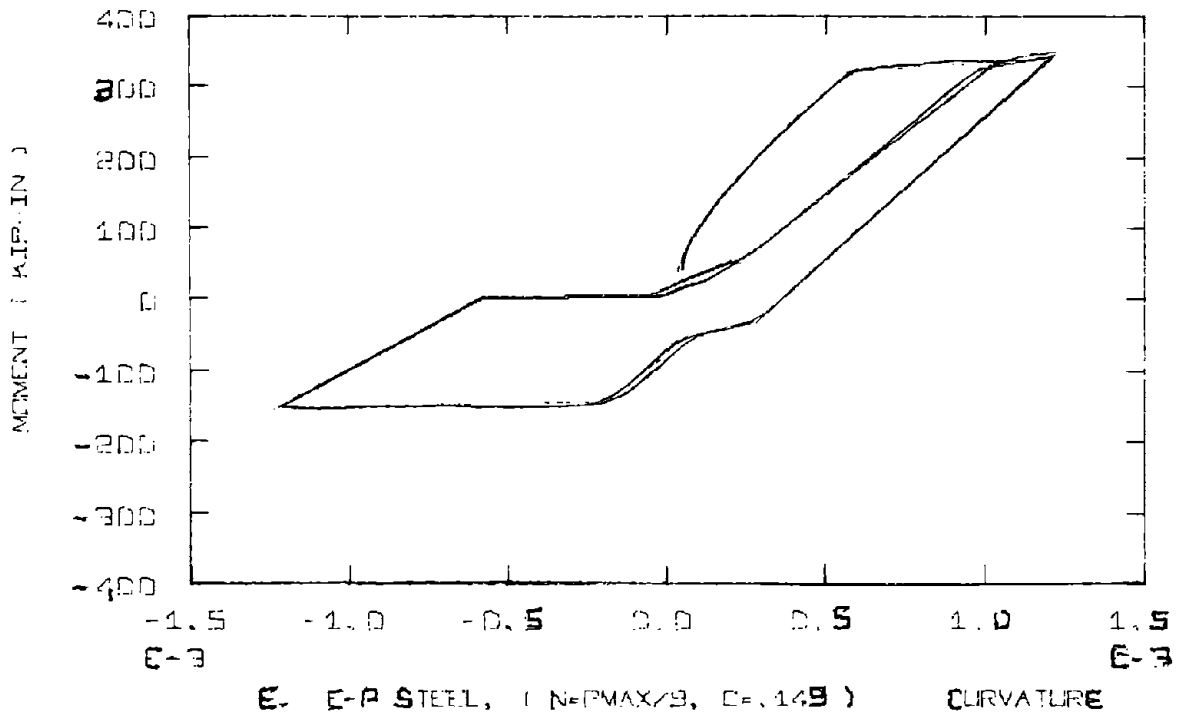


FIG. 4-22 (Continued)

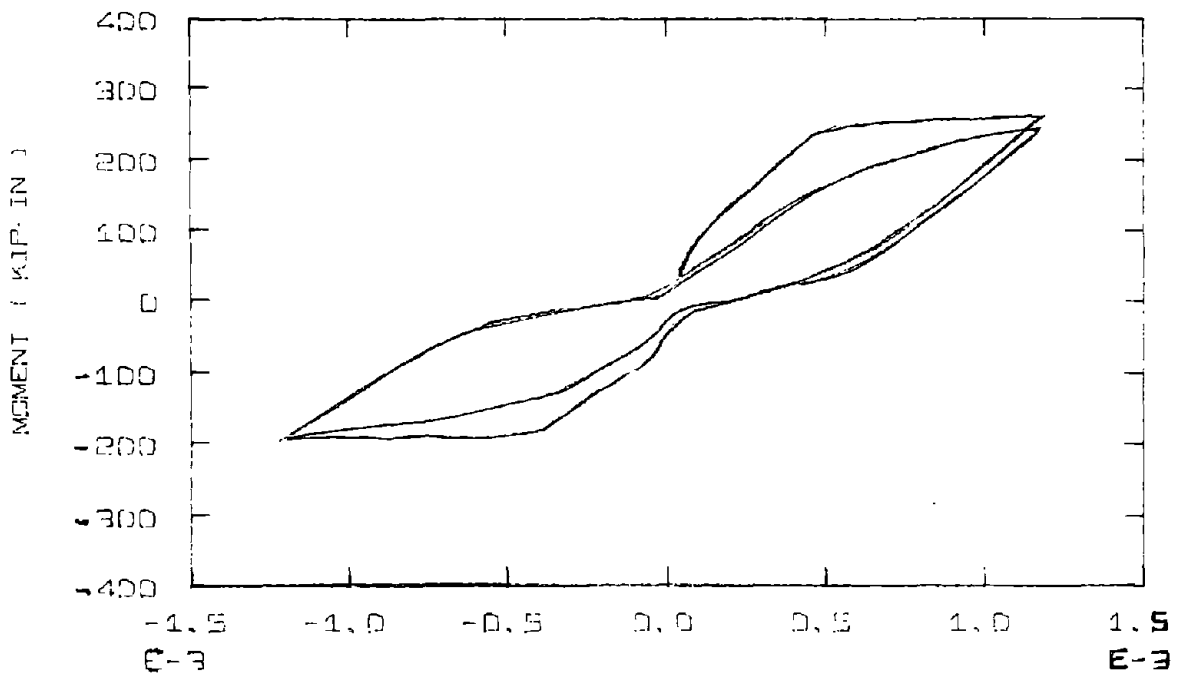
$c$  is reduced with smaller  $c$ .

Figure 4-23(A to E) shows the same loading conditions, but with the Improved SGT steel.

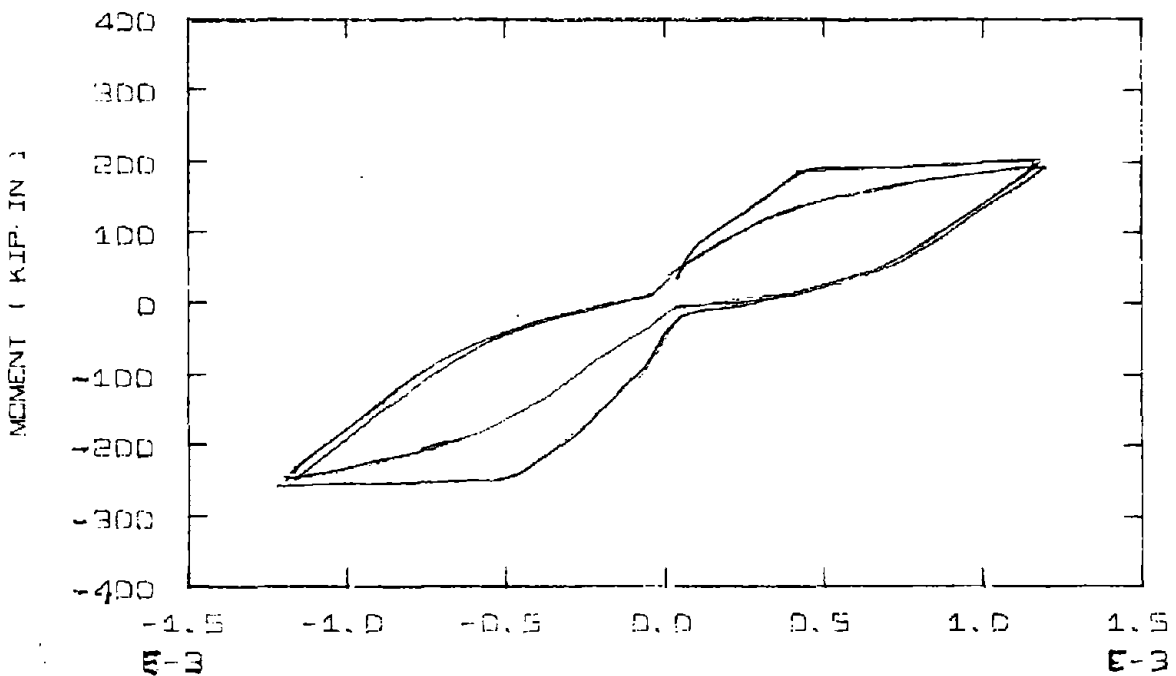
#### 4.6.4 Effect of Concrete Tensile Capacity on Moment-Curvature Relations with Axial Forces

Permitting tensile capacity in an incremental stiffness approach will lead to a violation of equilibrium when the fiber cracks, unless some means of correcting for this is implemented. A particular fiber may be carrying tensile stresses up to  $f_p$ , the modulus of rupture, then it cracks with additional stress and its tangent modulus becomes zero. Unless there is a scheme such as using a negative slope in the next step, equilibrium will not be satisfied: the tensile stress the fiber had before cracking has not been redistributed. The model with tensile capacity will then overestimate the moment capacity. Fig. 4-24(A to E) illustrates this effect for a tensile capacity of  $f'_c/10$  and various combinations of  $N$  and  $c$ . On the other hand, any scheme where there is iteration for stress equilibrium will correctly cause the redistribution of tensile stresses from the cracked fibers.

Since in the incremental approach, tensile capacity causes an overestimation of moment and since corrective action after cracking will involve a complicated iteration scheme, no tensile capacity in the concrete will be assumed



A. I-SBT STEEL, (  $N=P_{MAX}/9$ ,  $\alpha=+.05$  ) CURVATURE



B. I-SBT STEEL, (  $N=P_{MAX}/9$ ,  $\alpha=-.05$  ) CURVATURE

FIG. 4-23 - CYCLIC MOMENT-CURVATURE RELATIONS WITH A CONSTANT AXIAL FORCE PLUS AXIAL FORCE WHICH VARIES WITH MOMENT

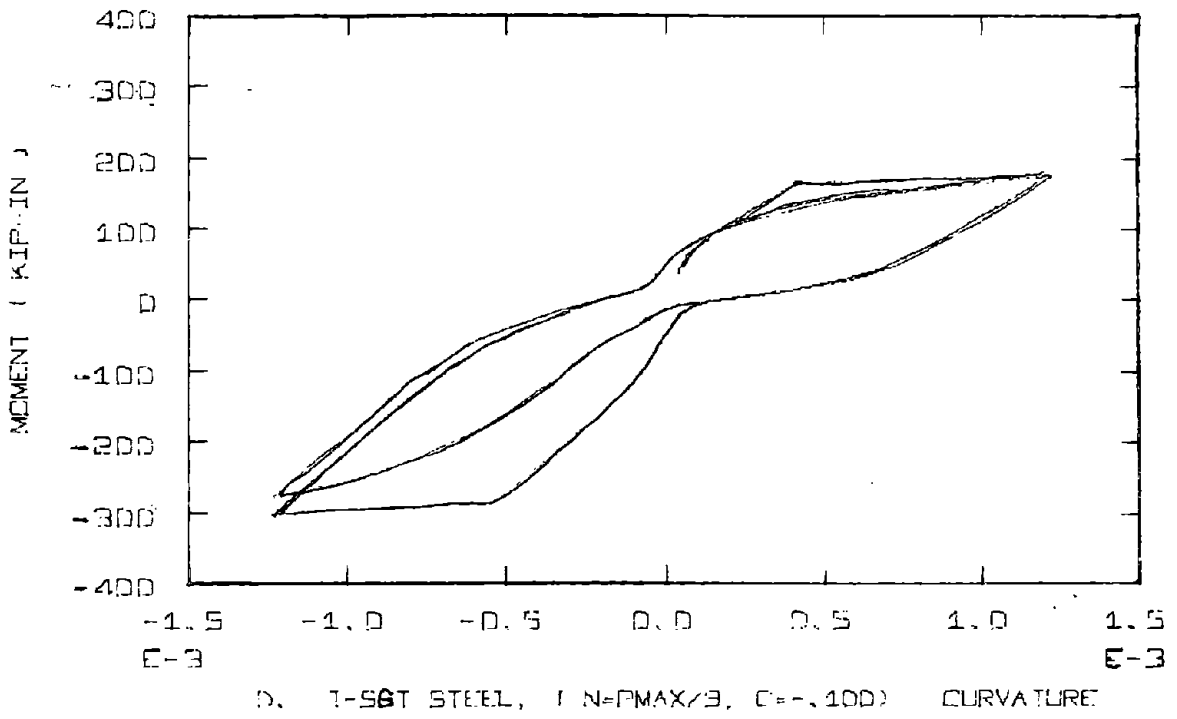
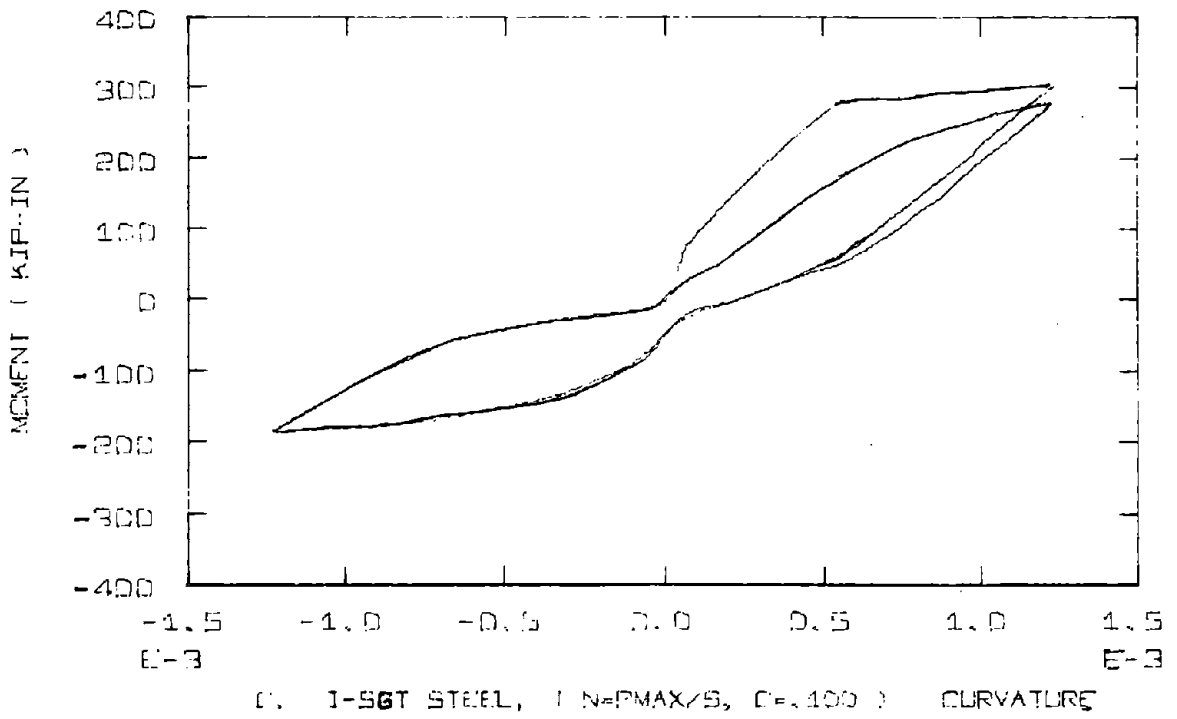


FIG. 4-23 (Continued)

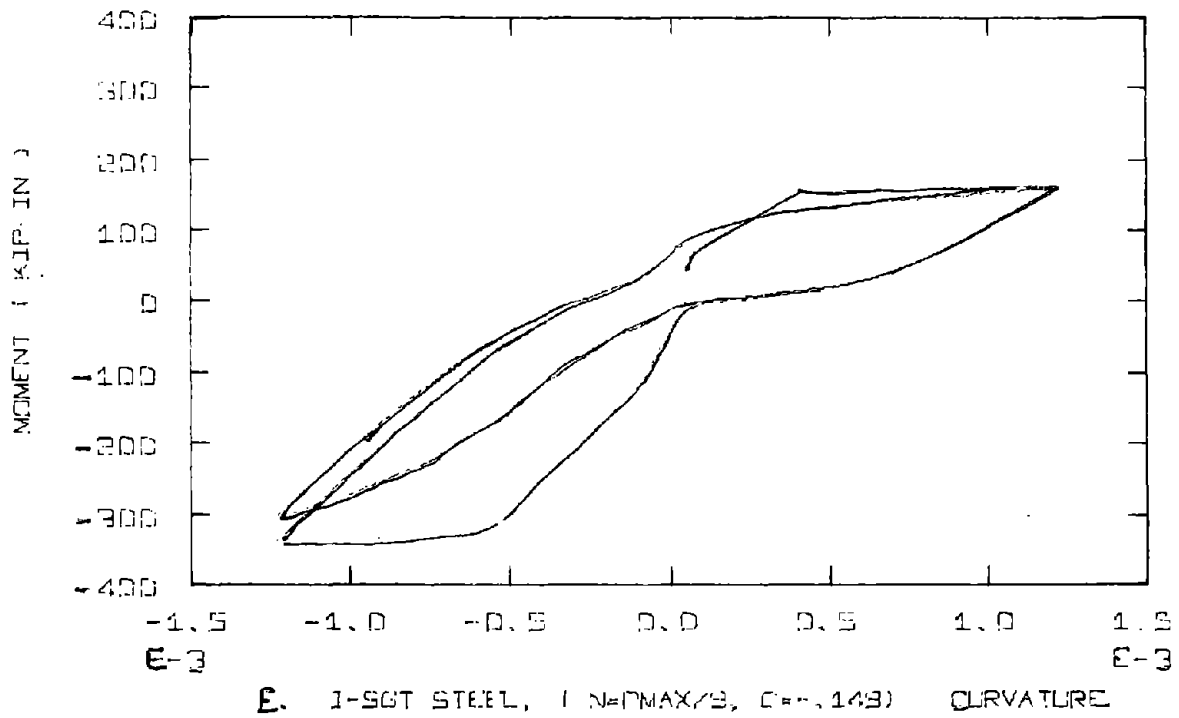
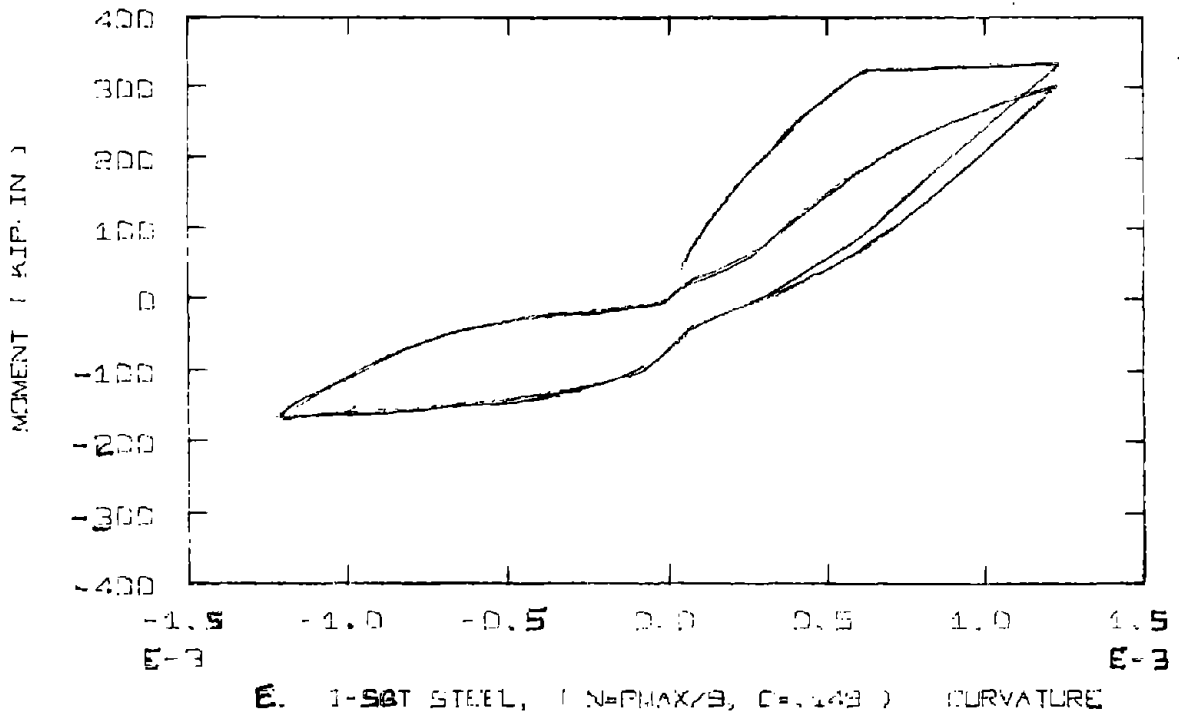


FIG. 4-23 (Continued)

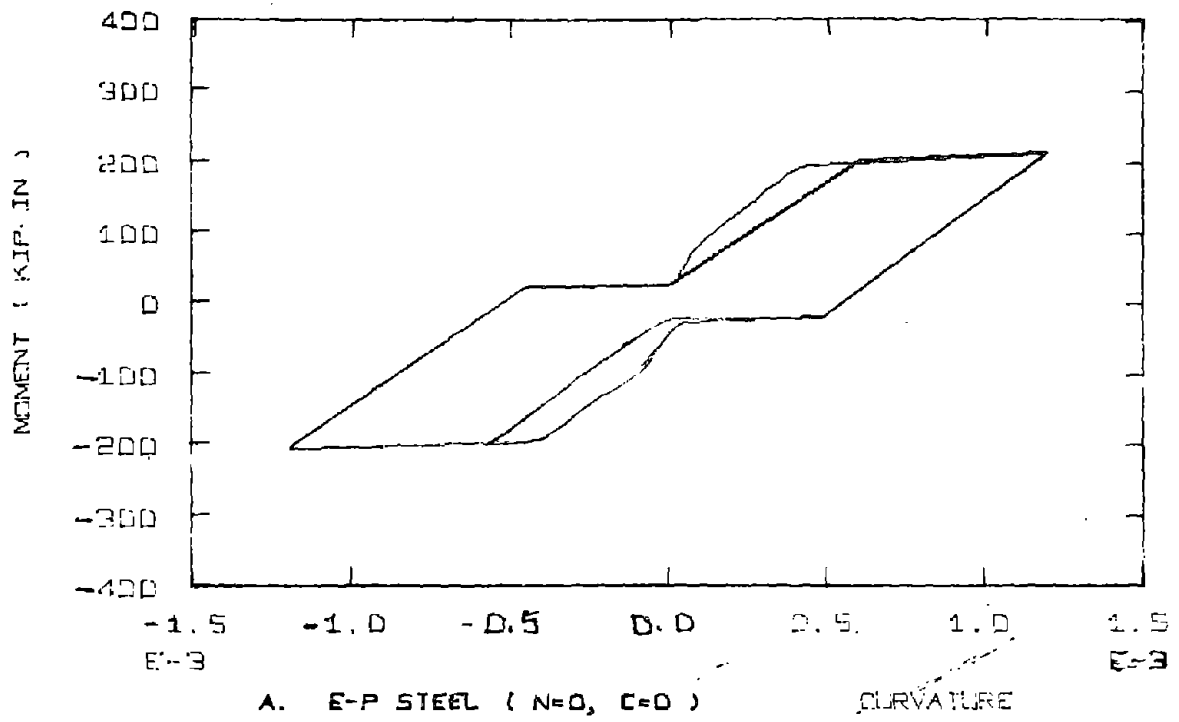


FIG. 4-24 - CYCLIC MOMENT-CURVATURE WITH AXIAL FORCE AND TENSILE CAPACITY IN CONCRETE

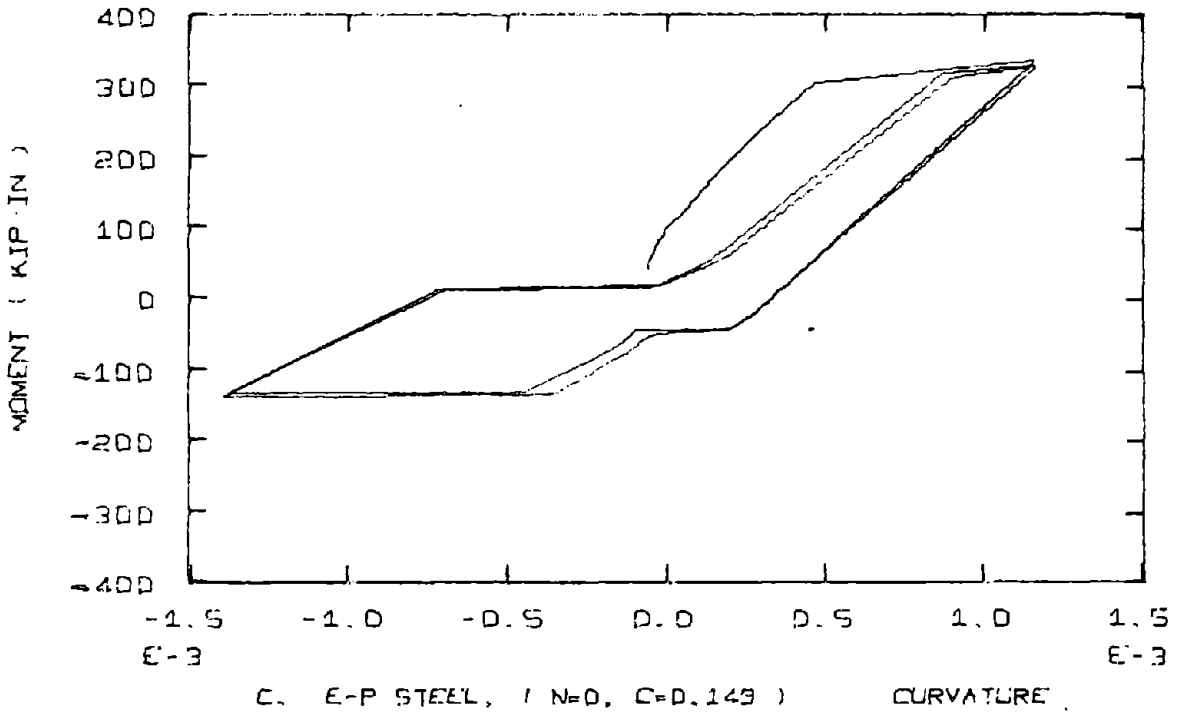
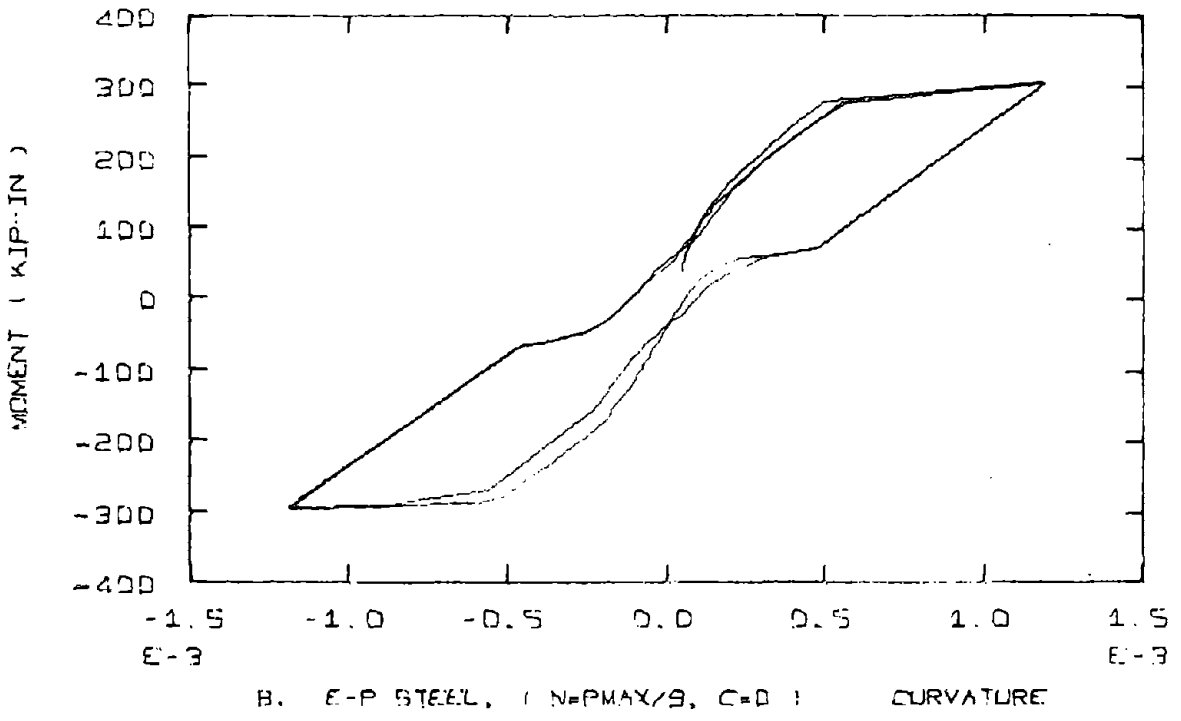


FIG. 4-24 (Continued)

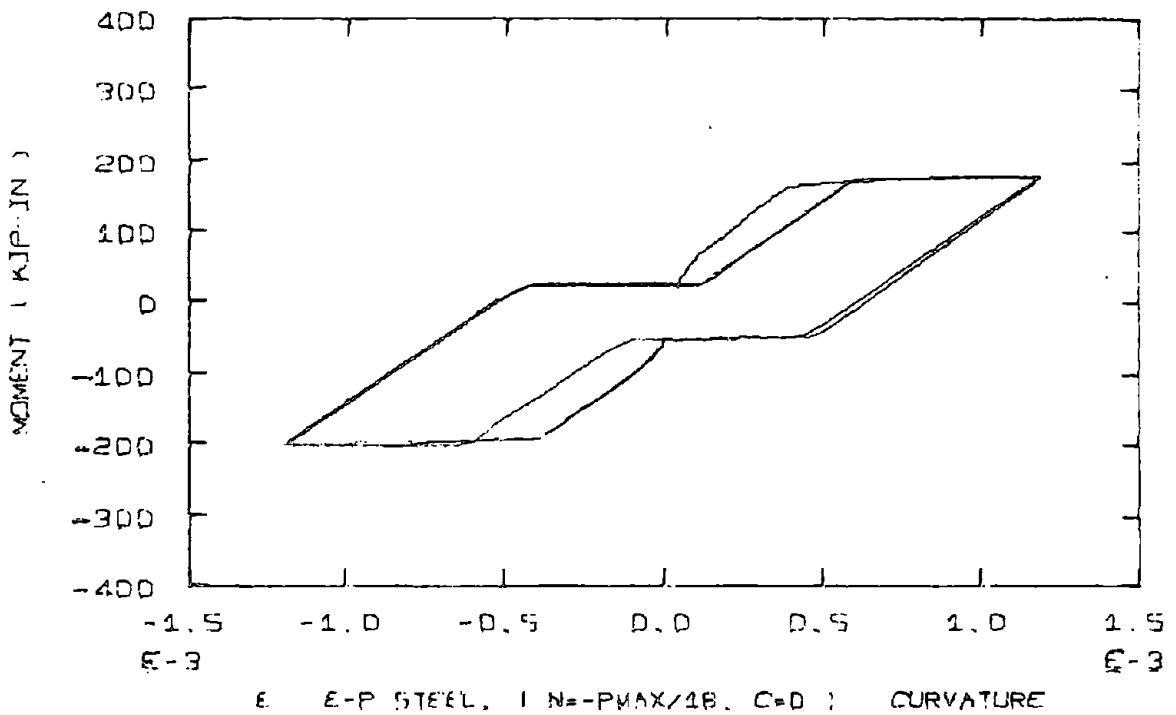
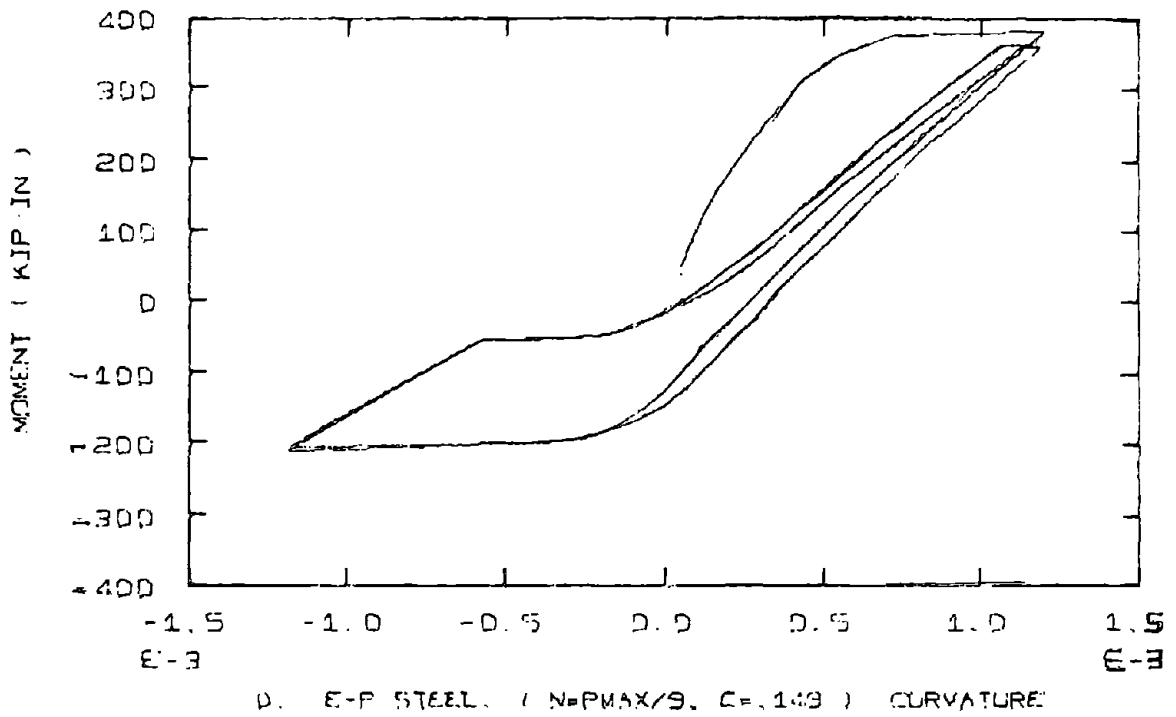


FIG. 4-24 (Continued)

#### 4.7 EFFECT OF SLIPPAGE BETWEEN CONCRETE AND THE STEEL REINFORCEMENT

In a reinforced concrete member there is slippage between the reinforcing steel and the adjacent concrete. As a result, there is a violation of the assumption that plane sections remain plane. In bending deformation of a member, the adjacent concrete is attempting to transfer stress to the steel and the lack of perfect bonding between the two materials leads to slippage.

Part of the observed stiffness degradation occurring in reinforced concrete members has already been explained in terms of the Bauschinger effect in the steel. The diminished participation of the concrete with increasing number of cycles is another aspect. The slippage of the reinforcement is also a factor.

Consider that the adjacent concrete fibers are attempting to transfer an increment of strain,  $\Delta\epsilon$ , and this results in an increment of steel strain and some slippage:

$$\Delta\epsilon = \Delta\epsilon_{\text{steel}} + \Delta\epsilon_{\text{slip}} \quad (4.8)$$

Let  $s$  be the ratio  $\frac{\Delta\epsilon_{\text{steel}}}{\Delta\epsilon}$ , so

$$\begin{aligned} \Delta\epsilon_{\text{steel}} &= s\Delta\epsilon \\ \Delta\epsilon_{\text{slip}} &= (1-s)\Delta\epsilon \end{aligned} \quad (4.9)$$

The slippage phenomena can be visualized as a "bond" spring transferring load from the concrete to the steel. The steel is also a spring in series with the bond spring.

$$\Delta f_s = (TM_{\text{steel}}) \Delta \epsilon_{\text{steel}} \quad (4.10)$$

where  $\Delta f_s$  is an incremental steel stress and  $TM_{\text{steel}}$  is the instantaneous tangent modulus (or steel spring stiffness). The fictitious bond spring stiffness is then

$$TM_{\text{slip}} = \left(\frac{s}{1-s}\right) TM_{\text{steel}} \quad (4.11)$$

which results from Eqns. 4.8, 4.9 and 4.10. The equivalent stiffness (tangent modulus) for the system is

$$TM_{\text{equiv.}} = \frac{TM_{\text{slip}} TM_{\text{steel}}}{TM_{\text{slip}} + TM_{\text{steel}}} = s(TM_{\text{steel}}) \quad (4.12)$$

Thus the effect of slippage between the steel and concrete is to reduce the effective stiffness supplied by the reinforcing steel. A loss of bond therefore reduces the cross-section stiffness.

In describing their results on steel bars encased in a concrete cylinder, Bresler and Bertero<sup>(29)</sup> reported that the stress transfer effectiveness (bond) was dependent upon the maximum peak stress in the steel. Larger stresses caused greater damage in the boundary layer between the steel and concrete and consequently the reduction in stress transfer became more severe.

Bond-slip relationships have been derived by researchers such as Nilson,<sup>(30)</sup> but they require an analysis where the location of cracks is maintained and the loading is monotonic.

One approach to including the effect of slippage would be to assume  $s$  is constant for a given cycle and is dependent on the maxi-

imum deformation (either steel strain or curvature for example). Experimentally it is difficult to measure because of the formation of cracks and the problems in instrumenting. Using data from Bertero, Bresler, Liao,<sup>(31)</sup> reporting the average curvature, concrete strains, and steel strains, the crude values obtained showed that  $s$  does decrease with larger curvatures. This indicates an increase in slippage. The problem with this type of determination of  $s$  is that in the model the concrete strains are "averaged over the cracks" whereas experimentally this type of concrete strain measurement has to be taken somewhere between the cracks.

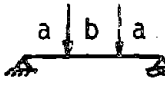
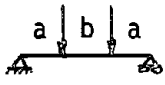
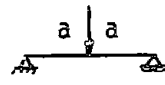
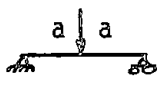
Another method would be to compare analytic moment-curvature curves with experimental ones and vary  $s$  for a given cycle until there is agreement in a least squares sense. However, the  $s$  values so determined would be strongly dependent on the assumed formulations for the reinforcing steel and concrete, and the assumed strain distribution.

Because of a lack of adequate data and variability of the other parameters considered in the formulation so far, the inclusion of the effect of slippage is a refinement not considered in this thesis.

#### 4.8 COMPARISON OF MOMENT-CURVATURE RELATIONS FOR DIFFERENT ANALYTICAL FORMULATIONS

In this section analytic moment-curvature relations, using the six steel formulations, are compared with experimental data which

TABLE 4-4 - PROPERTIES OF MEMBERS USED FOR MOMENT-CURVATURE COMPARISON IN SECTION 4-8

Section Properties	Aoyama <sup>(26)</sup> A2	Agrawal, Tulin Gerstle <sup>(24)</sup> #2	Kent <sup>(19)</sup> #24	Kent <sup>(19)</sup> #27
$A_s$ (in <sup>2</sup> )	.88	.20	.40	1.20
$A_s$ (in <sup>2</sup> )	.88	.20	.40	.40
b (in)	6.0	3.0	4.83	4.83
t (in)	12.0	6.0	8.0	8.0
$d'/d'_a$ (in)	2.0/2.6	1.0/1.0	1.25/1.67	1.25/1.10
$d/d_a$ (in)	10.0/10.0	5.0/4.8	6.75/6.33	6.56/5.80
$f_y$ (psi)	50000.	51000.	48400.	47000.
$f'_c$ (psi)	4900.	4400.	6950.	7490.
$\epsilon_o$	.0018	.0022	.0027	.0028
stirrups	#3	—	#2	#2
s (in)	6.	—	2.	2.
axial force (kip)	36.	—	—	—
loading				
a	3'0"	2'3"	4'2"	4'2"
b	6'0"	1'2"	—	—

represent a variety of cyclic loading conditions. Each of the models uses LINEAR3 for the concrete stress-strain relationship, and twenty concrete fibers and two steel fibers to represent the cross-section. The incremental stiffness approach uses the Euler method and an increment size of  $\Delta\phi \approx \phi_y/80$ . Table 4-4 lists the section properties for each of the members used.

#### 4.8.1 Aoyama's<sup>(26)</sup> Beam A2, Fig. 4.25 (A to G)

For this test the specimen was cycled through the following curvature limits: .00044, -.00117, .000911. With an axial force of 36 kips, the section barely yields in the initial loading, but has significant yielding in the other direction.

For all of the analytic models there is a sharp increase in stiffness when the curvature is nearly zero (in branch  $\overline{BC}$ ). At this point all the concrete fibers are participating because of the compressive strain caused by the axial force and the lack of tensile strain from bending. This increase in stiffness is not, however, apparent in the experimental curve.

Up to point c the behavior of the section is purely elasto-plastic, and there is no difference among the six steels. In the reloading curve,  $\overline{CD}$ , differences occur.

The Elasto-Plastic steel provides good agreement for the average stiffness up to point D', and then it is too stiff until the bottom steel yields in compression. The moment at the end of the cycle, point D, is close to the experimental value.

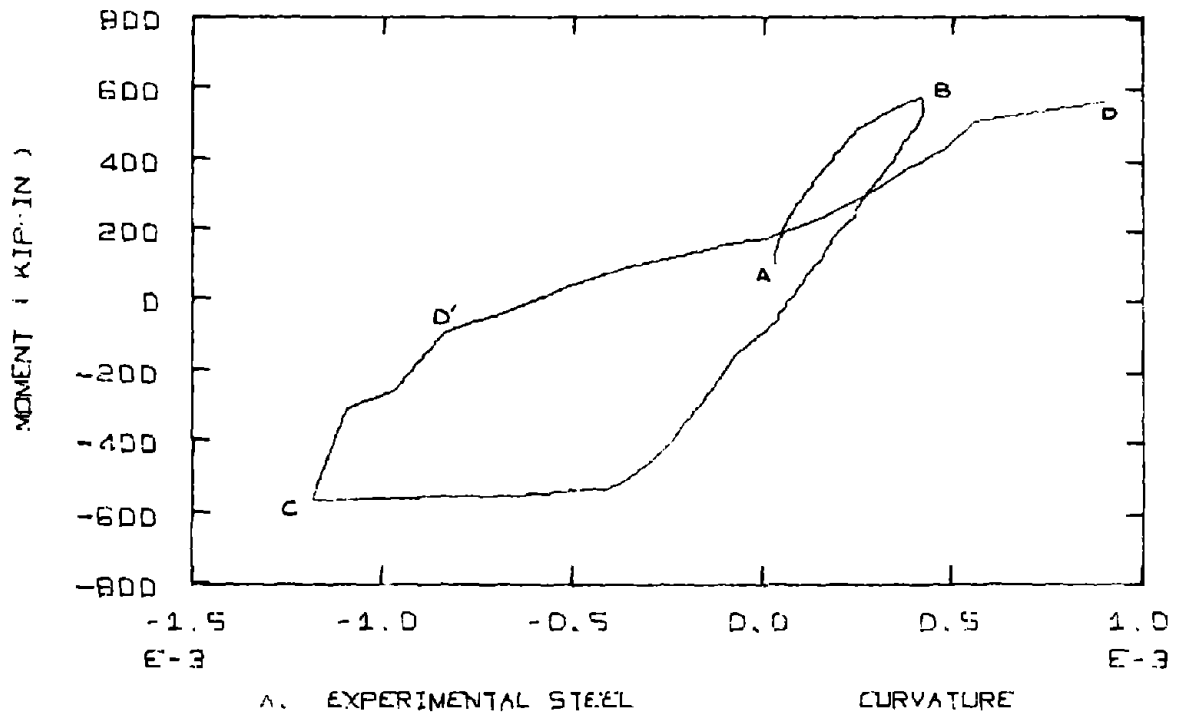


FIG. 4-25 - MOMENT-CURVATURE COMPARISONS  
FOR AOYAMA'S BEAM A2

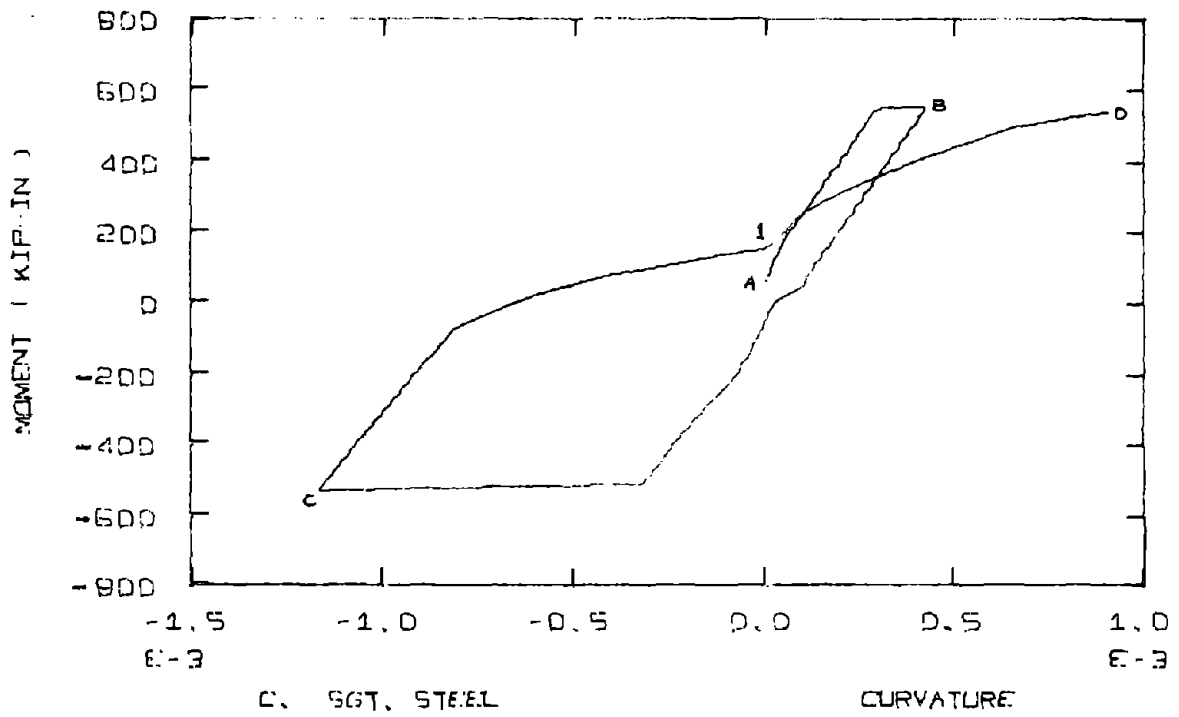
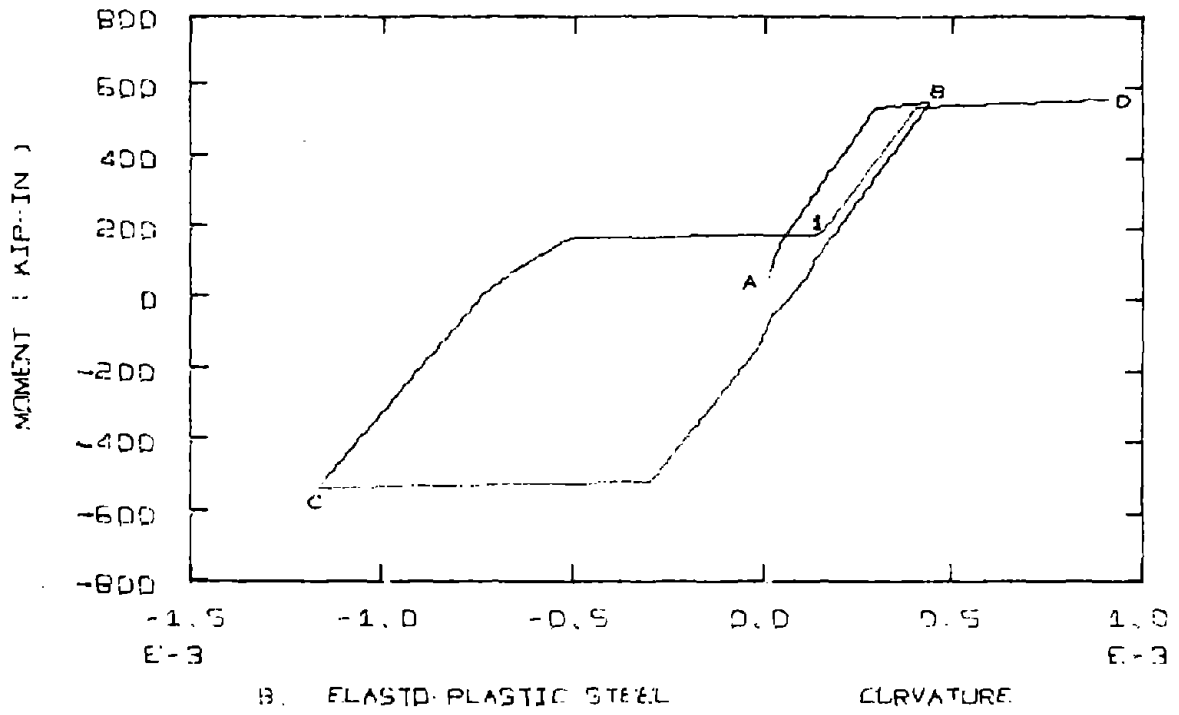


FIG. 4-25 (Continued)

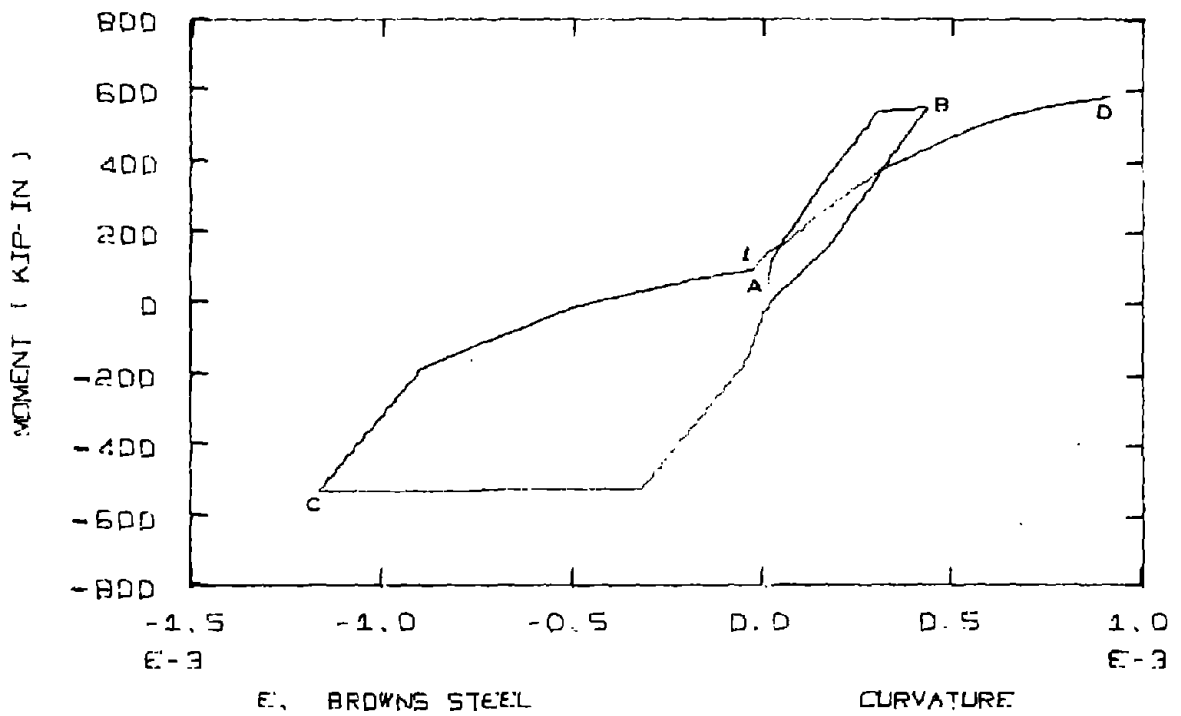
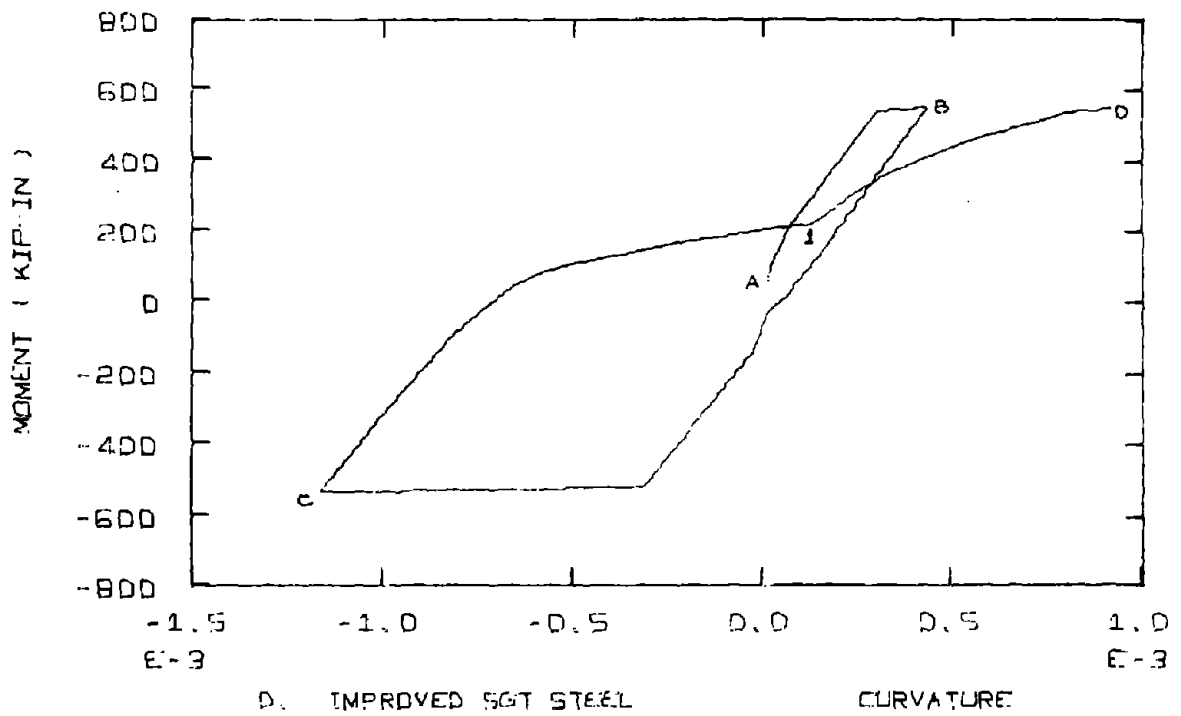


FIG. 4-25 (Continued)

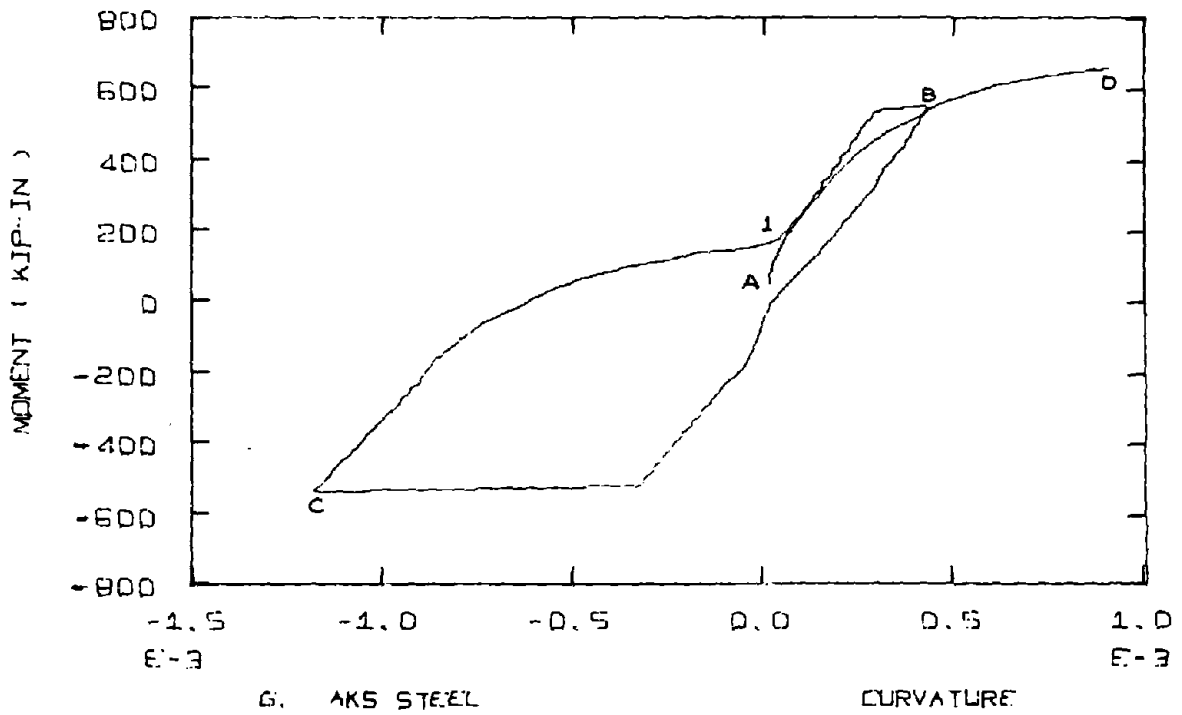
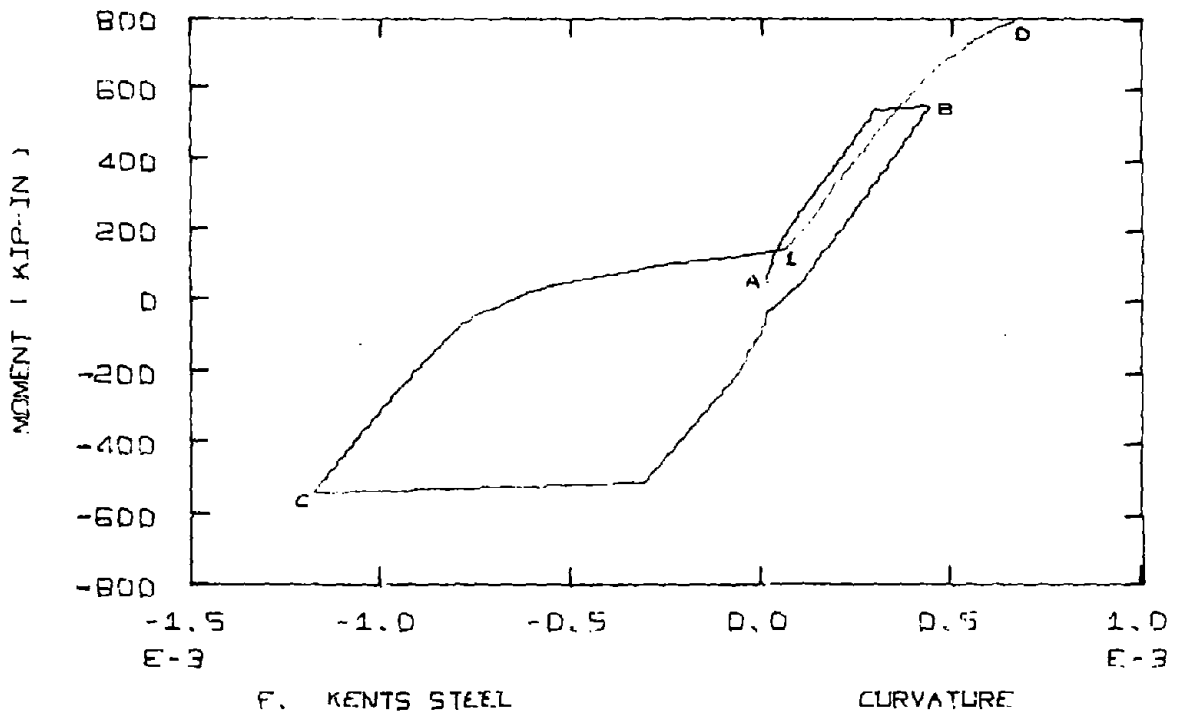


FIG. 4-25 (Continued)

Among the curvilinear steels, the SGT and Improved SGT provide good agreement. In the latter, the initial reloading branch, where the stiffness is due to the bottom concrete fibers still participating, is longer than experimental results. For Brown's steel, reloading is initially softer, then stiffer, but agreement is still reasonable. The problem with Kent's and AKS steel is that they become too stiff after the point where concrete stress is again supplied by the top fibers (point 1 on the analytic curves).

#### 4.8.2 Agrawal, Tulin, Gerstle<sup>(24)</sup> Beam #2, Fig. 4-26 (A to G)

This doubly reinforced section is unloaded and reloaded so that a positive curvature always exists. Unloading occurs without the section reaching its negative moment capacity.

The Elasto-Plastic steel overestimates the moment at the end of the unloading cycle by being too stiff and the loops formed are too narrow.

Of the curvilinear steels, Brown's (modified) and Kent's formulation provide the best overall fit. The AKS model in these cases greatly overestimates the positive moment capacity after the first reloading cycle. All the curvilinear models have a tendency to overestimate the unloading stiffness (such as  $\overline{AB}$  and  $\overline{CD}$ ) and underestimate the reloading stiffness ( $\overline{BC}$  and  $\overline{DE}$ ). For additional reloading straining they would become stiffer than observed, and this would lead to a larger than observed moment.

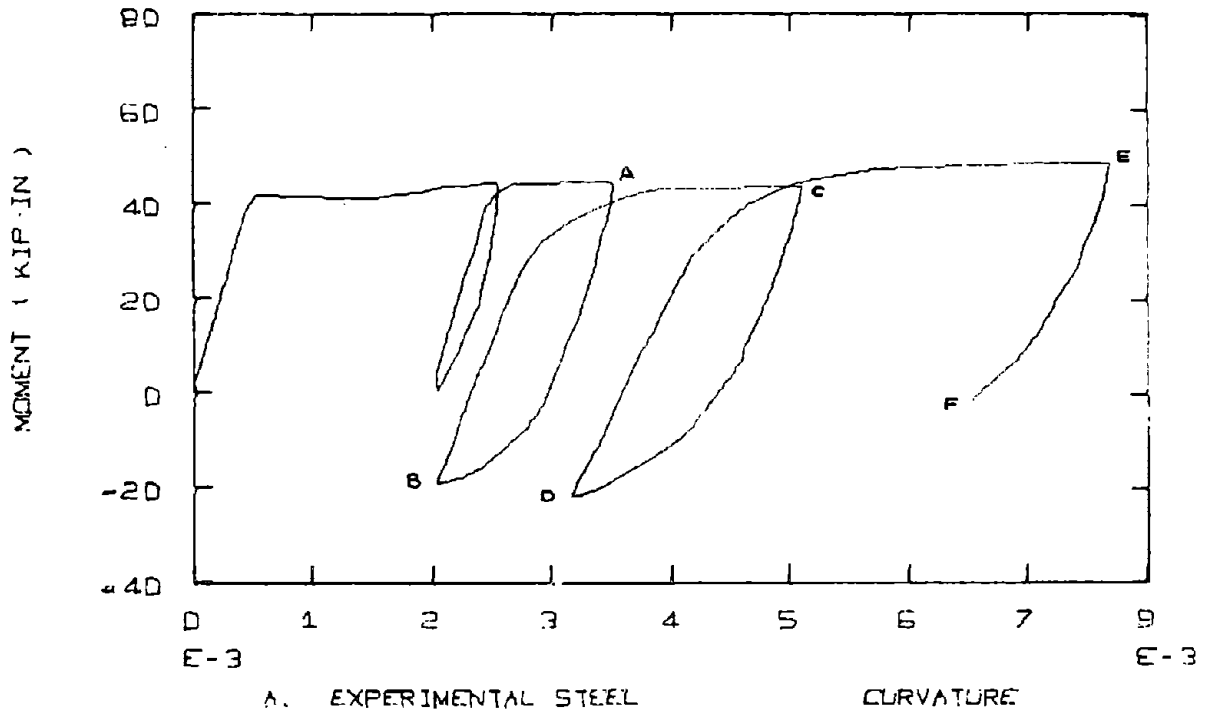


FIG. 4-26 - MOMENT-CURVATURE COMPARISONS FOR  
 AGRAWAL, TULIN, GERSTLE'S BEAM #2

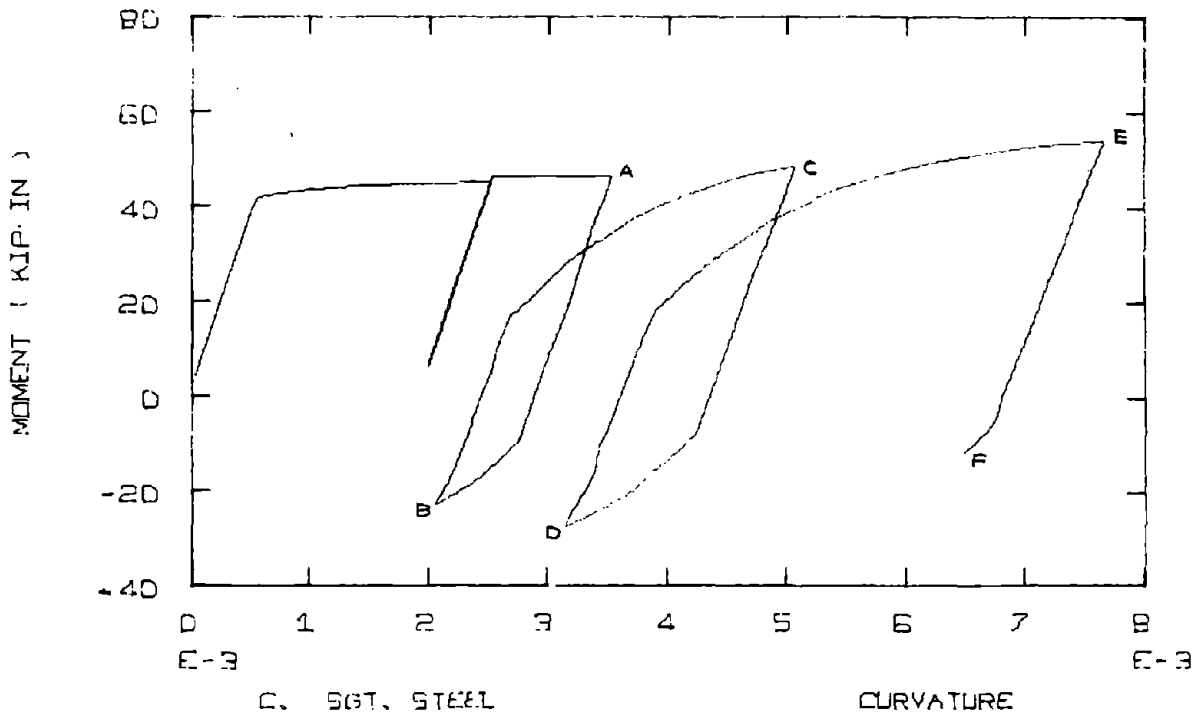
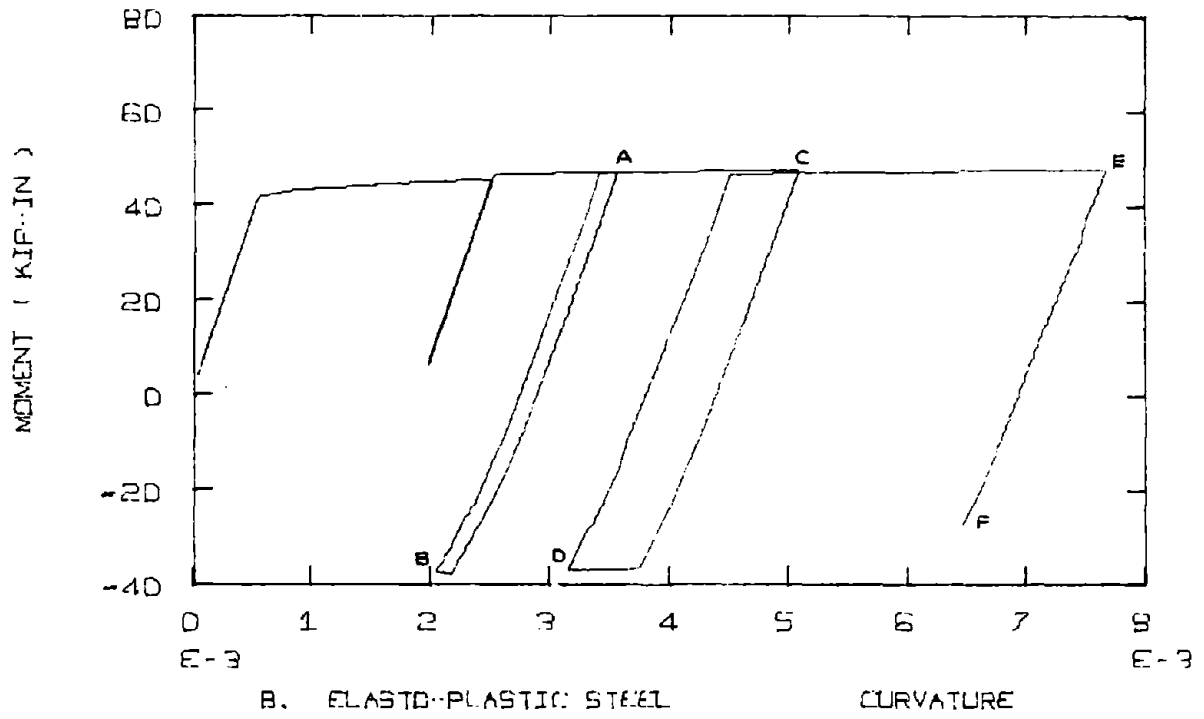


FIG. 4-26 (Continued)

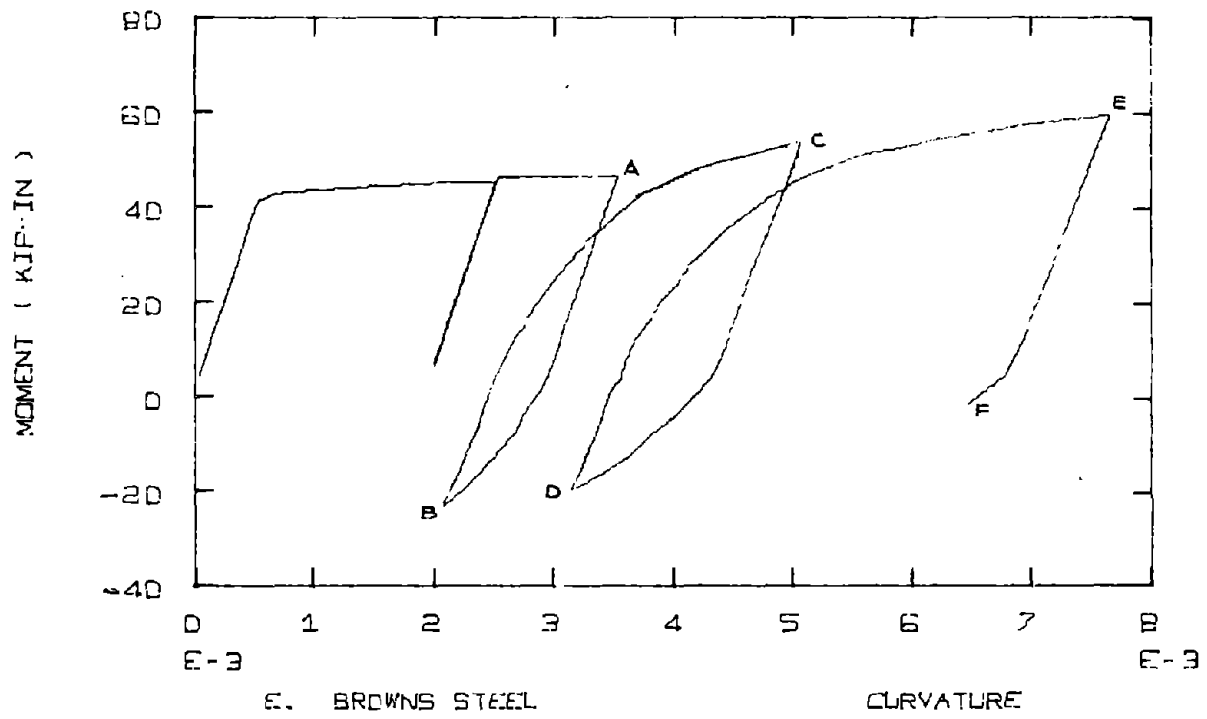
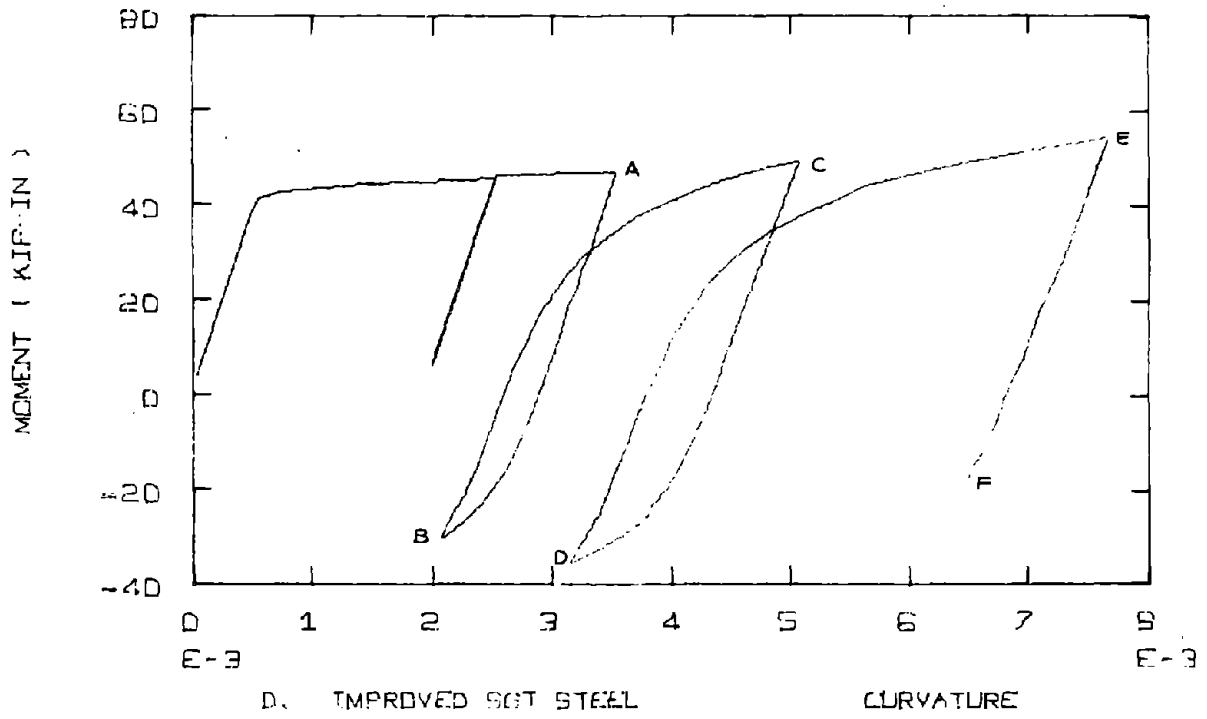


FIG. 4-26 (Continued)

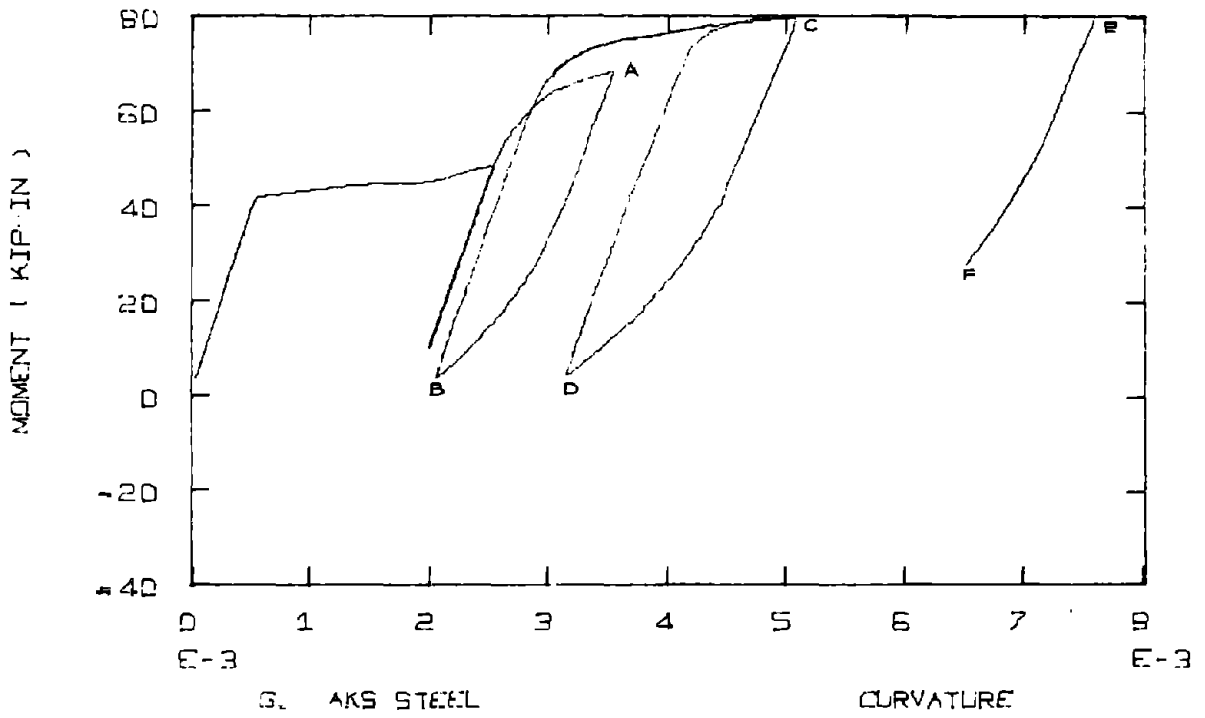
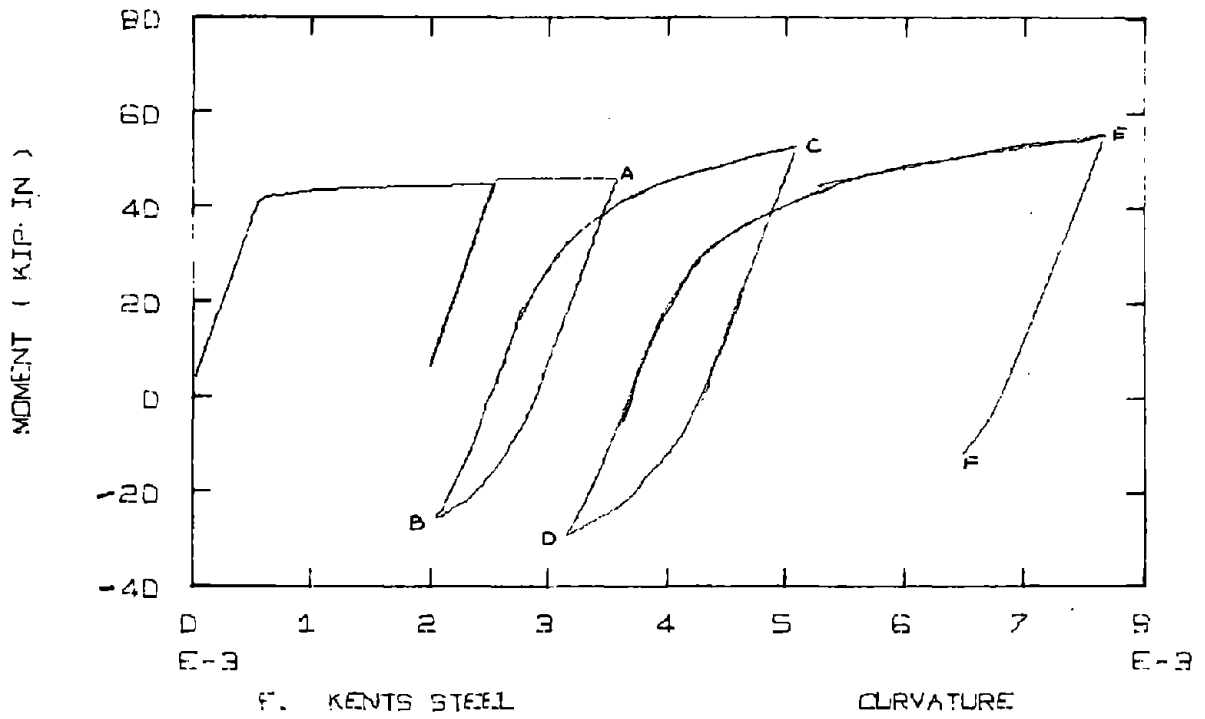


FIG. 4-26 (Continued)

#### 4.8.3 Kent's<sup>(19)</sup> Beam #24, Fig. 4-27 (A to G)

A symmetrically reinforced cross-section is cycled between curvature limits of  $-.00156$  to  $.00189$ . This is the same section used for many of the previous discussions of moment-curvature behavior.

Overall the Elasto-Plastic steel provides a good fit on the moment curvature relations. It should be noticed that there are changes in the stiffness provided by the concrete fiber participation. In the unloading curves  $\overline{BC}$  and  $\overline{DE}$  the Elasto-Plastic model is providing some of the observed stiffness degradation. This is due to fewer concrete fibers participating in  $\overline{DD'}$  than in  $\overline{BB'}$ . The stiffnesses after points B' and D' are the same because only the steel couple is participating. In general the end points appear to match well.

Generally the problem with all the curvilinear models seems to be in the reloading ( $\overline{CD}$  and  $\overline{EF}$ ), where they appear to be much softer than the experimental results. In a real beam there may be more concrete participation in reloading than the model provides.

Kent's and the Improved SGT formulations do very well on the unloading portions ( $\overline{BC}$ ,  $\overline{DE}$ ) and do slightly better on reloading than the other formulations. For larger curvatures, the AKS has the tendency to overestimate the moment.

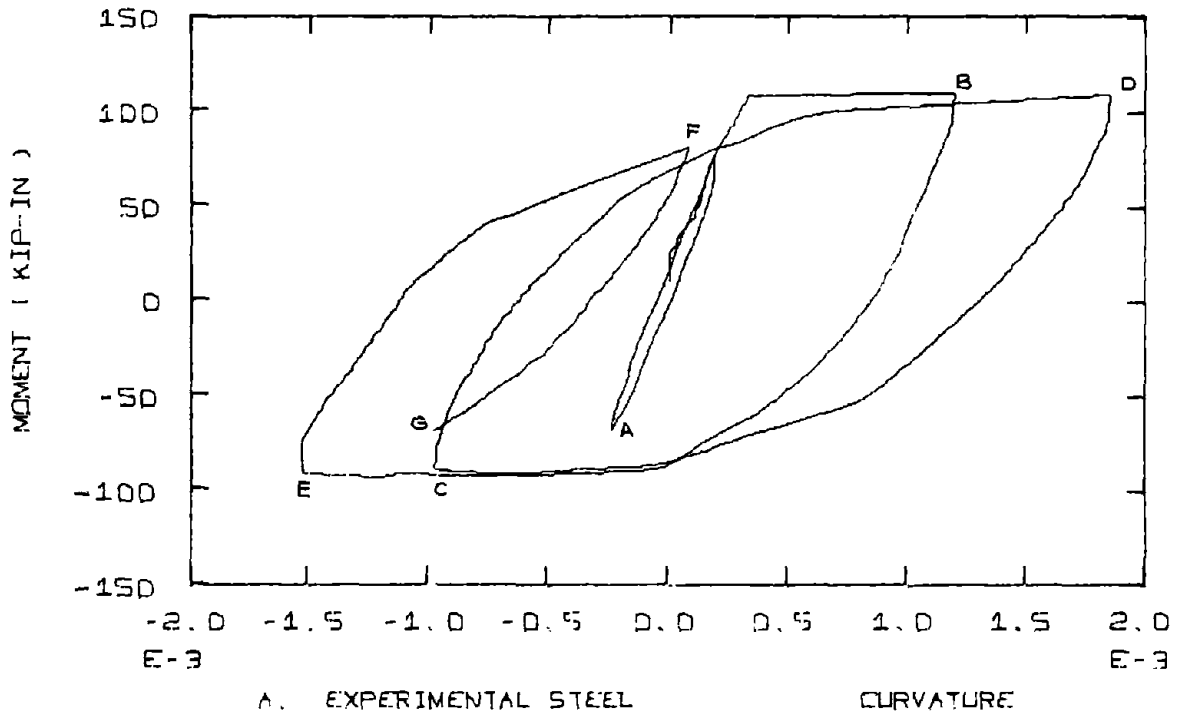


FIG. 4-27 - MOMENT-CURVATURE COMPARISONS  
FOR KENT'S BEAM #24

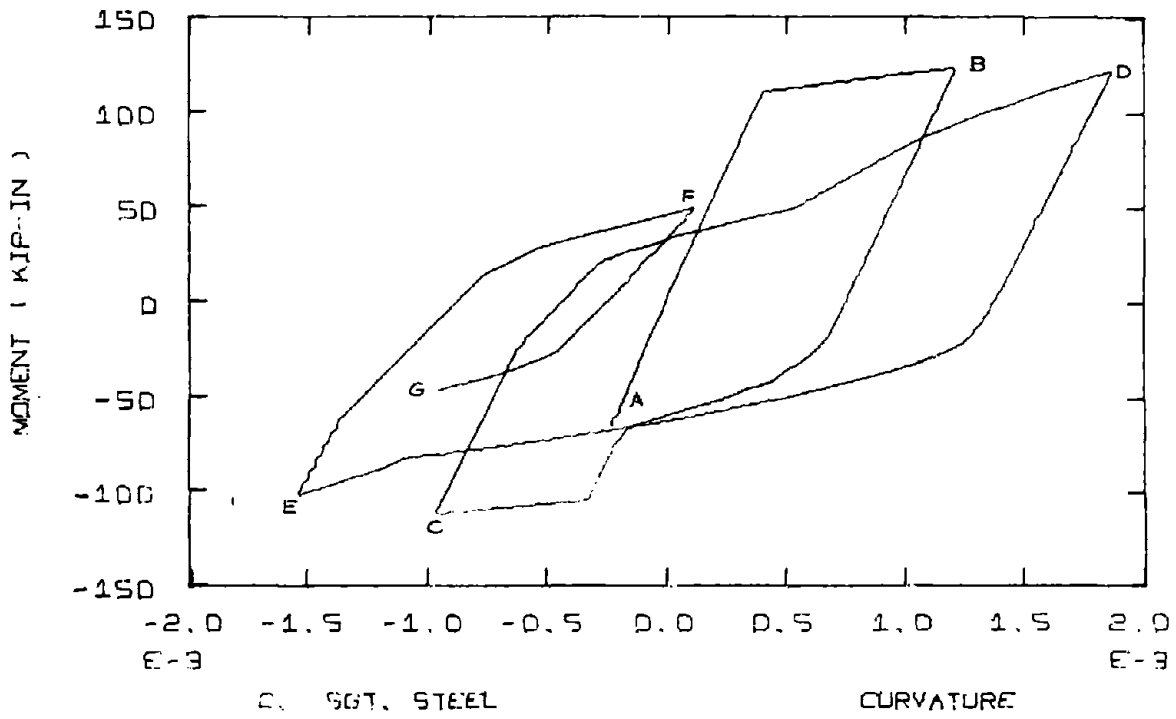
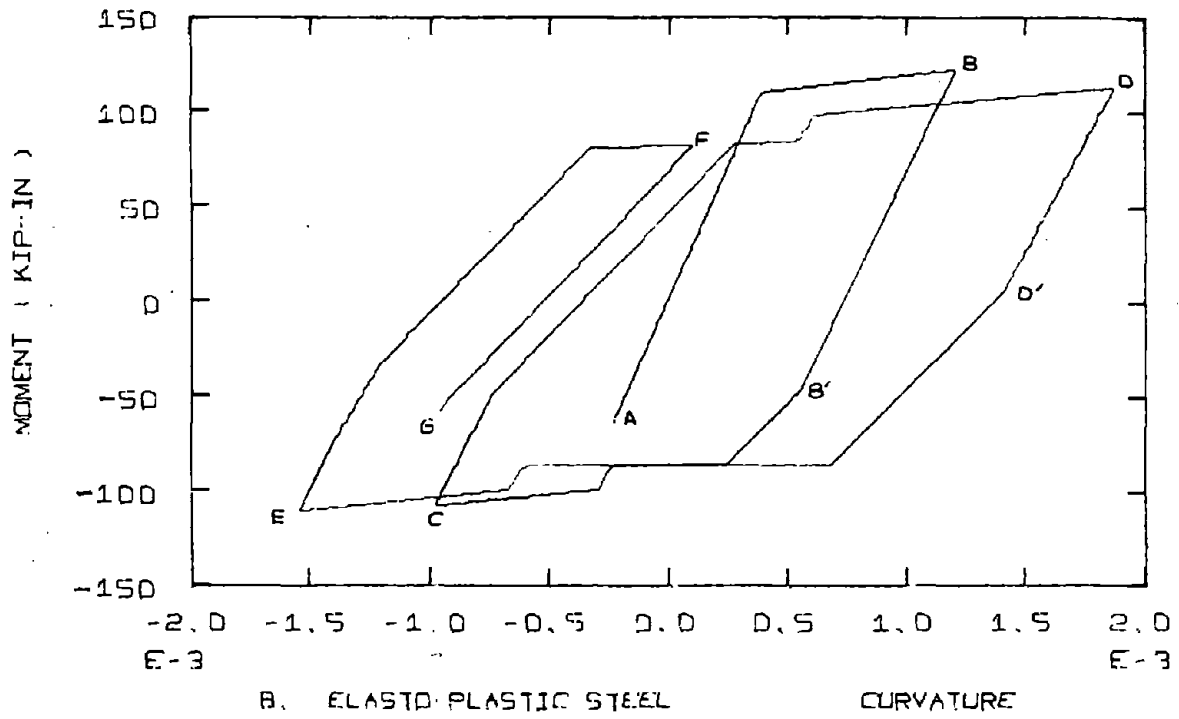


FIG. 4-27 (Continued)

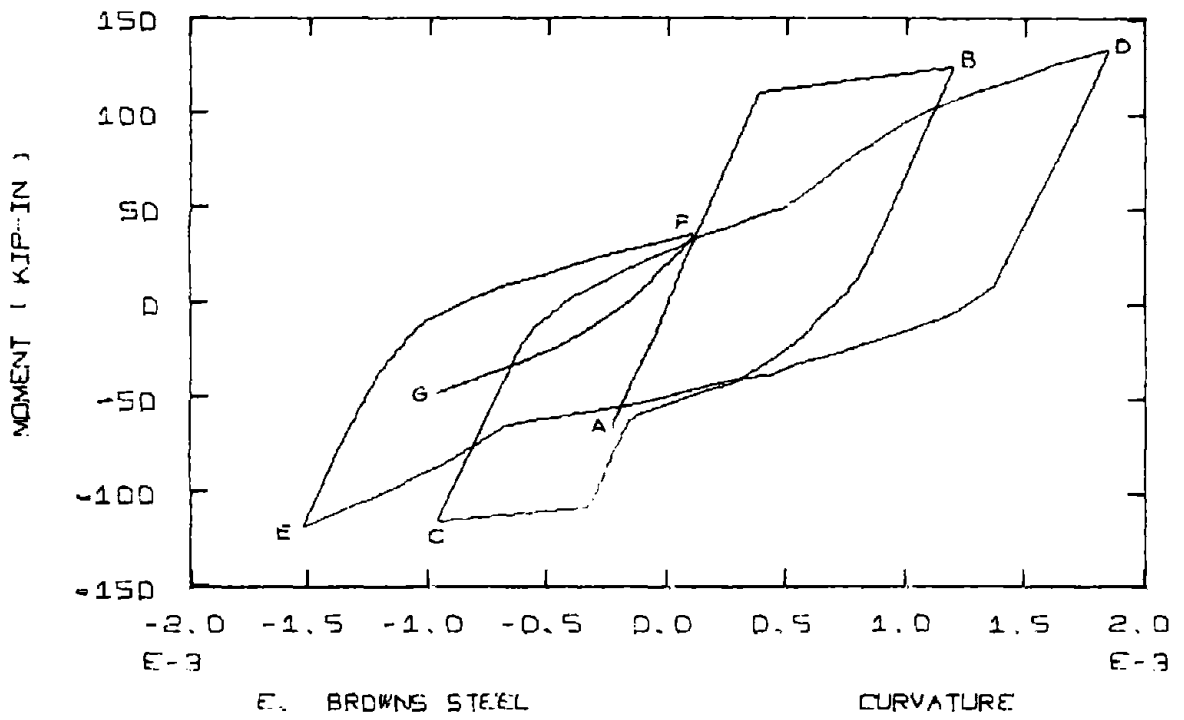
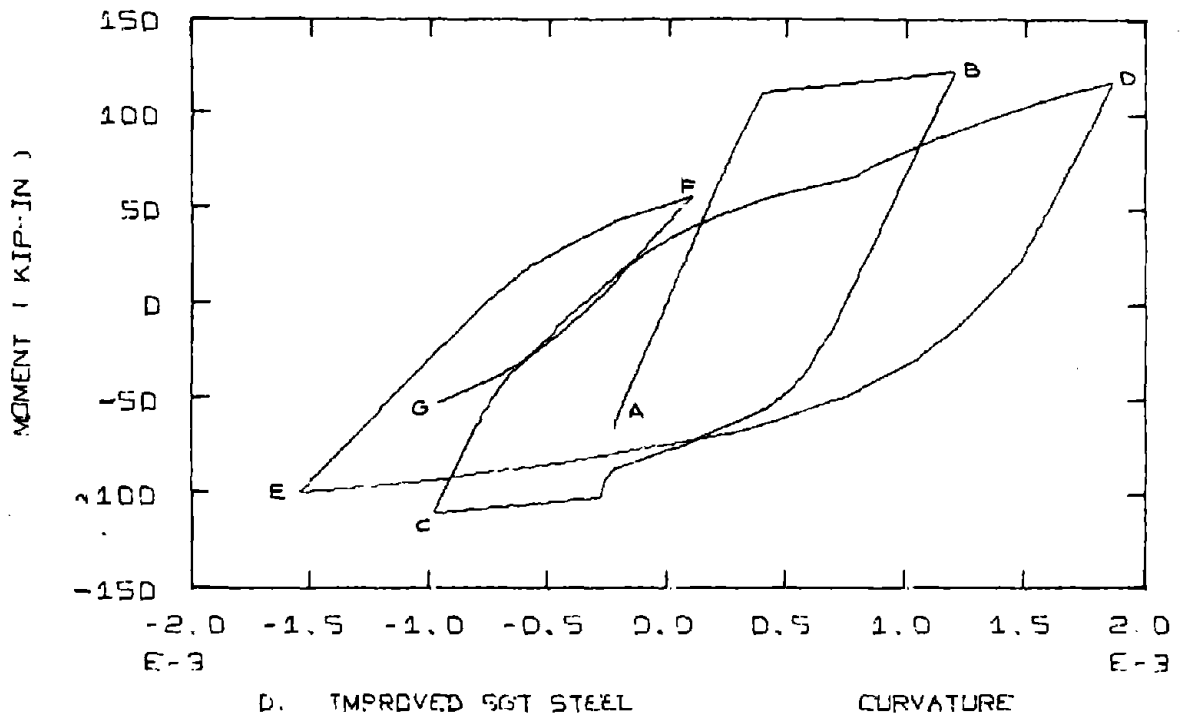


FIG. 4-27 (Continued)

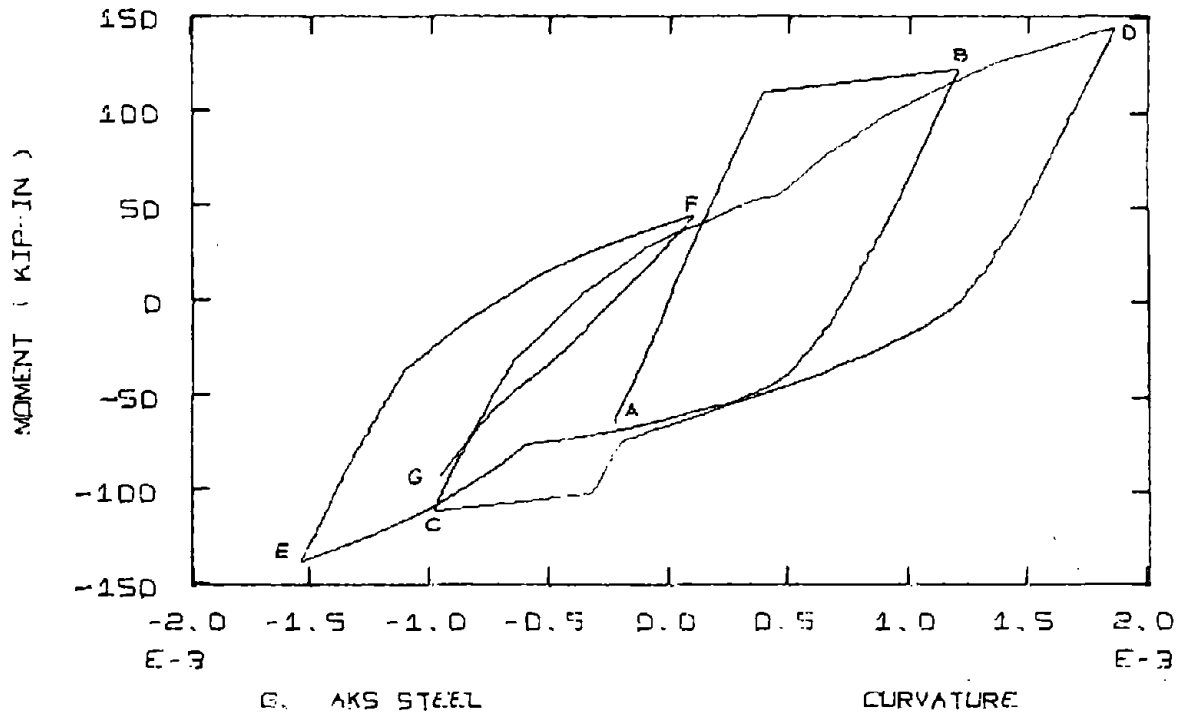
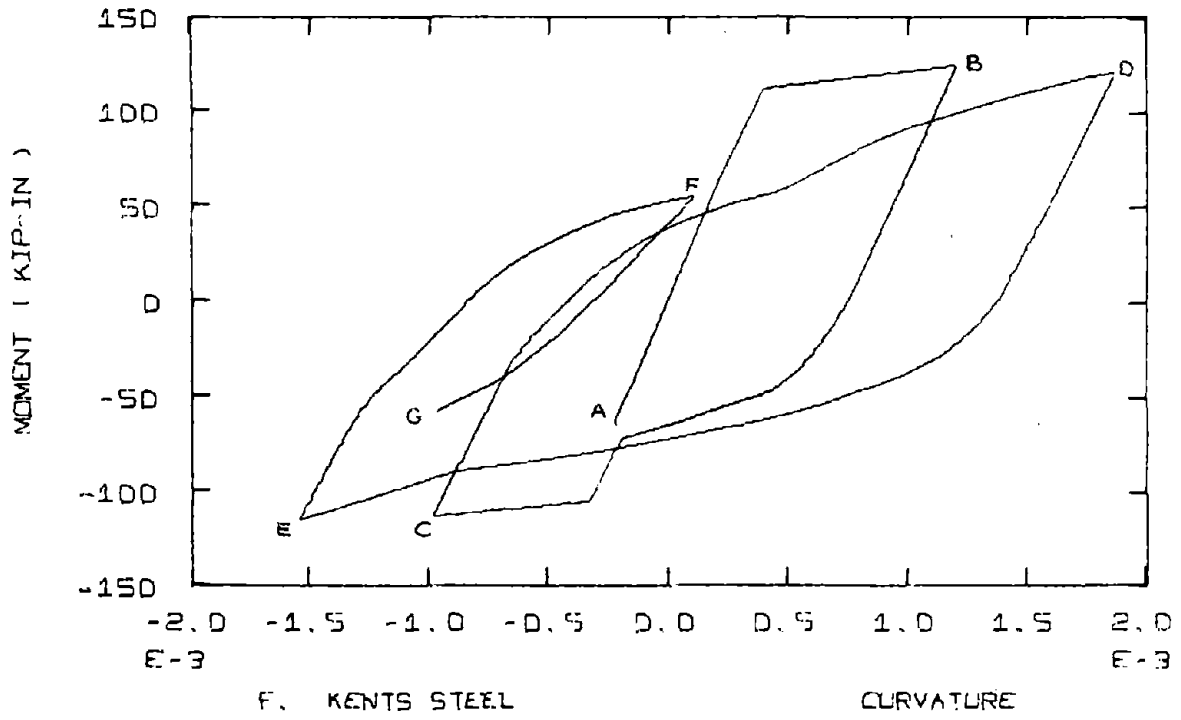


FIG. 4-27 (Continued)

#### 4.8.4 Kent's<sup>(19)</sup> Beam #27, Fig. 4-28 (A to G)

In this unsymmetrically reinforced section, the bottom steel area is three times the top steel ( $A_s = 1.20 \text{ in}^2$ ,  $A'_s = .40 \text{ in}^2$ ). This results in a significant difference in the observed moment capacities of +300 and -96 kip-in. Curvatures encountered in this loading ranged from -.000748 to .00208. From the experimental curves there seem to be a tendency to form closed loops. In the cycle  $\overline{BCD}$ , the reloading branch  $\overline{CD}$  passes very close to point B and  $\overline{EF}$  in cycle  $\overline{DEF}$  seems to be heading toward point D.

The Elasto-Plastic steel does very well in representing the unloading and reloading branches in an average sense. It has yield plateaus at points C' and E' which the test data does not have, but the end points of the cycles have good agreement.

The first three curvilinear steels, SGT, Improved SGT, and Brown's (modified) are very close to each other. Again the unloading curves,  $\overline{BC}$  and  $\overline{DE}$ , provide good agreement, but the reloading curves are too soft, particularly  $\overline{CC'D}$ . The experimental data is showing a distinct yield plateau which none of the curvilinear models have. However, these formulations provide a good estimate of the end point D.

In  $\overline{CD}$ , both Brown's and AKS formulations become very stiff after point C' and since the steels do not yield near point B, the maximum moment is greatly overestimated. The same thing happens in reloading branch EF.

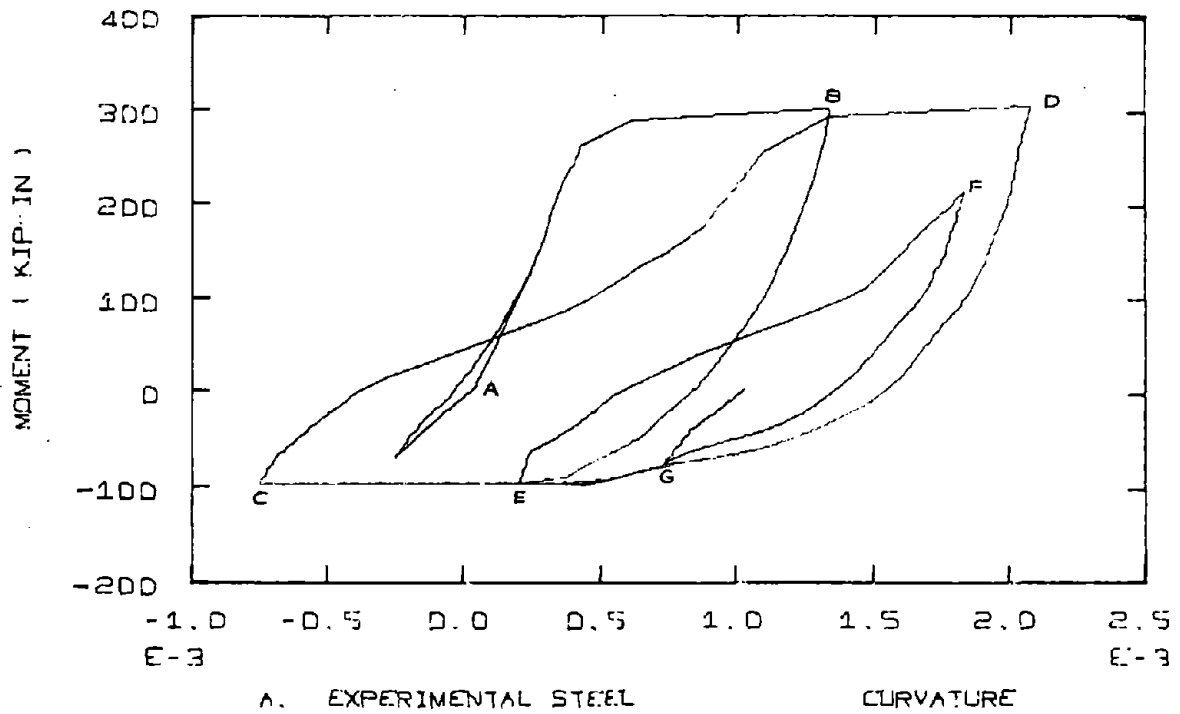


FIG. 4-28 - MOMENT-CURVATURE COMPARISONS  
FOR KENT'S BEAM #27

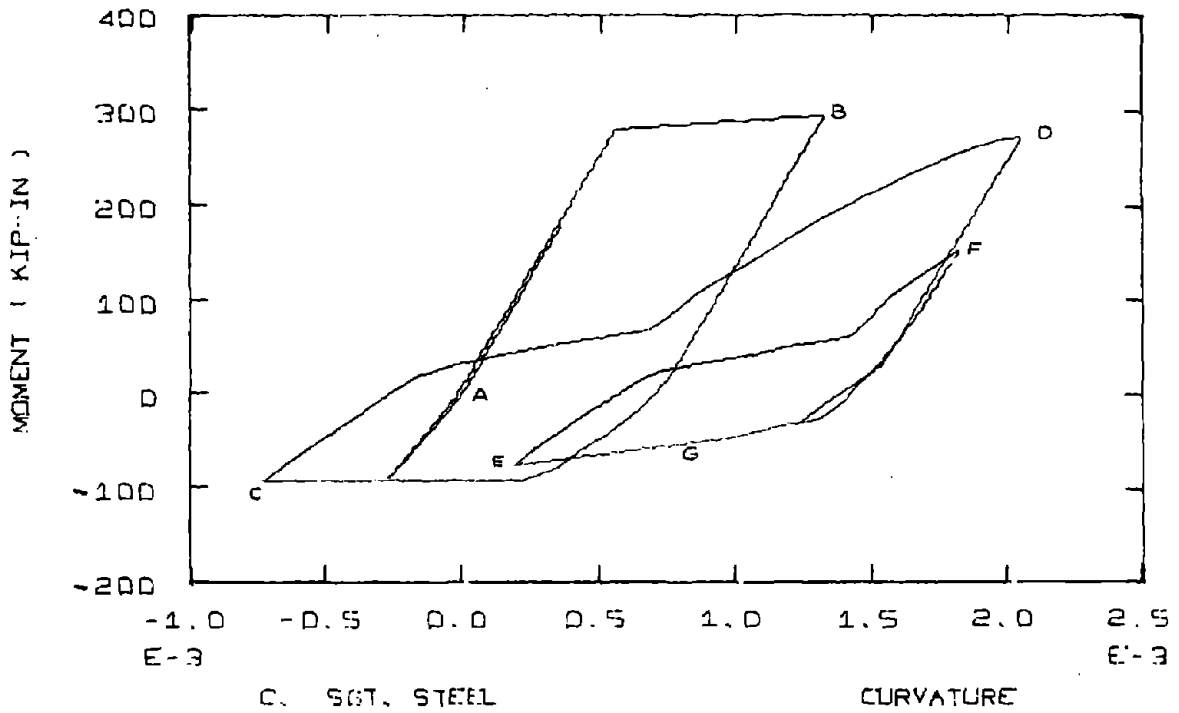
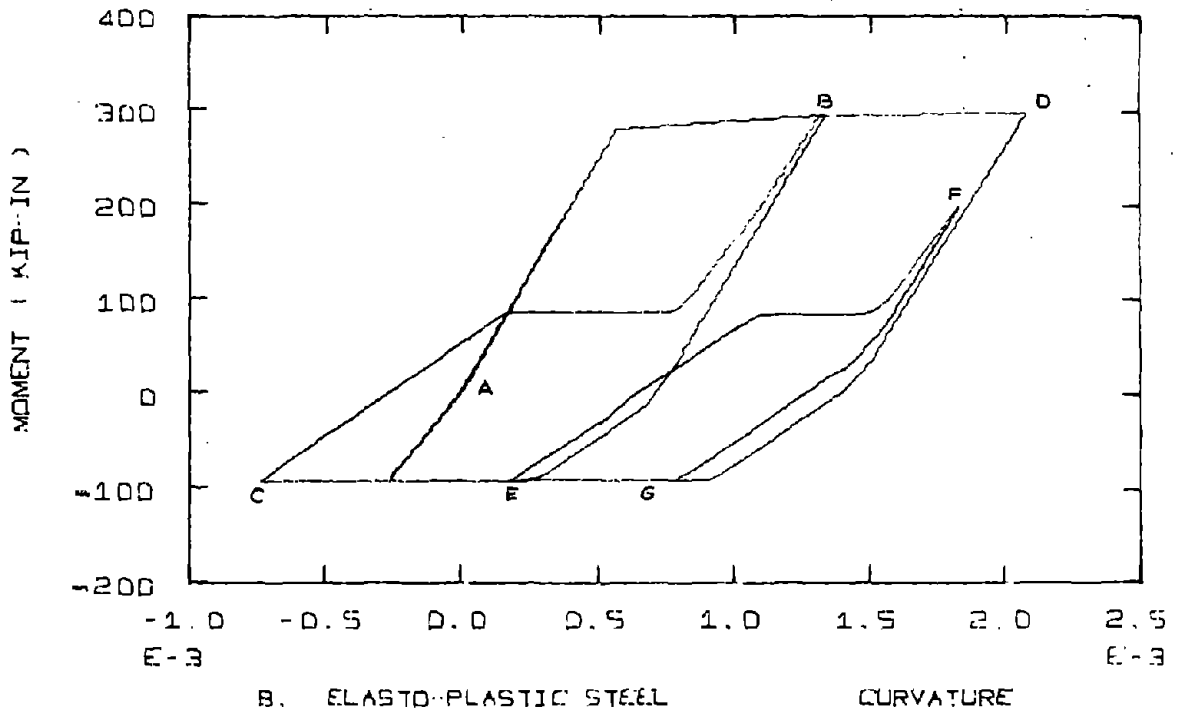


FIG. 4-28 (Continued)

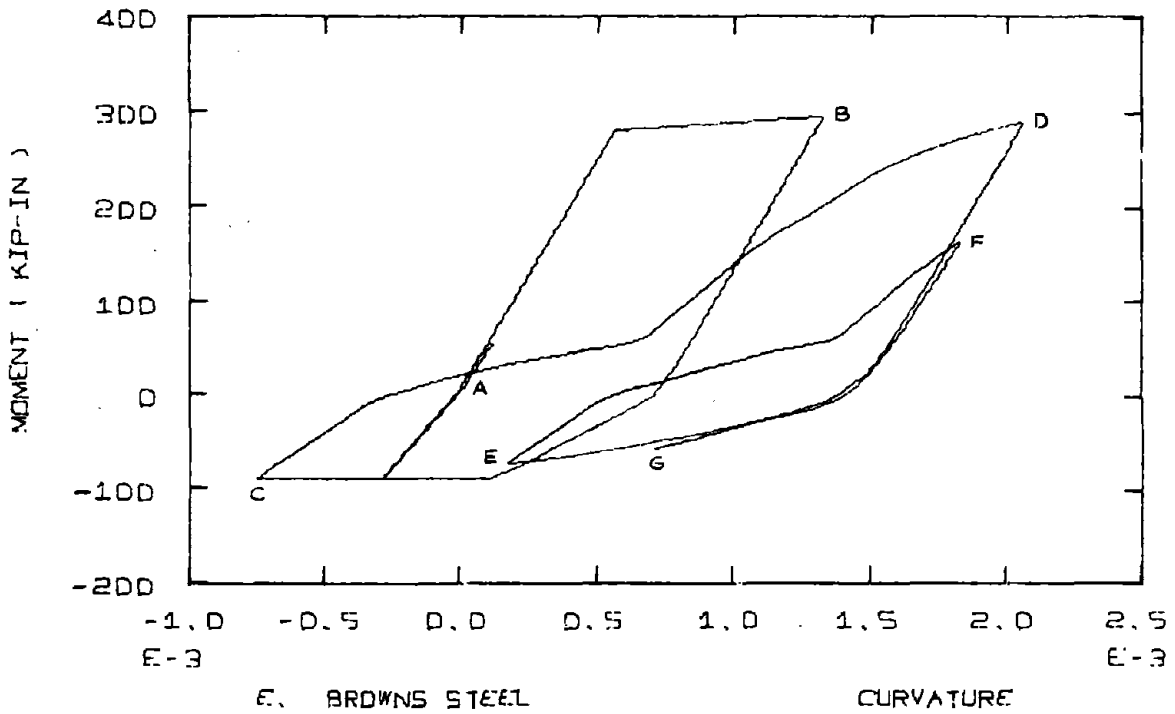
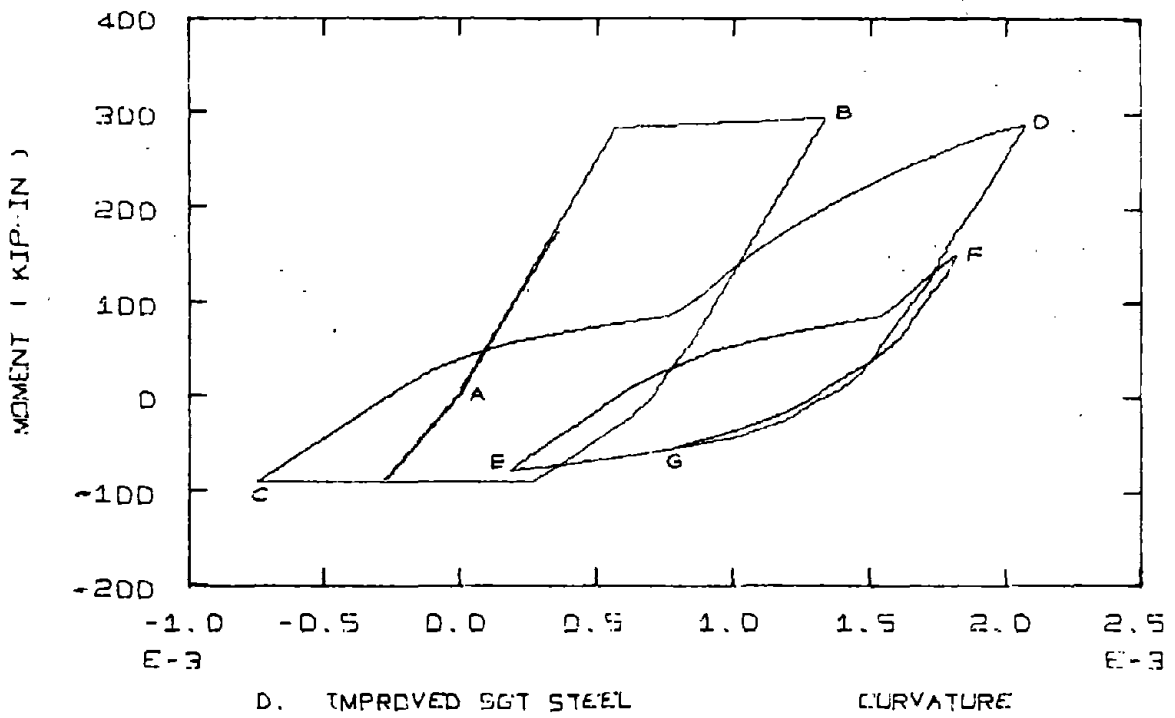


FIG. 4-28 (Continued)

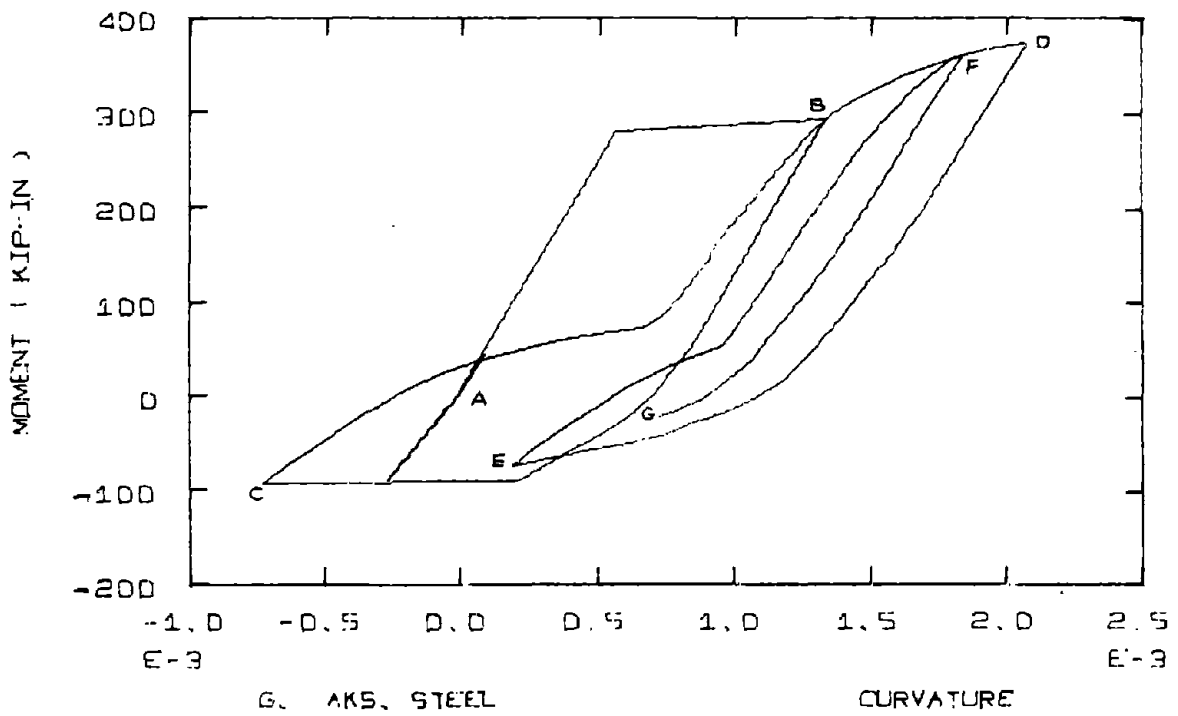
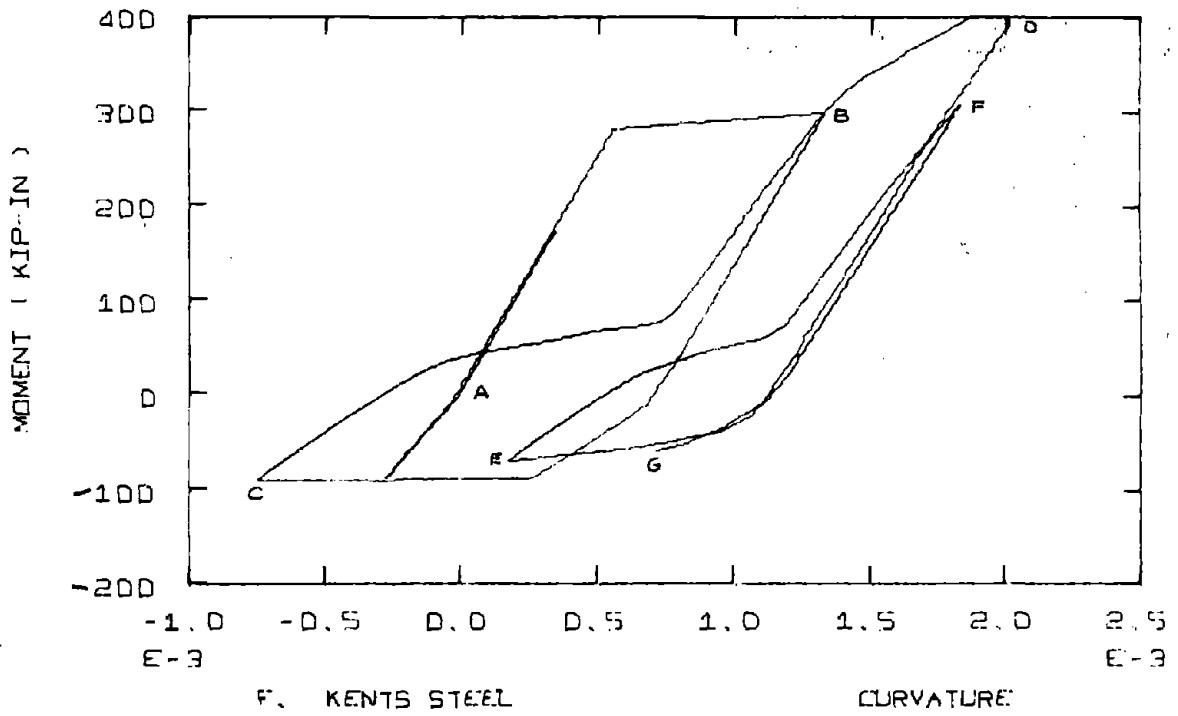


FIG. 4-28 (Continued)

#### 4.9 CONCLUSIONS

The fiber model with the incremental stiffness approach is able to represent the main features of the behavior of a reinforced concrete cross-section. The incremental stiffness approach is very sensitive to increment size, but for a given section reasonable values can be obtained by a trial and error procedure as described.

With the model representing the coupling between axial forces and bending, the "pinching-in" effect and changes in moment capacity under axial force have been reproduced. In addition, an axial force which varies with moment can significantly affect the moment-curvature relationship, by reducing the area of a typical loop.

None of the analytic models is able to represent, in a point by point correspondence, the observed moment curvature behavior. There is too much variability in the materials and their behavior to find a perfect model. Agreement has been reasonable only in a general sense. The Elasto-Plastic steel model provides better agreement than was expected and may have value in the subsequent member studies. All models with the curvilinear steels tend to represent well the unloading stiffness, but are softer than observed in reloading. The moment-curvature relations reflect strongly the assumed steel formulation, and the conclusions made in the previous chapter on the steel carry over for the section behavior. In the remaining chapter only the Elasto-Plastic steel and the Improved SGT steels will be used for comparisons.

## CHAPTER 5 - MEMBER STUDY

5.1 INTRODUCTION

In this chapter the fiber model along with the incremental stiffness approach is extended to study the behavior of members under cyclic loading. The structures considered are simply-supported beams, cantilever beams and simple frames.

The purpose of this chapter is to compare the analytic models (elasto-plastic and curvilinear steels) with experimental results and to discuss the advantages and limitations of the solution technique when extended beyond moment-curvature studies.

5.2 INCREMENTAL STIFFNESS ANALYSIS5.2.1 Solution Scheme

The stress-strain behavior of each fiber at a cross-section is monitored, during the loading process. From the tangent moduli, stiffness coefficients,  $a_{ij}$ , are obtained (Eq. 4.3). Inversion results in flexibility equations relating  $\Delta\epsilon$ ,  $\Delta\phi$  to  $\Delta N$ ,  $\Delta M$ . Using small deflection relations for the incremental strains and curvatures leads to

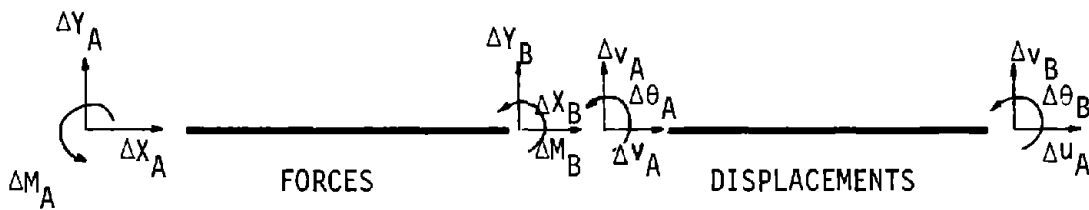
$$\begin{aligned}\Delta\epsilon &= \frac{d}{dx} (\Delta u) = b_{11} \Delta N + b_{12} \Delta M \\ \Delta\phi &= \frac{d^2}{dx^2} (\Delta v) = b_{21} \Delta N + b_{22} \Delta M\end{aligned}\tag{5.1}$$

where  $u$ ,  $v$  are the axial and lateral displacements of the member;  $x$  is the location of the cross-section; and  $b_{ij}$  are the flexibility coefficients.

Equation (5.1) is then integrated to obtain a flexibility relation for the member. This relates the end displacements  $\{\Delta u_j^i\}$  to the end forces  $\{\Delta p_j^i\}$ . The integration is carried out numerically by the trapezoidal rule at each of the twenty equally spaced cross-sections.

Finally inversion of the flexibility matrix yields the member stiffness matrix,

$$\{\Delta p_j^i\} = [K_j^i] \{\Delta u_j^i\} \quad (5.2)$$



where

$$\{\Delta p_j^i\} = \begin{Bmatrix} \Delta X_A^i \\ \Delta Y_A^i \\ \Delta M_A^i \\ \Delta X_B^i \\ \Delta Y_B^i \\ M_B^i \end{Bmatrix} \quad \{\Delta u_j^i\} = \begin{Bmatrix} \Delta u_A \\ \Delta v_A \\ \Delta \theta_A \\ \Delta u_B \\ \Delta v_B \\ \Delta \theta_B \end{Bmatrix}$$

$[K_j^i]$  is 6 x 6 and it is a tangential stiffness matrix; that is, it represents the instantaneous stiffness of the  $j^{\text{th}}$  member at step (i). Appendix A provides a detailed derivation of this matrix.

Once all the member stiffness matrices are computed, standard methods of assembling the total stiffness matrix for the structure and modifying for support conditions are used. The structures considered in this study are planar, and each member is assumed to be represented by a line element.

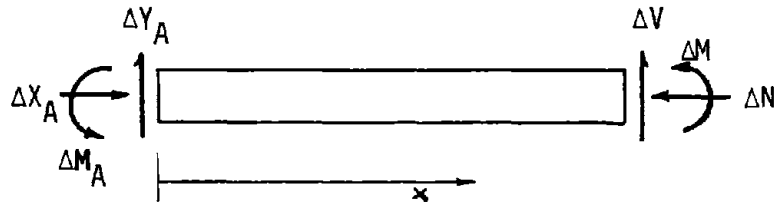
The Euler method is used in the member study to proceed from step (i) to (i+1). The incremental displacements at the joints are determined from:

$$\{\Delta U_T^i\} = [K_T^i]^{-1} \{\Delta P_T^i\} \quad (5.3)$$

where  $\{\Delta P_T^i\}$  may be forces due to specified displacements. The total displacements and forces at (i+1) are simply

$$\begin{aligned} \{U_T^{i+1}\} &= \{U_T^i\} + \{\Delta U_T^i\} \\ \{P_T^{i+1}\} &= \{P_T^i\} + \{\Delta P_T^i\} \end{aligned} \quad (5.4)$$

From the incremental joint displacements, member end forces can be determined from Eq. 5-2, once the displacements are rotated to member coordinates. To update the tangent stiffness matrix, the incremental axial forces and moments at each cross-section have to be determined.



$$\Delta N = \Delta X_A$$

(5.5)

$$\Delta M = \Delta M_A + \Delta Y_A x$$

This relationship assumes the member is represented by a straight line between joints. From these incremental forces and the flexibility coefficients at step (i), new strains, stresses and tangent moduli are computed at each cross-section. The tangent stiffness matrix is then determined for the structure at step (i+1).

### 5.2.2 Nonlinear Effects

After each application of an incremental load (or displacement), the geometry of the structure is updated, by adding the computed incremental displacements to the corresponding joint coordinates.

With the incremental stiffness equations, equilibrium is satisfied in the undeformed position, and corrective forces should be applied to satisfy equilibrium in the deformed position. This is particularly important in the case of members with axial forces and lateral displacements and is usually called the "P-Δ" effect. If the axial force is compressive, the lateral deflections of the member will

be amplified. Roesset<sup>(45)</sup> et al have shown that use of corrective lateral forces will reproduce the elastic stability (P-Δ effect) of the member. Latona<sup>(32)</sup> incorporates the corrective forces into the tangent stiffness matrix, thereby correcting before the next step. The following are changes to the member stiffness matrix: (Eq. 5.2).

$$\begin{aligned}
 K_{22} &= K_{22} + \frac{X_B}{L} \\
 K_{25} &= K_{25} - \frac{X_B}{L} \\
 K_{52} &= K_{52} - \frac{X_B}{L} \\
 K_{55} &= K_{55} + \frac{X_B}{L}
 \end{aligned}
 \tag{5.6}$$

These terms relate lateral forces to lateral displacements. Latona's scheme is included in the member study.

### 5.2.3 Limitations of the Incremental Stiffness Approach for the Member Study

As pointed out in the previous chapter, results from the incremental stiffness approach are very sensitive to increment size. An appropriate increment size was again chosen by trial (values used were on the order of yield deflection divided by 160). Although deflections are controlled in the member study, incremental forces  $\Delta M$ ,  $\Delta N$  are applied at the cross-section level. This can lead to large errors when there are sudden changes in the cross-section stiffness, such as when the steel yields.

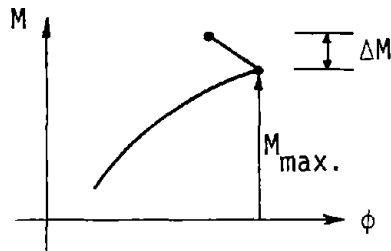
Since inversion of the stiffness coefficients  $a_{ij}$  is required in the solution scheme, numerical problems occur when  $a_{ij}$  approaches zero. This situation can occur when there is no concrete participation after a few cycles of loading, and both steel fibers yield. To prevent numerical instability, a 1% second slope on the steel stress-strain curve is provided.

A similar difficulty occurs when the moment-curvature relations have a descending branch following that of the concrete stress-strain curve. The stiffness coefficients can approach zero and even become negative, for large straining of the cross-section.

Consider the case of a cantilever beam with the deflection at the free end being increased. The maximum moment occurs at the fixed end. When this section's moment capacity is exceeded, the descending branch of the moment-curvature relationship is reached, and the rotational stiffness becomes negative. An inelastic hinge (such as Barnard<sup>(36)</sup> describes) has formed, and increased curvature results in a decrease in moment. In an experimental setup this means that if displacements are controlled, the applied load will drop, but if load is controlled, failure of the member will result.

Generally the analytic solution is able to represent this behavior. However, because the computation of the member stiffness involves integration by the trapezoidal rule (essentially a weighted averaging of section properties), it is possible that the member stiffness will not be negative even though the rotational stiffness at the

support is. If this occurs, increased deflection will lead to an increment of moment being applied to the cross-section, and the type of behavior illustrated below will occur.



The result is that the solution now becomes unstable, so the incremental stiffness method is not able to portray a descending branch for the load-deflection relationship, although it can indicate the point at which hinges form.

To prevent this problem, no descending branch on the concrete stress-strain curve was permitted. In Fig. 5-1 (A to B) moment-curvature curves are shown for Brown's cantilever beam, which will be studied in Section 5-4.1. The first shows the relationship with a descending branch and failure occurring at  $\phi \approx .005$ , defined by the extreme concrete fiber unloading to zero stress at  $\epsilon_c = .01$ . In Fig. 5-1B there is no limiting strain on the concrete, and infinite curvature is possible. Figures 5-1 (C and D) show the effect of 1% slope on the steel and strain hardening. These assumptions significantly change the shape of the  $M-\phi$  curve, but this is beyond the range when the member fails. In the useful range of curvatures such as segment  $\overline{AB}$  the difference is not large.

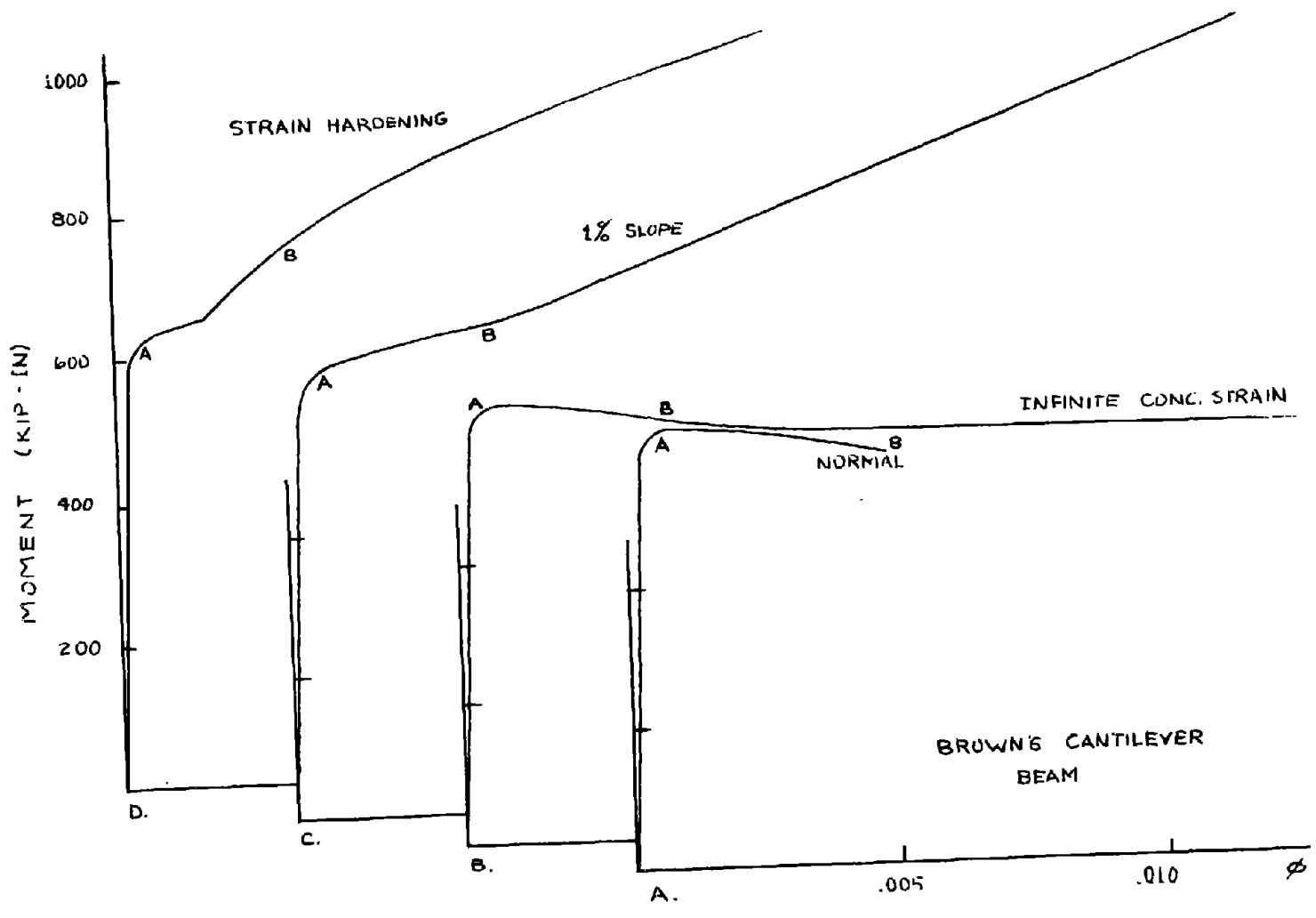


FIG. 5-1 - COMPARISON OF ASSUMPTIONS ON M- $\phi$  CURVES

One method of handling the problem of hinging would be to consider the formation of a semi-rigid joint when a section exceeded the maximum moment capacity (this formulation is discussed in Appendix B). As the hinging spread more sections could be considered in obtaining the moment-rotation relationship. In this way the member stiffness would become negative whenever any cross-section stiffness became negative. This, however, was not implemented.

### 5.3 SIMPLY SUPPORTED BEAM STUDY

#### 5.3.1 Kent's<sup>(19)</sup> Beam #24, Figure 5-2 (A to C)

This simply supported beam loaded at midspan is the same member used for a significant portion of the moment-curvature comparisons in Chapter 4. The loading is cyclic and deflections range from  $-.48''$  to  $.70''$ .

Both analytic models reproduce well the load-deflection behavior of this member under this cyclic loading with relatively small deflections. The average slopes of each half cycle and the end points agree with the experimental curves.

The analytic moment-curvature relations from this member study can be compared with the experimental one and those obtained analytically in the section study (Fig. 4-27). The elasto-plastic  $M-\phi$  curves in Fig. 5-2B show significantly larger curvatures than observed. Point D is at a curvature of  $.0031$ , while the measured value is  $.0018$ . This is a result of sharp changes in section stiffness after yielding and the  $M-\phi$  curve being incremented on  $\Delta M$  and  $\Delta N$ .

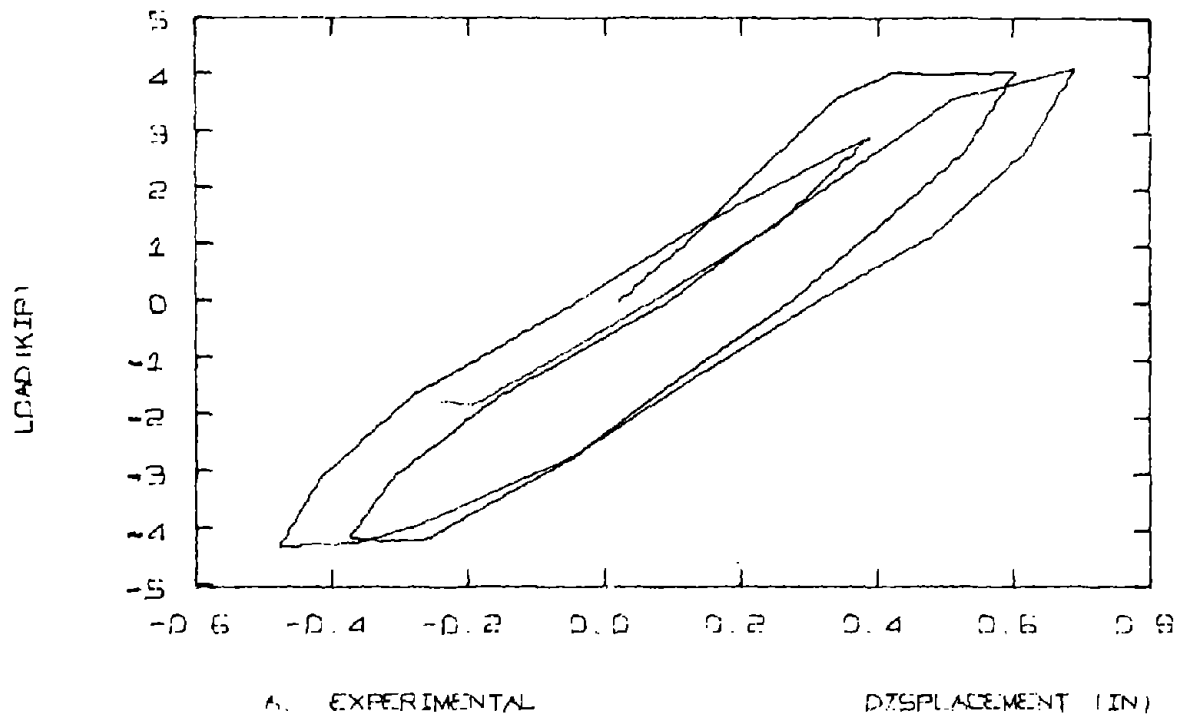


FIG. 5-2 - LOAD-DEFLECTION BEHAVIOR OF KENT'S BEAM #24

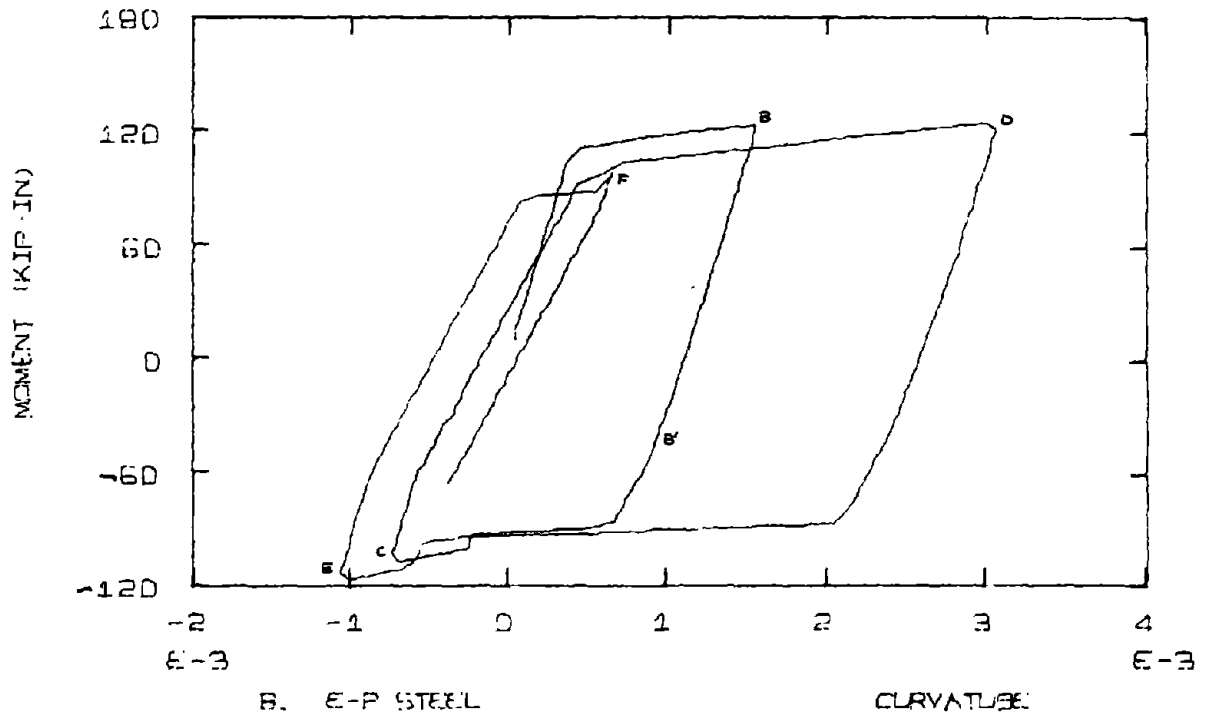
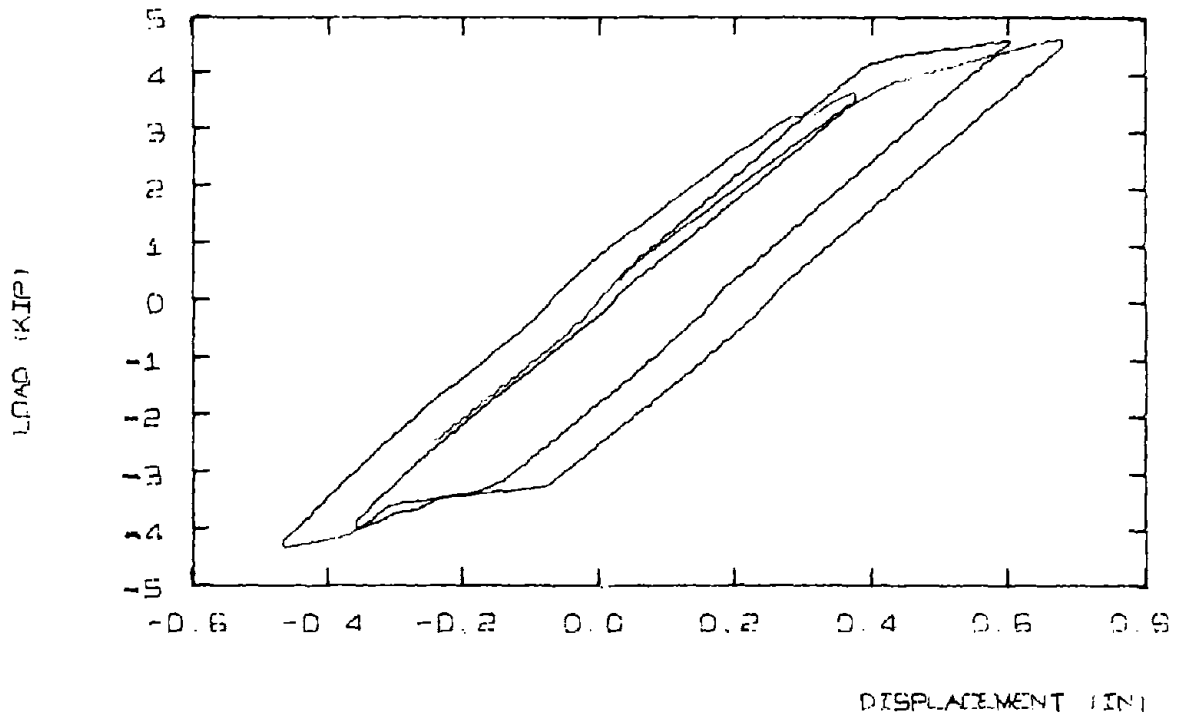


FIG. 5-2 (Cont.)

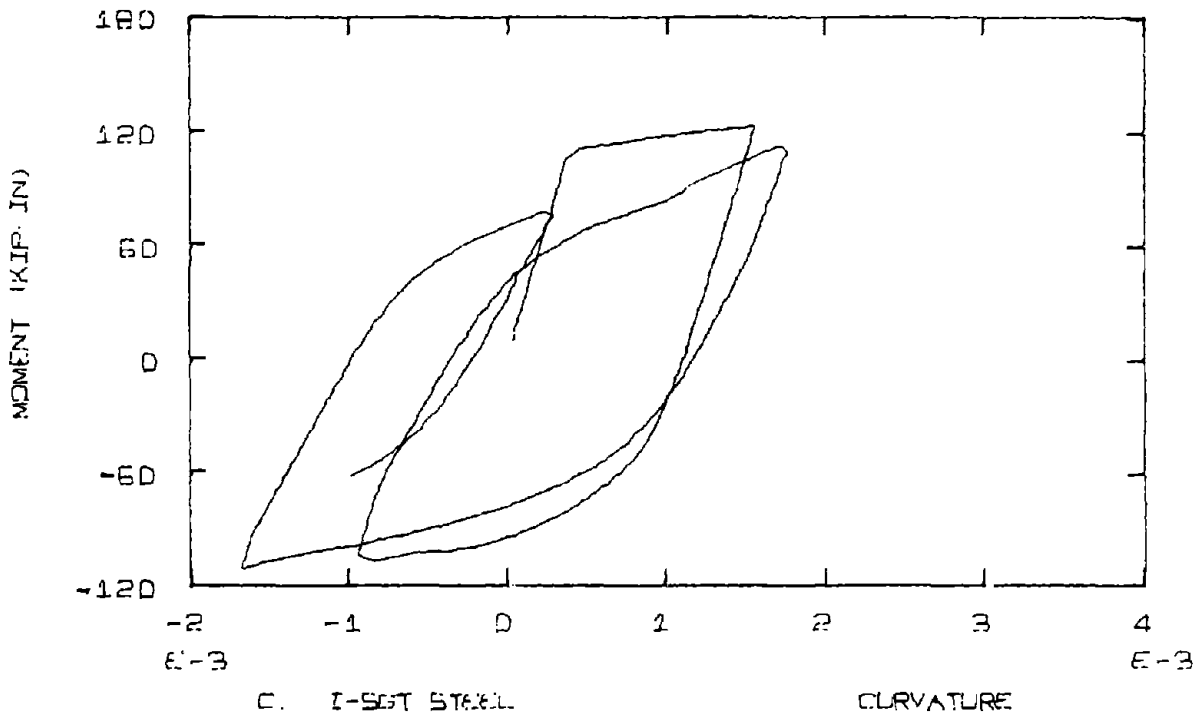
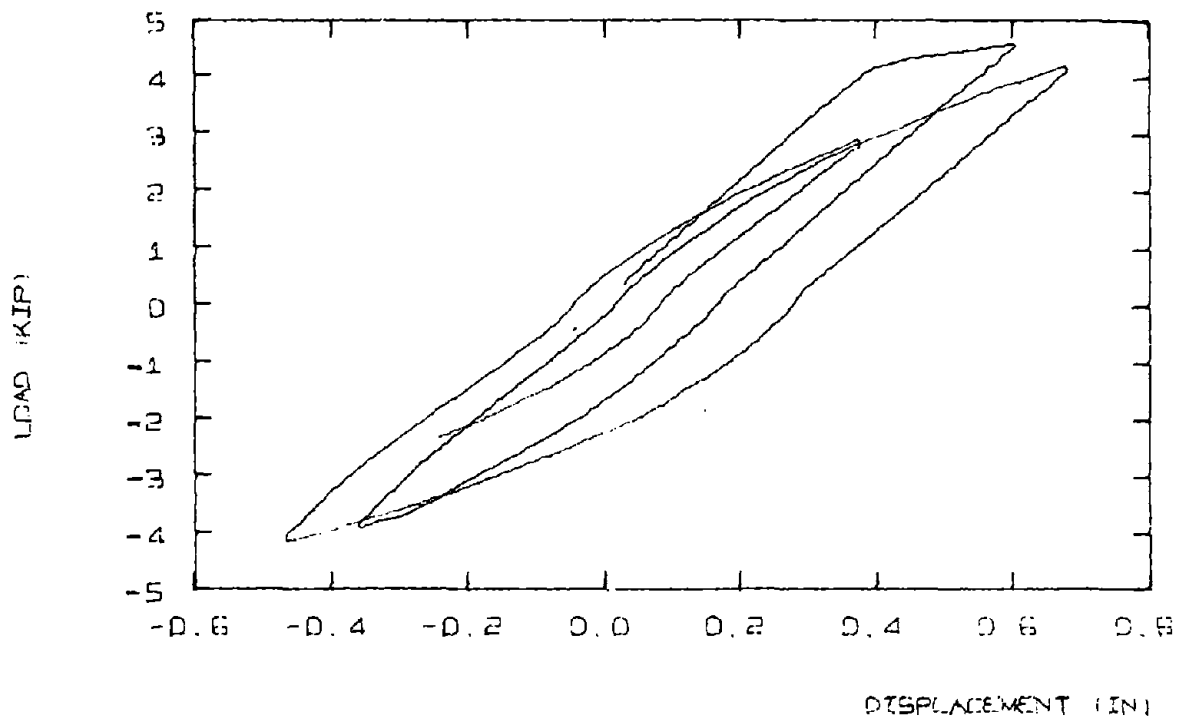


FIG. 5-2 (Cont.)

On the other hand, the  $M-\phi$  curve for the curvilinear steel is much closer to the experimental. The section stiffness changes gradually, and this leads to the incremental stiffness method being better behaved.

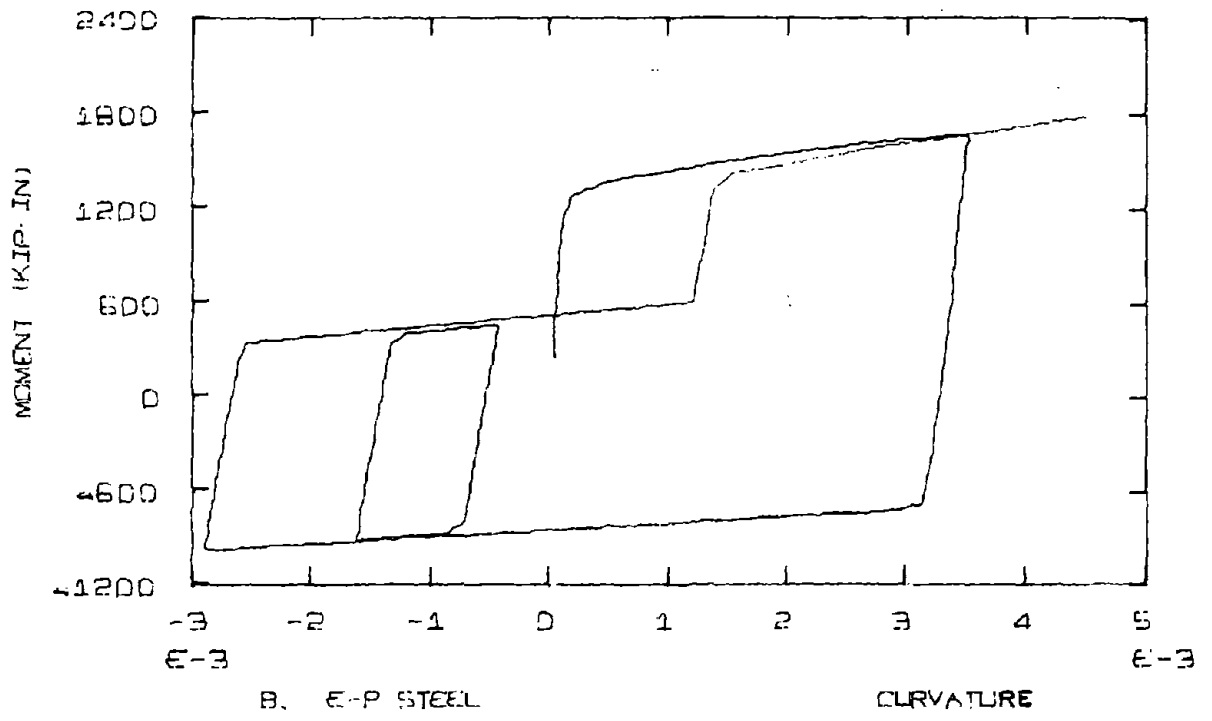
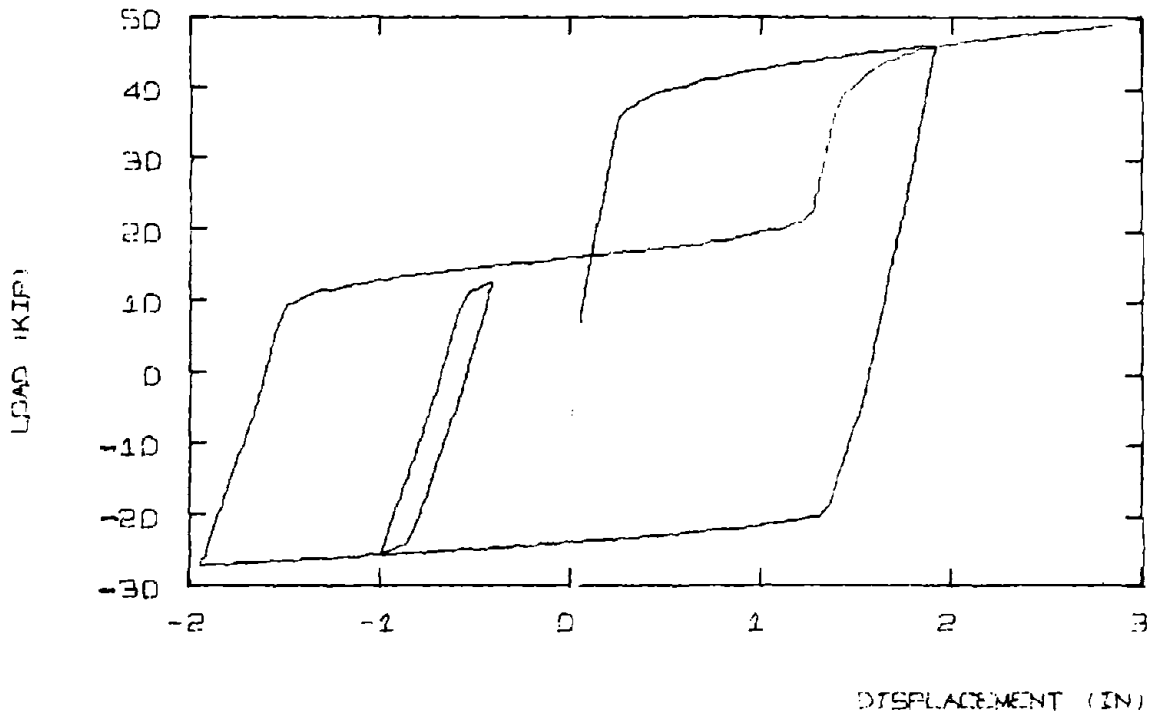
### 5.3.2 Burns and Siess<sup>(33)</sup> Beam J-12, Figure 5-3 (A to C)

This unsymmetrically reinforced member is a simply supported beam with loads applied at midspan. It has a length of 12'0", and deflections are on the order of 3".

For both analytic models, the unloading portion  $\overline{AB}$  provides good agreement with the experimental values as far as stiffness and end values are concerned. For segment  $\overline{DEF}$ , the experimental results indicate a noticeable change in stiffness after unloading to zero at point E. In segment  $\overline{DE}$  both models are stiffer. After E the experimental curve maintains a nearly constant slope, but the analytic models show abrupt changes when the concrete suddenly begins to participate again.

For the loop  $\overline{BCD}$ , the analytic models indicate a load reversal because they are stiffer than the observed curve. The loops for the elasto-plastic model are significantly wider. The curvilinear model is noticeably different in segment  $\overline{CD}$  because of the load reversal and resulting curvilinear behavior.





B. E-P STEEL

CURVATURE

FIG. 5-3 (Cont.)

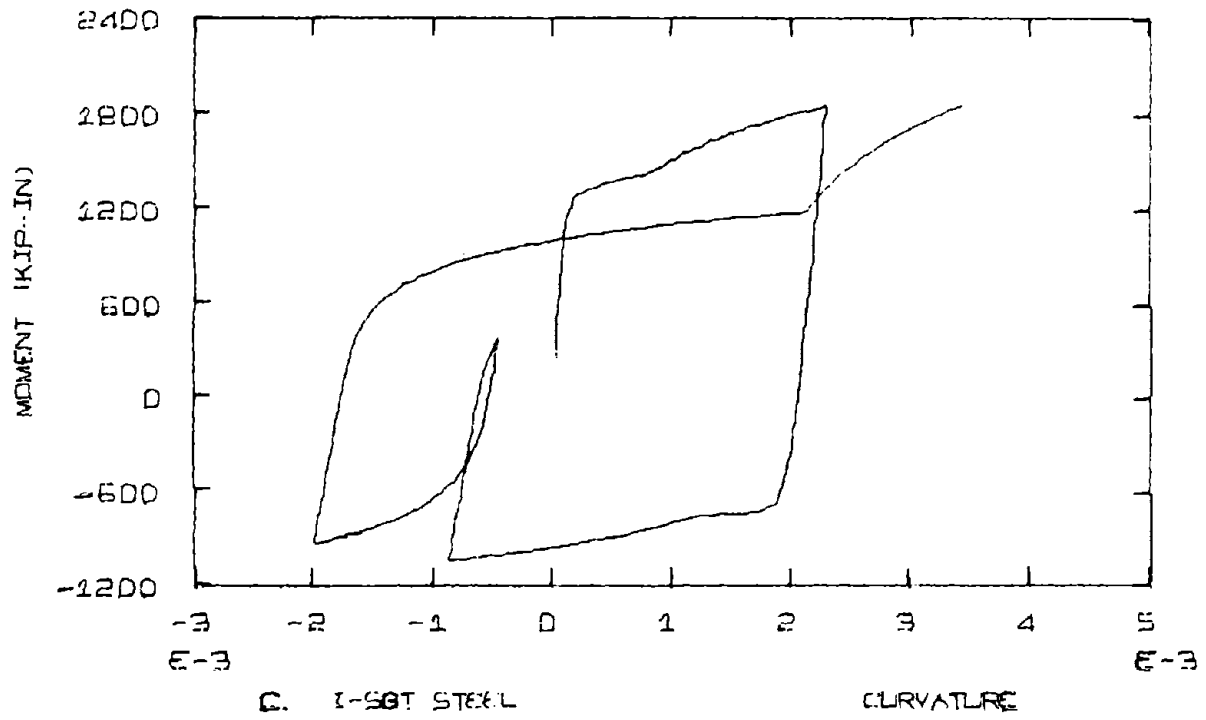
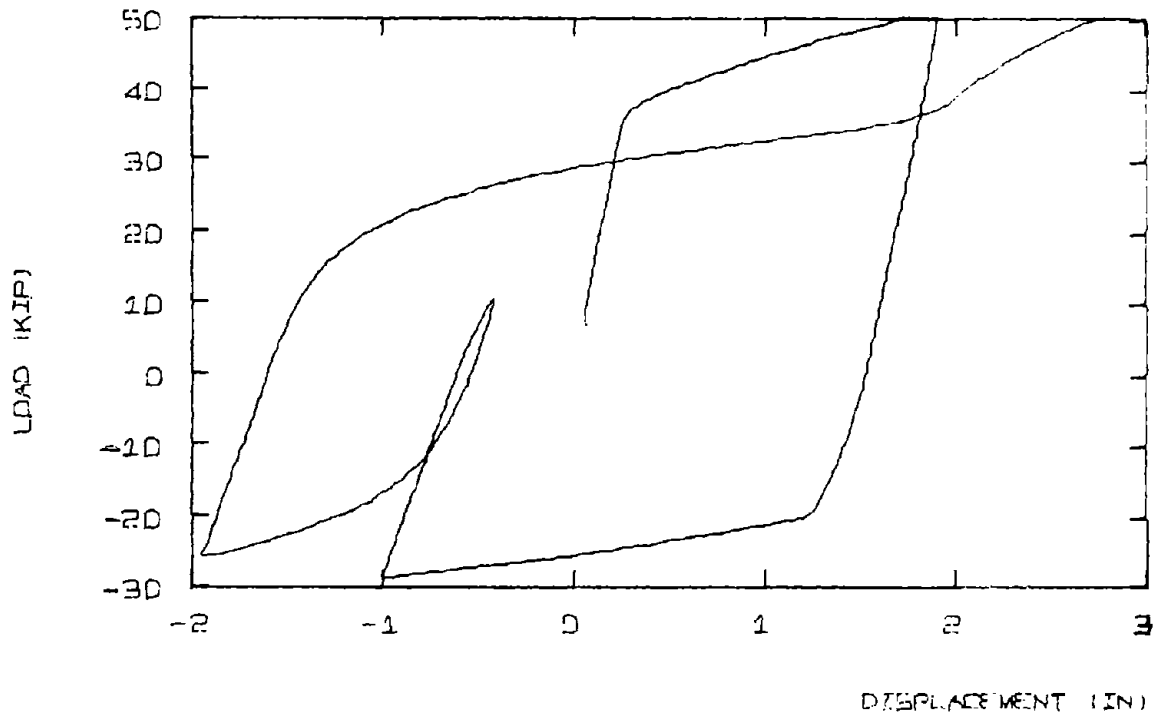


FIG. 5-3 (Cont.)

#### 5.4 CANTILEVER BEAM STUDY

##### 5.4.1 Brown's<sup>(17)</sup> Cantilever Beam 86-35-RV10, Figure 5-4 (A to E)

An unsymmetrically reinforced cantilever beam was subjected to very large deflections: 6.2" for an unsupported length of 60". These deflections are larger than can be accounted for by purely flexural deformations.

Figure 5-4 (B and C) indicate an attempt to obtain the observed deflections by only the bending deflections. The numerical procedure had stability problems, because by consideration of the maximum strains the section had failed. To obtain a numerical solution a 1% second slope on the steel and no descending branch for the concrete was assumed. Both analytic models produce load-displacements which compare as well as previous member studies do, with the same problems in not being able to obtain a point-to-point fit.

However, the deformations are beyond what the member can reasonably be expected to survive. Analytic curvatures of .025 are required, but an analysis (Fig. 5-1A) shows an ultimate curvature on the order of .005.

The rotation of the member at the "fixed" end, due to the slippage of the reinforcement anchorage, becomes very important in this case. Brown took actual measurements of the rotation during his cyclic loading tests. Using curve fitting techniques, he was able to formulate relations between  $\theta_{FE}$  and  $M_{FE}$ , the rotation and moment at the support. (Brown expressed these relations in terms of

$b = 6.00''$   
 $t = 12.00''$   
 $d = 9.88''$   
 $d' = 2.00''$

$A_s = 1.58 \text{ in}^2$   
 $A'_s = .88 \text{ in}^2$   
 $f_y = 45.0 \text{ ksi}$   
 $f'_c = 5.0 \text{ ksi}$

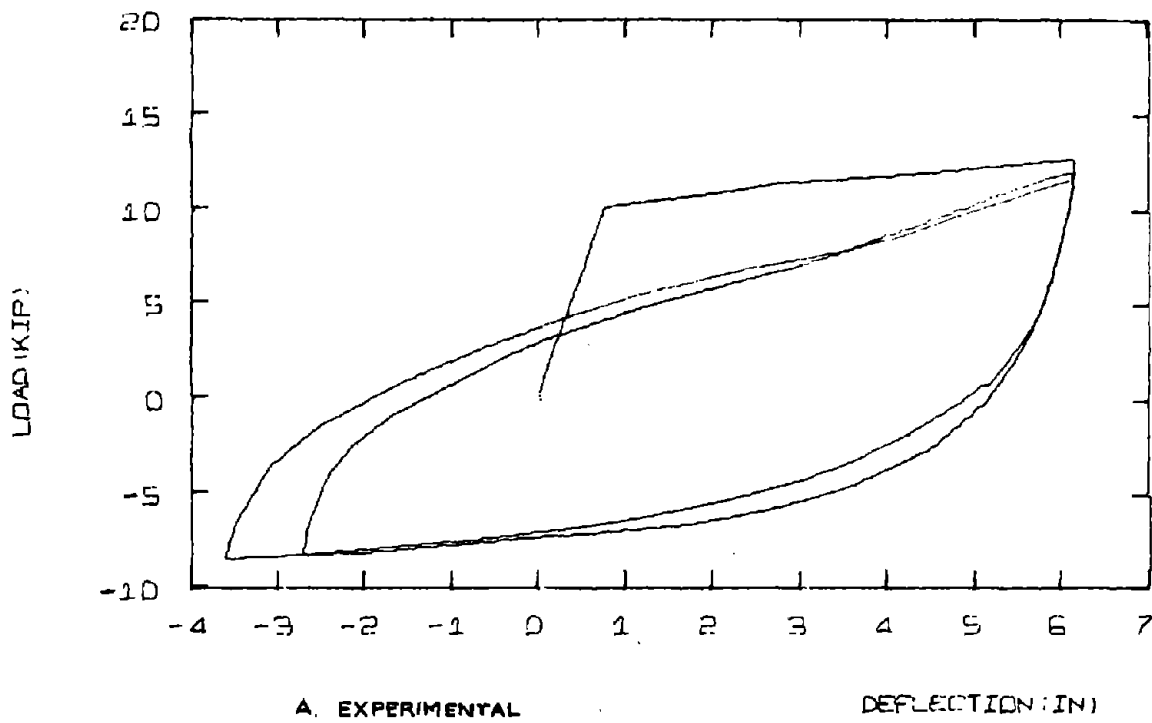
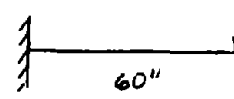
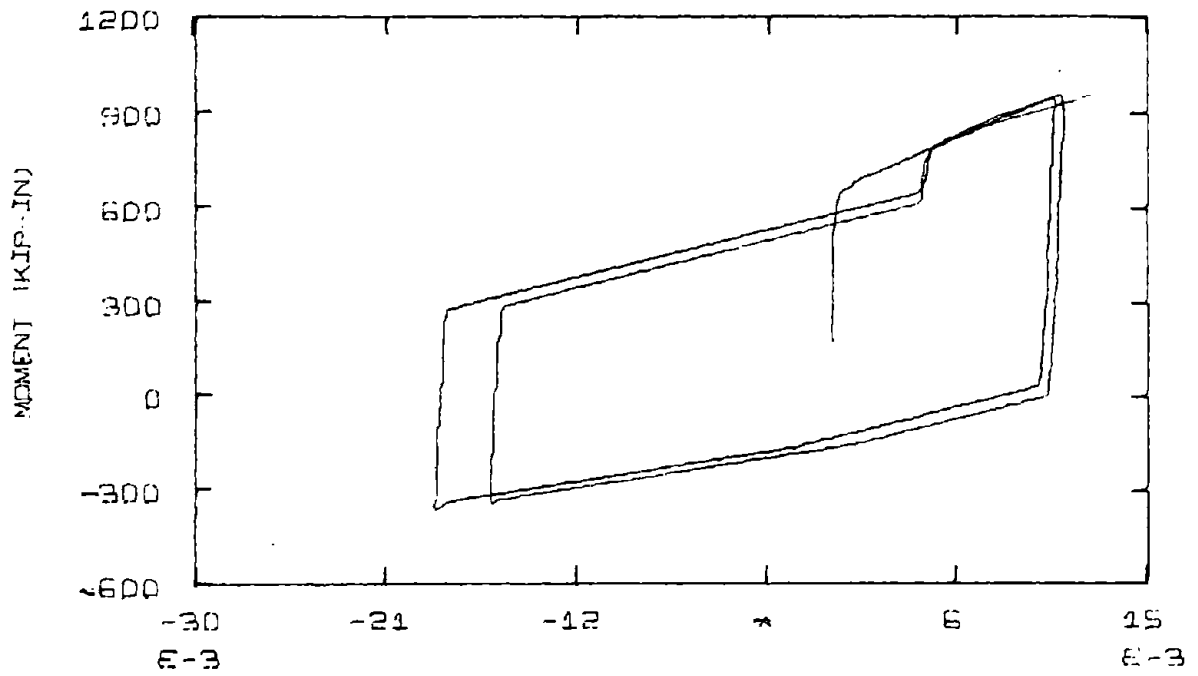
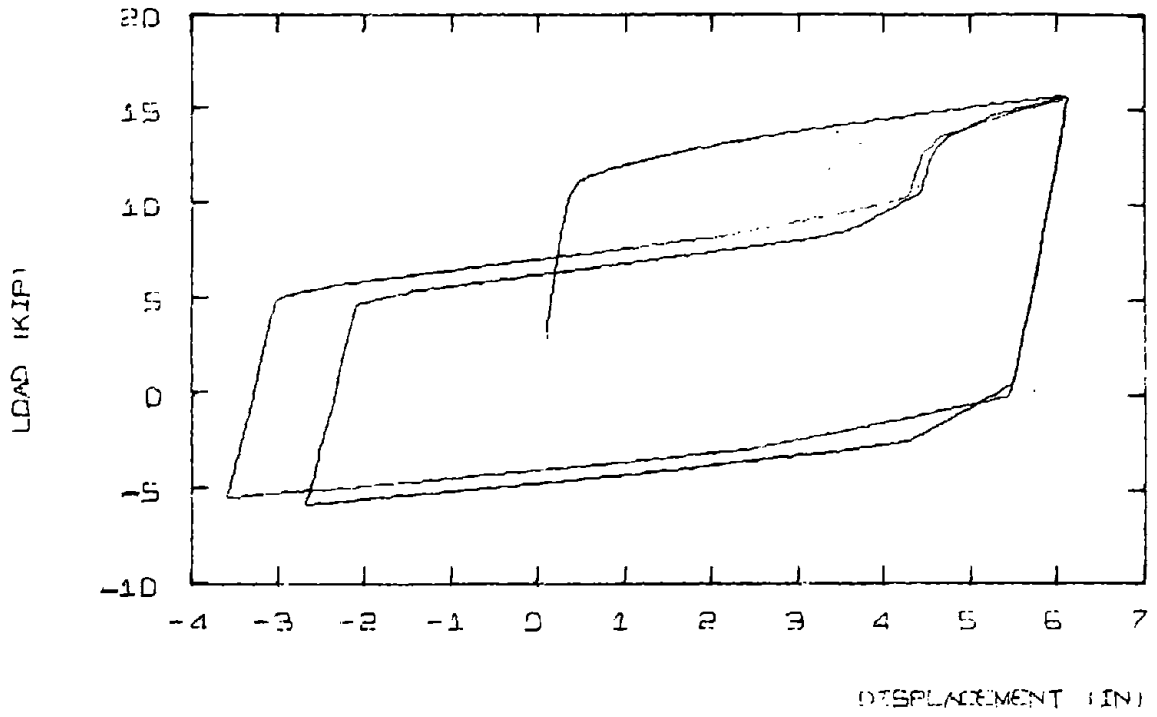
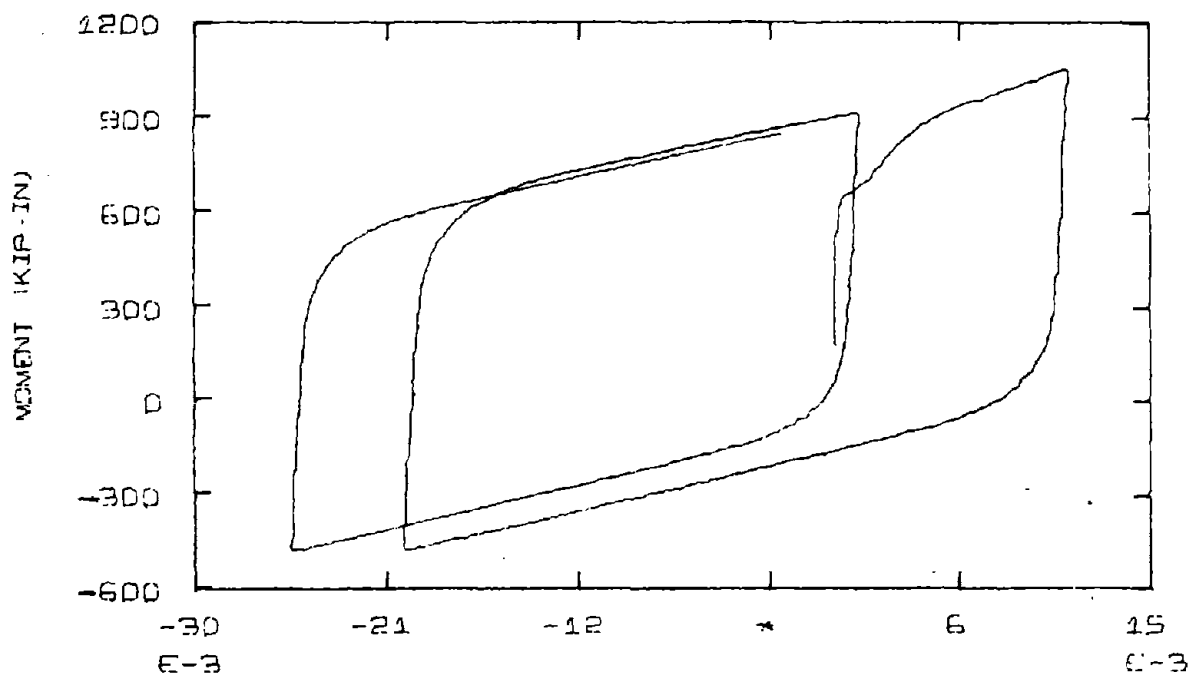
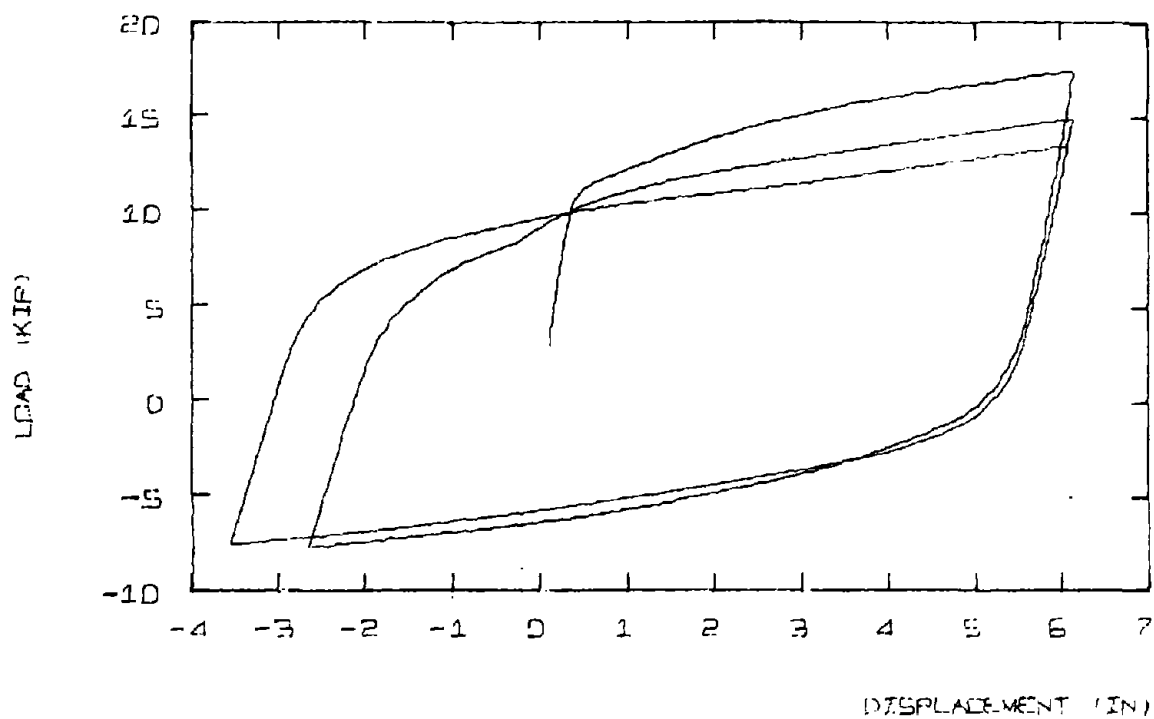


FIG. 5-4 - LOAD-DEFLECTION BEHAVIOR FOR BROWN'S CANTILEVER BEAM



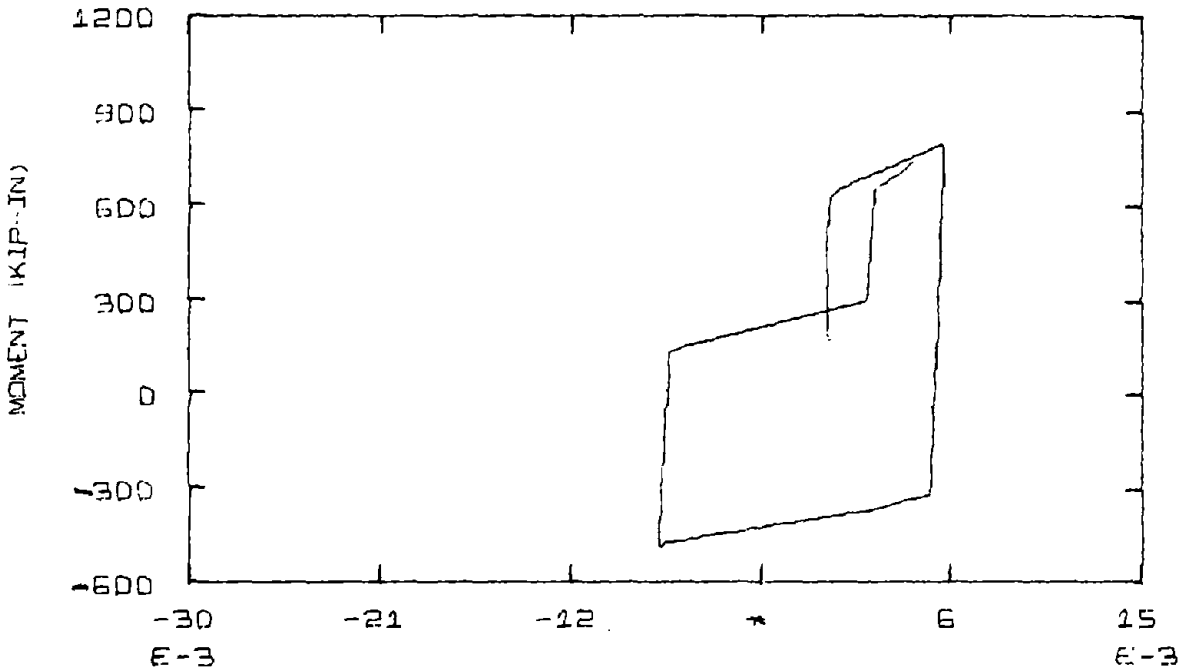
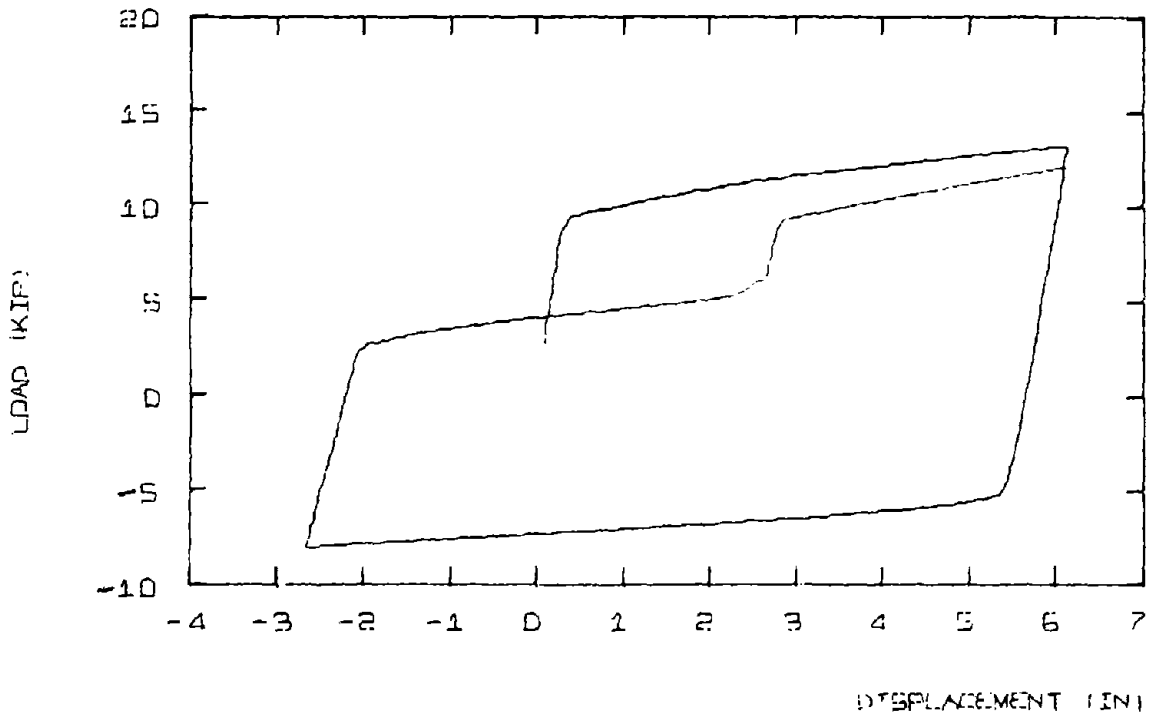
B. E-P STEEL

FIG. 5-4 (Cont.)



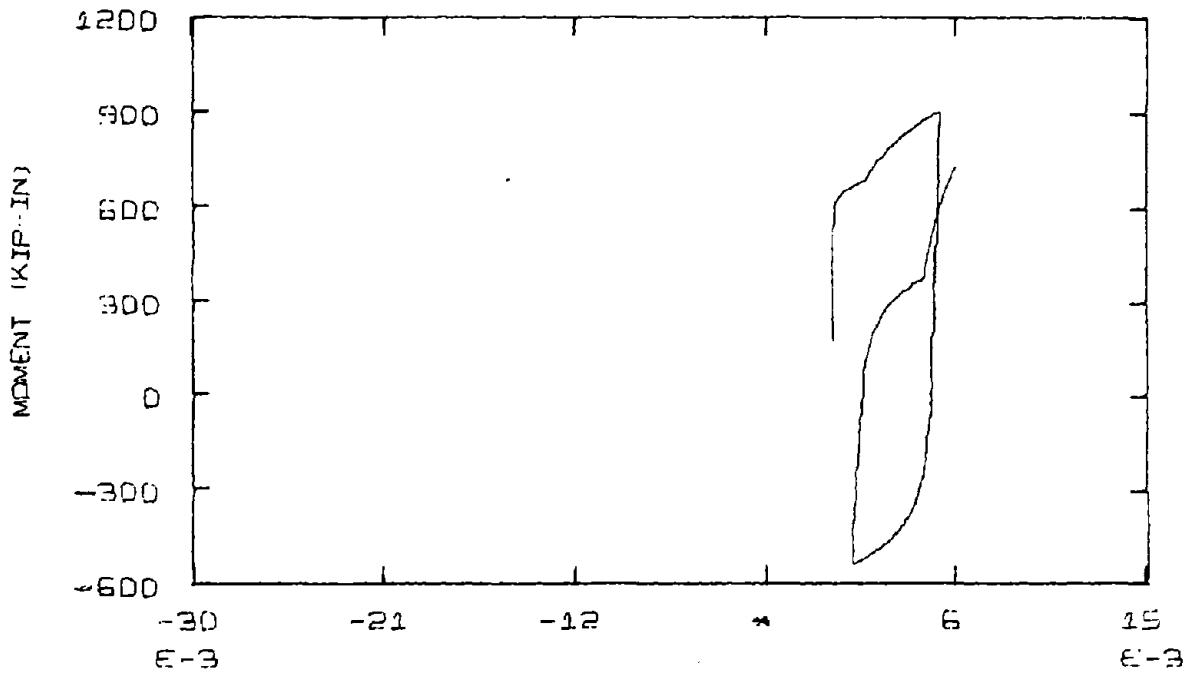
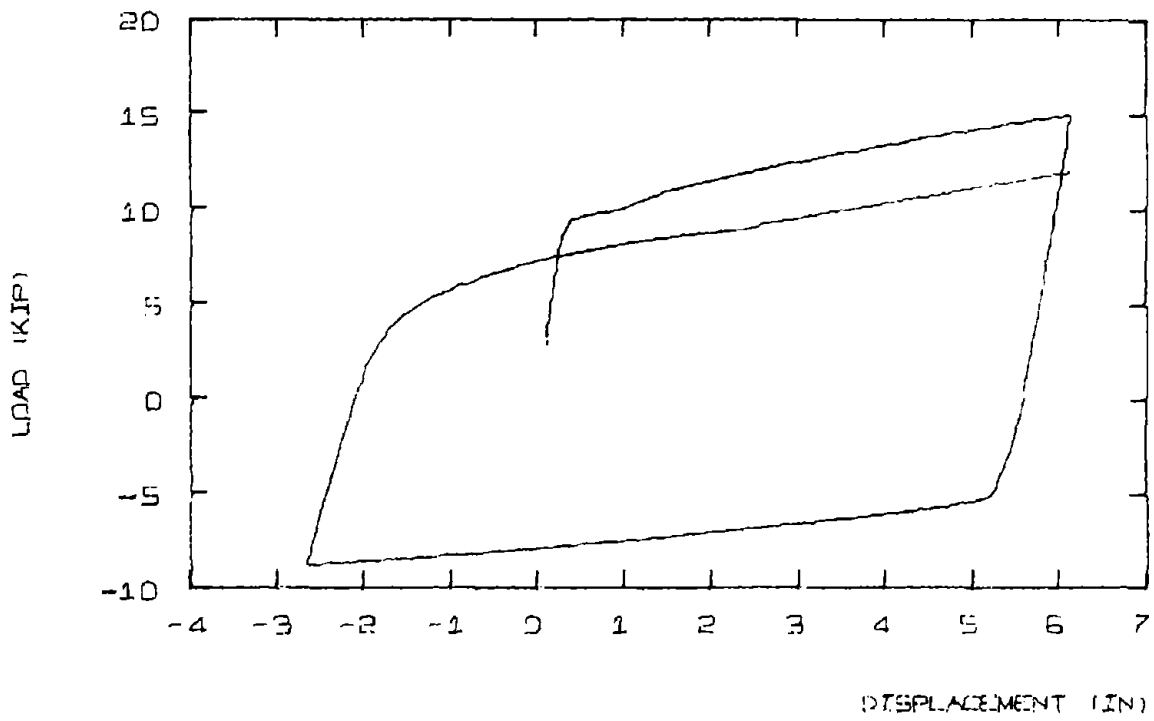
C. I-BEAM STEEL

FIG. 5-4 (Cont.)



D. E-P STEEL, JOINT ROTATION

FIG. 5-4 (Cont.)



E. Z-SGT STEEL, JOINT ROTATION

FIG. 5-4 (Cont.)

tensile force in the bars, but the relations presented here are modified to consider moment and rotation).

After first yielding

$$\theta_{FE} = \frac{D}{m' \sqrt{f'_c}} \frac{M}{(d-d')^2} - \frac{A_s f_y}{(d-d')} \quad (5.7)$$

For reversed loading, #8 bar

$$\theta_{FE} = \frac{.0005}{(d-d')^2} M + \frac{.000044 M^2}{(d-d')^3}$$

where the units are kip, in. and  $D$  is the bar diameter.  $m'$  is an experimentally derived coefficient which depends upon bar size).

The member now has a semi-rigid joint at the support, such that  $K_\theta = \frac{\Delta M}{\Delta \theta}$ . When  $K_\theta \rightarrow \infty$  the support is fixed (this is true before yielding occurs). Appendix B discusses how the effect of semirigid joints are incorporated into the member stiffness matrix.

For this particular member

$$\#8 \text{ 1st yield} \quad K_\theta = 3550. \text{ (Kip-in.)}$$

$$\#8 \text{ reversed load} \quad K_\theta = \frac{1}{3.274 \times 10^6 + 3.273 \times 10^{-7} M}$$

Figures 5-4 (D and E) show the effect of joint rotation on the elasto-plastic and curvilinear models. The analytical curvatures are now significantly smaller and are below the failure limits. This indicates that a sizeable portion of the tip deflection is due to the joint rotation. In the load-displacement curves the rotational

stiffness appears to dominate, once yielding occurs. The analytical load-displacement curves are close to the experimental results.

It must be remembered that Brown's joint rotation formulation is for a very specific member and type of loading condition. More study in this area is required if a general joint rotation formulation is to be developed.

5.4:2 Popov, Bertero, Krawinkler (34) Cantilever Beam, Figure 5-5(A-C)

This symmetrically reinforced cantilever beam is 78" long and is loaded cyclically such that the maximum deflection in a cycle gradually increases. The largest deflection is 3".

Being a very deep section ( $t = 29"$ ), shearing deformation becomes an important consideration. These researchers found that the large shear deformation causes a "pinching" effect. This occurs after several cycles of loading when flexural and diagonal tension cracks force the member to carry the shear principally by dowel action. In the experimental results (Fig. 5-5A) the pinching effect is more pronounced as the number of cycles and the maximum deformation increase.

Analytic models with both elasto-plastic and curvilinear steels were run to see if the model without shear deformation could reproduce any of the effects. In the moment-curvature study it had been shown that large deflections could cause a "pinching in" effect when the reinforcement which yielded previously in tension, yields in compression before the other steel fiber yields in tension. Figure 5-5(B & C)

$b = 15.00''$	$A_s = 6.0 \text{ in}^2$
$b = 29.00''$	$A'_s = 6.0 \text{ in}^2$
$d = 25.25''$	$f_y = 67.0 \text{ ksi}$
$d' = 3.75''$	$f'_c = 3.86 \text{ ksi}$

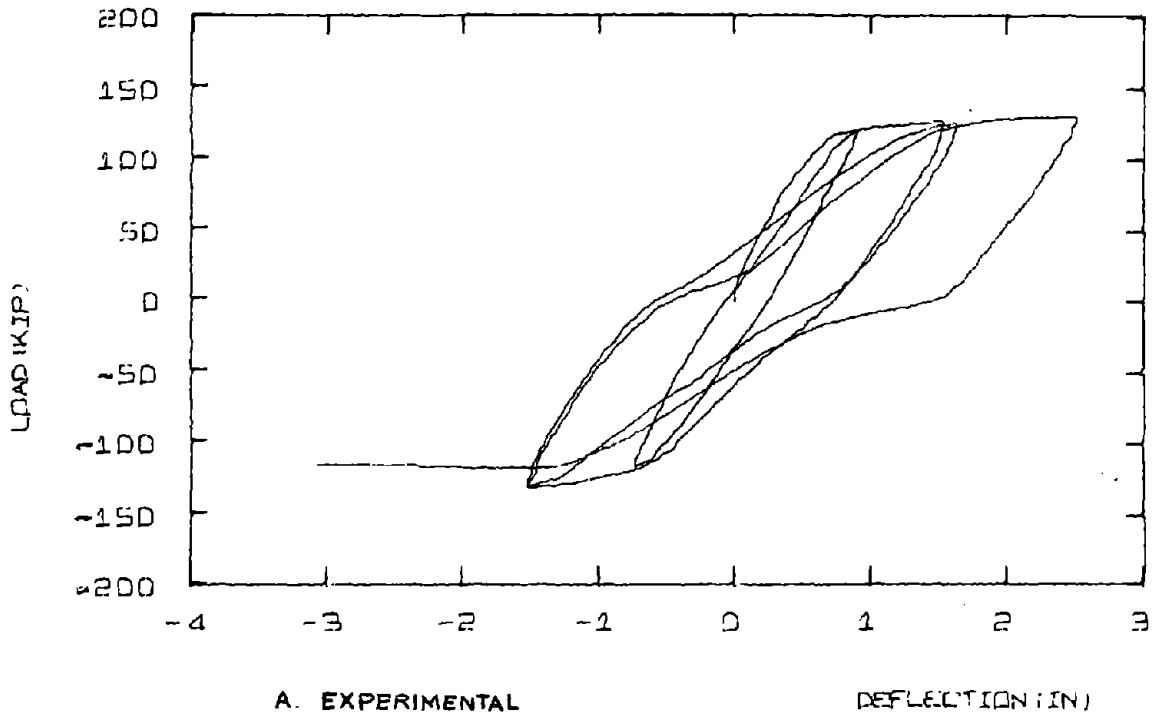
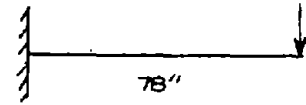
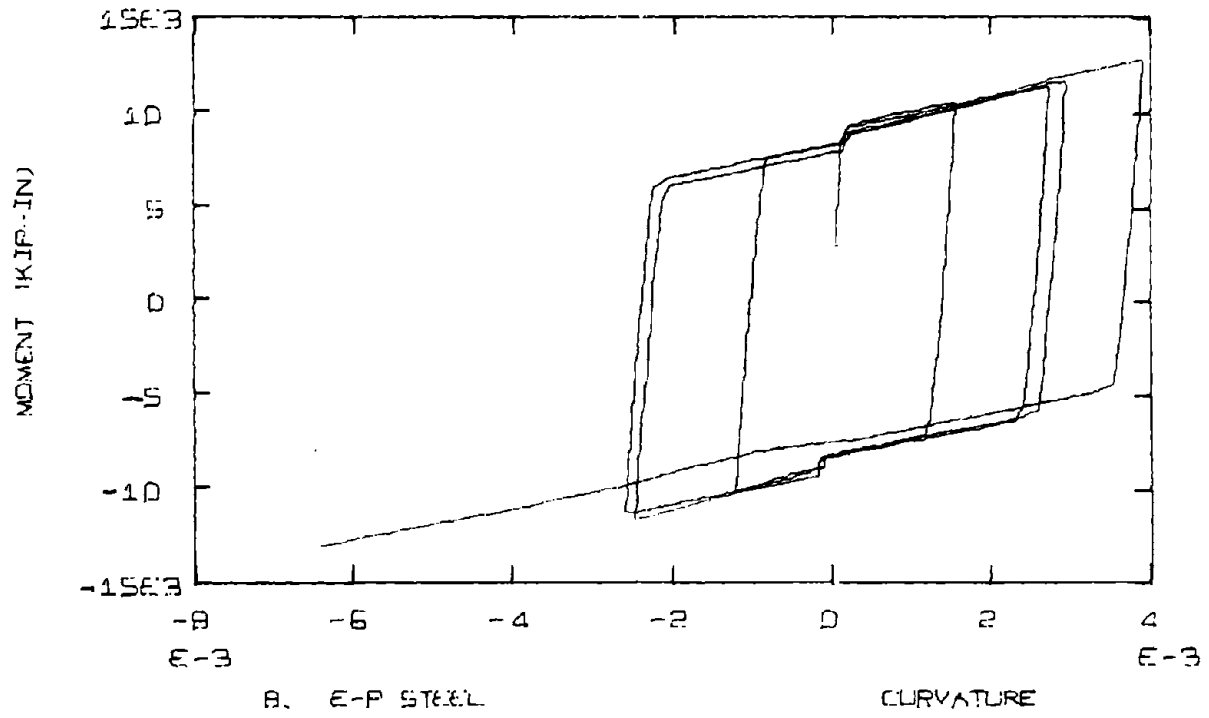
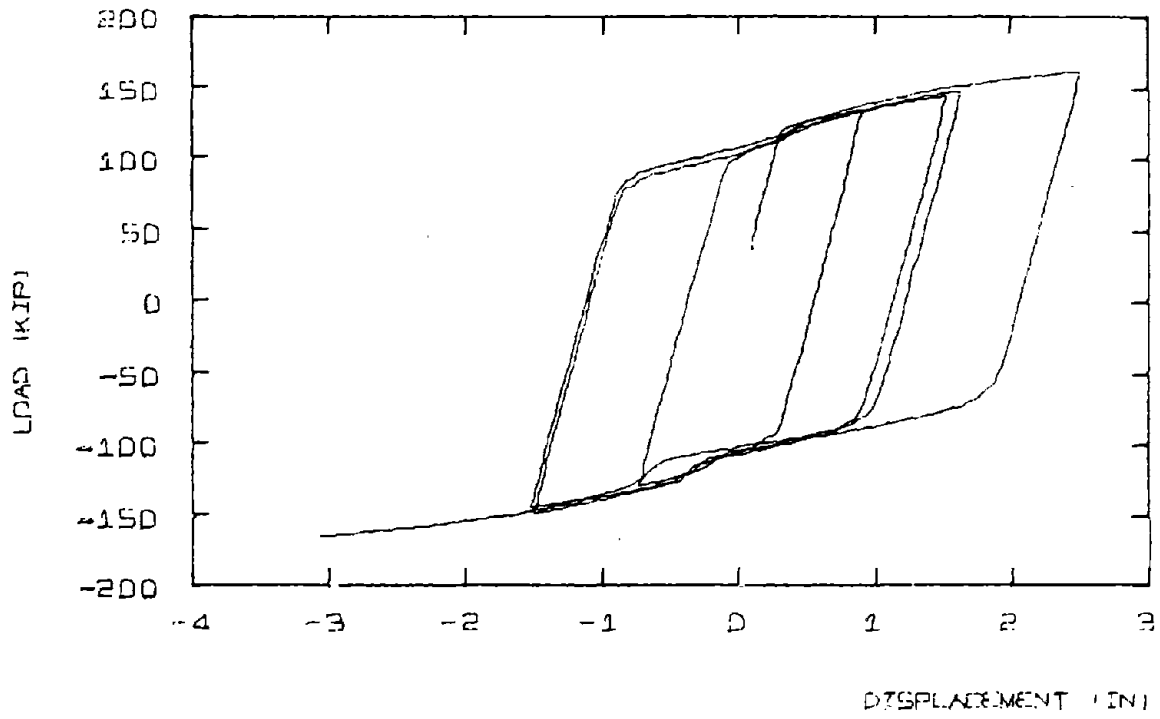


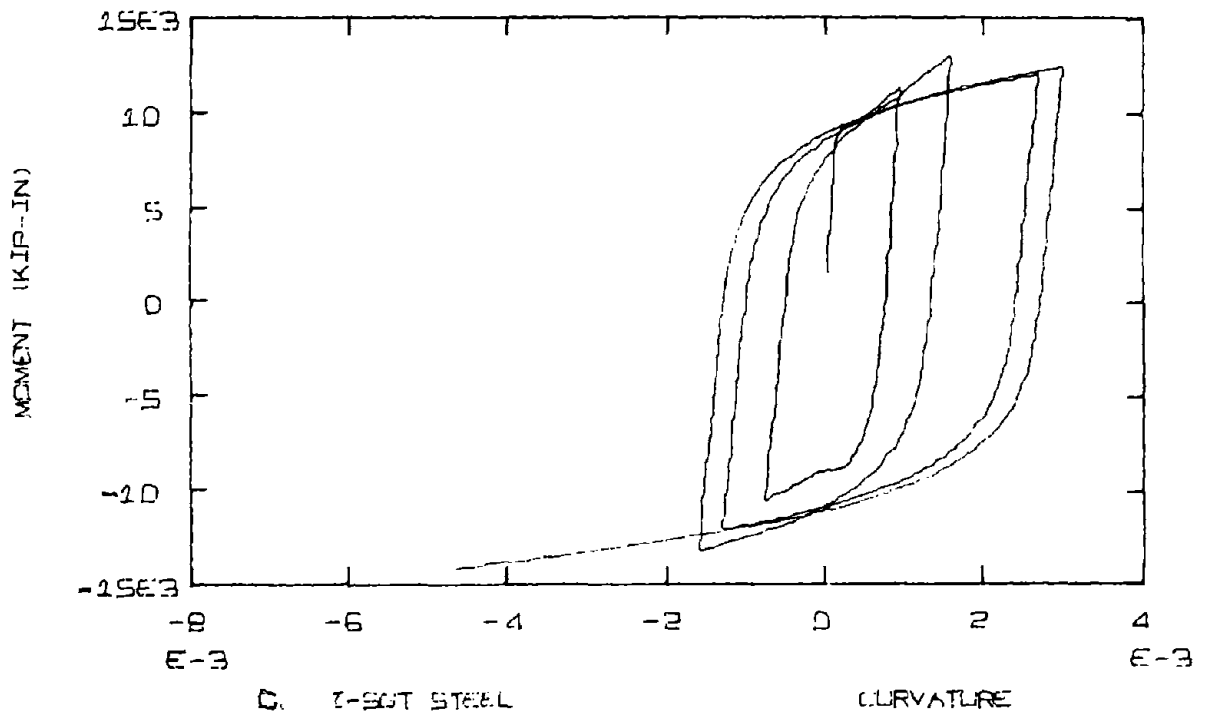
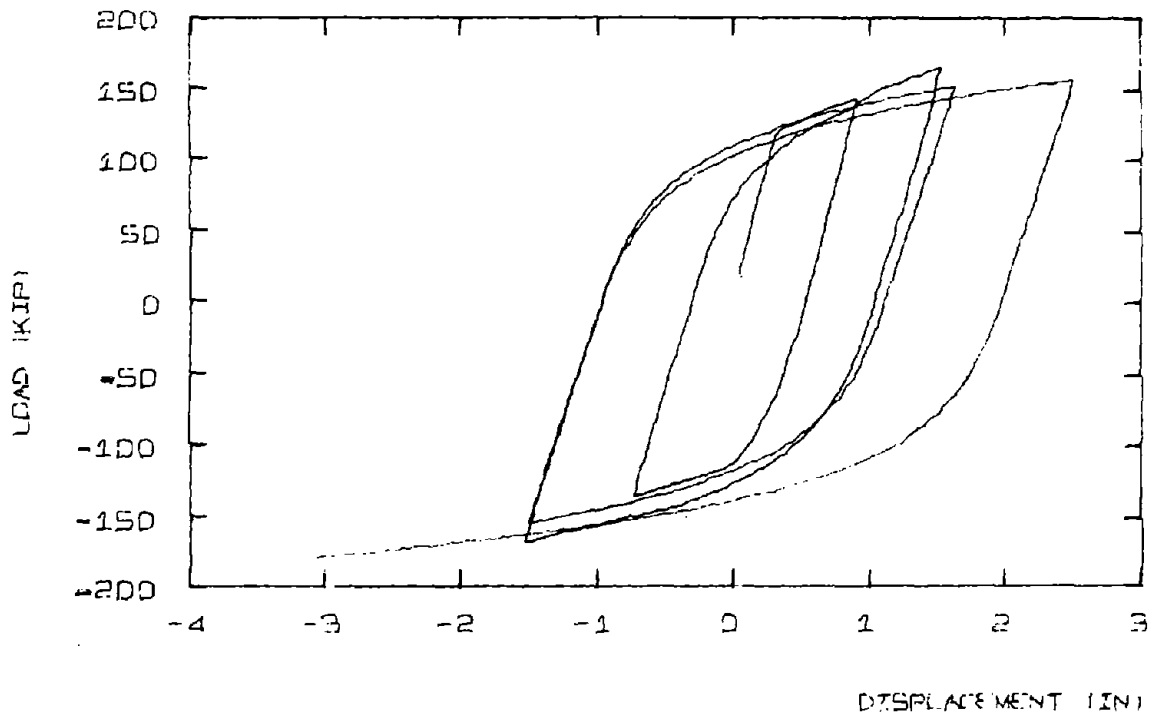
FIG. 5-5 - LOAD-DEFLECTION BEHAVIOR FOR POPOV, BERTERO, KRAWINKLER'S CANTILEVER BEAM



B. E-P STEEL

CURVATURE

FIG. 5-5 (Cont.)



C. I-BEAM STEEL

FIG. 5-5 (Cont.)

show that this was not true for these loading conditions. Both models are much stiffer than experimentally observed, and the loops enclose larger areas.

No attempt was made to include the effect into the analytic model. There are no clear-cut ways, however, of including this effect and for the types of frames to be considered in the dynamic analysis, shear deformation is not an important factor.

#### 5.5 FRAME STUDY: GULKAN'S<sup>(35)</sup> FRAME FS1, FIGURE 5-6 (A to C)

This frame was designed to have a very stiff girder in comparison to the columns. The clear distance of the columns is 26" and deflections range from -.4" to .3".

The analytic model used does not consider the effect of joint rotation nor shear deformation. Centerline dimensions are used for the member lengths.

Both analytic models are stiffer than the experimental results in unloading. The areas enclosed by the hysteresis loops in the analytic models are larger. However, the end point of the cycles show good agreement, so in an overall sense the models are representing the stiffness and behavior of the frame.

In Figures 5-6 (B2, B3, C2, C3), the moment-curvatures for each column of both analytic models are shown. Differences in shape and stiffness due to variation of axial forces in each column are noticeable but not drastic.

Columns

b = 5.00"  
 t = 5.00"  
 d = 4.26"  
 d' = .75"

$A_s = .22 \text{ in}^2$   
 $A'_s = .22 \text{ in}^2$   
 $f_y = 51.10 \text{ ksi}$   
 $f'_c = 5.20 \text{ ksi}$

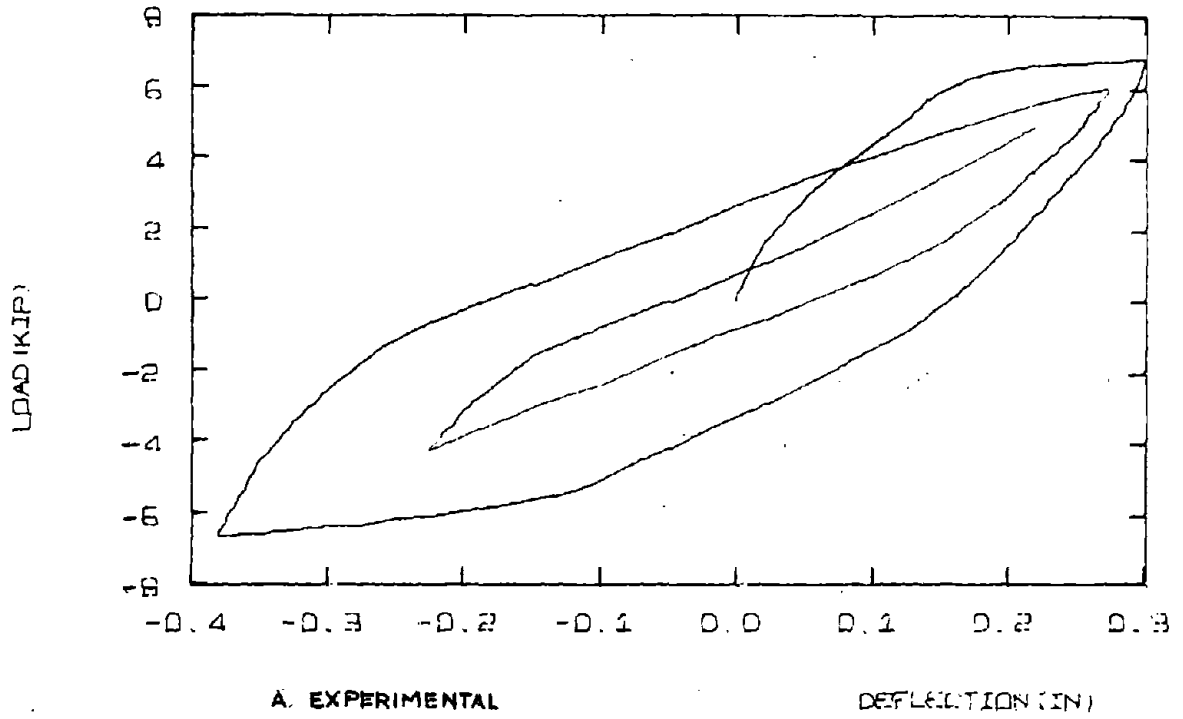
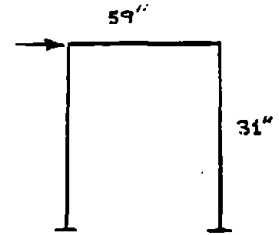


FIG. 5-6 - LOAD-DEFLECTION BEHAVIOR OF GULKAN'S FRAME F51

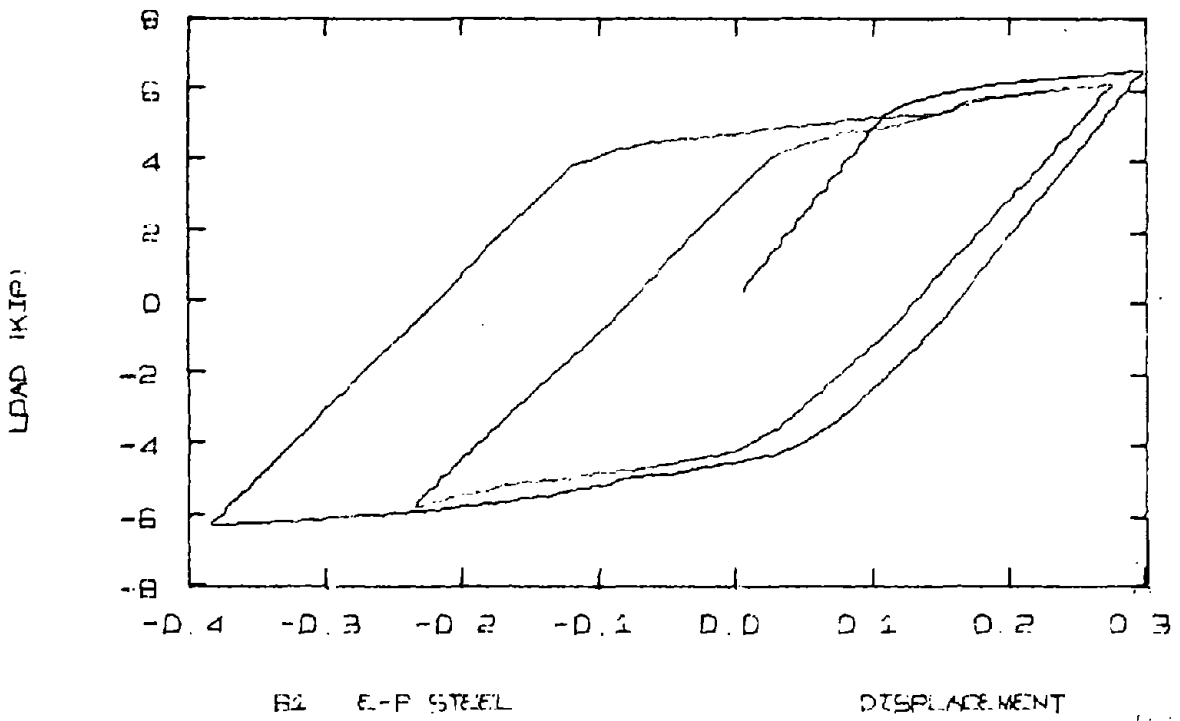


FIG. 5-6 (Cont.)

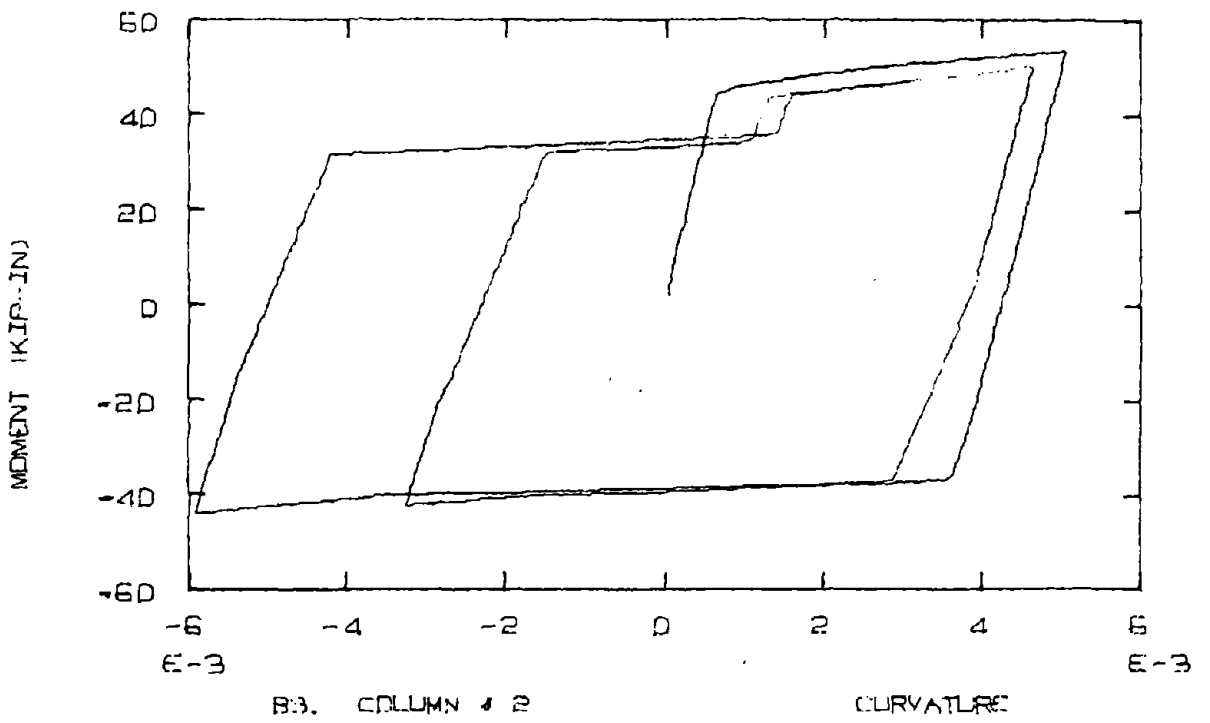
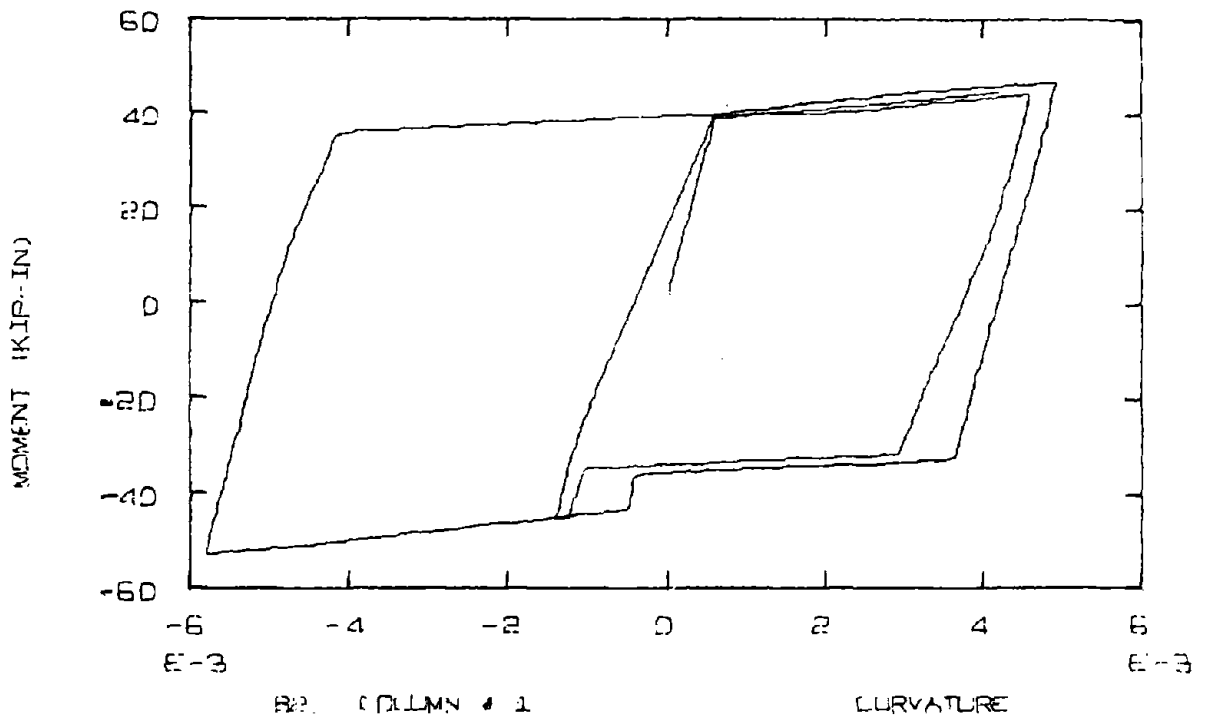


FIG. 5-6 (Cont.)

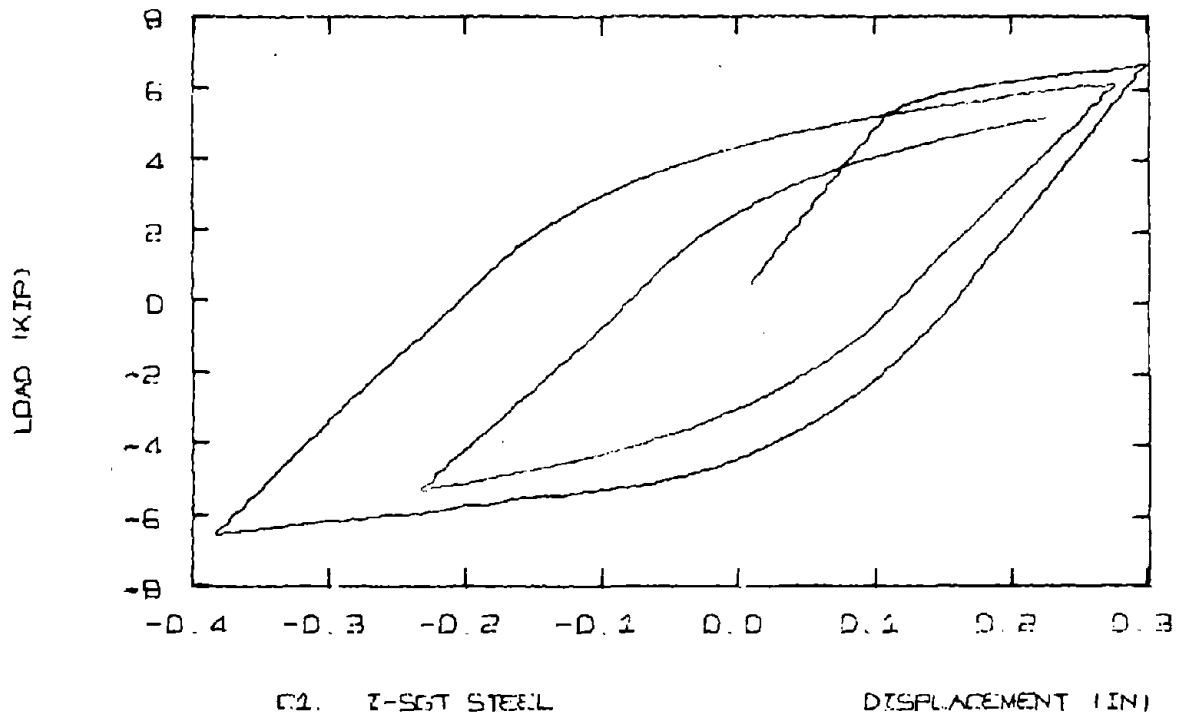


FIG. 5-6 (Cont.)

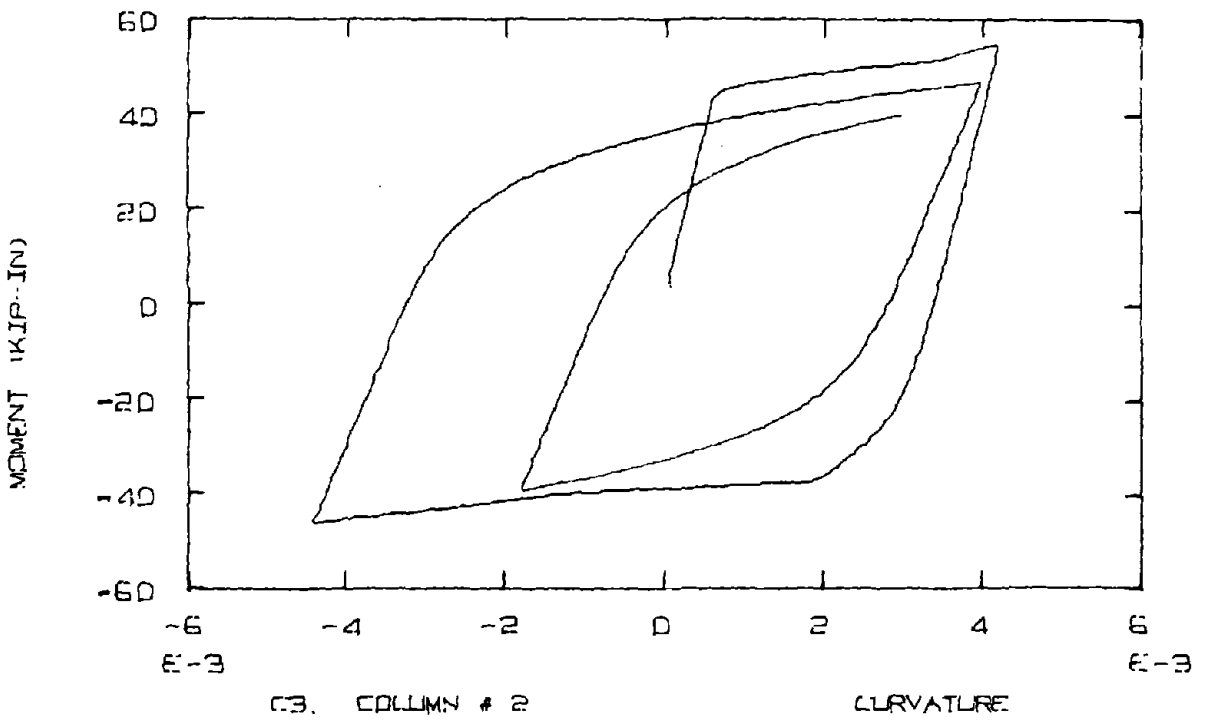
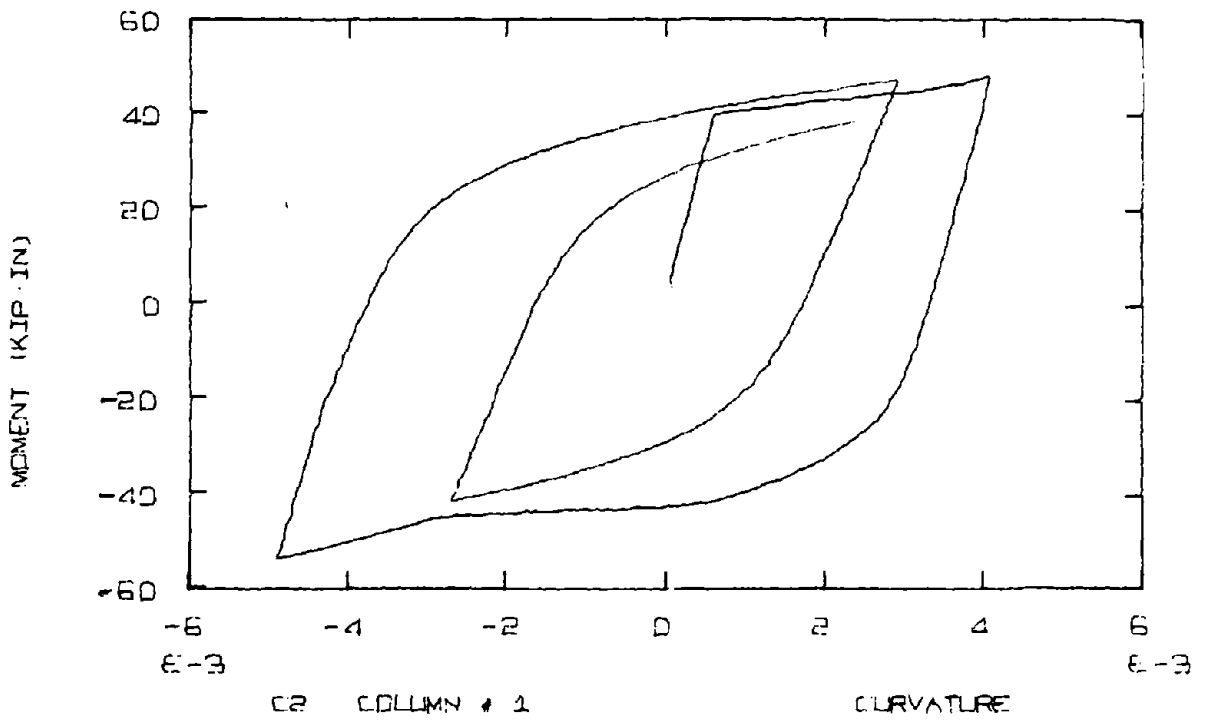


FIG. 5-6 (Cont.)

Probably the reason the models appear stiffer is that joint rotation due to slippage of anchorage reinforcement is not considered. Takeda, Sozen, Nielsen<sup>(37)</sup> show in an analysis of test results that 31% of the deflection could be attributed to joint rotation, 56% due to flexural deformation, and only 2% due to shear deformation. Although that was for another specimen, it indicates that joint rotation may be important.

#### 5.6 CONCLUSIONS AND RECOMMENDATIONS

The fiber model and the incremental stiffness approach have been extended to represent the behavior of simple structures. In an average sense the model can represent experimental results, but too many variables and uncertainties preclude having a point-to-point fit on the behavior.

The analytic model is sensitive to increment size, and numerical instability can occur when sections have zero or negative stiffness. This requires a modification of the model to include second slope on the steel and no descending branch on the concrete. A failure criteria is then limited to the determination of when some maximum concrete strain is exceeded, since descending branches (negative slope) for the load deflection relations cannot be reproduced.

The consideration of joint rotation due to slippage of anchorage reinforcement was shown to be a significant factor in the load-deflection behavior of reinforced concrete structures. However, more

research into the modeling of this effect is necessary. For deep members it may also be important to find a mechanism to account for shear deformations and the ensuing pinching effect.

## CHAPTER 6 - DYNAMIC ANALYSIS

6.1 INTRODUCTION

In this Chapter the fiber model and the incremental stiffness approach are used to study the dynamic response of reinforced concrete frames. In discussing this model's abilities and limitations, comparisons with simpler models will be made.

Two 1-bay, 1-story frames tested by Gulkan<sup>(35)</sup> will be used to compare models. The first frame has a sinusoidal base motion applied, and the second is subjected to a compressed El Centro earthquake component. It is not assumed that these frames represent the whole range of such structures, but many of the observations of their behavior will be generally valid.

## 6.2 DYNAMIC ANALYSIS WITH THE FIBER MODEL

6.2.1 Analytic Formulation

For dynamic response of the structures to be considered, the governing equations of motion, in matrix form, can be condensed to the form:

$$[M]\{\ddot{U}\} + [K_L]\{U\} = - [M]\{\ddot{U}_G\} \quad (6.1)$$

where  $[M]$  is a diagonal mass matrix in which the mass is lumped at each floor level ( $nfl \times nfl$ )

$[K_L]$  is the lateral stiffness matrix having 1 degree of freedom per floor ( $nfl \times nfl$ )

- $\{U\}$  relative displacement vector (with respect to ground),  
1 degree of freedom per floor
- $\{\ddot{U}\}$  relative acceleration vector
- $\{\ddot{U}_G\}$  ground acceleration vector.

The damping usually included in this equation represents an equivalent viscous damping and will not be considered in this model. Shiga et al.<sup>(39)</sup> have shown that the damping in reinforced concrete frames is hysteretic in nature and is proportional to the area enclosed by the loops of the load-deflection curves. It is of interest, therefore, to see how effectively the model represents this hysteretic damping.

To obtain the lateral stiffness matrix for the structure, the total stiffness matrix is condensed. The matrix equations relating forces to displacements can be partitioned in the following manner:

$$\begin{bmatrix} K_{LL} & K_{LR} \\ \text{-----} & \text{-----} \\ K_{RL} & K_{PR} \end{bmatrix} \begin{Bmatrix} U_L \\ \text{-----} \\ U_R \end{Bmatrix} = \begin{Bmatrix} P_L \\ \text{-----} \\ P_R \end{Bmatrix} \quad (6.2)$$

where the subscript L indicates lateral degrees of freedom and R indicates vertical and rotational ones. To simplify the subsequent equations, the brackets and braces will be left of the matrix quantities.

In response to earthquake motion the vertical and rotational inertial forces usually are smaller than the lateral inertial forces. If  $P_R$  is neglected with respect to  $P_L$ , then

$$K_{RL} U_L + K_{RR} U_R = 0$$

or

$$U_R = -K_{RR}^{-1} K_{RL} U_L \quad (6.3)$$

Then backsubstituting into Eq. 6.2 yields:

$$K_{LL} U_L - K_{LR} K_{RR}^{-1} K_{RL} U_L = P_L$$

and

$$K_L^* = K_{LL} - K_{LR} K_{RR}^{-1} K_{RL} \quad (6.4)$$

where  $K_L^*$  has only a lateral degree of freedom at each joint.

The next step in the condensation process uses the assumption that all joints at a floor level have the same lateral displacement. The lateral stiffness matrix,  $K_L$ , is obtained by adding the columns and rows of  $K_L^*$  which correspond to joints on the same floor.  $K_L$  now is (nfL x nfL) where nfL is the number of floors.

Once the lateral displacements are known, the vertical and rotational displacements can be obtained by backsubstitution into Eq. 6.3.

To advance the numerical solution in time, a central difference formulation is used for the acceleration vector. (The superscript refers to the time step.)

$$\ddot{U}^i = \frac{1}{(\Delta t)^2} [U^{i+1} - 2U^i + U^{i-1}]$$

or

$$U^{i+1} = 2U^i - U^{i-1} + (\Delta t)^2 \ddot{U}^i \quad (6.5)$$

Similarly

$$U^i = 2U^{i-1} - U^{i-2} + (\Delta t)^2 \ddot{U}^{i-1}$$

Let

$$\begin{aligned} \Delta U^i &= U^{i+1} - U^i = 2U^i - 3U^{i-1} - U^{i-2} + (\Delta t)^2(\ddot{U}^i - \ddot{U}^{i-1}) \\ &= 2\Delta U^{i-1} - \Delta U^{i-2} + (\Delta t)^2(\ddot{U}^i - \ddot{U}^{i-1}) \end{aligned} \quad (6.6)$$

where  $\Delta U^i$  is the change in displacement in the  $(i)^{\text{th}}$  step.

$$\text{From Eq. 6.1,} \quad \ddot{U} = -M^{-1} K_L U - \ddot{U}_G \quad (6.7)$$

Now  $K_L U$  is simply the forces in the structure and in an incremental fashion can be expressed as

$$K_L^i U^i = \sum_{j=1}^i K_t^{j-1/2} \Delta U^{j-1} \quad (6.8)$$

where  $K_t^{i-1/2}$  is the lateral tangent stiffness matrix at step  $(i-1/2)$ .

Notice that this uses the Modified Euler method. It was felt that the added accuracy of a second order method was needed for the dynamic analysis because of the sensitivity of the incremental stiffness method to increment size and the problems with propagation of errors.

$$\text{Now} \quad \ddot{U}^i - \ddot{U}^{i-1} = -M^{-1} [K_t^{i-1/2} \Delta U^{i-1}] - (\ddot{U}_G^i - \ddot{U}_G^{i-1}) \quad (6.9)$$

Finally the following recursive relationship is formulated

$$\begin{aligned} \Delta U^i &= 2 \Delta U^{i-1} - \Delta U^{i-2} \\ &\quad - (\Delta t)^2 [M^{-1} K_t^{i-1/2} \Delta U^{i-1} + (\ddot{U}_G^i - \ddot{U}_G^{i-1})] \end{aligned} \quad (6.10)$$

### 6.2.2 Behavior of the Fiber Model under Sinusoidal Base Motion

The structure used in this section is a 1-bay 1-story frame (with clear column height of 26") which Gulkan<sup>(35)</sup> subjected to steady-state base motion on the University of Illinois shaking table. This frame was designed to have the girder much stiffer than the columns, and a fixed support at the base.

In Fig. 6-1A, the base motion provided by the shaking table is shown. Although the variation in peaks and changes in frequency indicate that it is not purely sinusoidal, the major part of the study on the fiber model was run with a true sinusoid (Fig. 6-1B) having the average frequency and amplitude of the experimental excitation. This was an attempt to use a base motion where some engineering "feel" for the response existed.

Of interest are the effect of increment size, the effect of nonlinear geometry, the "P- $\Delta$ " effect, and the steel formulation used. Table 6-1 summarizes the effects included and the displacement averages for each of the nine comparison runs of the fiber model.

Figure 6-2 (A to I) has the displacement-time history for each of the runs plotted to the same scale. After the first couple of cycles the model's frequency of response matches the observed one. The initial difference is due to the variation of the input acceleration from the sinusoid assumed in the comparison. Maximum displacements ranged from .260" to .283", while the maximum and steady-state peak-to-peak amplitudes ranged from .388" to .409" and .262" to .301", respectively.

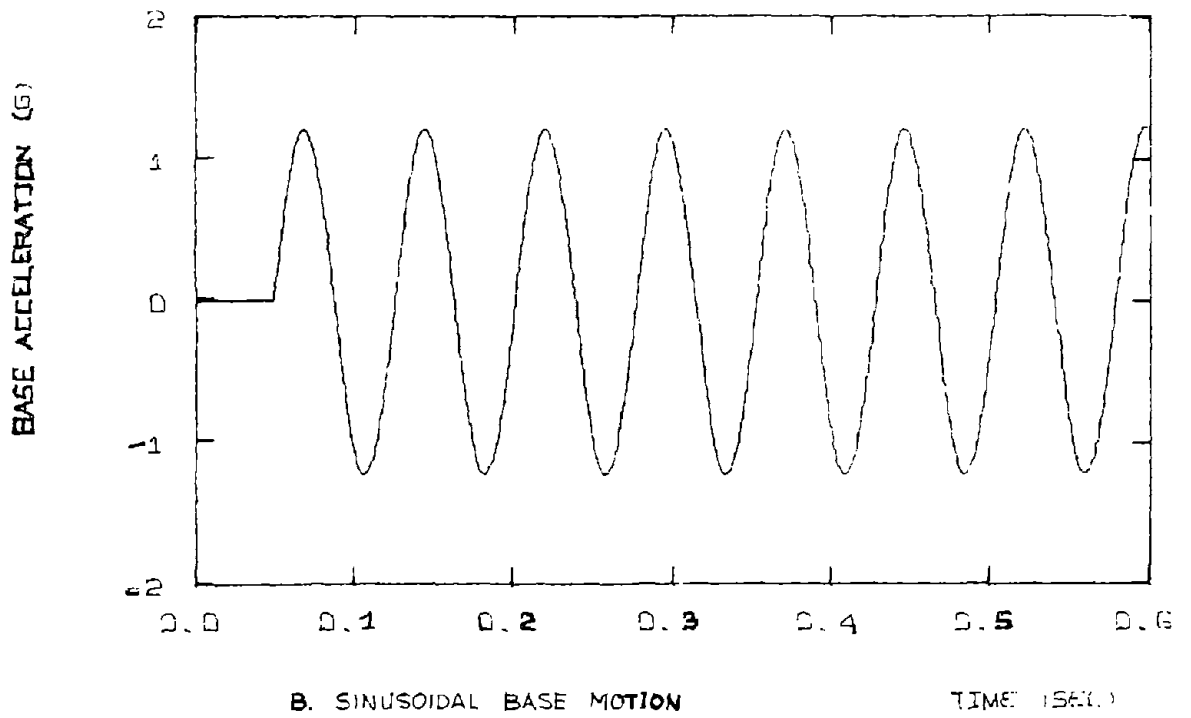
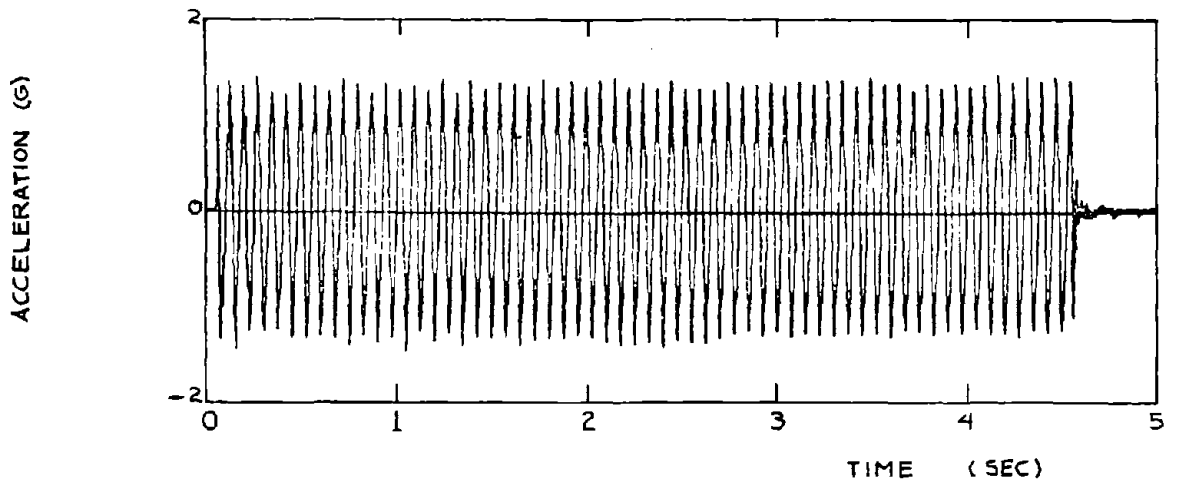


FIG. 6-1 - BASE MOTIONS USED IN THE DYNAMIC ANALYSIS

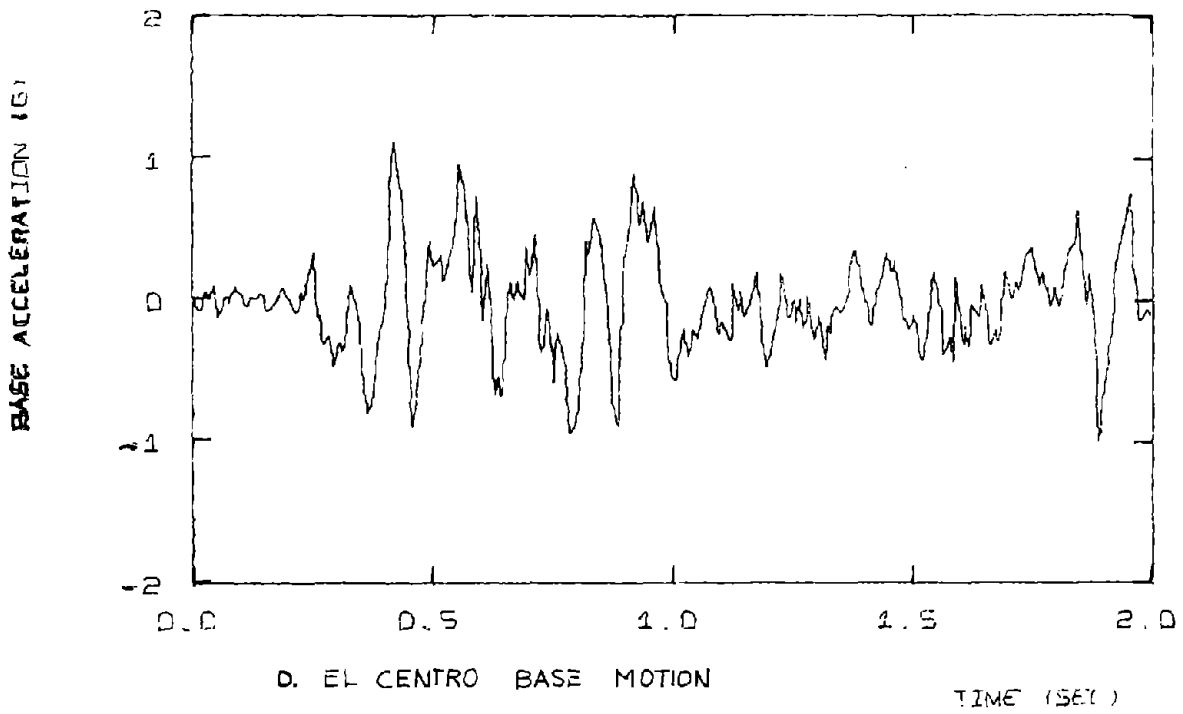
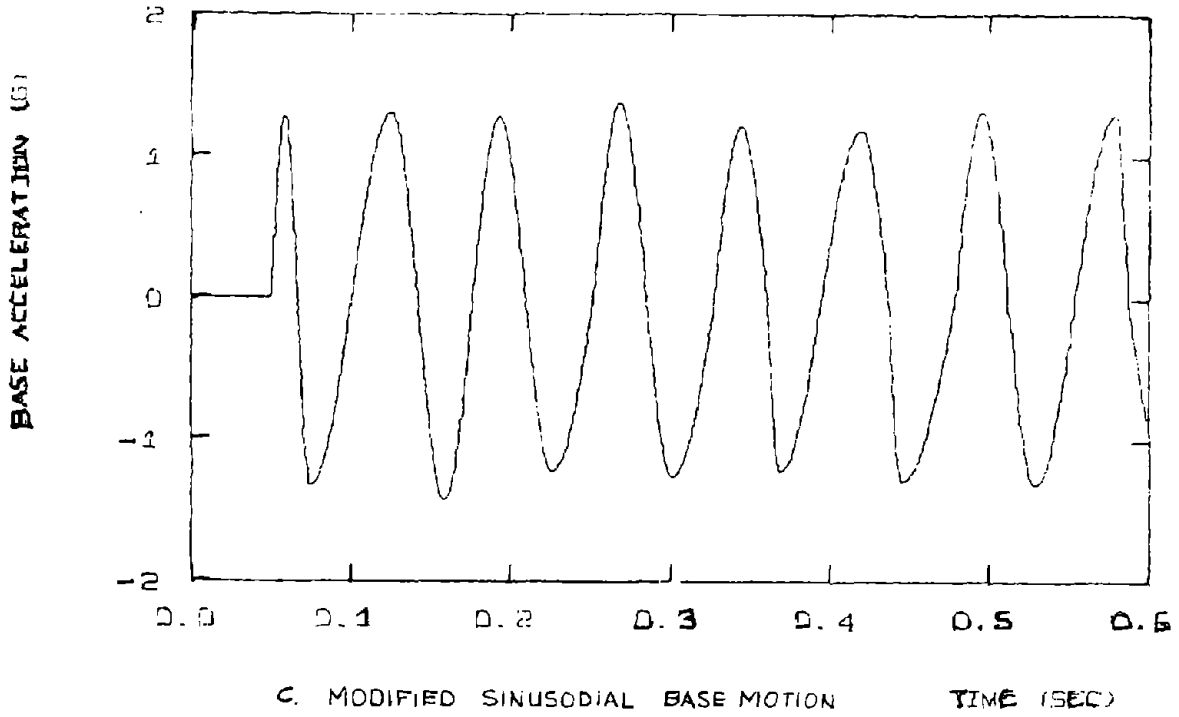


FIG. 6-1 (Cont.)

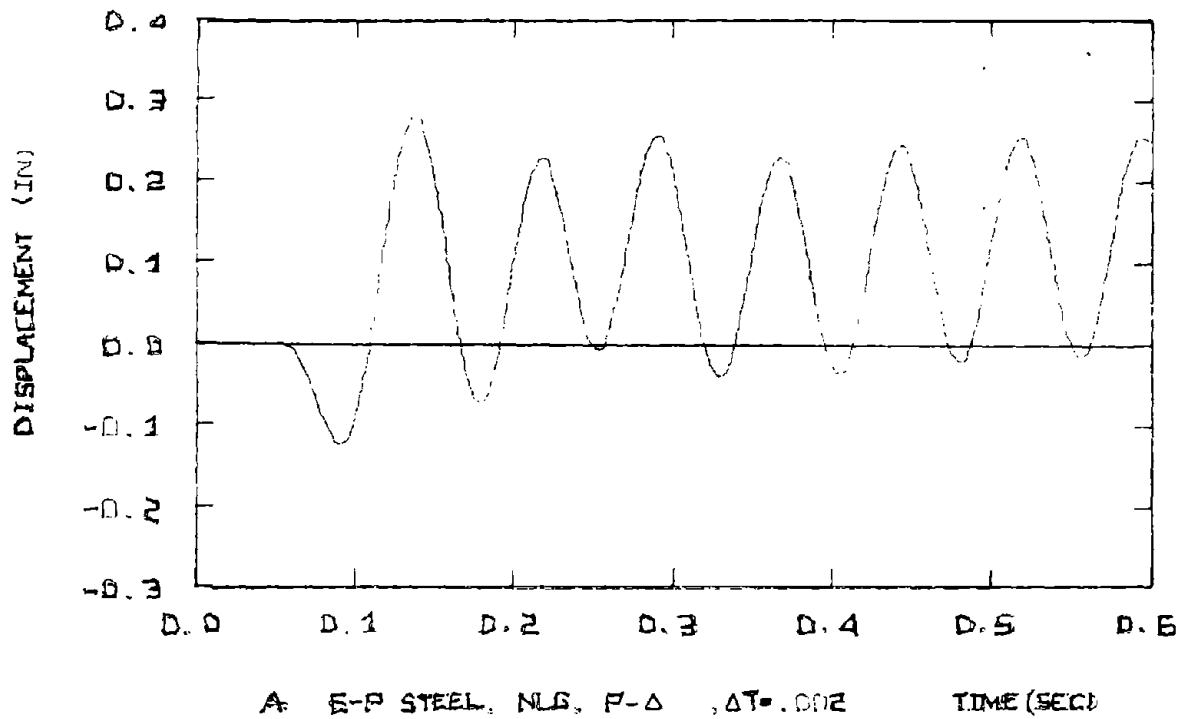


FIG. 6-2 - DISPLACEMENT-TIME RESPONSE FOR THE FIBER MODEL UNDER SINUSOIDAL BASE MOTION

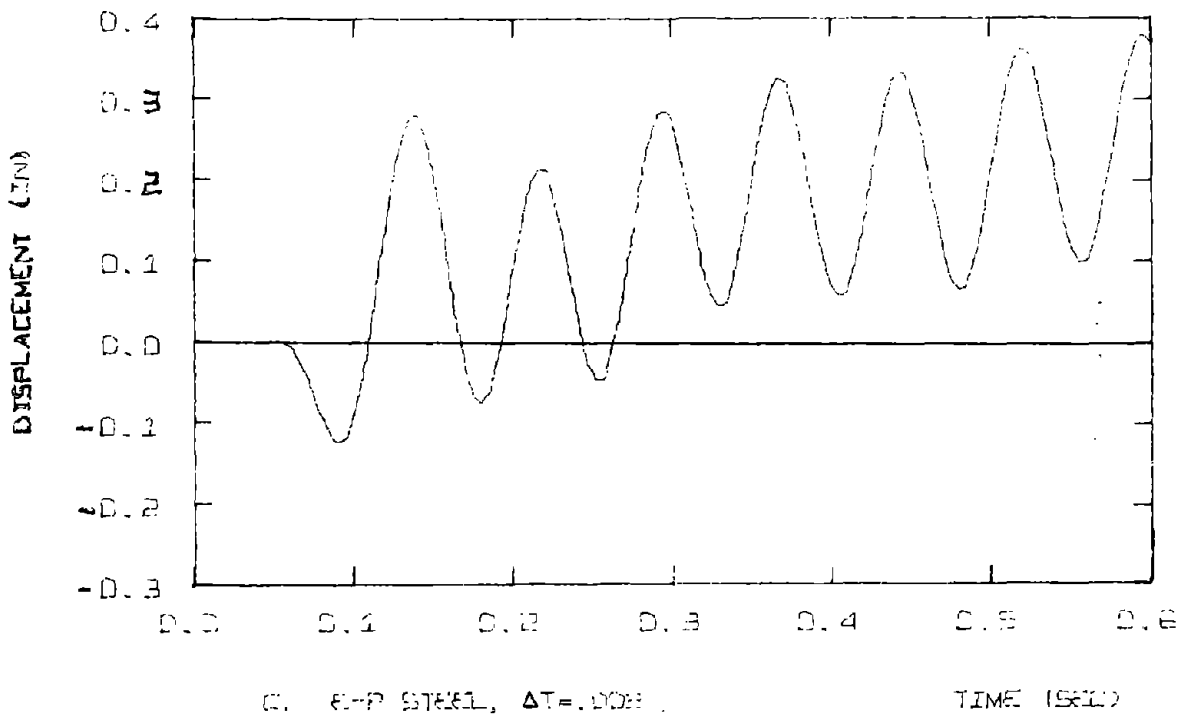
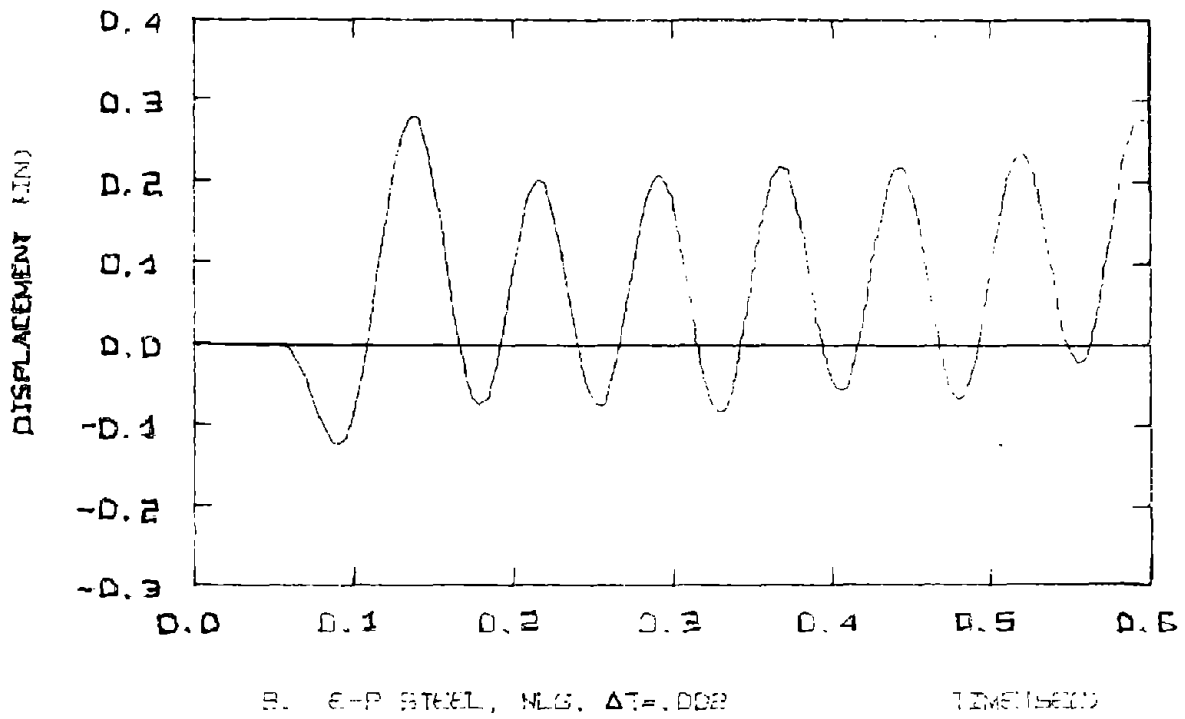


FIG. 6-2 (Cont.)

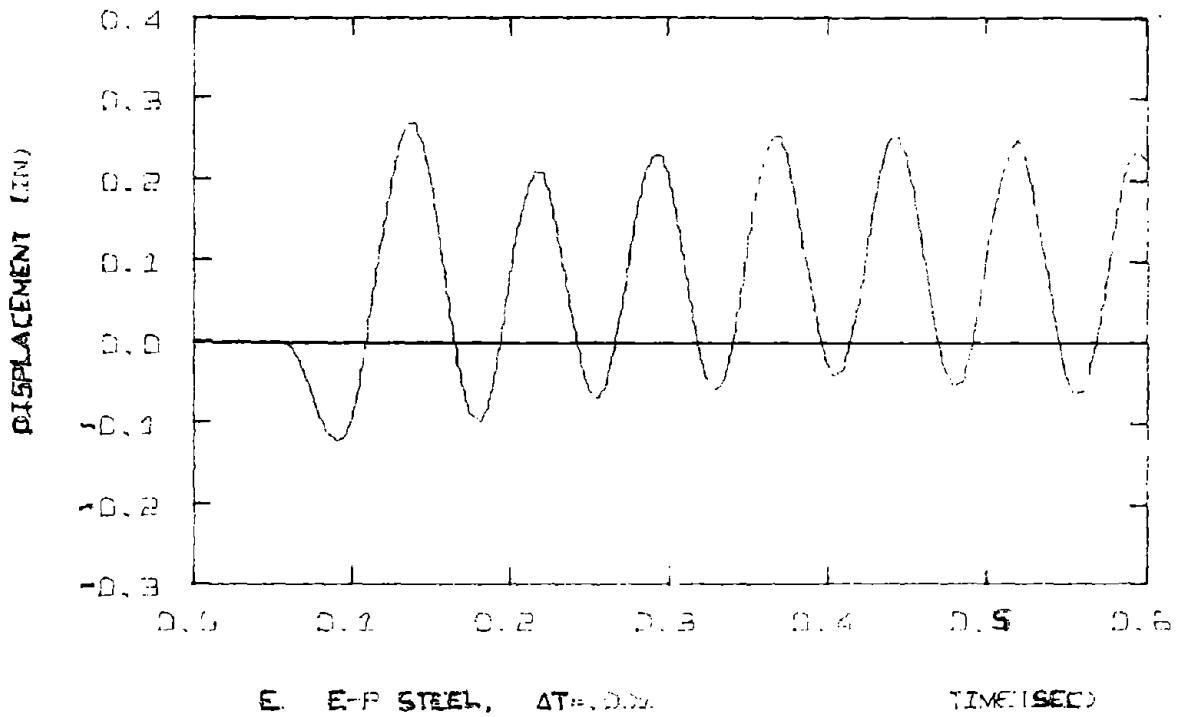
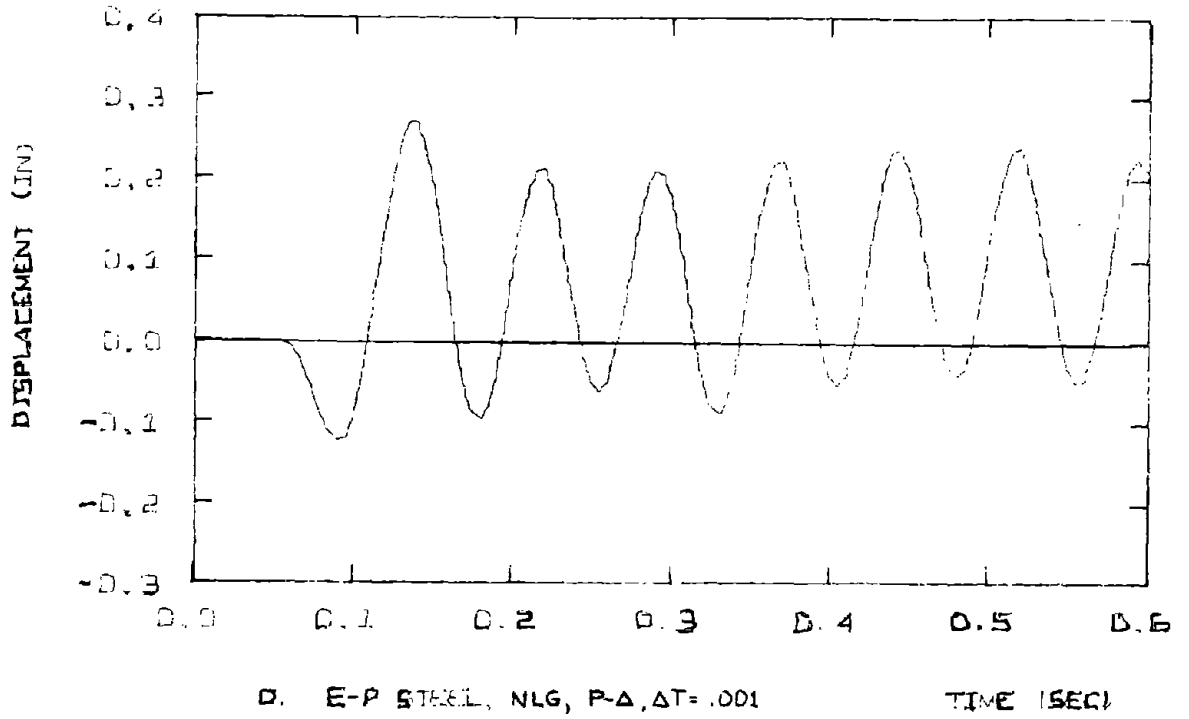
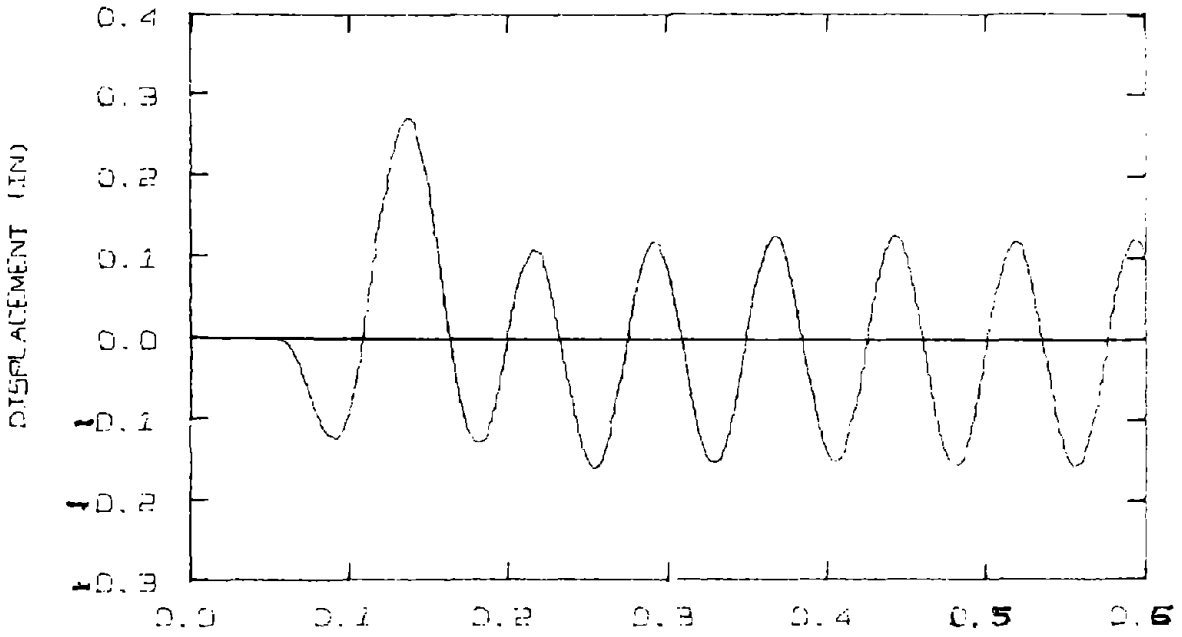
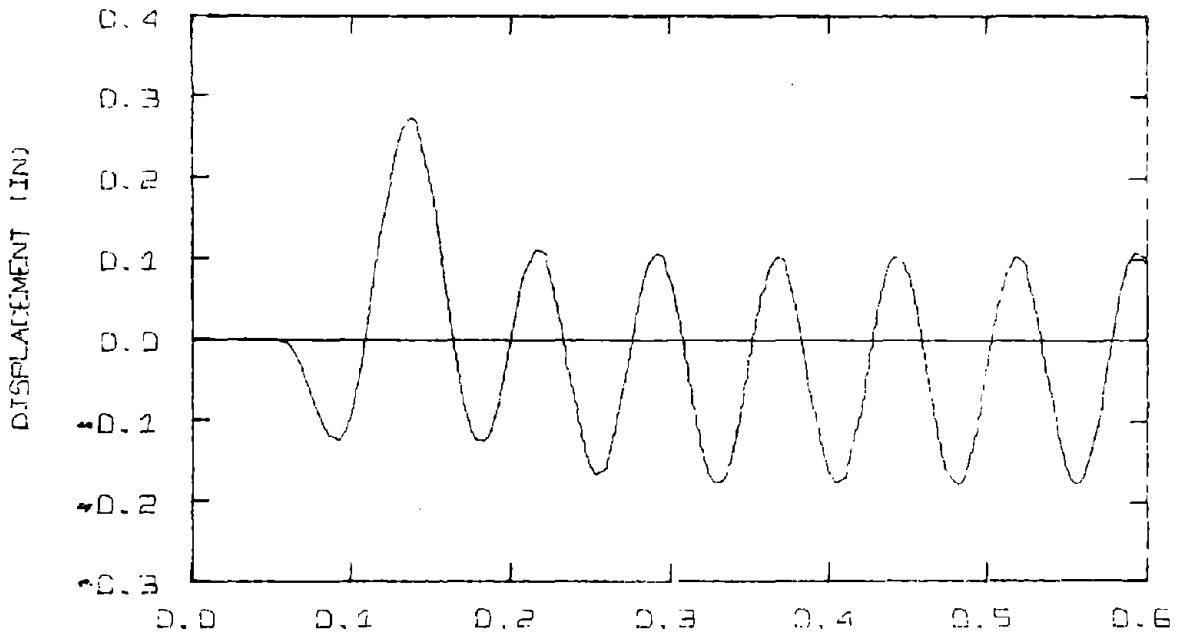


FIG. 6-2 (Cont.)

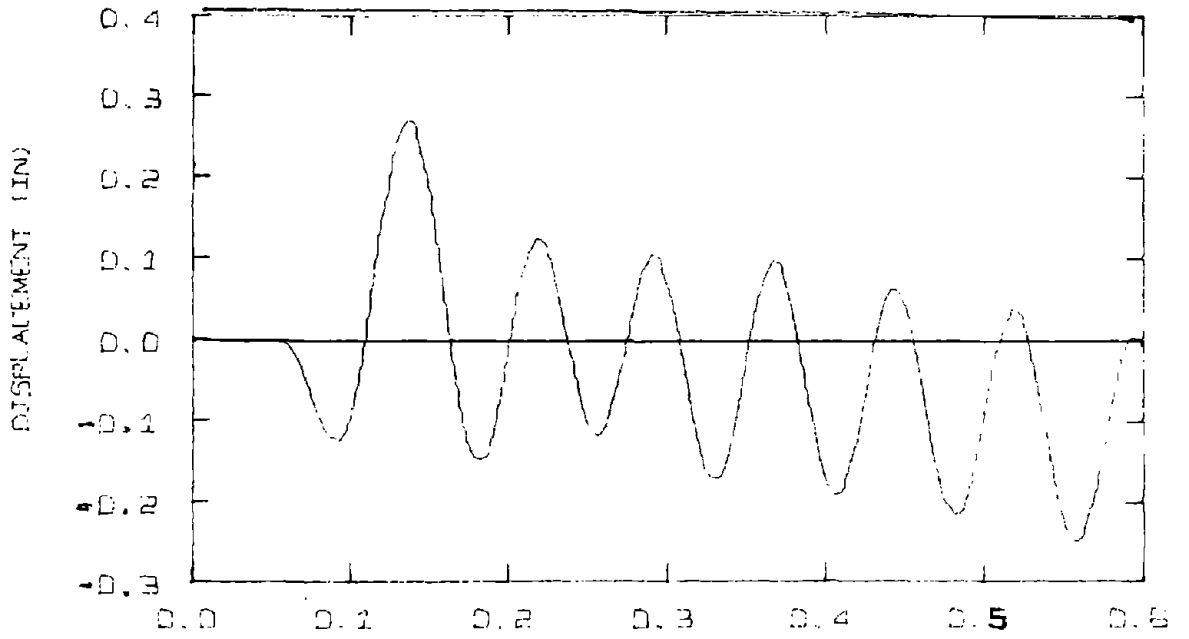


F. E-P STEEL, NLG, P- $\Delta$ ,  $\Delta T = .0005$  TIME (SEC)

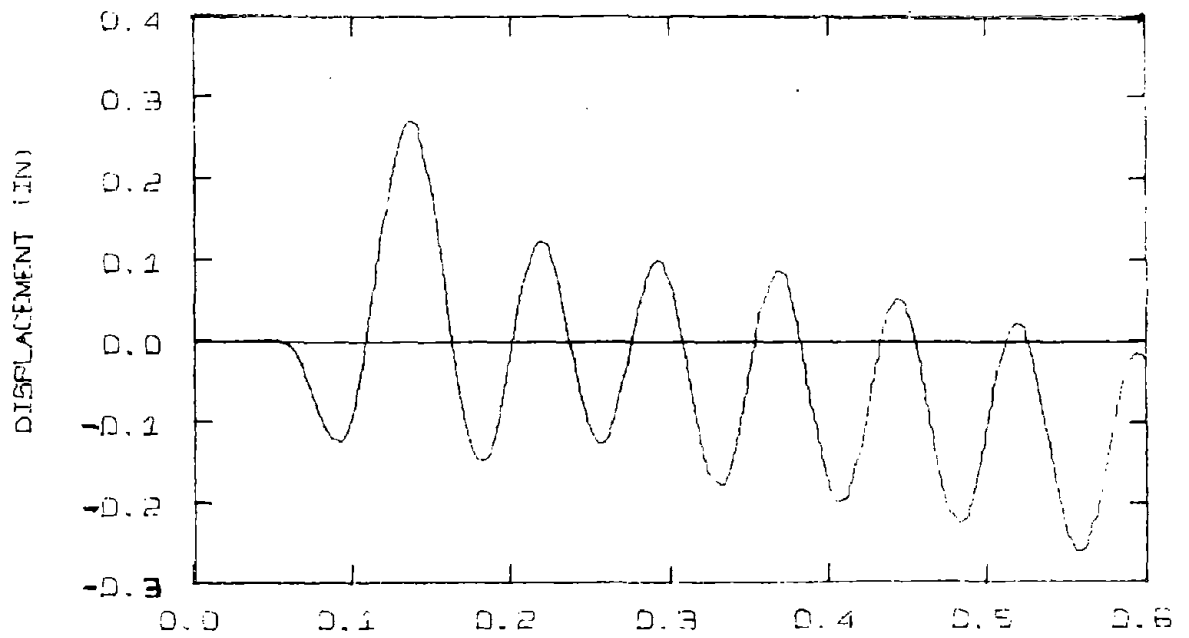


G. E-P STEEL,  $\Delta T = .0005$  TIME (SEC)

FIG. 6-2 (Cont.)



H. Z-SGT STEEL, NLG, P-A,  $\Delta T = .0005$  TIME (SEC)



I. I-SGT STEEL,  $\Delta T = .0005$  TIME (SEC)

FIG. 6-2 (Cont.)

In Fig. 6-2 (A, D, F) all nonlinear effects are included, and the increment size varies from  $\Delta t = .002$  to  $.0005$  sec. (The measured natural period of the structure varies from  $.063$  to  $.125$  sec.). For  $\Delta t = .002$  and  $.001$  there is a permanent set and some plastic drift. Both effects decrease with increment size and are not apparent at  $\Delta t = .0005$ . It was felt that accumulation of errors due to "overshooting" at direction changes was reduced sufficiently at the small increment size.

In Fig. 6-2 (C, E, G) the increment size is similarly varied, but now the nonlinear effects are not included. The effect of increment size reduction is obvious. Comparing runs A and C, the nonlinear effects appear to decrease the calculated plastic drift. A comparison of B and C, where B has only the nonlinear geometry effect, shows that this effect is more responsible than the  $P-\Delta$  for the reduction. Differences in the models with and without the nonlinear effects become less apparent at a smaller increment size.

Run H is for a curvilinear steel, and it corresponds to the elasto-plastic run F. Up to the third peak there is very little difference, since the behavior in both models is essentially elasto-plastic. Afterwards the curvilinear steel begins to exhibit a significant plastic drift which is not observed in either the elasto-plastic case or in the experimental results.

The corresponding moment-curvature relations (runs F, G, and H) for a cross-section at the top of each column are plotted in Fig. 6-3 (A to C). Significant differences may occur for each column in a

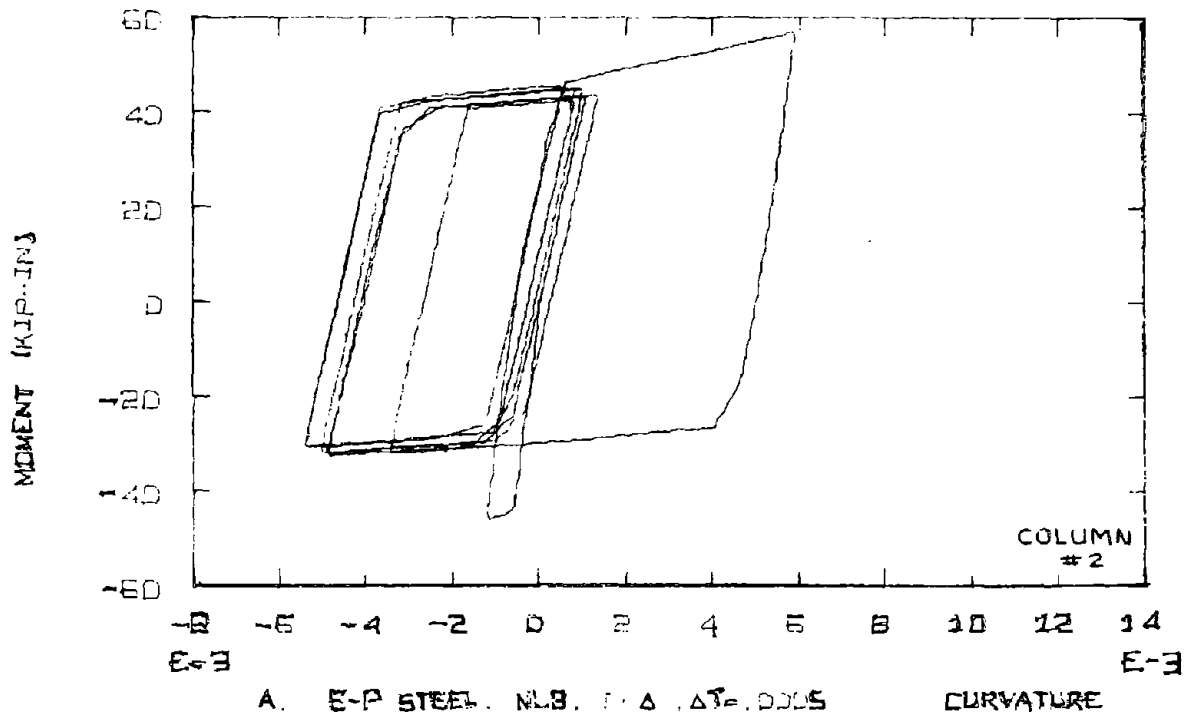
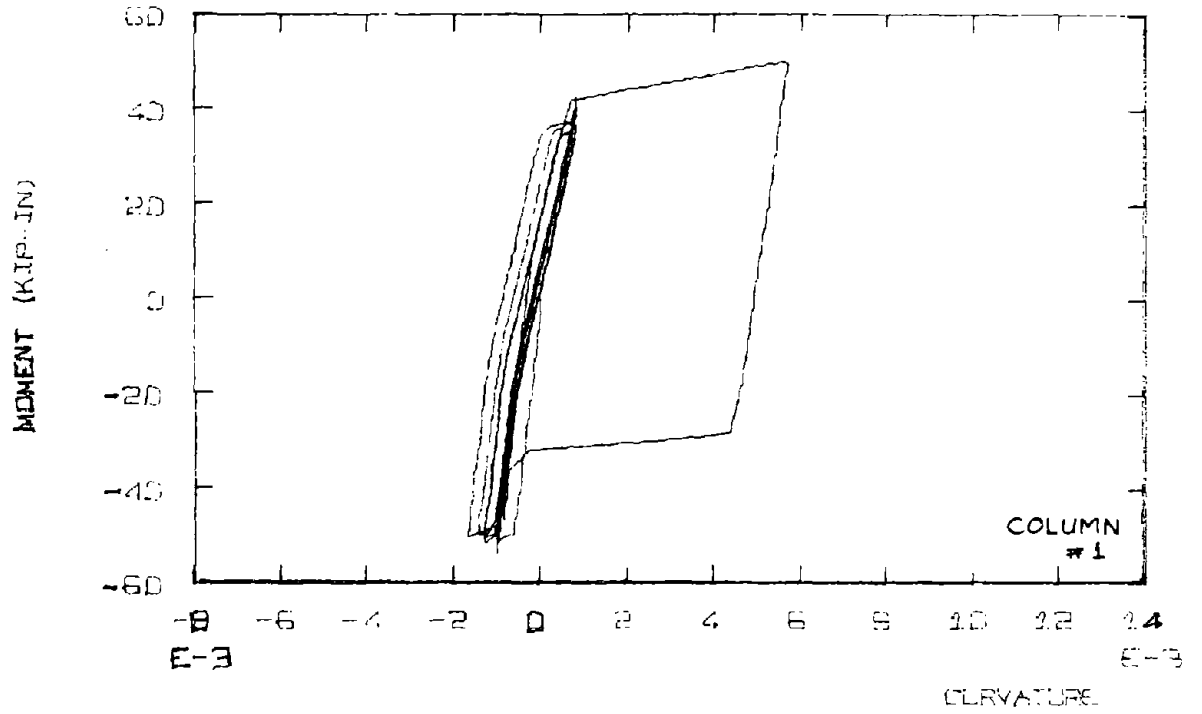


FIG. 6-3 - TYPICAL MOMENT-CURVATURE RELATIONS FOR THE COLUMNS

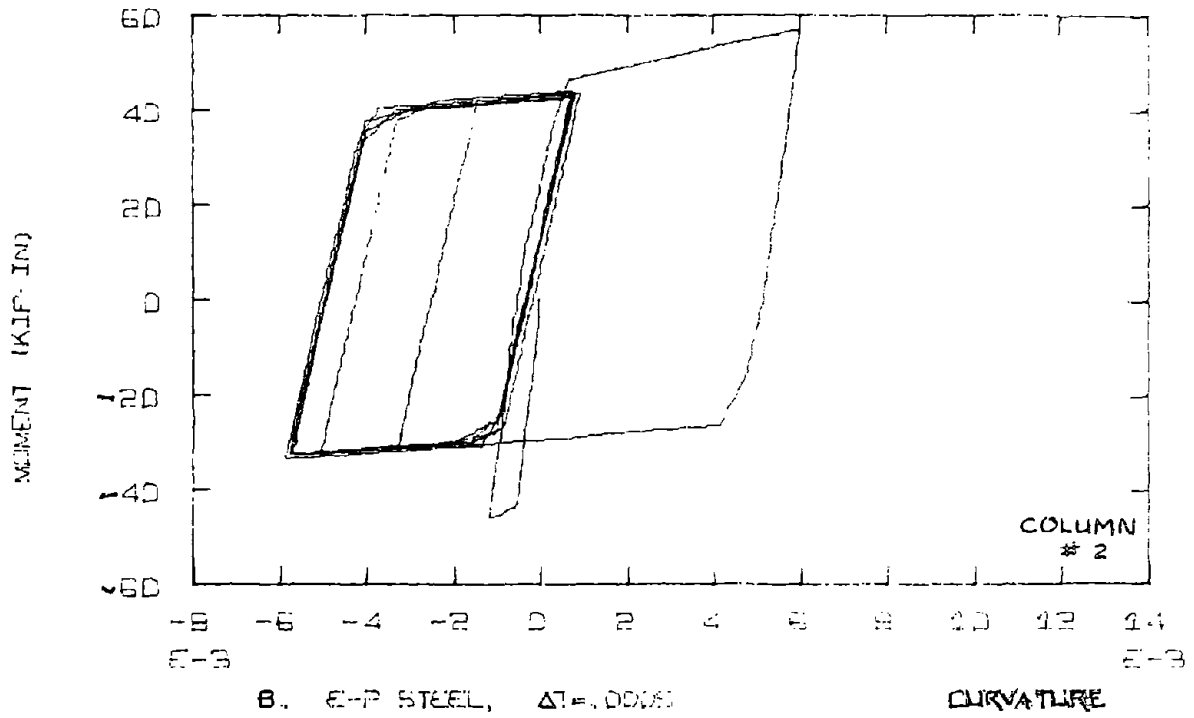
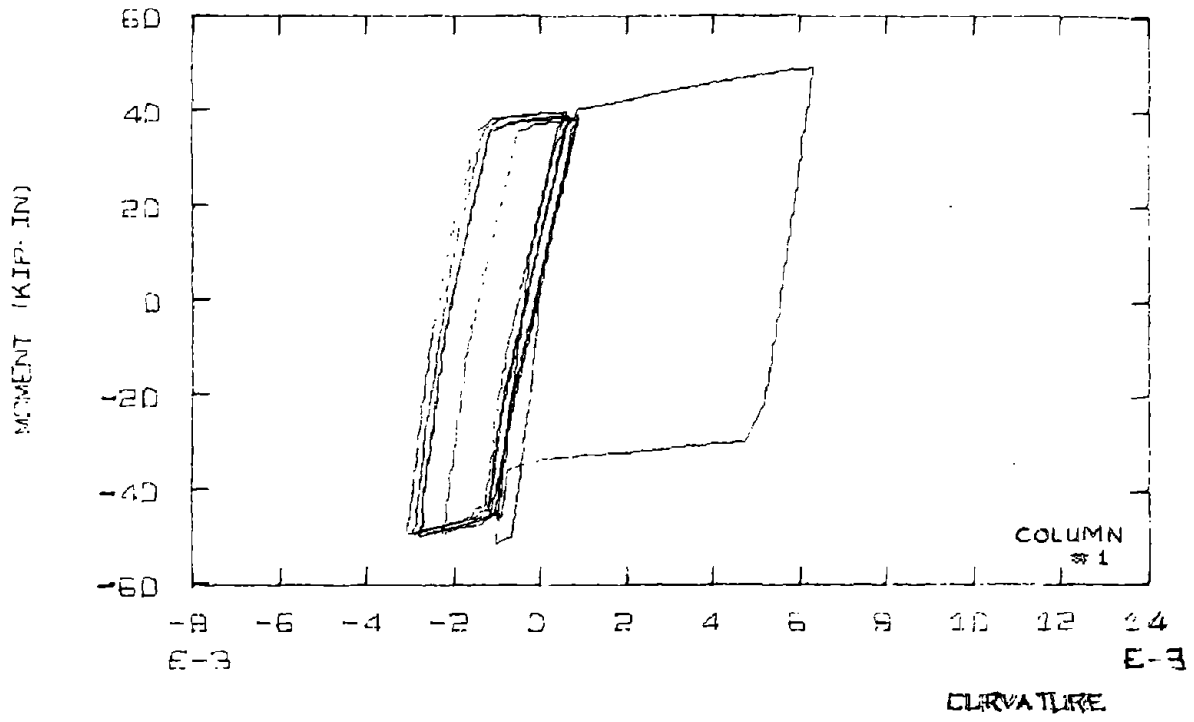


FIG. 6-3 (Cont.)

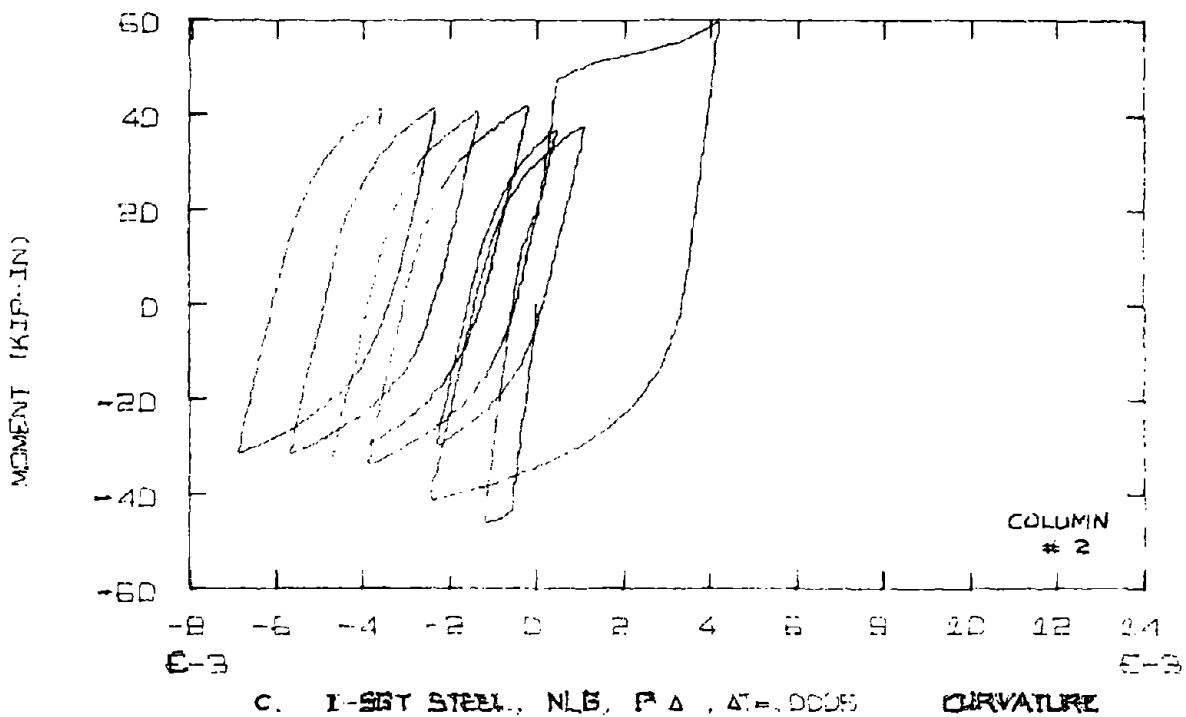
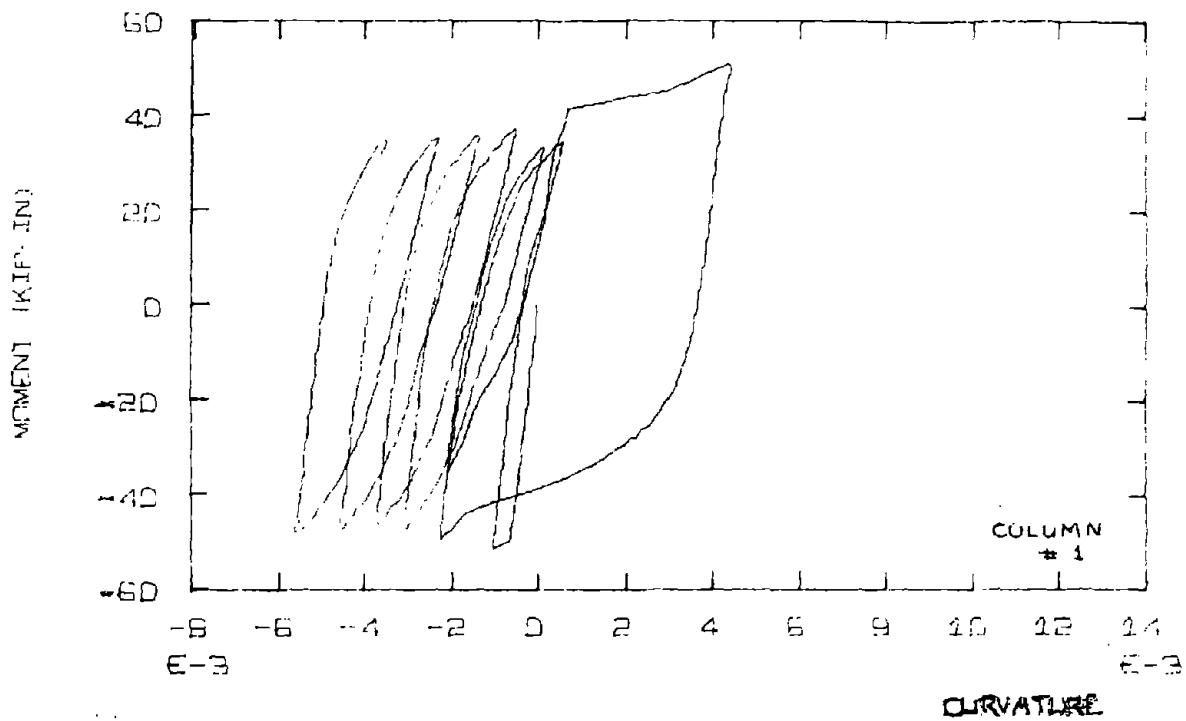


FIG. 6-3 (Cont.)

frame. Laterally-induced axial forces cause differences in the moment-curvature relations and in the resultant stiffness of each column.

For the elasto-plastic steel (F and G) the loops formed become stable, but for the curvilinear steel they do not. This reflects two aspects previously pointed out: 1) The I-SGT model and other curvilinear models discussed do poorly for repetitive loadings with small strain reversals; 2) The moment-curvature relation with I-SGT steel tends to be softer in reloading in the initial loading direction than in the opposite direction. Additional refinement of the steel formulation may be required to meet these criteria of performance.

For comparison with the simpler models to be discussed in Section 3, the load-deflection relationships for runs F and H are displayed in Fig. 6-4 (A and B). These generally reflect the corresponding moment-curvature relations. The loops for the elasto-plastic steel begin to show some rounding.

In the dynamic response of the frame there can be considerable variation in the lateral stiffness (Fig. 6-4). Sudden changes in the lateral stiffness correspond to changes in the loading direction where the steel yields or begins to unload. The frame is initially uncracked, and the stiffness eventually oscillates in a range lower than the initial lateral stiffness. In the response of the structure to a sinusoidal motion, the detailed variation of

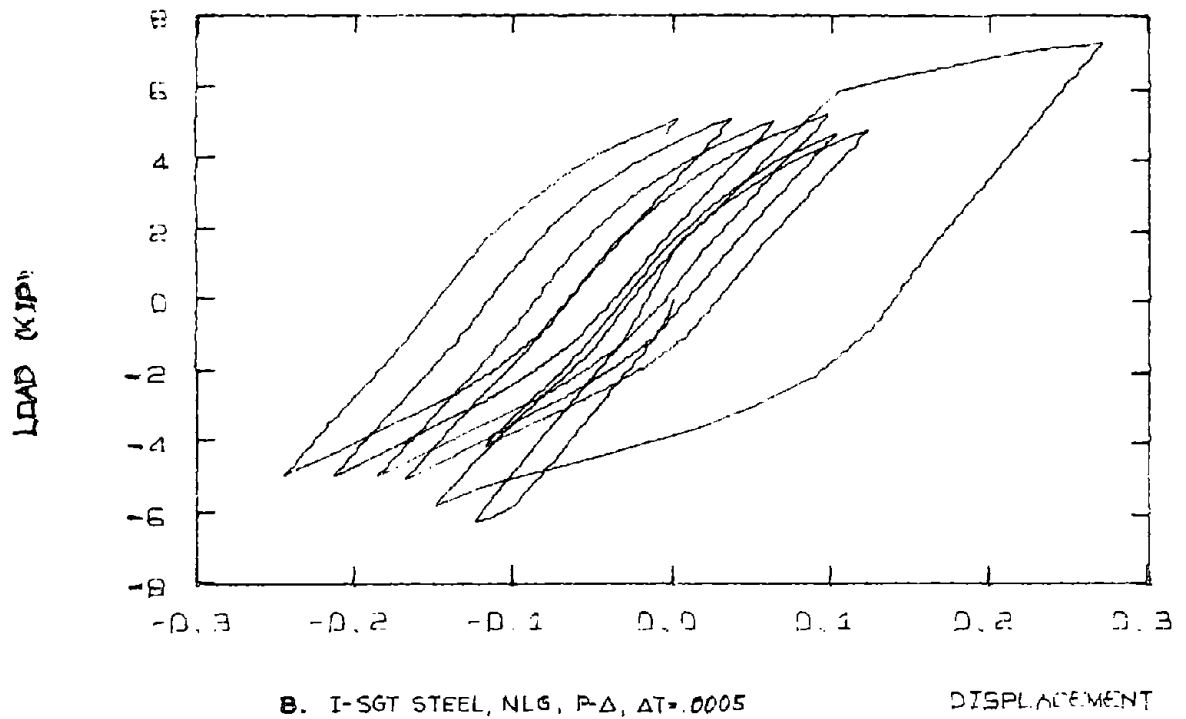
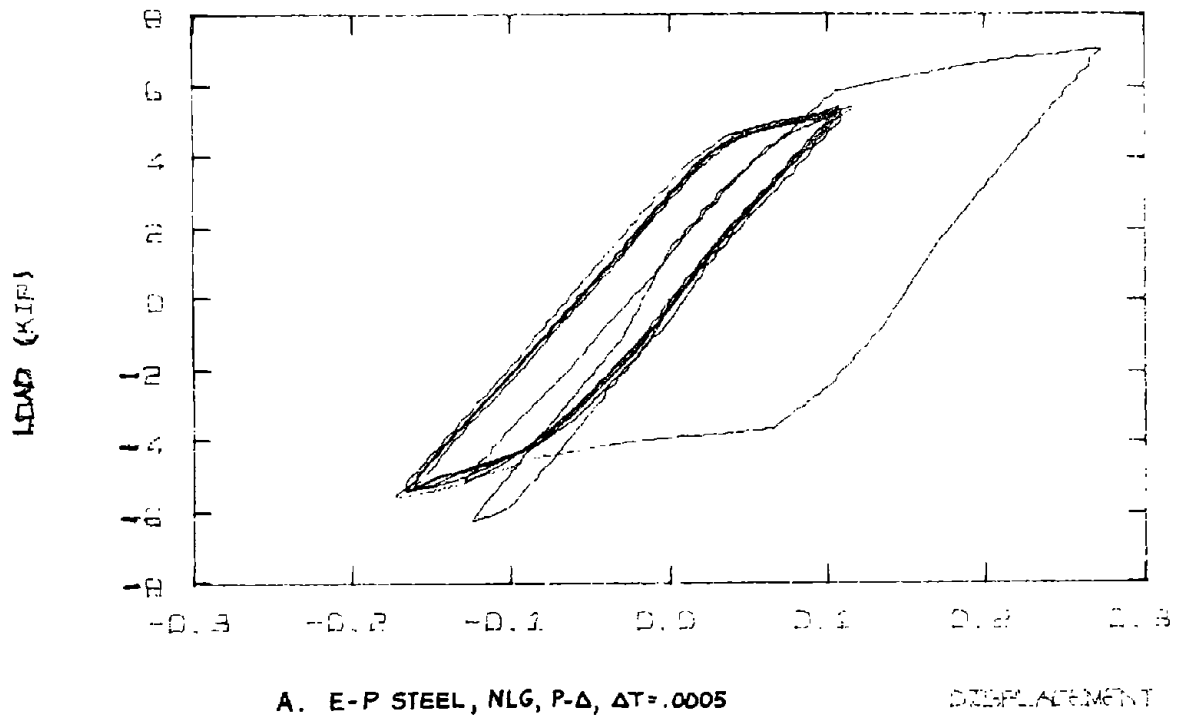


FIG. 6-4 - LOAD-DEFLECTION RELATIONSHIPS

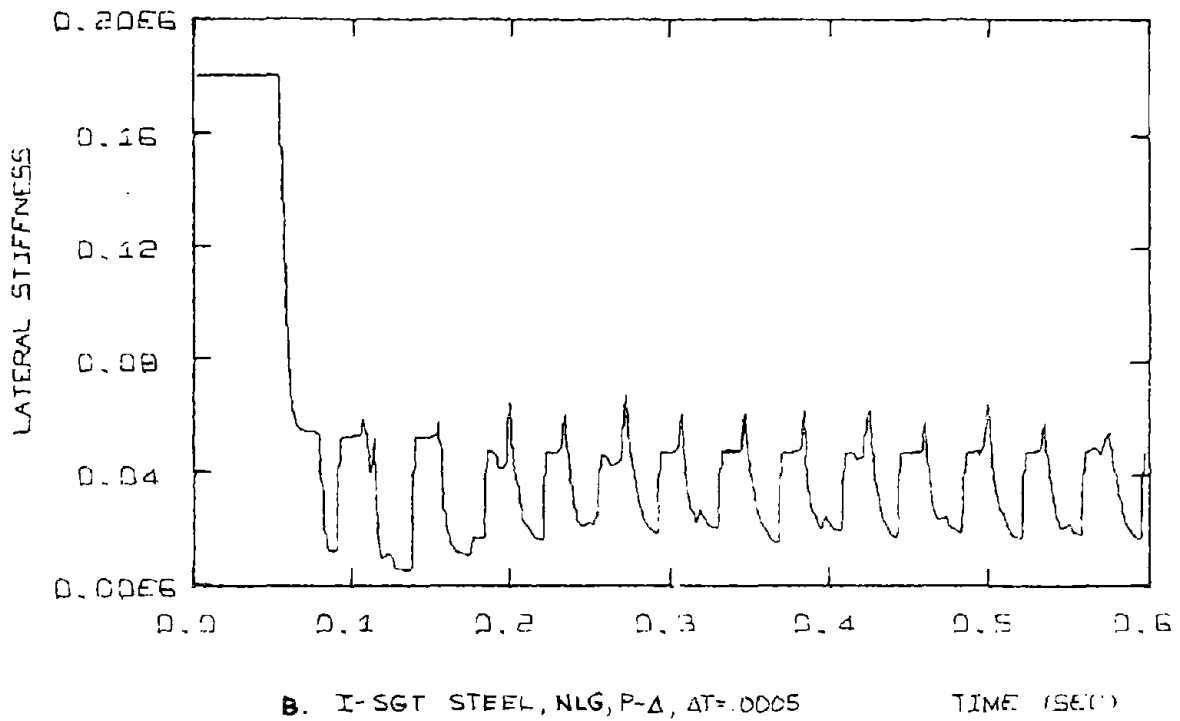
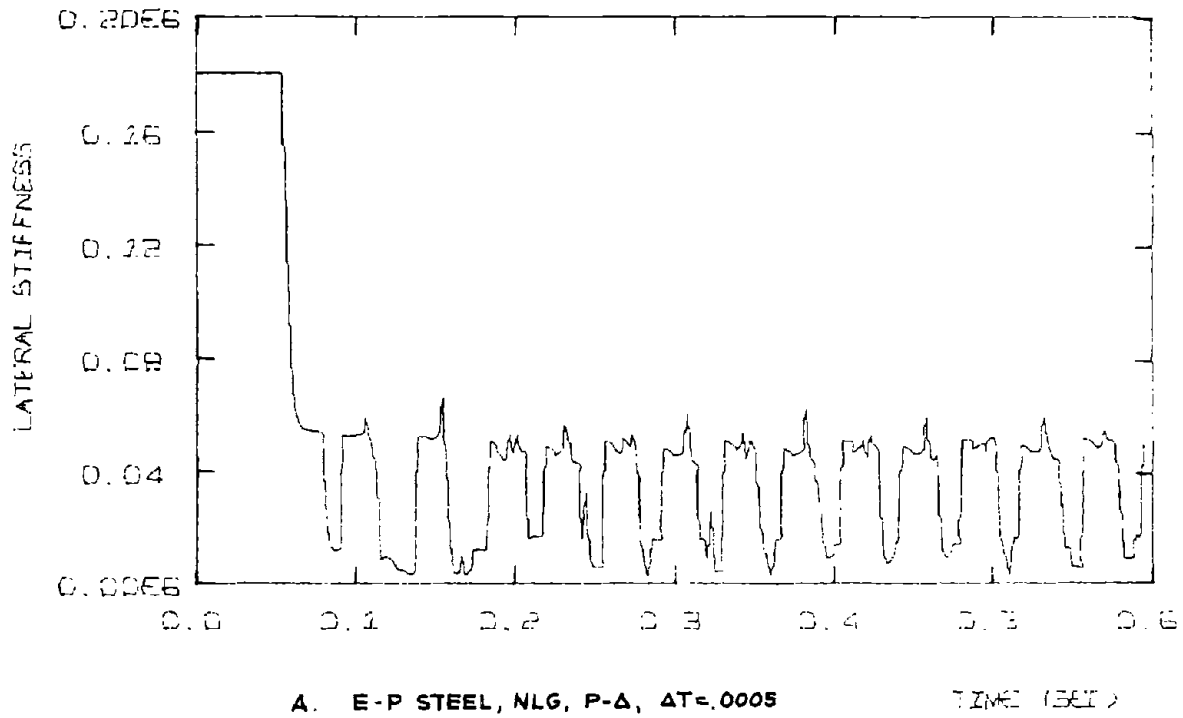


FIG. 6-5 - VARIATION OF LATERAL STIFFNESS

TABLE 6-1 COMPARISON OF PEAK DISPLACEMENTS FOR FIBER MODEL UNDER SINUSOIDAL BASE MOTION

$\Delta T$ NLG P- $\Delta$ Steel	A .002 Yes Yes E-P	B .002 Yes No E-P	C .002 No No E-P	D .001 Yes Yes E-P	E .001 No No E-P	F .000f Yes Yes E-P	G .0005 No No E-P	H .0005 Yes Yes I-SGT	I .0005 No No I-SGT
Peak #									
1	-.126	-.126	-.126	-.125	-.125	-.126	-.125	-.126	-.125
2	.282	.287	.283	.273	.274	.274	.260	.273	.273
3	-.075	-.077	-.076	-.099	-.101	-.131	-.129	-.150	-.150
4	.231	.202	.215	.215	.213	.110	.112	.126	.125
5	-.009	-.078	-.049	-.065	-.073	-.163	-.169	-.119	-.128
6	.259	.209	.287	.208	.273	.119	.107	.104	.099
7	-.043	-.086	.042	-.092	-.061	-.156	-.180	-.173	-.179
8	.232	.219	.322	.225	.257	.125	.102	.098	.087
9	-.038	-.059	.055	-.057	-.044	-.155	-.179	-.193	-.201
10	.247	.219	.333	.237	.254	.125	.103	.063	.082
11	-.024	-.070	.064	.044	-.055	-.159	-.179	-.217	-.226
12	.255	.236	.361	.240	.248	.120	.103	.037	.022
13	-.020	-.026	.095	-.053	-.066	-.162	-.180	-.249	-.262
Max. Displ.	.281	.283	.283	.273	.274	.273	.260	.273	.273
Max. Peak to Peak Displ.	.407	.409	.409	.398	.398	.404	.388	.243	.243
Ave. Peak to Peak Displ.	.272	.281	.262	.267	.301	.279	.283	.273	.276
Drift at t=.6 sec.	.112	.105	.228	.094	.091	-.021	.039	-.106	-.120

the stiffness becomes of particular importance because of the possibility of resonant excitation.

As was previously pointed out, the actual base acceleration is not exactly a sinusoid. Figure 6-1 C shows a modified sinusoid which has the same peak amplitudes and zero crossings as the shaking table acceleration. The elasto-plastic model was run from this base motion with the nonlinear effects and  $\Delta t = .0005$  (Fig. 6-7). Comparing this with the experimental response in Fig. 6-6, there is good agreement in the frequency of response. There is better agreement with the first three peaks than in previous runs with the sinusoidal excitation, but the agreement deteriorates later. The change in response caused by a small change in the excitation is worth noticing.

### 6.2.3 Behavior of the Fiber Model under Earthquake Base Motion

Another frame (with a clear column height of 13"), designated HE1, was tested by Gulkan using the El Centro (N-S) component compressed in time as the base motion (Fig. 6-1D). The experimental response is shown in Fig. 6-8. Due to the expense of the computation required for the fiber model, only two seconds of response were computed (this required 17 minutes on the IBM 370/M165) at an increment  $\Delta t = .0005$ .

For the elasto-plastic steel shown in Fig. 6-9A, there is a very good match with the response of the structure for the first 1.1 seconds if the response is shifted in time .04 seconds (the large

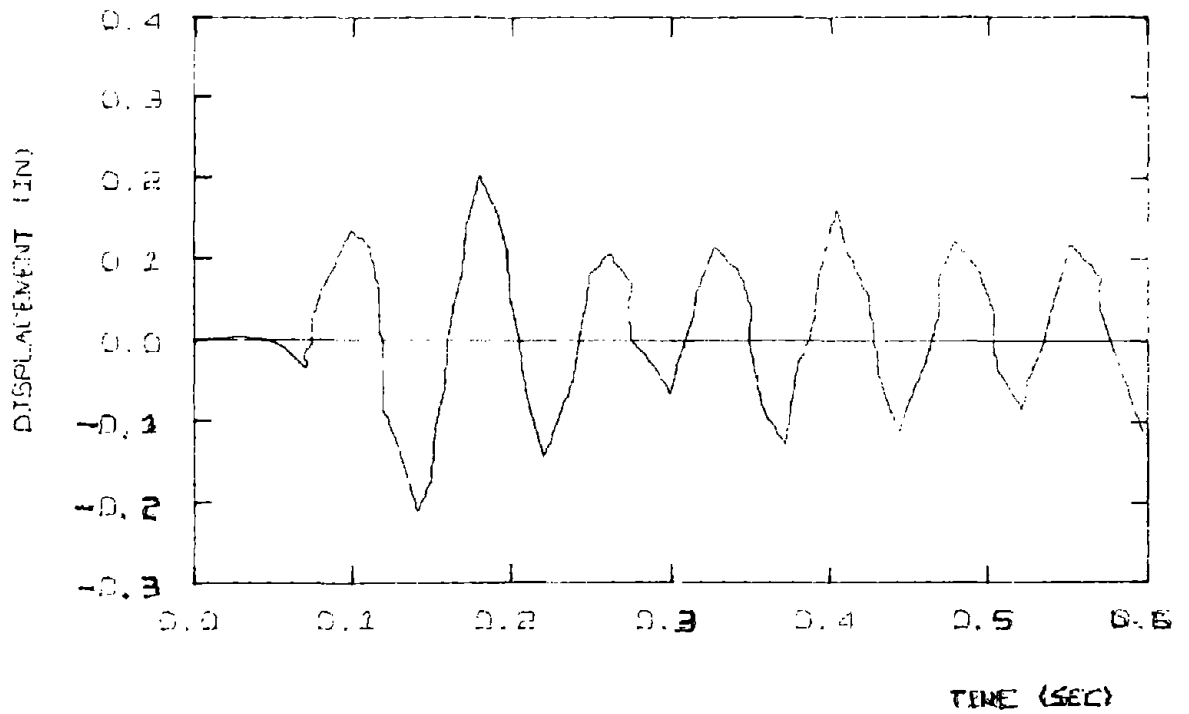


FIG. 6-6 - EXPERIMENTAL RESPONSE OF FRAME FD1 TO  
STEADY STATE BASE MOTION

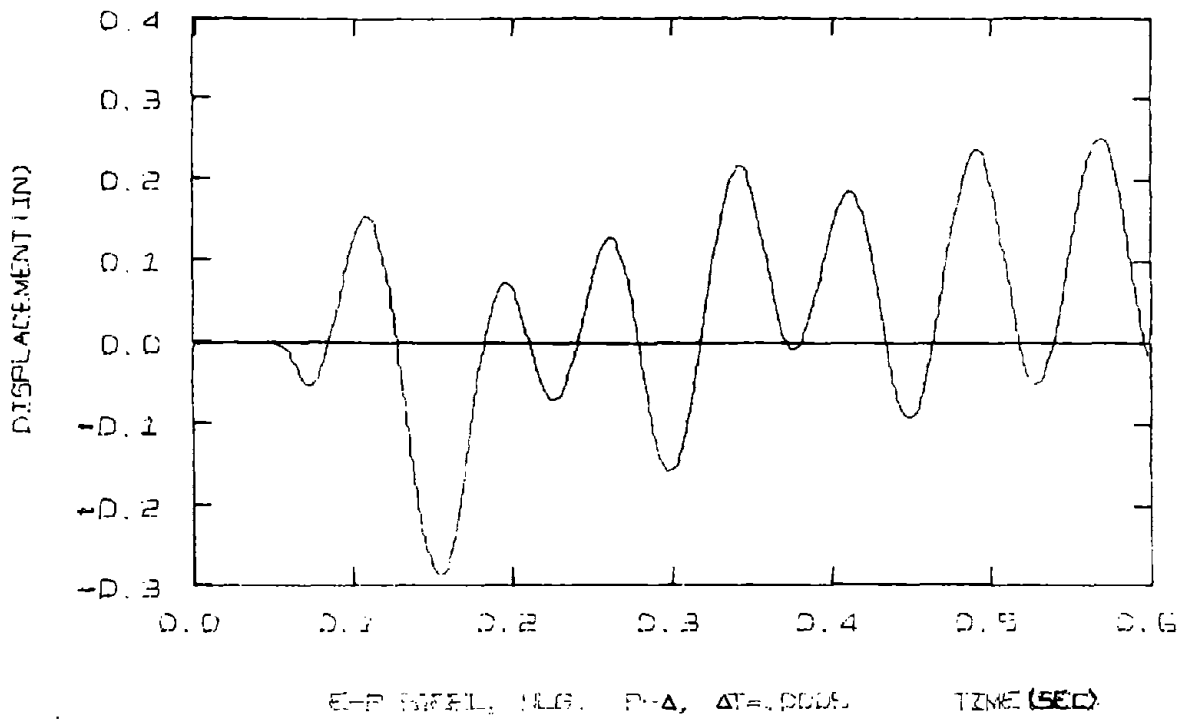


FIG. 6-7 - RESPONSE OF FIBER MODEL TO STEADY STATE BASE MOTION

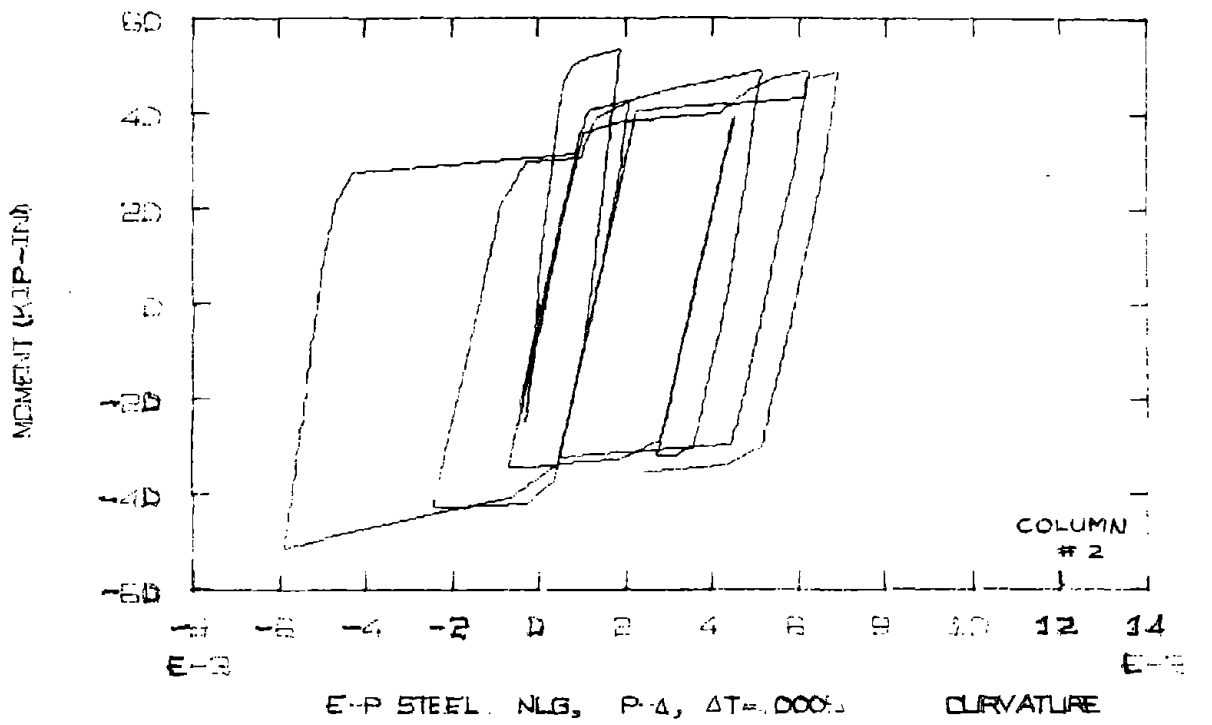
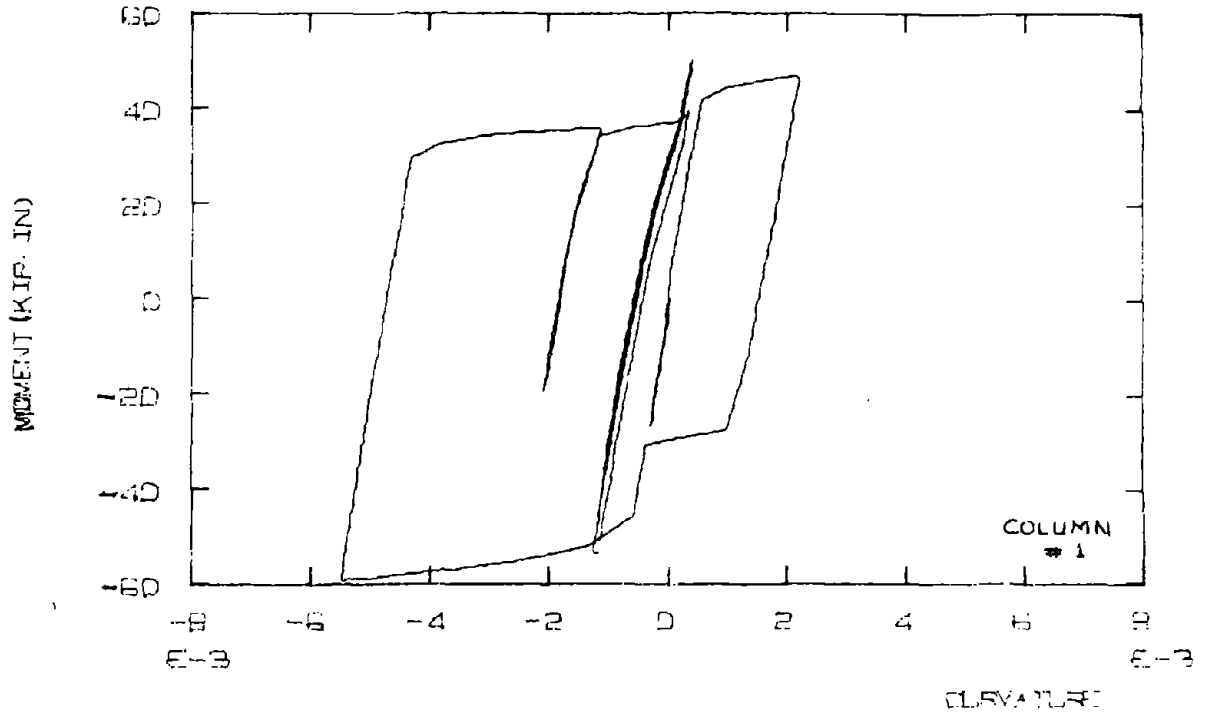


FIG. 6-7 (Cont.)

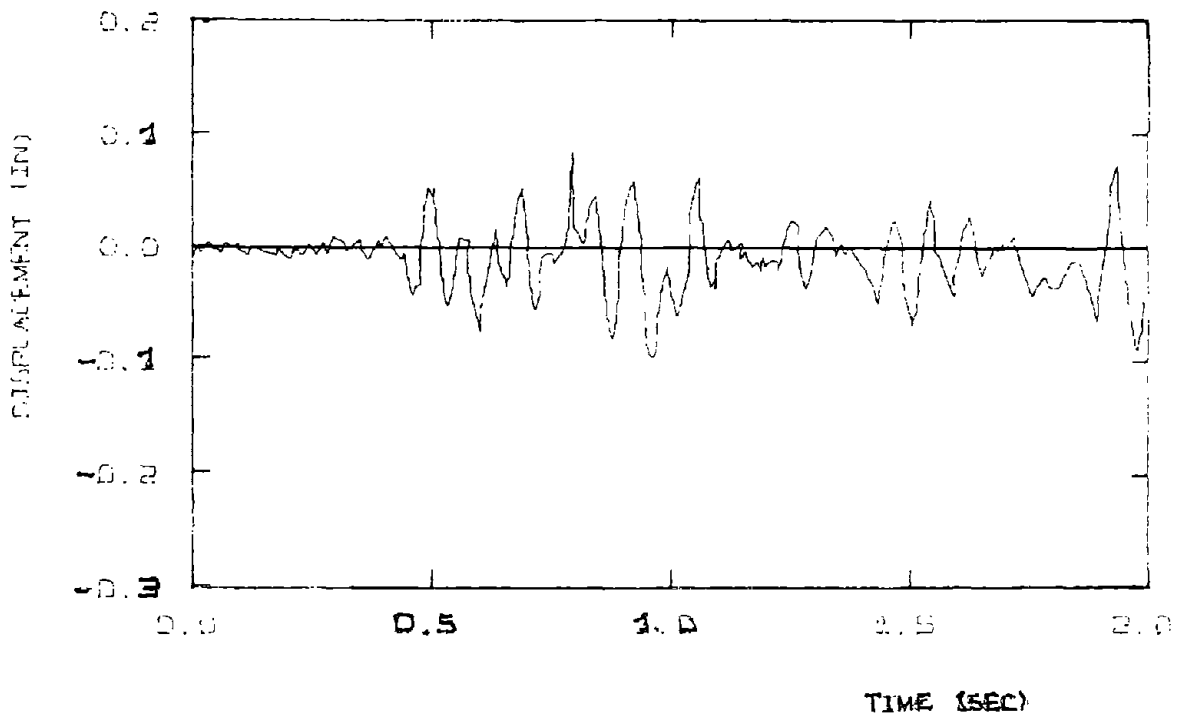


FIG. 6-8 - EXPERIMENTAL RESPONSE OF FRAME HE1 TO  
EL CENTRO EARTHQUAKE

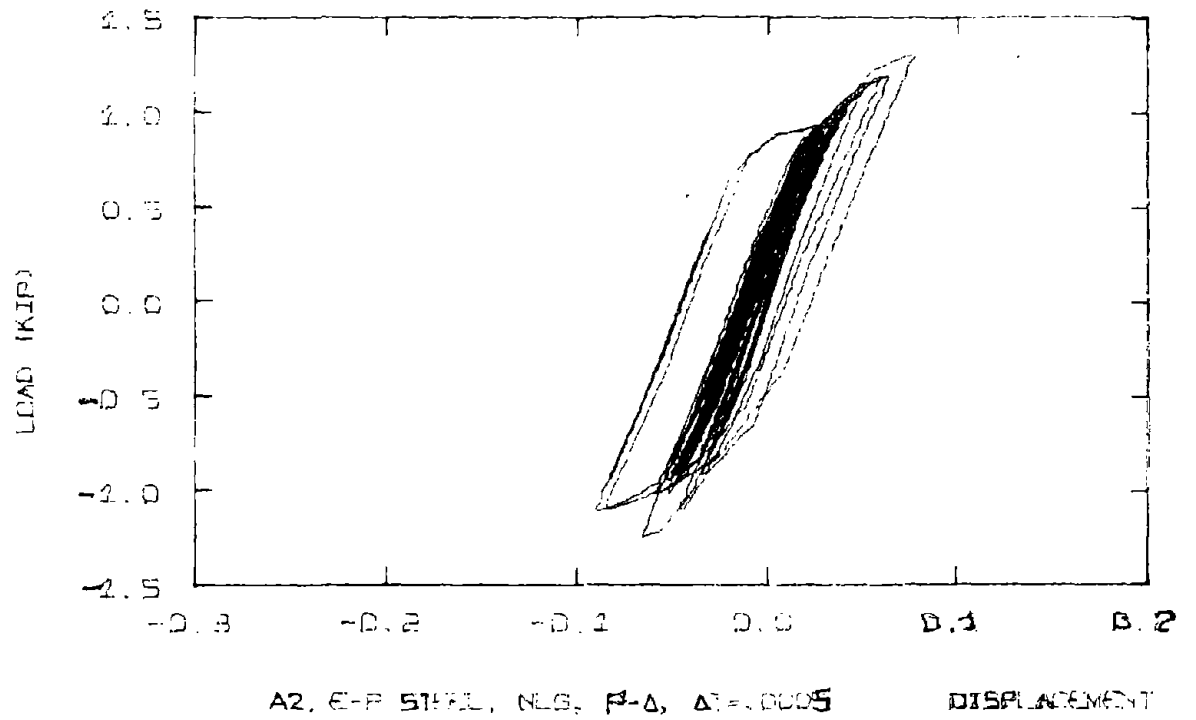
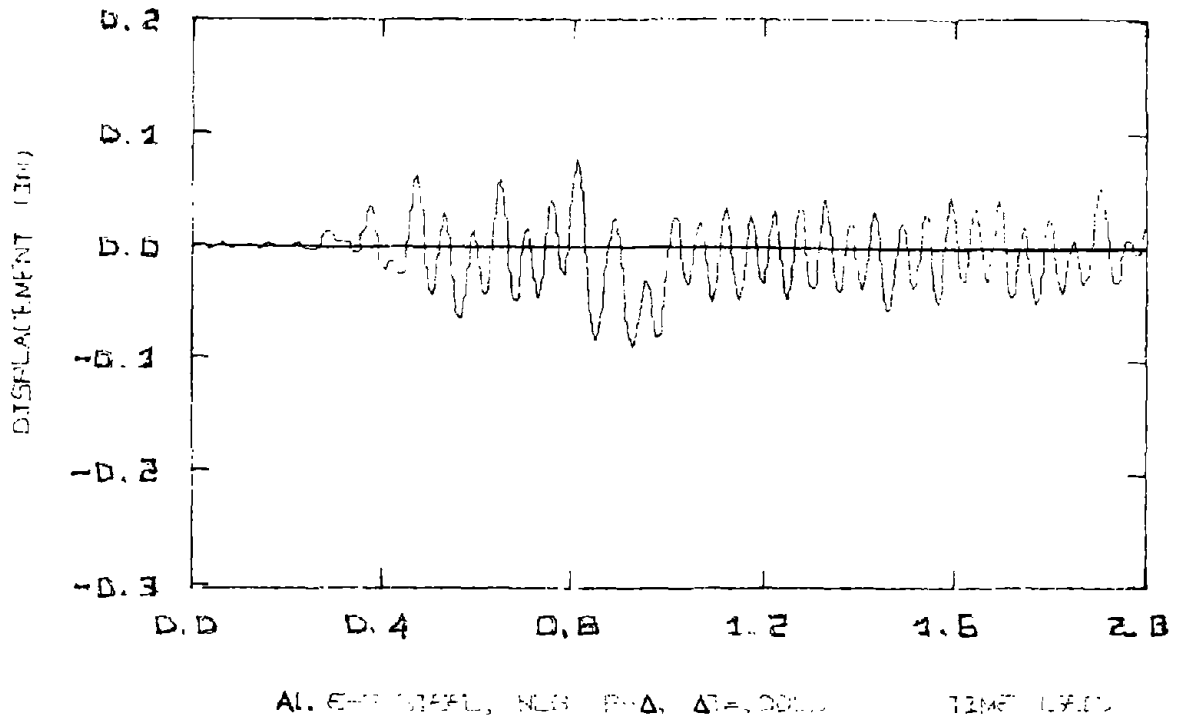


FIG. 6-9 - RESPONSE OF FIBER MODEL TO EL CENTRO EARTHQUAKE

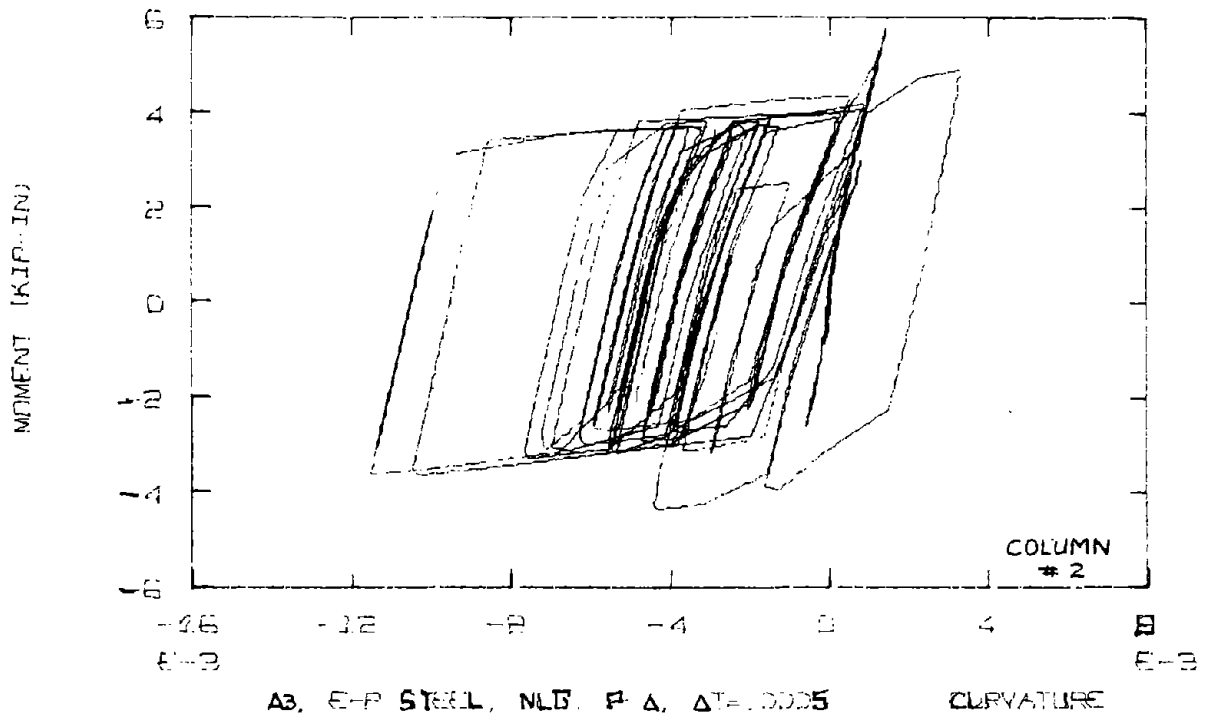
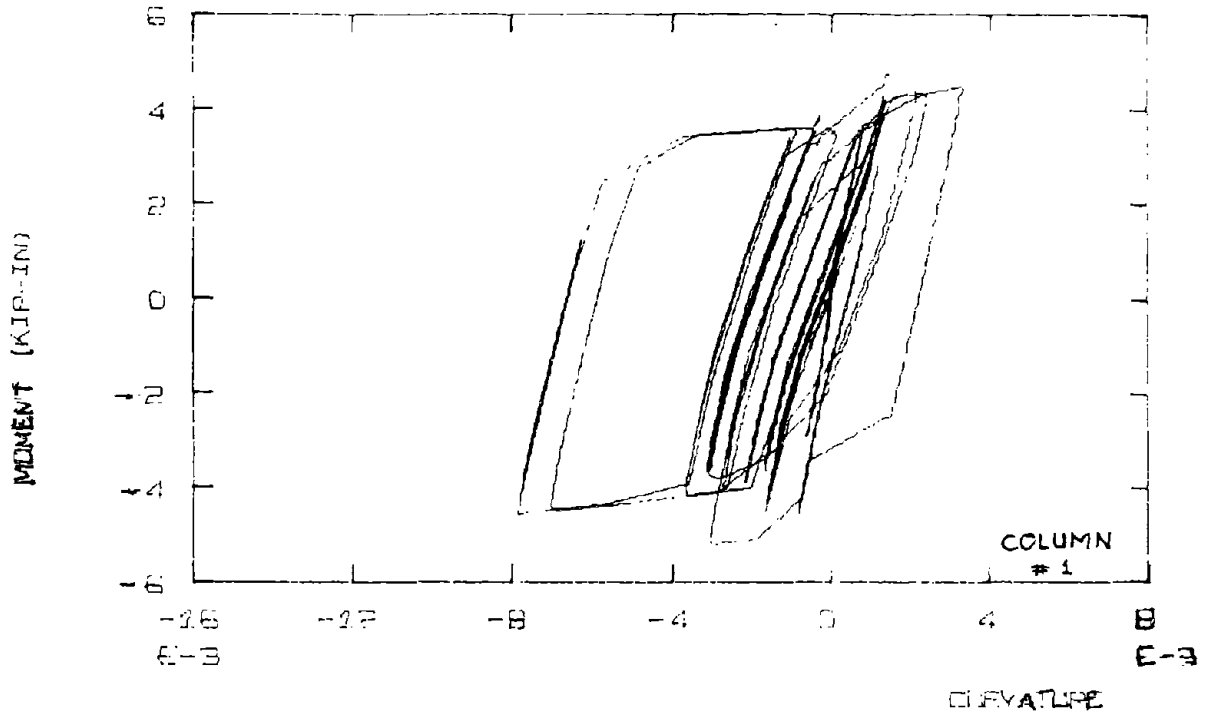
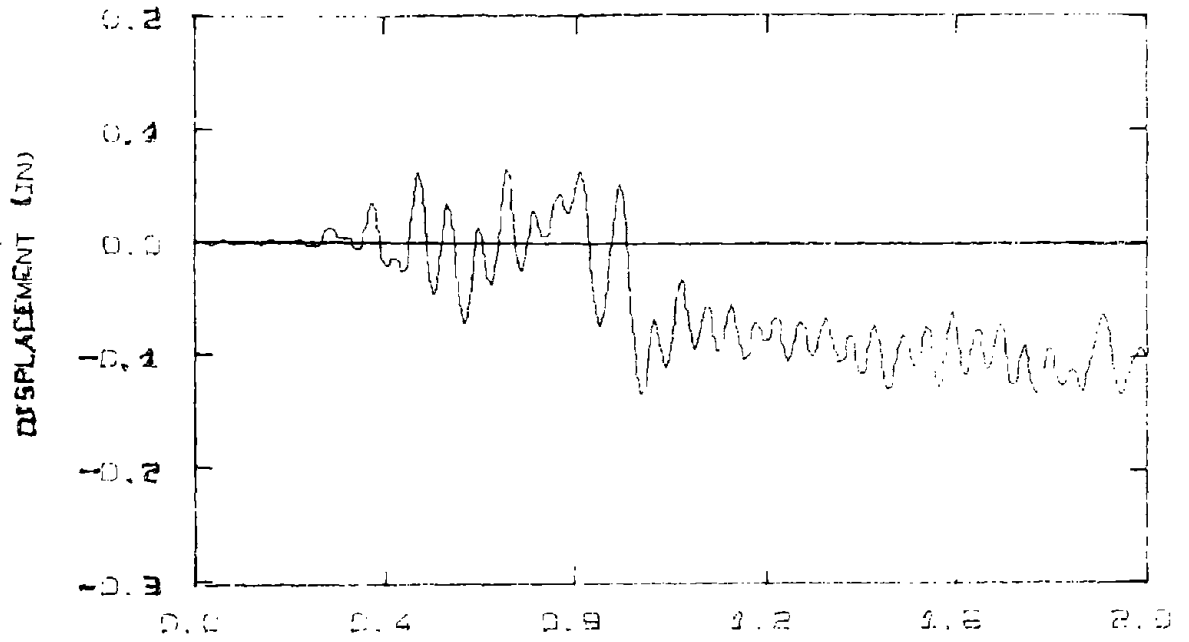
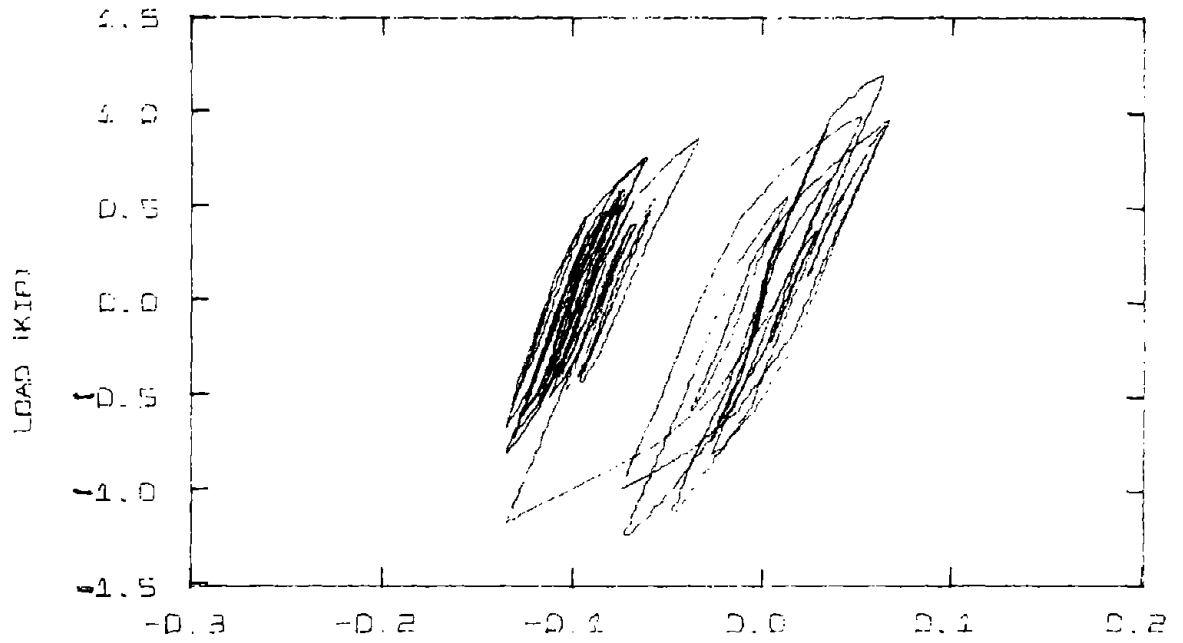


FIG. 6-9 (Cont.)

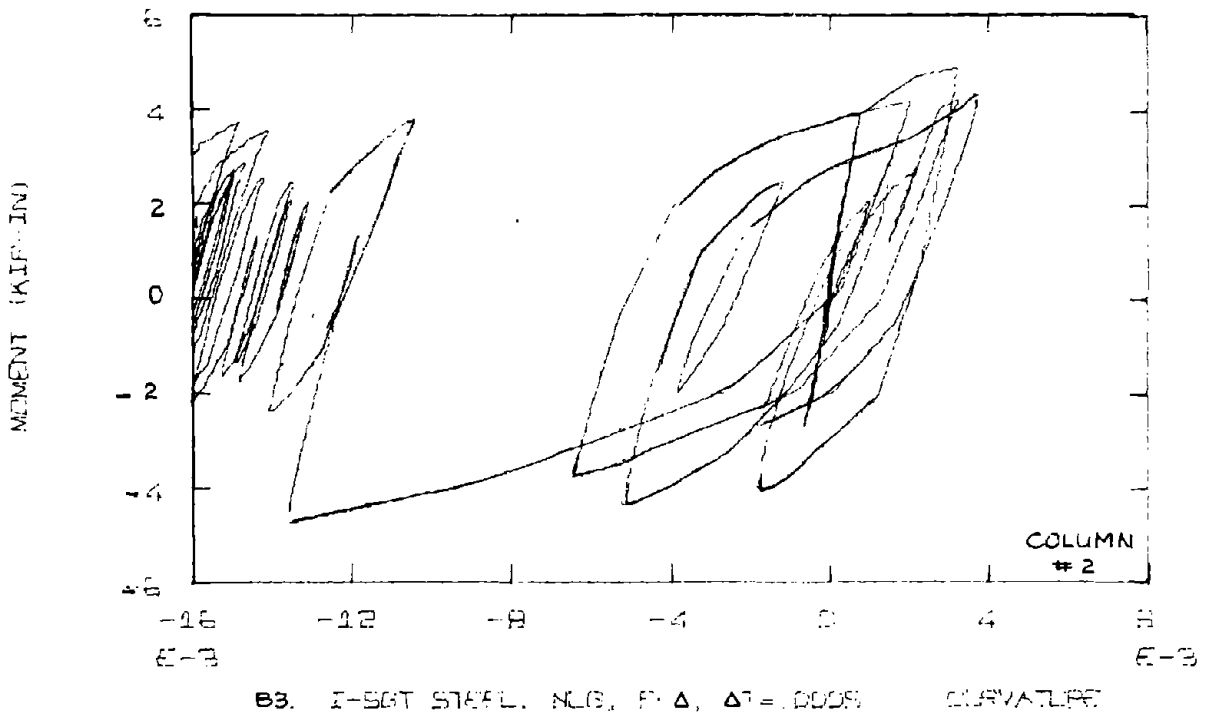
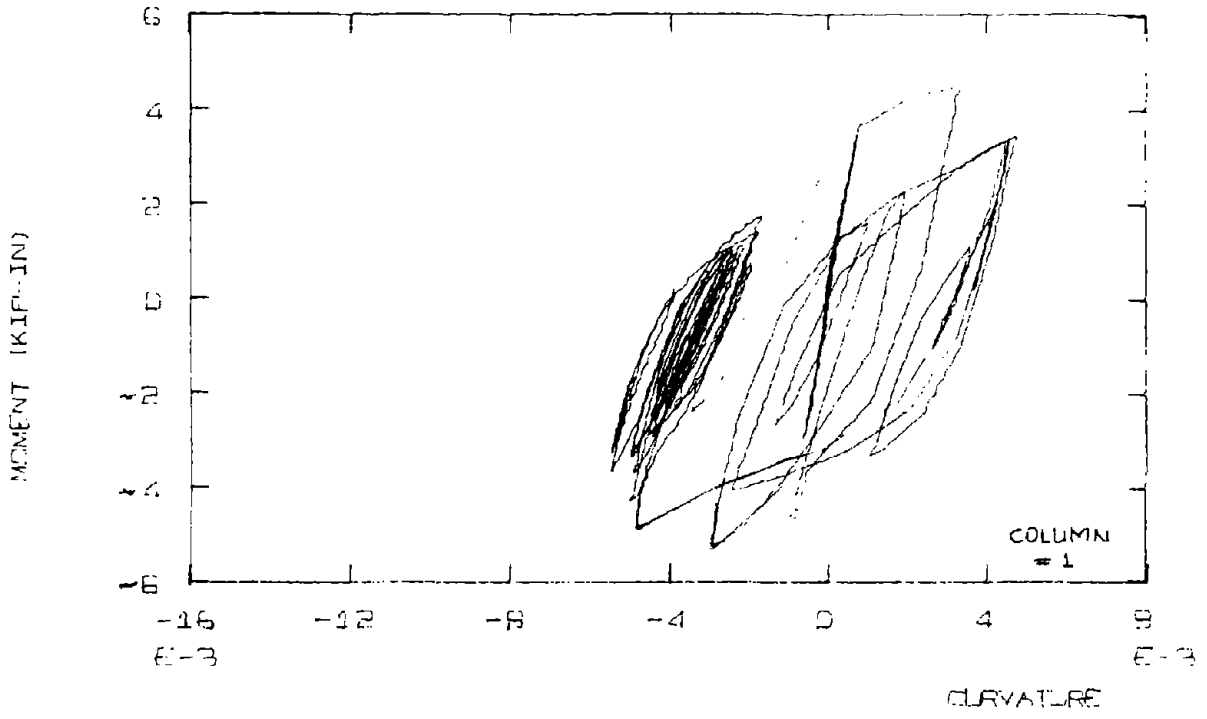


B1. I-BEAM STEEL, NLG, P-Δ, ΔT=.0005 TIME (SEC)



B2. I-BEAM STEEL, NLG, P-Δ; ΔT=.0005 DISPLACEMENT

FIG. 6-9 (Cont.)



B3. I-SBT STEEL. NLG.  $P/\Delta$ ,  $\Delta T = 0.009$

FIG. 6-9 (Cont.)

amplitude peaks occur sooner in the analytic model). The amplitude of response and location of peaks then show good agreement in this range. In the remaining part of the response the analytic response frequency is noticeably greater. From this load-deflection curve it appears that the frame is more-or-less elastic because there is little yielding. The maximum calculated deflection is .078", while experimentally the value is .084". Maximum peak-to-peak values are .151" and .143" for the analytic and experimental results.

The model with the curvilinear steel, however, displays a significant permanent set after .92 seconds. The permanent set is reflected in the moment-curvature and load-deflection relations, where during one cycle there is a large deformation, after which the loops become stable. Whether this is due to error propagation in the model or to the momentary excitation of some resonant frequency was not determined.

### 6.3 COMPARISON OF SIMPLE MODELS FOR FRAME BEHAVIOR

For use in design the fiber model is far too expensive (in terms of computer time). Simpler models which attempt to represent the overall behavior of reinforced concrete frames will be compared in this Section. There is no attempt to imply that the models used represent a complete survey of those available.

The following were used:

- 1) Elastic            This model is used more as a comparison with other models than as a representation of concrete frame behavior.
- 2) Bilinear           This model is essentially elasto-plastic, with a small second slope.
- 3) Trilinear          The initial and final slope correspond to the elasto-plastic, but the second branch has a slope  $.2K_0$  and begins at half the yield force.
- 4) Clough's<sup>(47)</sup> Model    This has an elasto-plastic envelope and unloads with the initial stiffness, but has stiffness degradation in the reloading part of the relationship.
- 5) Anagnostopoulos' Model<sup>(45)</sup> This model further adds stiffness degradation for the unloading branches according to:
 
$$\frac{K}{K_0} = \left( \frac{\delta_y}{\delta_{max.}} \right)^{.35}$$
- 6) Takeda<sup>(37)</sup> Hysteresis Laws    These were used by Gulkan to obtain his analytic results and are reproduced here for comparison. Slight differences in this model may exist due to the digitizing of a small-scale record.

The models (1 through 5) were formulated as 1 d.o.f. springs which related the lateral force and displacement of the simple frame. From Gulkan's experimental work, the average initial stiffness and yield values were obtained. These models were subjected to the same base motions as the fiber model was (modified sinusoid and El Centro).

### 6.3.1 Behavior of Simple Models to Sinusoidal Base Motions

The simple models were subjected to the modified sinusoid base motion shown in Fig. 6-1 C. Fig. 6-10 (A to E) presents the displacement-time history and corresponding force-displacement relations.

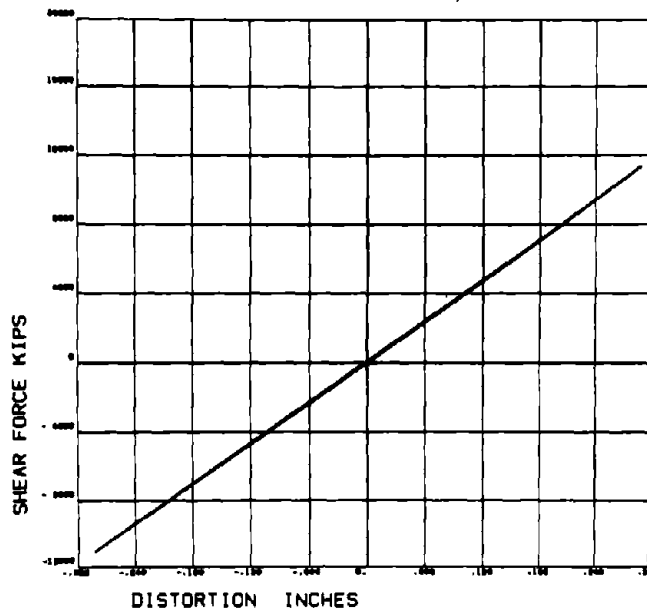
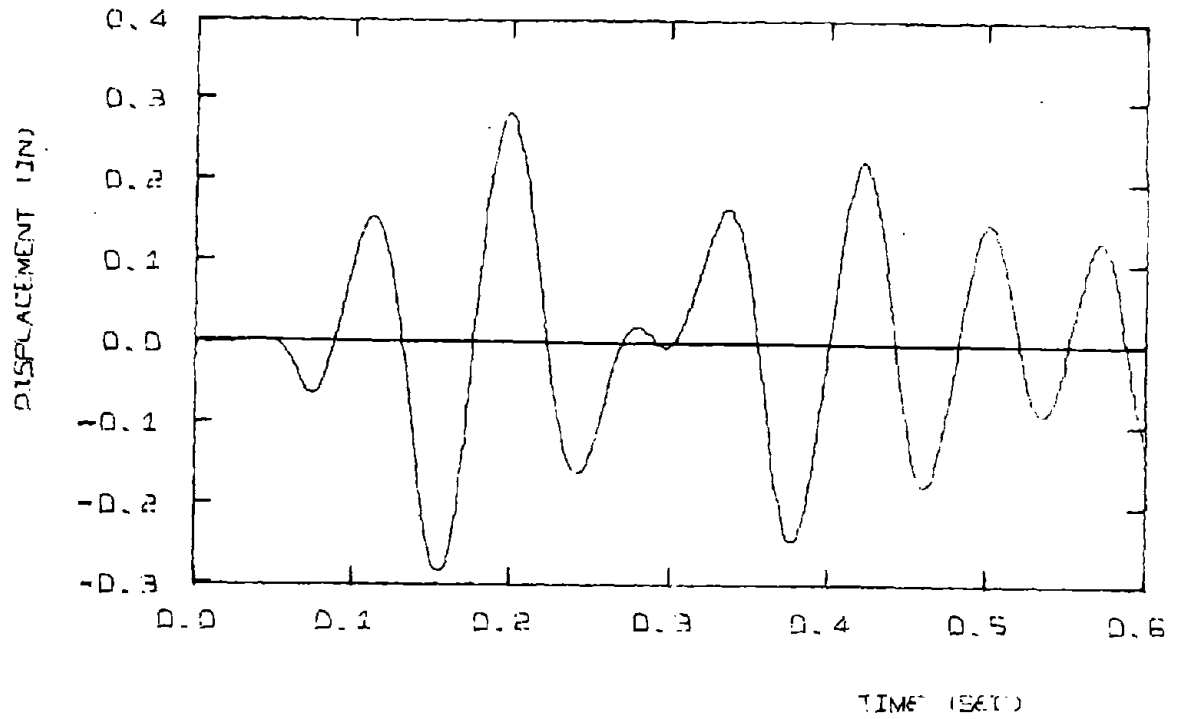
Generally all the models agree with the number of peaks, and thus with the average frequency of response. The location of the peaks correspond except for a slight shift in the time axis of .015 sec., since the test frame appears to respond sooner.

In comparing the Anagnostopoulos and Clough models it appears that response is not sensitive to the parameter used in the unloading stiffness degradation (.35 for the former and 0. for the latter). That is, whether there is degradation in the unloading branches does not seem to be important. These two models overestimate the magnitude of response displacement.

The bilinear model indicates a permanent set contrary to the observed response, and the average peak-to-peak response is again larger. In the trilinear model used, the force-displacement does not reach the final yield level. Except for a low fourth peak, the agreement is reasonable. The elastic model produces significantly larger response, especially for the second and third peaks.

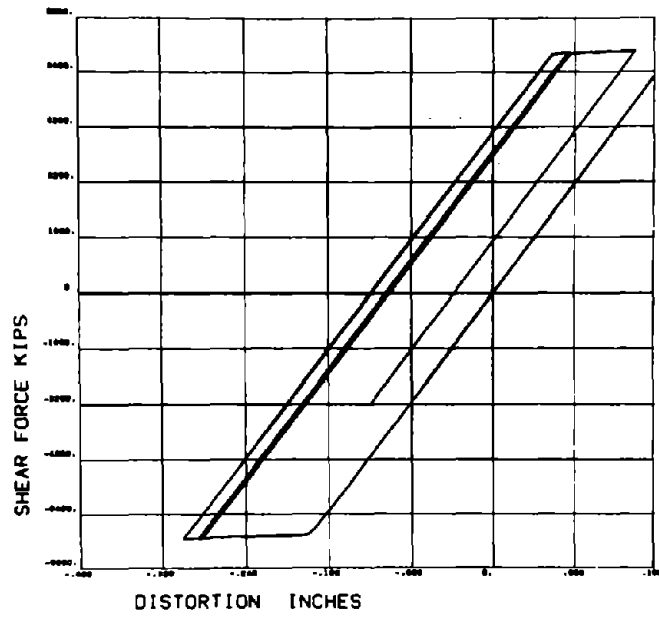
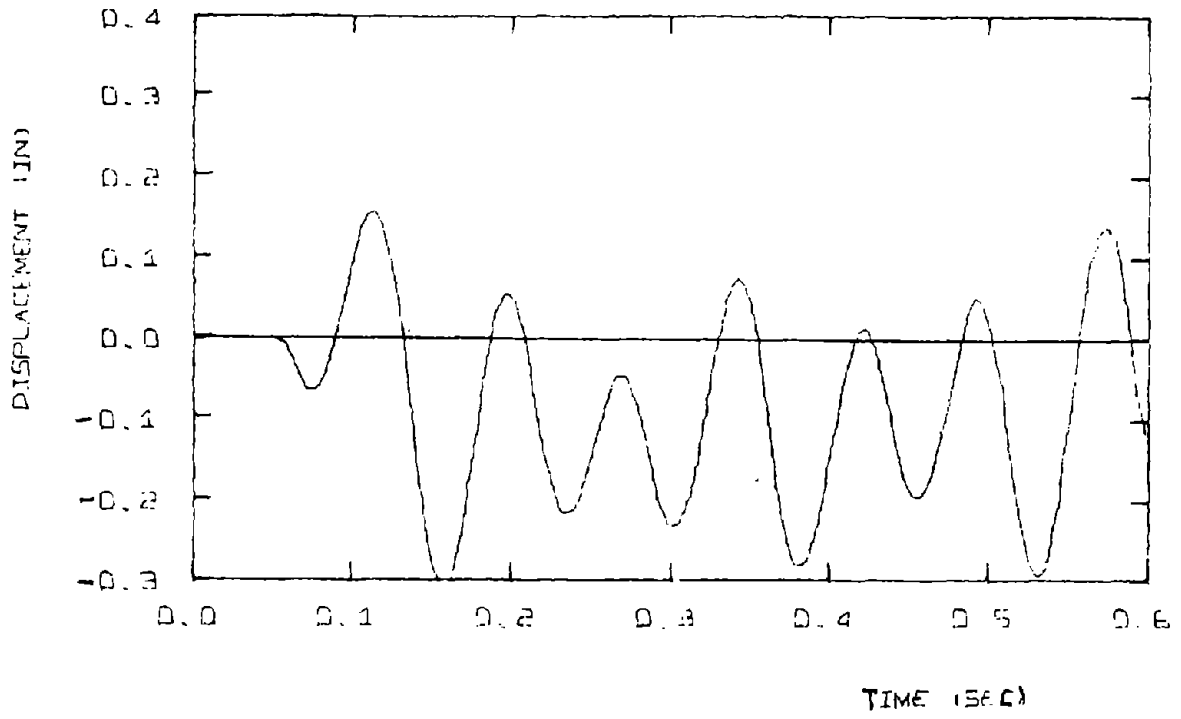
The jaggedness of the Takeda displacement response plot is the result of enlarging a small scale figure. The overall agreement is reasonable.

TABLE 6-2 COMPARISON OF MODELS FOR MODIFIED SINUSOIDAL LOADING						
Peak #	Elastic	Bilinear	Trilinear	Clough	Anagnosto- poulos	Takeda
1	-.067	-.068	-.067	.067	-.068	-.040
2	.159	.158	.169	.157	.157	.131
3	-.285	-.309	-.203	-.307	-.306	-.214
4	.287	.058	.022	.076	.101	.145
5	-.163	-.218	-.121	-.064	-.033	-.105
6	.021	-.044	.108	.031	.035	.013
7	-.006	-.233	-.141	-.228	-.216	-.100
8	.167	.076	.150	.143	.158	.141
9	-.283	-.044	-.143	-.145	-.145	-.214
10	.225	.013	.120	-.040	-.048	.122
11	-.180	-.200	-.135	-.175	-.168	-.088
12	.152	.051	.167	.55	.155	.021
13	-.094	-.294	-.076	-.241	-.245	-.113
14	.129	.141	.188	.090	.109	.141
Max. Displ.	.287	.309	.203	.307	.306	.214
Max. Peak-to- Peak Displ.	.448	.467	.372	.464	.463	.359
Ave. Peak- to-Peak Displ.	.300	.323	.255	.282	.287	.235



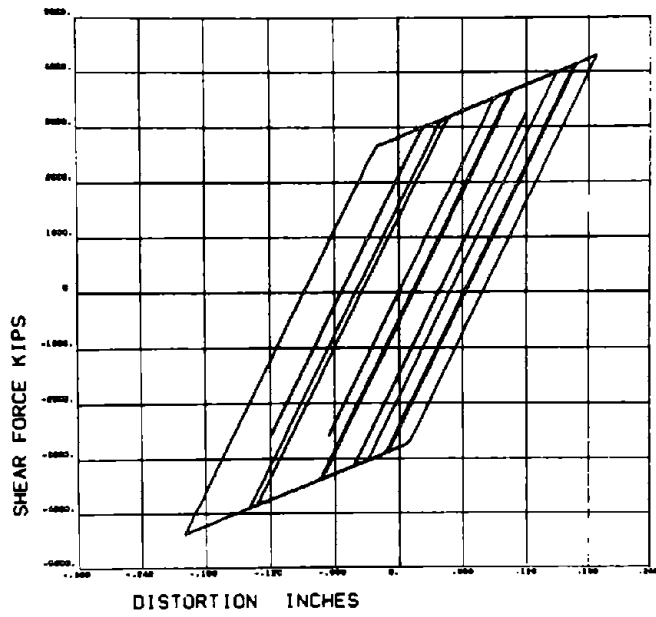
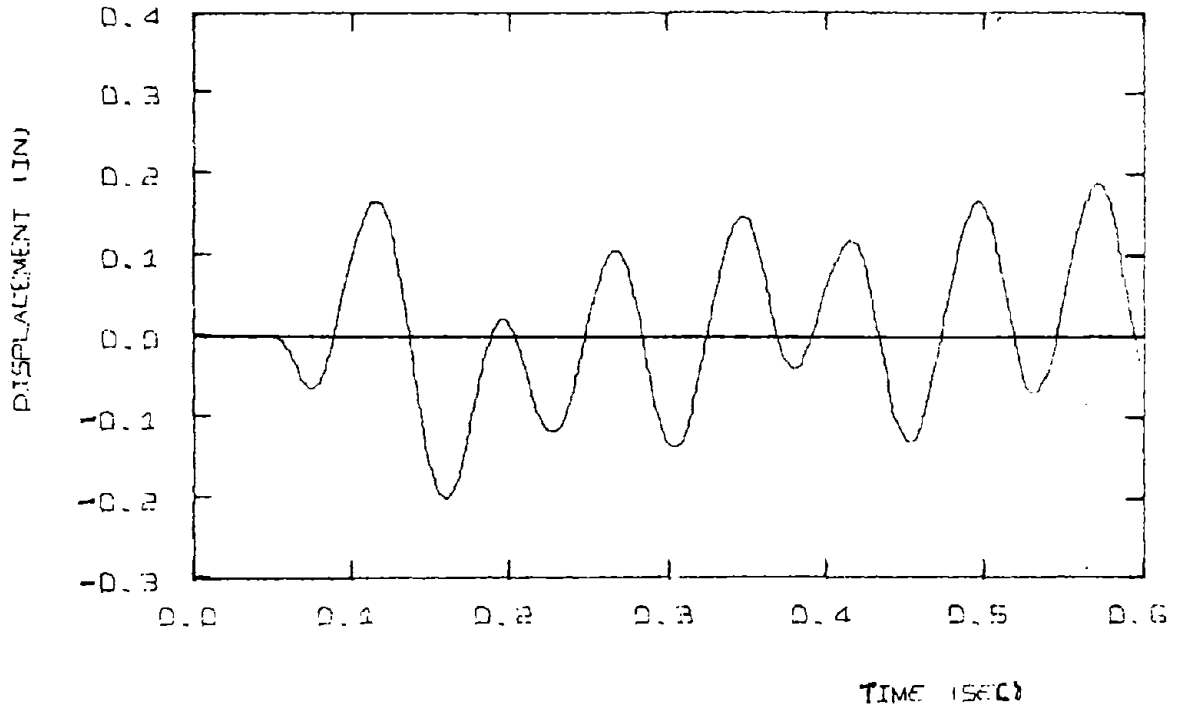
A. ELASTIC MODEL

FIG. 6-10 - RESPONSE OF SIMPLE MODELS TO STEADY STATE BASE MOTION



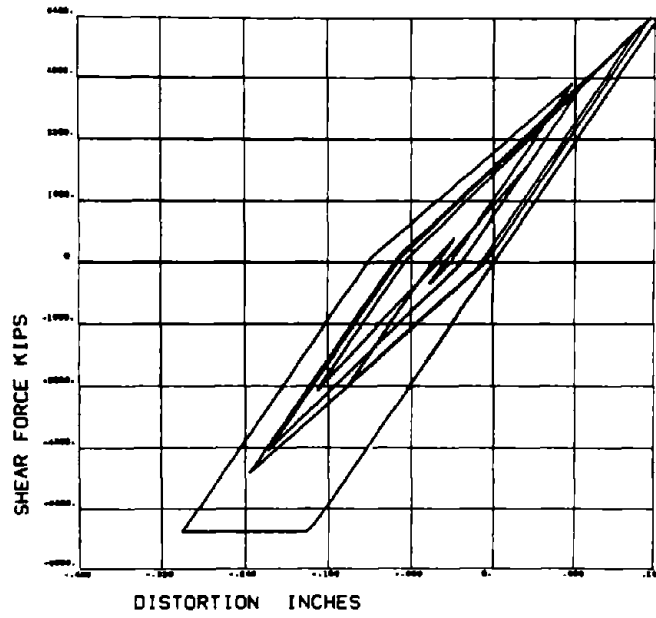
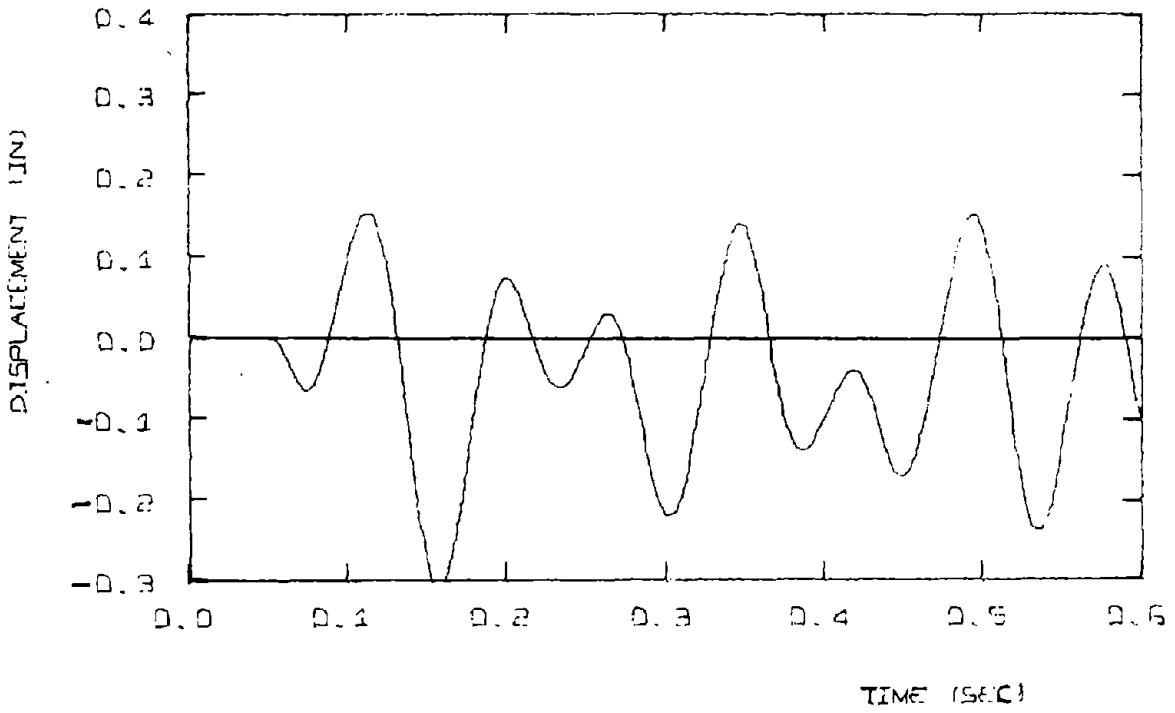
B. BILINEAR MODEL

FIG. 6-10 (Cont.)



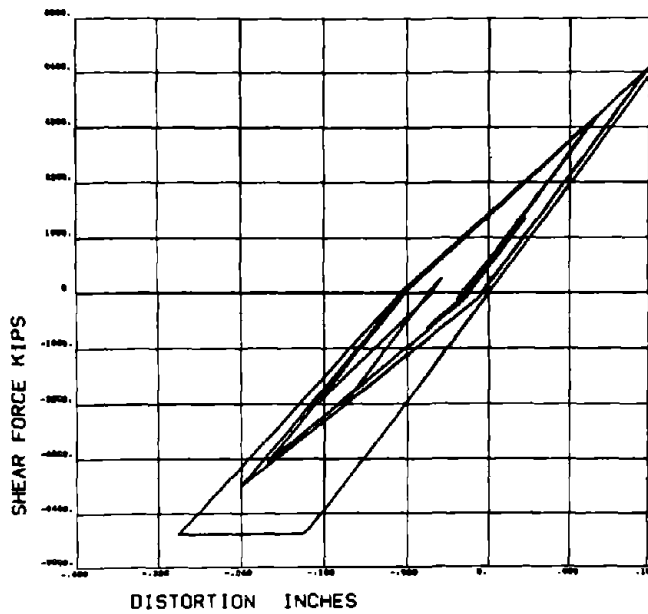
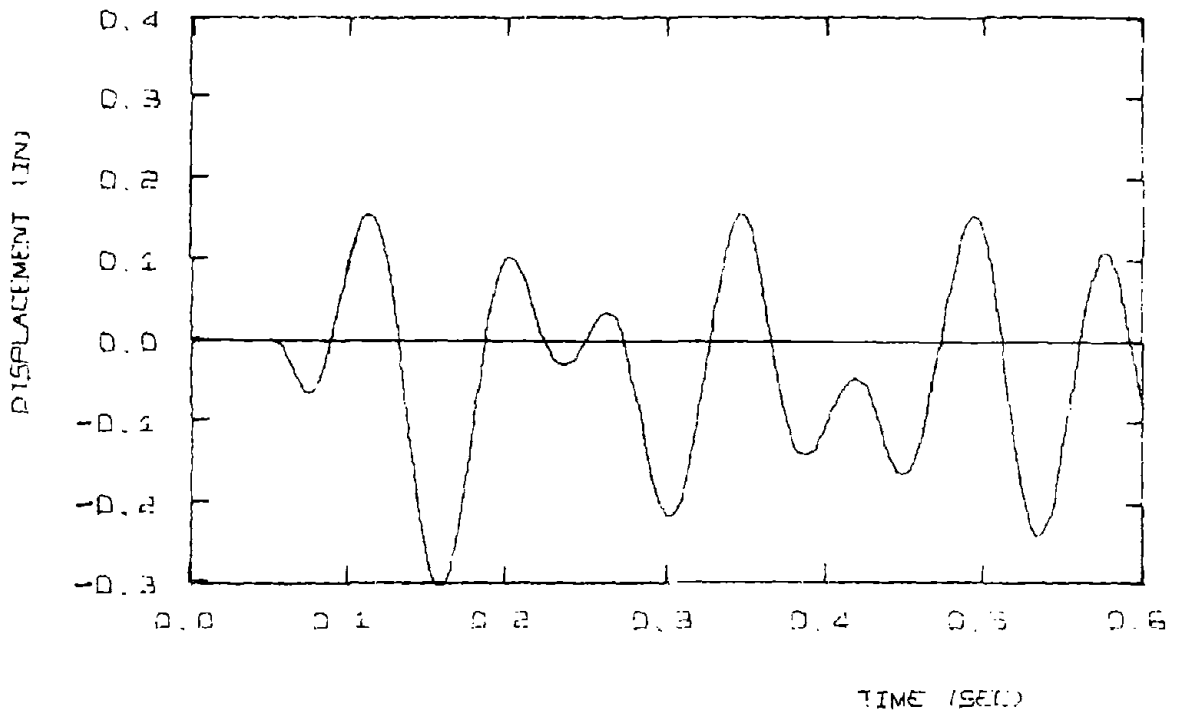
C. TRILINEAR MODEL

FIG. 6-10 (Cont.)



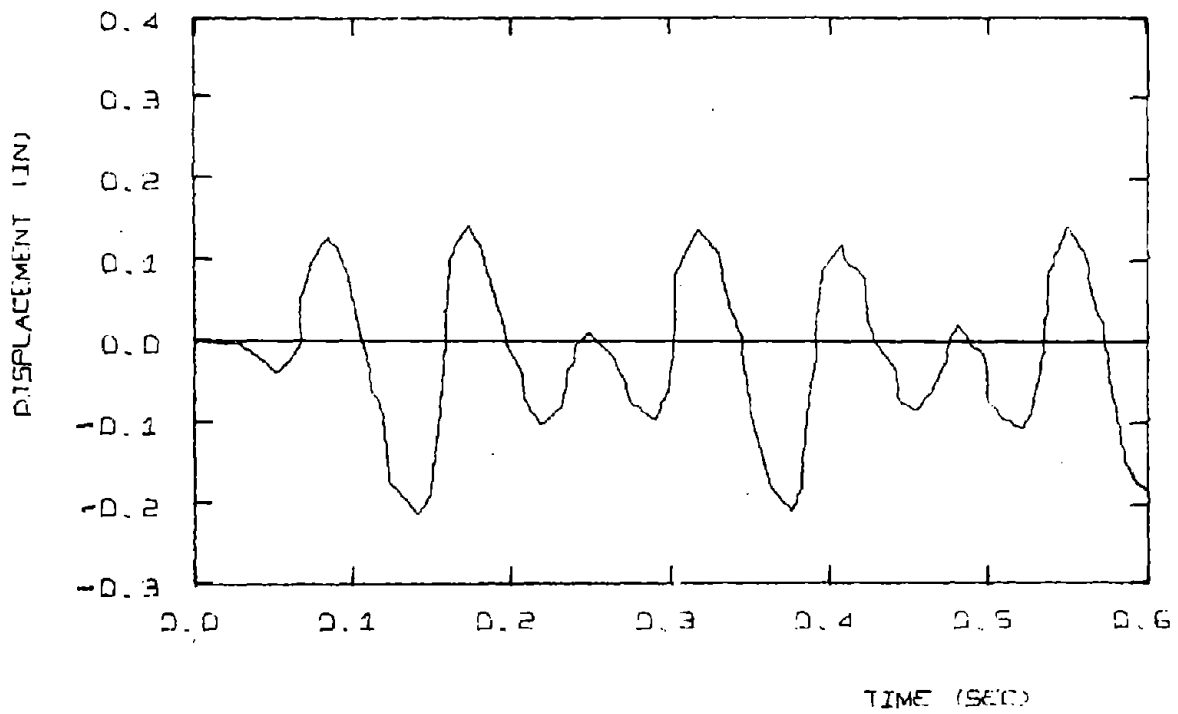
D. CLOUGH'S MODEL

FIG. 6-10 (Cont.)



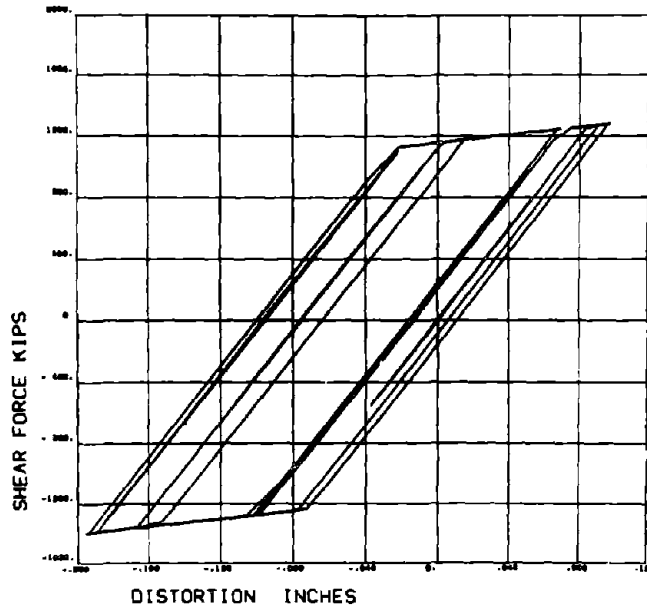
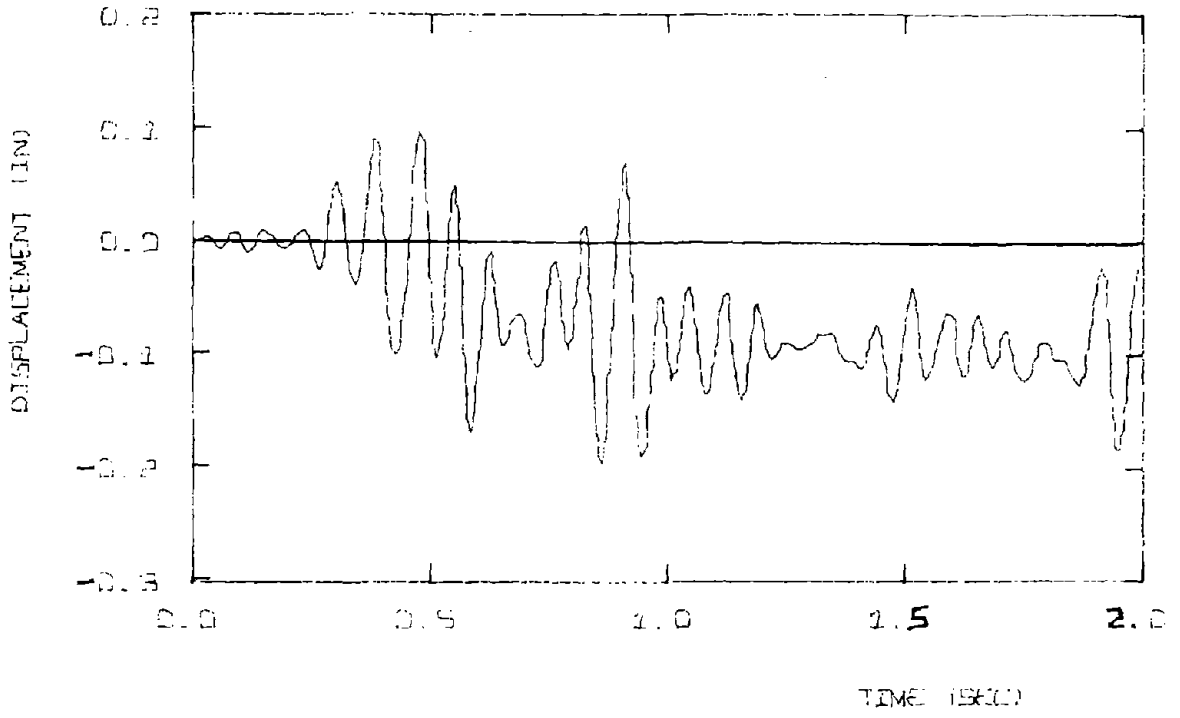
E. ANAGNOSTOPOULOS' MODEL

FIG. 6-10 (Cont.)



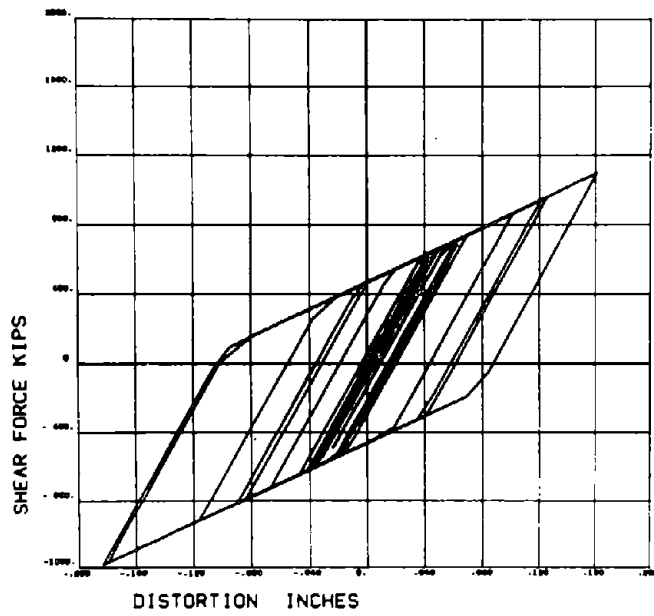
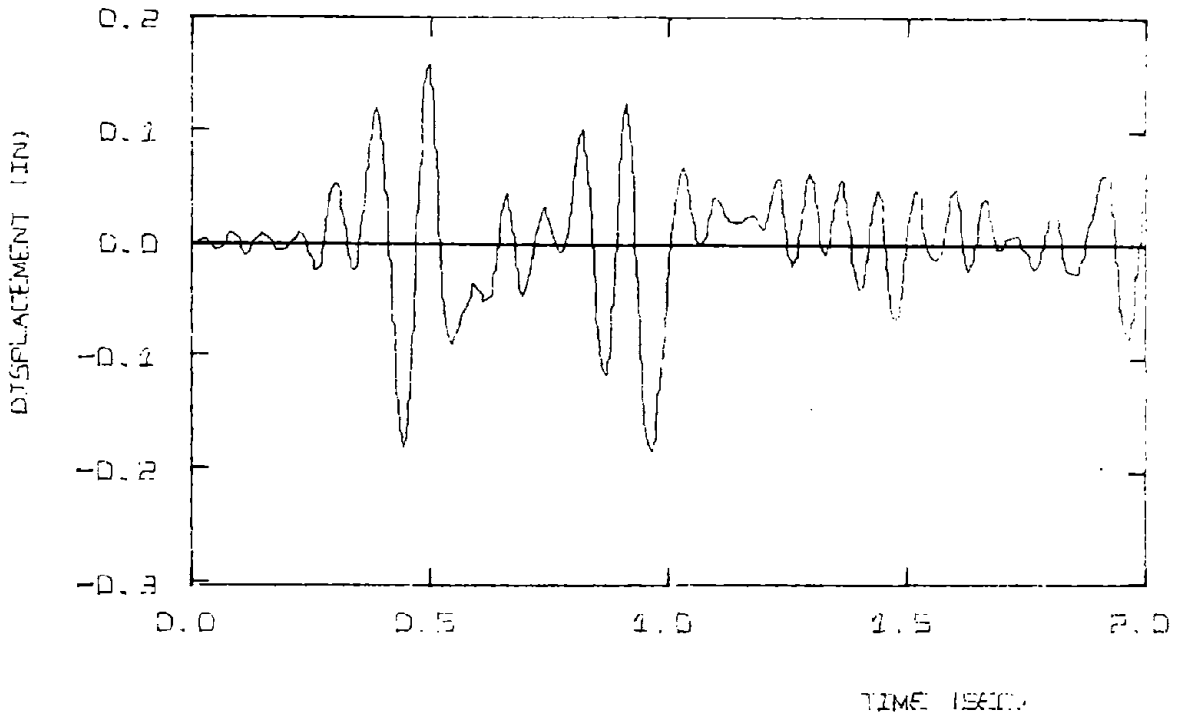
F. TAKEDA'S MODEL

FIG. 6-10 (Cont.)



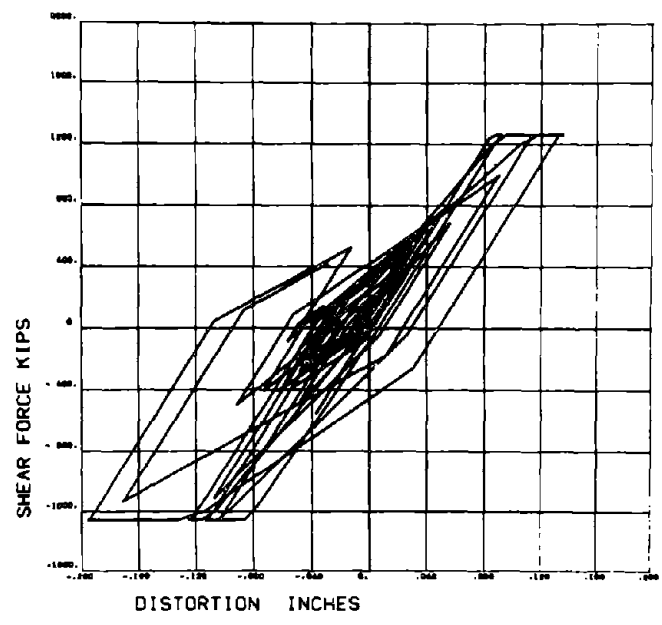
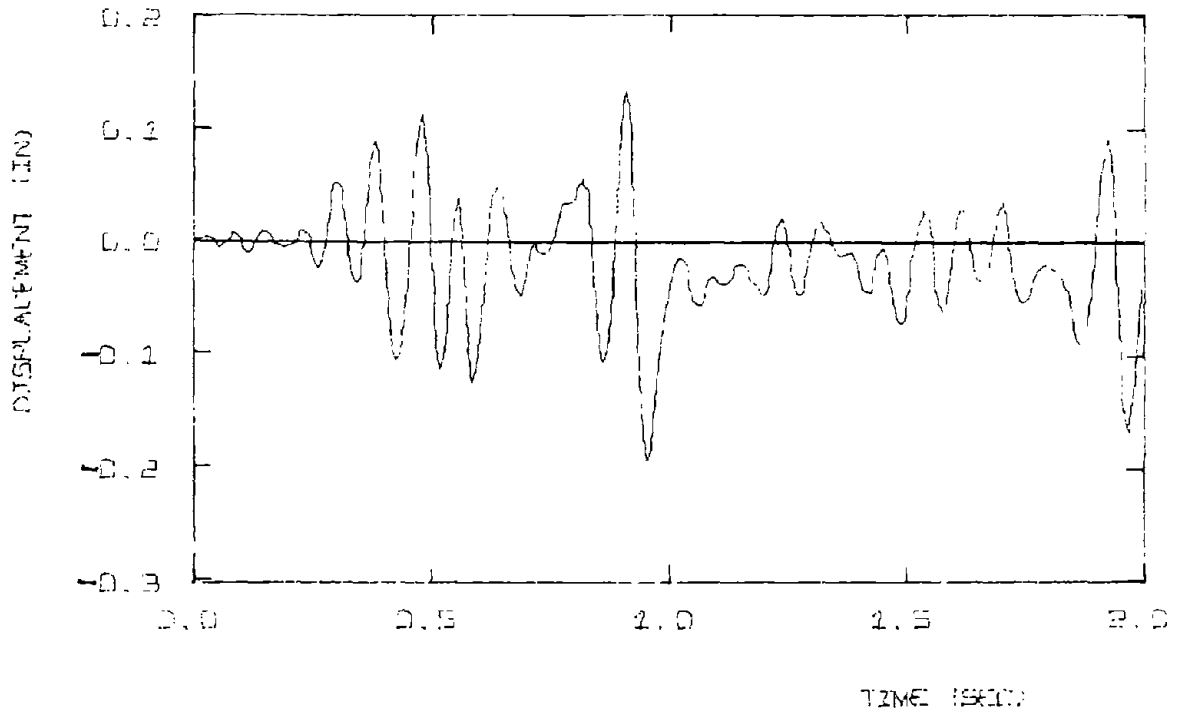
A. BILINEAR MODEL

FIG. 6-11 - RESPONSE OF SIMPLE MODELS TO EL CENTRO EARTHQUAKE



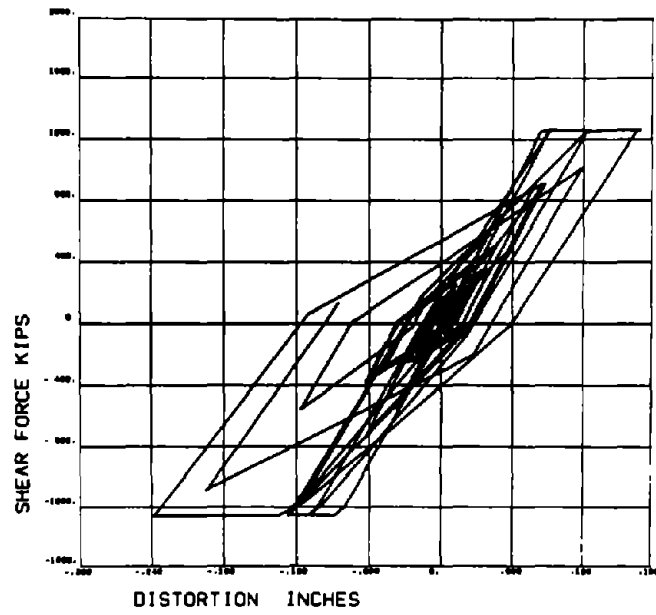
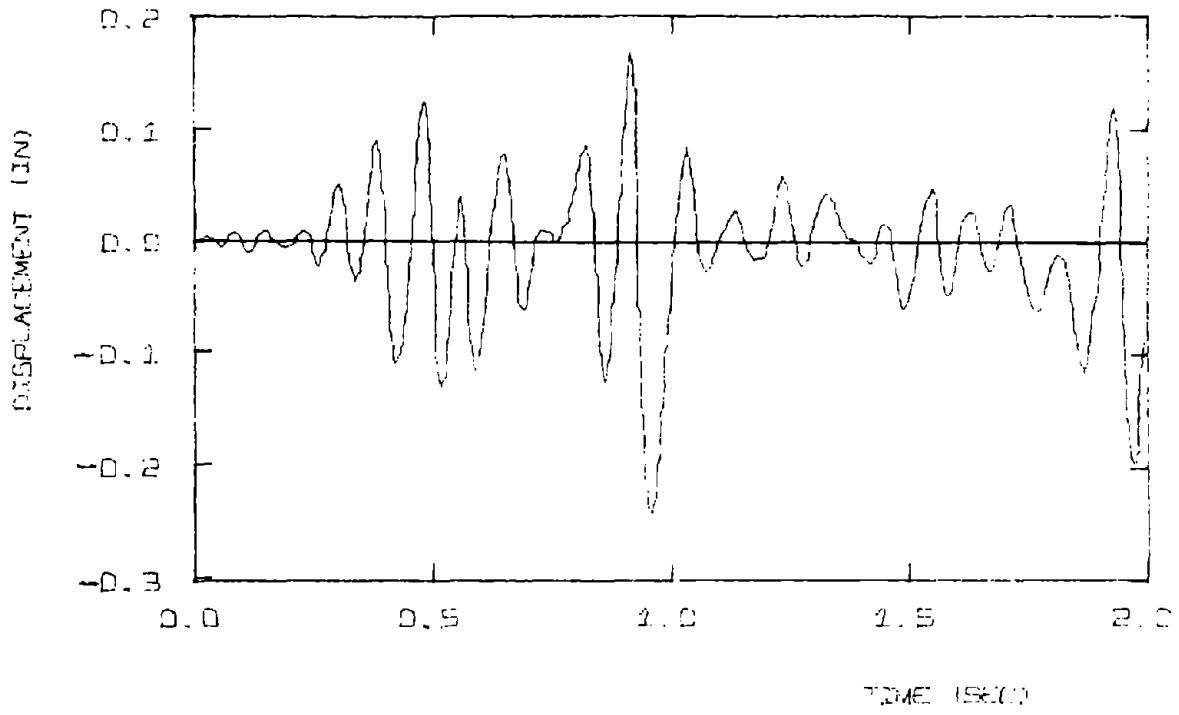
B. TRILINEAR MODEL

FIG. 6-11 (Cont.)



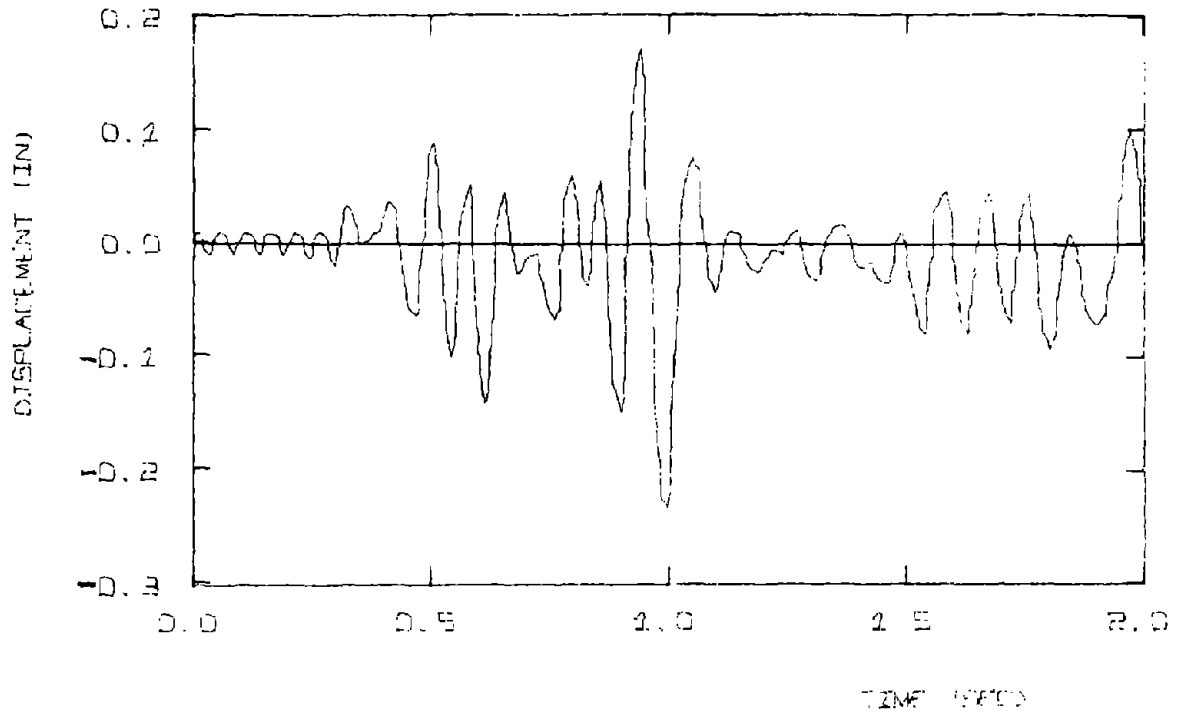
C. CLOUGH'S MODEL

FIG. 6-11 (Cont.)



D. ANAGNOSTOPOULOS' MODEL

FIG. 6-11 (Cont.)



E. TAKEDA'S MODEL

FIG. 6-11 (Cont.)

### 6.3.2 Behavior of Simple Models to Earthquake Base Motion

The simple models are used to represent the response of frame HE1 under the El Centro earthquake motion. The predicted responses are displayed in Fig. 6-11 (A to E). (The elastic model was not included because large amplitude forces were required for the spring to be elastic, causing the response to be very different from that observed.)

Three of the models, Anagnostopoulos, Clough, and Takeda, produce results that are nearly identical with each other. However, they overestimate the magnitude of response, although they seem to agree well with the location of the peaks. (Maximum displacements and peak-to-peak displacements are .234", .408", while experimentally they are .084", .143".)

Both the bilinear and trilinear models also overestimate the magnitude of displacement. In addition, the bilinear model has again a permanent set.

## 6.4 CONCLUSIONS

The fiber model and incremental stiffness approach can represent reasonably well the dynamic behavior of a reinforced concrete frame. But to be able to obtain a better fit to the experimental data, a more sophisticated model would be required. One important aspect would be a refinement of the curvilinear steel model which has been shown to respond poorly to small repetitive loadings. Other

effects such as slippage at the joints could be added.

For the simple models, it seemed that they could all represent well the location of peaks, but had difficulty with their magnitudes. In particular all the simple models overestimated the deflections for the simulated earthquake motion. The fiber model did better in this respect, and overall it appeared to represent the dynamic response better.

## CHAPTER 7 - CONCLUSIONS AND RECOMMENDATIONS

1. To properly represent the behavior of reinforced concrete structures with a fiber model, the stress-strain relationship for the reinforcing steel is a key parameter. Although the curvilinear steel formulation developed represented the behavior for large cyclic straining, it was poor in reproducing the behavior under small repetitive loadings. On the other hand, the elasto-plastic formulation was reasonable for many circumstances. As far as the overall behavior of the members was concerned, the concrete formulation was less important.

2. The model is able to reproduce the axial-bending coupling in the members. Under axial load a pronounced pinching of the cyclic moment-curvature and load-deflection curves appeared consistent with experimental observations. For axial forces which vary with moment, such as in a laterally loaded frame, the moment-curvature behavior may be significantly altered. While the fiber model is reasonable in predicting cross-section behavior, an added refinement would be the consideration of slippage of the reinforcement along the member.

3. The fiber model is able to represent in an average sense the behavior of members under static cyclic loadings. It is important, however, to be able to reproduce the rotation of the joints due to slippage of the anchorage reinforcement. For deep members shear deformation should also be considered. These are improvements which

were not implemented in this work, but which should be undertaken in the future if the fiber model is to be used.

4. In the dynamic frame analysis it was not possible to produce perfect agreement with experimental results. For sinusoidal excitation, results obtained with the simpler models were of the same order, but for the earthquake excitation the fiber model seemed to predict better the observed response. Additional refinements of the model may improve the performance, but the necessity of using a very small time increment makes it expensive to run, and more of an academic tool, rather than a practical design aid. Considering all the uncertainties involved in the material properties, it may be hard to justify this complexity versus attempting to improve the simpler models.

## References

1. S. Popovics, "A Review of Stress-Strain Relationships of Concrete," Journal of the ACI, March 1970, pp. 243-48.
2. H. Rüsçh, "Research Toward a General Flexural Theory for Structural Concrete," Journal of the ACI, July 1960, pp. 1-28.
3. I.C. Medland, D.A. Taylor, "Flexural Rigidity of Concrete Column Section," Journal of the Structural Division, ASCE, February 1971, pp. 573-586.
4. A.H. Mattock, L.B. Kriz, E. Hognestad, "Rectangular Concrete Stress Distribution in Ultimate Strength Design," Journal of the ACI, February 1961, pp. 875-928.
5. H.E.H. Roy, M.A. Sozen, "Ductility of Concrete," Flexural Mechanics of Reinforced Concrete, Proceedings of the International Symposium, Miami, Florida, 1964.
6. P.M. Ferguson, Reinforced Concrete Fundamentals, J. Wiley & Sons, New York, 1965.
7. I.D. Karson, J.O. Jirsa, "Behavior of Concrete under Compressive Loadings," Journal of the Structural Division, ASCE, December 1969, pp. 2543-63.
8. I.D. Karson, J.O. Jirsa, "Behavior of Concrete under Varying Strain Gradients," Journal of the Structural Division, ASCE, August 1970, pp. 1675-95.
9. G.M. Sturman, S.P. Shah, G. Winter, "Effects of Flexural Strain Gradients on Microcracking and Stress-Strain Behavior of Concrete," Journal of the ACI, July 1965, pp. 805-22.
10. S.P. Shah, G. Winter, "Response of Concrete to Repeated Loadings," RILEM International Symposium on the Effects of Repeated Loadings on Materials and Structural Elements, Mexico, September 1966.
11. B.P. Shina, K.H. Gerstle, L.G. Tulin, "Stress-Strain Relations for Concrete under Cyclic Loading," Journal of the ACI, February 1964, pp. 195-212.
12. M.A. Sozen, Personal communication with J.M. Roesset on behavior of concrete under cyclic loadings.

13. W. Ramberg, W.R. Osgood, "Description of Stress-Strain Curves by Three Parameters," TN No. 902, National Advisory Committee for Aeronautics, Washington D.C., July 1943.
14. N.H. Burns, C.P. Siess, "Load-Deformation Characteristics of Beam-Column Connections in Reinforcing Concrete," Civil Engineering Studies, Structural Research Series No. 234, University of Illinois, Urbana, January 1962.
15. A. Singh, K.H. Gerstle, L.G. Tulin, "The Behavior of Reinforcing Steel under Reversed Loading," Materials Research & Standards, January 1965, pp. 12-17.
16. R.H. Brown, J.O. Jirsa, "Reinforced Concrete Beams under Load Reversals," Journal of the ACI, May 1971, pp. 380-390.
17. R.H. Brown, "Reinforced Concrete Cantilever Beams under Slow Cyclic Loadings," Ph.D. Thesis, Civil Engineering Department, Rice University, May 1970.
18. D.C. Kent, R. Park, "Flexural Members with Confined Concrete," Journal of the Structural Division, ASCE, July 1971, pp. 1969-1990.
19. D.C. Kent, "Inelastic Behavior of Reinforced Concrete Members with Cyclic Loading," Ph.D. Thesis, Civil Engineering Department, University of Canterbury, New Zealand, 1969.
20. A.E. Aktan, B.I. Karlsson, M.A. Sozen, "Stress-Strain Relationships of Reinforcing Bars Subjected to Large Strain Reversals," Civil Engineering Studies, Structural Research Series No. 397, University of Illinois, Urbana, June 1973.
21. H. Grandholm, A General Flexural Theory of Reinforced Concrete, J. Wiley & Sons, New York, 1965.
22. E.O. Pfrang, C.P. Siess, M.A. Sozen, "Load-Moment-Curvature Characteristics of Reinforced Concrete Cross Sections," Journal of the ACI, July 1964, pp. 763-777.
23. B.P. Shina, K.H. Gerstle, L.G. Tulin, "The Response of Singly Reinforced Concrete Beams to Cyclic Loading," Journal of the ACI, August 1964, pp. 1021-1038.
24. G.L. Agrawal, L.G. Tulin, K.H. Gerstle, "Response of Doubly Reinforced Concrete Beams to Cyclic Loading," Journal of the ACI, July 1965, pp. 823-834.

25. K.H. Gerstle, "Flexural Characteristics of R.C. Members," ASCE-IABSE, International Conference on Planning & Design of Tall Buildings, Lehigh University, August 1972.
26. H. Aoyama, "Moment-Curvature Characteristics of Reinforced Concrete Members Subjected to Axial Load and Reversal of Bending," Flexural Mechanics of Reinforced Concrete, Proceedings of the International Symposium, Miami, November 1964.
27. A. Parducci, A. Samuelli Ferretti, "Prismatic Reinforced Concrete Members, Alternate Bending beyond the Yielding of Reinforcement under Axial Loads", Proceedings, Fifth World Conference on Earthquake Engineering, Rome, 1973.
28. S.H. Crandall, Engineering Analysis, McGraw-Hill Book Company, New York 1956.
29. B. Bresler, V. Bertero, "Reinforced Concrete Prism under Repeated Loads," RILEM International Symposium on the Effects of Repeated Loadings on Materials and Structural Elements, Vol. III, 1966, Mexico.
30. A.H. Nilson, "Internal Measurement of Bond Slip," Journal of the ACI, July 1972, pp. 439-441.
31. V.V. Bertero, B. Bresler, H. Liao, "Stiffness Degradation of Reinforced Concrete Members Subjected to Cyclic Flexural Moments," Report No. EERC 69-12, University of California, Berkeley, Dec. 1969.
32. R.W. Latona, "Nonlinear Analysis of Building Frames for Earthquake Loading," Dept. of Civil Engineering Research Report R70-65, MIT, Cambridge, Mass., 1970.
33. N.H. Burns, C.P. Siess, "Repeated and Reversed Loading on Reinforced Concrete," Journal of the Structural Division, ASCE, Oct. 1966, pp. 65-78.
34. E.P. Popov, V.V. Bertero, H. Krawinkler, "Cyclic Behavior of Three Flexural Members with High Shear," Report No. EERC 72-5, University of California, Berkeley, October 1972.
35. P. Gulkan, M.A. Sozen, "Response and Energy-Dissipation of Reinforced Concrete Frames Subjected to Strong Base Motions," Civil Engineering Studies, Structural Research Series No. 377, University of Illinois, Urbana, May 1971.
36. P.R. Barnard, "The Collapse of Reinforced Concrete Beams, Flexural Mechanics of Reinforced Concrete, Proceedings of the International Symposium, Miami, November 1964.

37. T. Takeda, M.A. Sozen, N.N. Nielson, "Reinforced Concrete Response to Simulated Earthquakes," Journal of the Structural Division, ASCE, December 1970, pp. 2557-2573.
38. H. Aoyama, T. Endo, T. Minami, "Behavior of Reinforced Concrete Frames Subjected to Reversal of Horizontal Forces," Proceedings of the Japanese Earthquake Symposium - 1966, Tokyo, October 1966, pp. 315-320.
39. T. Shiga, J. Ogawa, A. Shibata, J. Shibuya, "The Dynamic Properties of Reinforced Concrete Frames," Proceedings of U.S.-Japan Seminar on Earthquake Engineering with Emphasis on Safety of School Buildings, Japan, September 1970, pp. 346-363.
40. W.R. Walpole, R. Shepherd, "Elasto-Plastic Seismic Response of Reinforced Concrete Frames," Journal of the Structural Division, ASCE, October 1969, pp. 2031-2055.
41. S. Otani, M.A. Sozen, "Behavior of Multistory Reinforced Concrete Frames during Earthquakes," Civil Engineering Studies, Structural Research Series, No. 392, University of Illinois, Urbana, Nov. 1972.
42. V.V. Bertero, G. McClure, "Behavior of Reinforced Concrete Frames Subjected to Repeated Reversible Loads," Journal of the ACI, October 1964, pp. 1305-1329.
43. N.W. Hanson, H.W. Connor, "Seismic Resistance of Reinforced Concrete Beam-Column Joints," Journal of the Structural Division, ASCE, October 1967, pp. 533-560.
44. W.H. Ruiz, G. Winter, "Reinforced Concrete Beams under Repeated Loads," Journal of the Structural Division, ASCE, June 1969, pp. 1189-1211.
45. J.M. Roesset, K.R. Reinschmidt, R.E. Efimba, The Use of ICES-STRUDEL in Design Courses, Dept. of Civil Engineering Research Report R68-72, MIT, Cambridge, Mass., 1968.
46. R.K. Livesley, Matrix Methods of Structural Analysis, Pergamon Press, London, 1964.
47. R.W. Clough, S.B. Johnston, "Effect of Stiffness Degradation on Earthquake Ductility Requirements," Proceedings of the Japan Earthquake Engineering Symposium, 1967.
48. S.A. Anagnostopoulos, "Nonlinear Dynamic Response and Ductility Requirements of Building Structures Subjected to Earthquakes," Dept. of Civil Engineering Research Report R72-54, MIT, Cambridge, Mass. 1972.

## BIOGRAPHY

## KENNETH MUN SUNG MARK

Born on June 8, 1946, the author has spent most of his life in sunny Hawaii.

In 1968 he graduated from the University of Hawaii, with highest honors in Civil Engineering. While an undergraduate he was a compulsive joiner of such honorary societies as Phi Eta Sigma, Omicron Delta Kappa, Phi Kappa Phi, and Chi Epsilon. In addition he served as president of the student chapter of ASCE and as chairman of the Engineers' Council.

With the aid of a doctoral support fellowship, the author attended the University of Illinois at Urbana. The draft cut his planned education short, but he managed to get a M.S. in Civil Engineering with a major in structures. Military service with the U.S. Army Corps of Engineers found him stationed overseas in Honolulu, Hawaii. There he was fortunate to get some engineering experience in design and construction.

With no hard feelings against the Army, he began his doctoral work at M.I.T. in the Fall of 1971, supported by an NSF Traineeship and later by an NDEA Fellowship. He has since worked as a Teaching Assistant in Information Systems and as a Research Assistant in a project leading to his doctoral thesis.

APPENDIX AFORMULATION OF THE MEMBER INCREMENTAL STIFFNESS MATRIX

The incremental stiffness equations for a cross-section were formulated in Chapter 4, and from them the flexibility relations are obtained by inversion.

$$\begin{aligned}\Delta\varepsilon &= b_{11} \Delta N + b_{12} \Delta M \\ \Delta\phi &= b_{21} \Delta N + b_{22} \Delta M\end{aligned}\tag{A.1}$$

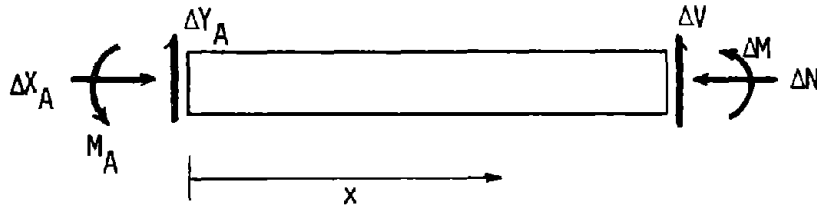
$$\text{where } [b_{ij}] = [a_{ij}]^{-1}$$

If the beam is considered to be represented by a line element and the deflections are small, then the following relationships hold:

$$\begin{aligned}\varepsilon &= \frac{du}{dx} \\ \phi &= \frac{d^2v}{dx^2} \\ \theta &= \frac{dv}{dx}\end{aligned}\tag{A.2}$$

where  $u$  and  $v$  are the horizontal and vertical displacements;  $\theta$  is the chord rotation; and  $x$  is the distance along the centroid of the member.

The ends of the member will be labeled A and B and the length of the member is  $L$ .



In the above figure a portion of the member is shown with the forces acting at end A and at the cross-section a distance  $x$  away. By considering equilibrium,

$$\Delta N = \Delta X_A \quad (\text{A.3})$$

$$\Delta M = -\Delta M_A + x \Delta Y_A$$

Substitution of the relations in (A.3) and (A.2) into (A.1) leads to the following

$$\Delta \epsilon = \frac{d}{dx} (\Delta u) = b_{11} \Delta X_A + b_{12} x \Delta Y_A - b_{12} \Delta M_A \quad (\text{A.4})$$

$$\Delta \phi = \frac{d^2}{dx^2} (\Delta v) = b_{21} \Delta X_A + b_{22} x \Delta Y_A - b_{22} \Delta M_A$$

(A.4) can be integrated across the length of the member to obtain:

$$\Delta u_A - \Delta u_B = - \int_0^L b_{11} dx \Delta X_A + - \int_0^L x b_{12} dx \Delta Y_A + \int_0^L b_{12} dx \Delta M_A$$

$$\Delta \theta_A - \Delta \theta_B = - \int_0^L b_{12} dx \Delta X_A + - \int_0^L x b_{22} dx \Delta Y_A + \int_0^L b_{22} dx \Delta M_A$$

$$\begin{aligned} \Delta v_A - \Delta v_B + L \Delta \theta_A = & \int_0^L (L-x) b_{12} dx \Delta X_A + - \int_0^L x(L-x) b_{22} dx \Delta Y_A \\ & + \int_0^L (L-x) b_{22} dx \Delta M_A \quad (\text{A.5}) \end{aligned}$$

These equations can be easily be expressed in matrix form

$$\begin{Bmatrix} \Delta u_A - \Delta u_B \\ \Delta v_A - \Delta v_B + L\Delta\theta_A \\ \Delta\theta_A - \Delta\theta_B \end{Bmatrix} = \begin{bmatrix} f_{11} & f_{12} & f_{13} \\ f_{21} & f_{22} & f_{23} \\ f_{31} & f_{32} & f_{33} \end{bmatrix} \begin{Bmatrix} \Delta X_A \\ \Delta Y_A \\ \Delta M_A \end{Bmatrix} \quad (\text{A.6})$$

where  $[f_{ij}]$  is the flexibility matrix relating incremental displacements to the incremental forces of end A.

If  $[f_{ij}]$  is inverted then:

$$\begin{Bmatrix} \Delta X_A \\ \Delta Y_A \\ M_A \end{Bmatrix} = \begin{bmatrix} k_{11} & k_{12} & k_{13} \\ k_{21} & k_{22} & k_{23} \\ k_{31} & k_{32} & k_{33} \end{bmatrix} \begin{Bmatrix} \Delta u_A - \Delta u_B \\ \Delta v_A - \Delta v_B + L\Delta\theta_A \\ \Delta\theta_A - \Delta\theta_B \end{Bmatrix} \quad (\text{A.7})$$

where  $[k_{ij}] = [f_{ij}]^{-1}$

This matrix equation can be expanded and rearranged to get

$$\begin{Bmatrix} \Delta X_A \\ \Delta Y_A \\ \Delta M_A \end{Bmatrix} = \begin{bmatrix} k_{11} & k_{12} & (k_{13} + Lk_{12}) \\ k_{21} & k_{22} & (k_{23} + Lk_{22}) \\ k_{31} & k_{32} & (k_{33} + Lk_{33}) \end{bmatrix} \begin{Bmatrix} \Delta u_A \\ \Delta v_A \\ \Delta\theta_A \end{Bmatrix} + \begin{bmatrix} -k_{11} & -k_{12} & -k_{13} \\ -k_{21} & -k_{22} & -k_{23} \\ -k_{31} & -k_{32} & -k_{33} \end{bmatrix} \begin{Bmatrix} \Delta u_B \\ \Delta v_B \\ \Delta\theta_B \end{Bmatrix} \quad (\text{A.8})$$

$$\{\Delta P_A\} = [K_{AA}] \{\Delta U_A\} + [K_{AB}] \{\Delta U_B\} \quad (\text{A.9})$$

From the condition of equilibrium

$$\begin{Bmatrix} \Delta X_B \\ \Delta Y_B \\ \Delta M_B \end{Bmatrix} = \begin{bmatrix} -1 & 0 & 0 \\ 0 & -1 & 0 \\ 0 & L & -1 \end{bmatrix} \begin{Bmatrix} \Delta X_A \\ \Delta Y_A \\ \Delta M_A \end{Bmatrix} \quad (\text{A.10})$$

or

$$\begin{aligned} \{\Delta P_B\} &= [T] \{\Delta P_A\} \\ &= [T][K_{AA}]\{\Delta U_A\} + [T][K_{AB}]\{\Delta U_B\} \\ &= [K_{BA}]\{\Delta U_A\} + [K_{BB}]\{\Delta U_B\} \end{aligned} \quad (\text{A.11})$$

so

$$\begin{aligned} [K_{BA}] &= [T] [K_{AA}] \\ [K_{BB}] &= [T] [K_{AB}] \end{aligned} \quad (\text{A.12})$$

With (A.9) and (A.11) the incremental member stiffness relations have been obtained, relating incremental forces to the incremental displacements.

## APPENDIX B

SEMI-RIGID JOINTS TO ACCOUNT FOR ROTATIONS  
DUE TO SLIP OF ANCHORAGE REINFORCEMENTS

An alternate method\* of obtaining a member stiffness matrix from the member flexibility matrix and to include semi-rigid joints is described.

The flexibility matrix is now defined in the following way:

$$\begin{Bmatrix} \Delta u_B \\ \Delta v_B \\ \Delta \theta_B \end{Bmatrix} = \begin{bmatrix} \bar{F}_{11} & \bar{F}_{12} & \bar{F}_{12} \\ \bar{F}_{21} & \bar{F}_{22} & \bar{F}_{23} \\ \bar{F}_{31} & \bar{F}_{32} & \bar{F}_{33} \end{bmatrix} \begin{Bmatrix} \Delta X_B \\ \Delta Y_B \\ \Delta M_B \end{Bmatrix} \quad (\text{B.1})$$

$$\{\Delta u_B\} = [\bar{F}_{ij}] \{\Delta P_B\}$$

This flexibility matrix differs from the one derived in Appendix A (Eq. A.6), but can be obtained from it by considering end A to be fixed ( $\Delta u_A = \Delta v_A = \Delta \theta_A = 0$ ), and using the following result of equilibrium:

$$\{\Delta P_A\} = - \begin{bmatrix} -1 & 0 & 0 \\ 0 & -1 & 0 \\ 0 & -L & -1 \end{bmatrix} \{\Delta P_B\} \quad (\text{B.2})$$

or

$$\{\Delta P_A\} = - [H] \{\Delta P_B\}$$

---

\* One source of this type of derivation is Livesley. (46)

From these equations:

$$\begin{bmatrix} \bar{f}_{11} & \bar{f}_{12} & \bar{f}_{13} \\ \bar{f}_{21} & \bar{f}_{22} & \bar{f}_{23} \\ \bar{f}_{31} & \bar{f}_{32} & \bar{f}_{33} \end{bmatrix} = \begin{bmatrix} f_{11} & (f_{12} + L f_{13}) & f_{13} \\ f_{12} & (f_{21} + L f_{23}) & f_{23} \\ f_{13} & (f_{31} + L f_{33}) & f_{32} \end{bmatrix} \quad (\text{B.3})$$

Through use of the definition

$$\begin{Bmatrix} \Delta P_A \\ \Delta P_B \end{Bmatrix} = \begin{bmatrix} K_{AA} & K_{AB} \\ K_{BA} & K_{BB} \end{bmatrix} \begin{Bmatrix} \Delta u_A \\ \Delta u_B \end{Bmatrix} \quad (\text{B.4})$$

and the fact that  $K_{BA} = K_{AB}^T$ , it can be shown that

$$\begin{aligned} [K_{AA}] &= [H] [F_{ij}]^{-1} [H]^T & [K_{AB}] &= - [H] [F_{ij}]^{-1} \\ [K_{BA}] &= -[H] [F_{ij}]^{-1} & [K_{BB}] &= [F_{ij}]^{-1} \end{aligned} \quad (\text{B.5})$$

These are the same member stiffness matrices as previously described, in Appendix A.

Consider now that the member has semi-rigid joints; it then can be visualized as having rotational springs attached to each end.



$$K_A^\theta = M_A \quad \text{and} \quad K_B^\theta = M_B \quad (\text{B.6})$$

Returning to the definition of the flexibility matrix (Eq. B.1), the displacement at end B now is composed of the member distortions plus the distortions due to the rotational springs at the ends of the member. Thus

$$\{u_B\}_{\text{total}} = \left[ [F_{ij}] + [f_{ij}]_A + [f_{ij}]_B \right] \{P_B\} \quad (\text{B.7})$$

where  $[f_{ij}]_A$  and  $[f_{ij}]_B$  are the flexibility matrices due to the rotation springs at joints A and B, respectively.

$$[f_{ij}]_A = \begin{bmatrix} 0 & 0 & 0 \\ 0 & \frac{L^2}{K_A} & \frac{L}{K_A} \\ 0 & \frac{L}{K_A} & \frac{1}{K_A} \end{bmatrix}$$

(B.8)

$$\text{and } [f_{ij}]_B = \begin{bmatrix} 0 & 0 & 0 \\ 0 & 0 & 0 \\ 0 & 0 & \frac{1}{K_B} \end{bmatrix}$$

Finally, the flexibility matrix for the member becomes:

$$[f_{ij}]_{\text{total}} = \begin{bmatrix} \bar{f}_{11} & \bar{f}_{12} & \bar{f}_{13} \\ \bar{f}_{21} & (\bar{f}_{22} + \frac{L^2}{K_A}) & (\bar{f}_{23} + \frac{L}{K_A}) \\ \bar{f}_{31} & (\bar{f}_{31} + \frac{L}{K_A}) & (\bar{f}_{33} + \frac{1}{K_A} + \frac{1}{K_B}) \end{bmatrix} \quad (\text{B.9})$$

Substitution of this matrix into Eq. B.4 will yield the stiffness matrices for the member. Note that if  $K_A$  and  $K_B$  are equal to infinity, the member stiffness matrix will revert to that of Appendix A.





